

# FLUID FLOW DURING CONTINENTAL REWORKING

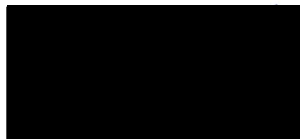
A study of shear zones in the Arunta Inlier, central Australia

Caroline M. Read (BSc hon.)

A thesis submitted for the degree of Doctor of Philosophy (Earth Sciences)  
at Monash University

February, 2002

This thesis contains no material that has been accepted for the award of any other degree or diploma in any university or other institution. To the best of my knowledge, this thesis contains no material previously published or written by another person except where due reference is made in the text.



Caroline Margaret Read  
February, 2002

## **Copyright Notices**

### **Notice 1**

Under the Copyright Act 1968, this thesis must be used only under the normal conditions of scholarly fair dealing. In particular no results or conclusions should be extracted from it, nor should it be copied or closely paraphrased in whole or in part without the written consent of the author. Proper written acknowledgement should be made for any assistance obtained from this thesis.

### **Notice 2**

I certify that I have made all reasonable efforts to secure copyright permissions for third-party content included in this thesis and have not knowingly added copyright content to my work without the owner's permission.

## ACKNOWLEDGMENTS

I would like to thank my fantastic supervisor Ian Cartwright for being calm and concise about everything, always. Ian taught me a great deal (though I failed on the commas) and especially made me realise that interpreting geological processes from geochemical data is not stressful. Thank you for taking me on as a student and for funding all of my fieldwork, analytical work, conference attendance and fieldtrips and especially for your practical support after the crash with university administration.

I would like to acknowledge the abundant technical support from: Marlin Yanni, Mary Jane, Jodie Miller, Roland Maas, Shane Reeves, Robert Douglass, Chris Pierson, Gary McWilliams, John Tsiros and Dave Phillips, without which I would have very little data! I would like to thank Karen Bond and Florita Herincus for their administrative help and excellent cheer. And I want to especially thank Karen for tracking down my computer that tried to escape to the psychology department!

In the production of this thesis I would like to thank the following people for their helpful reviews of different chapters; Marteen Krabendam, Patricia Lavery, Catherine Spaggiari, Ulli Troitzsch, Ricardo Zucchetto, Jannene McBride, Marion Anderson. And especially Matthew Leavesley and Catherine Spaggiari for help with the final production. Also I would like to thank Dave Phillips who was patient and helpful with the argon analyses and for his constructive review and comments for Chapter Seven and also Paul Bons for his advice on vein formation and the mechanics of fluid-flow and for letting me attend the Portugal Geotraverse. The following people also helped considerably in discussions (big and small) and with their evaluations (not always positive) of my data at conferences and in the field; Ian Buick, Jodie Miller, Bob Holdsworth, Mike Sandiford, Rick Sibson, Bruce Yardley, and Phaedra Upton. I also am grateful to have been able to attend Andy McCaig's trip to the Pyrenees, where I got to see the big picture in actual 3D, at the top of a mountain, in the snow with a glass of wine, fantastic!

I would also like to thank all the people that came into the field with me, who contributed (some in their own special way) to my fieldwork; Emily Neil, Ian Fitzsimons, Tony Rudge, Chris Doyle, Cath Spaggiari, Christian Biermeir, Geoff Pike, Ben Foley, Susan Shand, Matthew Leavesley and especially Jodie Miller, who taught me a great deal about geochemical sample collection and Ian Cartwright who found all the shear zones he was looking for with relative ease that I was surprised I couldn't do the same thing the following year. Also in central Australia, thanks to the guys from the Northern Territory Geo Survey, especially Dot Close, Bunge Scrimingcoir, Christine Edgoose and Ali Dean for having a laugh/chat/beer when I was in town. A special thanks to Barry who came and picked Ian Fitz and I up after the crash on a Sunday morning when there was probably much more interesting things to be doing. Thanks also to Cookie at Aileron Roadhouse, and the Nurse at Tea Tree community. Thanks to Patricia Lavery, Martin Hand and Ian Buick for taking me into the Harts Range and showing me some really spectacular rocks! And a big thanks to the station owners and managers who allowed me access to their wonderful beautiful (I'm overlooking environmentally stuffed) properties.

I benefited immensely from my stay at Durham University where I was able to discuss the role of fluids in reactivation with Bob Holdsworth. I am also grateful for the help with microstructural analysis from Lee Watts as well as his and Janines kindness and generosity while I was in Durham. And thanks to Megan QB for periodically having me to stay in Newcastle and treating a broke student to a couple of pints and a curry.

My excellent and sometimes even excellently odd friends at Monash and La Trobe have provided great inspiration, support and fun over the years especially Catherine for your friendship and for taking me with you on some excellent trips into the Bush - long may they continue. Thanks also to Mary not least for all the technical help over the years but your friendship and dream analysis discussions. A huge thanks to Jodie for all the support and guidance which were invaluable to me, especially in the beginning of my thesis and your continued friendship now that you are off and away.

Thanks to Beryl and John for making me feel like one of the family and for being very generous and kind. Thanks also to Jannene and Kerrin for having me to stay in your wonderful house, and feeding me wonderful treats in those last weeks. Life in Canberra would certainly have been duller if it wasn't for millions of cups of tea with Melissa. I am also grateful to have been able to use a microscope at the University of Canberra.

I am truly grateful and indebted to Matthew Leavesley for all his support over the last couple of years and especially his help and patience in this last week - luckily you will be writing up in a few months and I will have

the chance to repay all that reference checking! And finally thank you to my Mum and Dad for loving me and believing in me and visiting me in Australia. The beers on you Mum!

---

## ABSTRACT

The continental crust preserves ancient metamorphic terrains that record repeated periods of tectonic rejuvenation. Shear zones commonly represent sites of crustal reworking where new structural fabrics, new mineral growth and chemical alteration occur. Deformation, metamorphism and alteration within shear zones are facilitated by the presence of fluids. This study investigates the role of fluids in middle crustal reworking by examining shear zones in central Australia.

Petrological and geochemical analysis of the shear zones in the Arunta Inlier suggest that large volumes of fluid infiltrated the middle crust during the Alice Springs Orogeny. The resulting composition domains within some of the shear zones developed over repeated cycles of seismically-activated fluid infiltration, vein development and stress-induced dissolution at the brittle-ductile transition. The shear zones suggest that the location of the brittle-ductile transition is highly-dependant on the tectonic regime and the abundance of fluid. In addition, heterogeneous alteration of individual samples within the shear zones suggests that geochemical techniques used for interpreting fluid volumes and fluid flow directions may not be applicable to complex shear zones.

Rb-Sr and  $^{40}\text{Ar}/^{39}\text{Ar}$  data show that greenschist- to amphibolite-facies shearing in the northern Arunta Inlier occurred from ~360 Ma to ~300 Ma during the Alice Springs Orogeny.  $^{40}\text{Ar}/^{39}\text{Ar}$  *in situ* laser probe analysis of reworked mylonites in the Redbank High Strain Zone, southern Arunta Inlier, show the mylonites reached temperatures of  $>500^\circ\text{C}$  during Alice Springs Orogeny, contrary to previous interpretations. In addition, the laser analysis shows that heterogeneous excess argon contamination occurred within the Redbank High Strain Zone mylonites as a result of interaction with an argon-bearing fluid during the Alice Springs Orogeny. The data indicate that excess argon contamination may be common within fluid-dominated shear zone environments and high spatial resolution is required when using  $^{40}\text{Ar}/^{39}\text{Ar}$  to date reworking events.

$\delta^{18}\text{O}$  values as low as  $-6.4\text{‰}$  within the shear zones show re-equilibration with a low  $^{18}\text{O}$  fluid during shearing. Calculated  $\delta^{18}\text{O}_{\text{fluid}}$  and  $\delta D_{\text{fluid}}$  values indicate that the infiltrating fluid was

predominantly derived from formation waters in the overlying basins, suggesting that the surface represents an important reservoir for fluid required to hydrate the middle crust.

The Alice Springs Orogeny may represent a contractional response to substantial crustal thinning during the extensional Larapinta Event (~490 Ma) that led to the opening of the Larapinta Seaway. Permeable connectivity between the surface and the middle crust may have been substantial at this time and led to the infiltration of large volume of fluids that became trapped in the crust as tectonism reversed and deformation became predominantly ductile. Fluid then escaped predominantly via seismic pumping up through the shear zones.

There is substantial evidence that large volumes of surface-derived fluid infiltrated shear zones in central Australia during tectonic rejuvenation. This suggests that connectivity with the surface is important for rehydrating the middle crust, especially where other fluid sources are unavailable, such as within intraplate tectonic settings.

---

**TABLE OF CONTENTS**
**Chapter One: The role of fluids in crustal reworking.**

1.1 Introduction	1
1.1.1 Fluids within the crust	1
1.2 Shear zones reworking the middle crust	2
1.2.1 Shear zones as PTt indicators	3
1.2.2 Shear zones as conduits for fluid flow	3
1.2.3 Hydration of middle crustal shear zones – what fluid source?	4
1.2.4 Timing of fluid flow and deformation	6
1.3 Research aims	6
1.4 Methodology	7
1.4.1 Suitability of study area	7
1.4.2 Arunta Inlier sampling transect	7
1.4.3 Analytical techniques	8
1.4.3.1 Oxygen isotopes	8
1.4.3.2 Hydrogen isotopes	9
1.4.3.3 Whole rock geochemistry	9
1.4.3.4 Mineral chemistry	9
1.4.3.5 Rb-Sr age determination analysis	9
1.4.3.6 $^{40}\text{Ar}/^{39}\text{Ar}$ analysis by furnace step heating	10
1.4.3.7 $^{40}\text{Ar}/^{39}\text{Ar}$ laser probe analysis	10
1.5 Layout of this thesis	11
1.6 Nomenclature and classification of shear zone rocks	12
1.6.1 Mylonites	12
1.6.2 Other terms	12
1.6.3 Abbreviations	13

**Chapter Two: The geology of the Arunta Inlier, central Australia.**

2.1 Introduction	15
2.2 Regional geology of central Australia	15
2.3 The Arunta Inlier	17
2.3.1 Rock nomenclature and divisions within the Arunta Inlier	19
2.3.2 Tectonic and metamorphic history	19
2.3.2.1 Mount Stafford Event	20
2.3.2.2 Strangways Orogeny	20
2.3.2.3 Argilke Event	21
2.3.2.4 Chewings Orogeny	21
2.3.2.5 Anmatjira Uplift Phase	23
2.3.2.6 Dyke Swarm	23
2.3.2.7 Larapinta Event	23
2.3.2.8 Alice Springs Orogeny	24
2.4 The Alice Springs Orogeny	24
2.4.1 An intraplate orogeny	25
2.4.2 The Centralian Superbasin	25
2.4.3 Effects of the Alice Springs Orogeny within the Arunta Inlier	27
2.4.4 Summary	29

2.5 Local Geology	30
2.6 Northern Province	30
2.6.1 Paragneisses of the Northern Province	30
2.6.1.1 The Weldon Metamorphics	32
2.6.1.2 P-T conditions	33
2.6.1.3 The Mount Freeling Schist	35
2.6.2 Orthogneisses of the Northern Province	35
2.6.2.1 The Napperby Gneiss	38
2.6.2.2 The Mount Airy Orthogneiss	38
2.6.2.3 The Alooya Gneiss	38
2.6.3 Tectonic evolution of the Anmatjira and Reynolds Ranges	39
2.6.4 Shearing and fluid flow	40
2.7 Central Province	41
2.7.1 Lithologies	41
2.7.2 Tectonic history	43
2.7.3 Crustal reworking	44
2.8 Redbank High Strain Zone	44
2.8.1 Deep structure of the Redbank High Strain Zone	44
2.8.2 Mylonites of the Redbank High Strain Zone	46
2.8.3 Tectonic history	46
2.9 Southern Province	47
2.9.1 The Wigley Zone	48
2.9.1.1 Madderns Yard Metamorphic Complex	49
2.9.1.2 Iwupataka Metamorphic Complex	50
2.9.2 Tectonic and metamorphic history	51
2.10 Summary	51

***Chapter Three: The role of fluids in mechanical and chemical partitioning within shear zones of the northern Arunta Inlier, Central Australia.***

3.1 Introduction	53
3.2 Geological setting	54
3.3 Structure and petrography of shear zones	56
3.3.1 Sample collection	56
3.3.2 The Yalbadjandi Shear Zone, Anmatjira Range	58
3.3.2.1 Mica schists	58
3.3.2.2 Protomylonites	59
3.3.2.3 Phyllonites	60
3.3.2.4 Foliated cataclasites	60
3.3.3 Blue Bush Swamp Shear Zone, Reynolds Range	61
3.3.3.1 Sheared Mount Freeling Schist	61
3.3.3.2 Sheared orthogneiss and pegmatites	64
3.3.4 Shear Zones in the Napperby Gneiss, Reynolds Range	64
3.3.4.1 Orthoschist	64
3.3.4.2 Muscovite-chlorite phyllonite	68
3.3.4.3 Biotite phyllonite	68
3.3.4.4 Xenolith-hosted shear zone rocks	69
3.3.5 Shear Zones in the Mount Airy Orthogneiss, Anmatjira Range	69
3.3.6 Shear Zones in the Alooya Gneiss, Anmatjira Range	69
3.4 Characteristics of deformation	70

3.4.1 Yalbadjandi Shear Zone	71
3.4.2 Napperby Gneiss shear zones	72
3.4.3 Blue Bush Swamp Shear Zone	73
3.4.4 Summary	73
3.5 Hydration and metamorphic reactions	73
3.5.1 Orthogneiss-hosted shear zones	74
3.5.2 Pelite-hosted shear zones	76
3.6 Major element geochemistry	77
3.6.1 Variability within the host gneisses	78
3.6.2 The Yalbadjandi Shear Zone	82
3.6.2.1 Mount Airy Orthogneiss	82
3.6.2.2 Weldon Metamorphics	84
3.6.3 Napperby Gneiss	86
3.7 Discussion	88
3.7.1 Development of the shear zones	88
3.7.2 SiO <sub>2</sub> redistribution during fluid flow	89
3.8 Conclusions	91
3.8.1 Problems with quantifying time-integrated fluid fluxes	92
3.8.2 Implications for how fluids migrate through shear zones	92

***Chapter Four: The infiltration of surface-derived fluids into middle crustal shear zones in the northern Arunta Inlier.***

4.1 Introduction	93
4.2 Geological setting	94
4.2.1 Host rocks	95
4.2.1.1 Weldon Metamorphics	95
4.2.1.2 Mount Airy Orthogneiss	96
4.2.1.3 Napperby Gneiss	96
4.3 Sample collection	97
4.4 O and H isotope results	97
4.4.1 Yalbadjandi Shear Zone	97
4.4.2 Orthogneiss-hosted shear zones, SE Anmatjira Range	98
4.4.3 Napperby Gneiss-hosted shear zones	100
4.4.4 Blue Bush Swamp Shear Zone	102
4.5 Temperature of shearing	103
4.5.1 Shearing characteristics	106
4.6 Fluid-rock interaction	107
4.6.1 Blue Bush Swamp Shear Zone	109
4.7 Fluid composition	109
4.7.1 Oxygen isotopes	109
4.7.2 Hydrogen isotopes	111
4.8 Fluid origin	112
4.9 Characteristics of fluid flow	113
4.9.1 Yalbadjandi Shear Zone	113
4.9.2 Blue Bush Swamp Shear Zone	113
4.9.3 Napperby Gneiss-hosted shear zones	113
4.10 Formation waters in the middle crust	114
4.11 Conclusions	115

**Chapter Five: A new perspective on the timing of shearing in the Northern Arunta Inlier using Rb-Sr and  $^{40}\text{Ar}/^{39}\text{Ar}$  dating.**

5.1 Introduction	117
5.2 Geological setting	118
5.3 Sample collection and petrography	120
5.3.1 Yalbadjandi Shear Zone	120
5.3.2 Blue Bush Swamp Shear Zone	121
5.3.3 Napperby Gneiss-hosted shear zones	122
5.4 Dating	123
5.4.1 Rb-Sr results	123
5.4.2 $^{40}\text{Ar}/^{39}\text{Ar}$ results	123
5.5 Interpretation of age data	126
5.6 Tectonic synthesis	128
5.6.1 Stratigraphic and geochronological constraints	128
5.6.2 Structural constraints	131
5.6.3 Shear Zone development through time	131
5.6.4 Fluid flow during Alice Springs age shearing	133
5.7 Conclusions	133

**Chapter Six: Characteristics of fluid flow in the Redbank High Strain Zone.**

6.1 Introduction	135
6.2 Geological setting	136
6.2.1 Host rocks	138
6.2.2 Mylonite zones	139
6.3 Sample collection	143
6.4 Petrography	143
6.4.1 Quartzofeldspathic mylonite zones	143
6.4.1.1 Brumby Bore	143
6.4.1.2 Hamilton Downs	147
6.4.1.3 Ilyabba Dam	154
6.4.1.4 Supplejack Dam	155
6.4.2 Quartz-epidote mylonites	156
6.4.2.1 Cataclasis and shearing at Mount Forster	156
6.4.3 Mafic mylonites at Mount Forster	157
6.4.4 Littlers Yard shear zones	160
6.4.4.1 Ellery Granitic Complex migmatite gneiss	160
6.4.4.2 Protomylonite	160
6.4.4.3 Mylonite	161
6.4.4.4 Ultramylonite	162
6.4.5 Shearing characteristics	162
6.4.5.1 Quartz-epidote mylonites	164
6.4.5.2 Mafic mylonites	165
6.4.5.3 Littlers Yard	165
6.5 Stable isotope geochemistry	166
6.5.1 Quartzofeldspathic mylonite zones	167
6.5.2 Quartz-epidote mylonites	168
6.5.3 Mafic mylonites	169

6.5.4 Hydrogen isotopes	169
6.5.5 Littlers Yard shear zones	170
6.6 Discussion	171
6.6.1 Fluid flow in the Redbank High Strain Zone	173
6.7 Conclusions	174

**Chapter Seven: Excess argon in reactivated mylonites of the Redbank High Strain Zone: Implications for fluid flow during shearing.**

7.1 Introduction	175
7.2 Tectonic framework	179
7.3 Geology of the Redbank High Strain Zone	181
7.4 Sample selection and description	182
7.4.1 CR98BB235 Granitic protomylonite	183
7.4.2 CR98BB245 Mica-rich quartzofeldspathic mylonite	184
7.4.3 CR98BB246 Granitic protomylonite	184
7.4.4 CR98BB269 Granodioritic mylonite	185
7.4.5 CR98BB546 Granodioritic protomylonite-gneiss	185
7.4.6 CR98BB342 Quartzofeldspathic mylonite	186
7.4.7 Discussion	186
7.5 Results	187
7.5.1 Step-heating analyses	187
7.5.2 Laser <i>in situ</i> analyses	188
7.5.2.1 Hornblende porphyroclasts	188
7.5.2.2 Biotite porphyroclasts	189
7.5.2.3 Biotite matrix	193
7.6 Interpretation of data	194
7.6.1 Hornblende porphyroclasts	194
7.6.2 Biotite porphyroclasts	194
7.6.3 Biotite matrix	194
7.7 Excess argon contamination	195
7.8 Implications for fluid flow during shearing	196
7.9 Conclusions	197

**Chapter Eight: The role of shear zones in crustal fluid flow.**

8.1 Introduction	199
8.2 Characteristics of shearing during the Alice Springs Orogeny	200
8.2.1 Geochronology	200
8.2.3 Conditions of shearing	202
8.2.2 Fluid-rock interaction	203
8.3 Central Australian continental reworking: a failed rift?	204
8.4 Shear zone hydration: implications for middle-crustal fluid recycling	205
8.5 Further work	207
<b>References</b>	209

# CHAPTER ONE

## THE ROLE OF FLUIDS IN CRUSTAL REWORKING

### **Abstract**

Orogenic belts record crust-forming and crustal-reworking processes occurring at continental edges and within continental interiors. Crustal reworking, including deformation and recrystallisation, facilitate chemical transport at variable scales throughout the crust and provide a mechanism for geochemical recycling and redistribution. Deformation and recrystallisation in crustal reworking are enhanced by the presence of fluids. This study investigates fluid flow during crustal reworking within shear zones, using examples from the Arunta Inlier in central Australia. The research aims to identify what and how fluids were moved through the middle crust during shearing events, specifically in continental interiors where available fluid sources were reduced by the absence of a devolatilizing hydrous slab. In addition, the research aims to document how fluids contribute to the evolution of shear zones in association with deformation in order to understand their role during crustal reworking. Using field and petrological observations, mineral compositions, whole rock geochemistry and O, H, Rb-Sr and  $^{40}\text{Ar}/^{39}\text{Ar}$  isotope ratios, the characteristics of fluid flow are investigated through the identification of: 1) fluid flow pathways; 2) volumes and directions of fluid flow; 3) sources of fluids; 4) timing of fluid infiltration; 5) geochemical effects of fluid-rock interaction and; 6) mechanisms of fluid infiltration.

### **1.1 INTRODUCTION**

The interpretation of metamorphic and deformation processes in the crust provides an opportunity to describe how the continents have evolved, leading to an understanding of the history of the Earth. This history is preserved in part within ancient metamorphic terrains, through the superimposition of fabrics, and the chemical and physical characteristics of minerals (Best, 1982), as well as through crustal and mantle anisotropies (Silver, 1996). The tectonic history of the crust intimately involves processes of fluid flow, as fluids are known to be fundamental in thermal, chemical and mechanical processes (Best, 1982; Yardley, 1989; Bowman *et al.*, 1994), particularly the redistribution of matter and the transfer of heat. Therefore, an understanding of the role of fluids in different geological processes enables a more comprehensive interpretation of the physical and chemical record of rocks.

#### **1.1.1 Fluids within the crust**

Fluids are abundant throughout the lithosphere, as surface waters (ocean, meteoric and formation), mantle fluids, crustal fluids (metamorphic and magmatic) and as geothermal fluids, that are both meteoric and crustal in origin. There is evidence of large-scale fluid circulation throughout the crust (Fyfe *et al.*, 1979; Kerrich and Hyndman, 1986; Rumble,

1994; Hoefs, 1997). Processes involved in this large-scale fluid flow may include; geothermal convection (Etheridge *et al.*, 1983), subduction of hydrous slabs at convergent margins (eg. Jambon and Zimmerman, 1990; Bebout and Barton, 1993; Becker *et al.*, 2000), and fluid-rock interaction in deep contractional and extensional fault zones (e.g. McCaig *et al.*, 1990; Koons and Craw, 1991; Upton *et al.*, 1995; Barker *et al.*, 2000; Manatschal *et al.*, 2000). The movement of large volumes of fluid throughout the crust is constrained by rock permeability (Ferry, 1994; Rumble, 1994; Henderson and McCaig, 1996). Thus, as fluids are intimately involved in the processes that create permeability, they play a significant role in the development of fluid flow pathways throughout the crust (Gueguen *et al.*, 1991; Wintsch *et al.*, 1995).

Faults and shear zones are important fluid flow pathways as they represent sites of high transient permeability within the lithosphere. In the brittle upper crust, under conditions of high pore fluid pressures, rocks deform predominantly by instantaneous fracturing, frictional sliding and cataclasis (Fig. 1.1) and, as such, can host substantial volumes of fluid (Sibson, *et al.*, 1975; Sibson, 1990). Shear zones represent coherent, narrow, planar zones of rock where displacement occurs over long periods of time by ductile (predominantly crystal plastic) deformation. Ductile, viscous creep mechanisms operate under nonhydrostatic conditions at temperatures above  $\sim 300^{\circ}\text{C}$  (Best, 1982; Passchier and Trouw, 1996) and become dominant in rocks at  $\sim 10$  kilometres depth, below the brittle-ductile transition (Fig. 1.1). Thus, fluid flow through shear zones is likely to involve migration along grain boundaries during mass-transfer and metamorphic reactions (Wintsch *et al.*, 1995).

However, brittle structures can occur within ductile shear zones (Henderson and McCaig, 1996) and ductile deformation may occur at low temperatures in fluid-dominated systems (van Staal *et al.*, 2001). Shear zones that underwent both brittle and crystal-plastic deformation occur at the brittle-ductile transition (Fig. 1.1), typically at temperatures of  $250\text{-}350^{\circ}\text{C}$  (Snoke and Tullis, 1998). The brittle-ductile transition separates the brittle upper crust, from the essentially aseismic lower crust (Schmid and Handy, 1991). Thus the location of the brittle-ductile transition is dependant on mechanical and chemical properties of the rocks and thus may be influenced by the presence of fluids (Imber *et al.*, 1997; Stewart *et al.*, 2000; Holdsworth *et al.*, 2001). The evaluation of the fluid flow pathways and the mode of fluid transfer through the crust are, therefore, invaluable in the overall understanding of fluid flow. This thesis investigates whether shear zones can act as potential fluid flow pathways driving fluid circulation throughout the middle crust.

## 1.2 SHEAR ZONES REWORKING THE MIDDLE CRUST

In many multiply deformed metamorphic provinces, shear zones commonly preserve the best evidence of late- or post-regional metamorphic events. This is because shear zones often show mineral growth and fabric development that post-dates regional metamorphism. The scale of movement and reworking that can occur along these narrow structures in the middle crust is variable (Ramsay, 1980; Knipe, 1989). On a large scale, the juxtaposition of crustal blocks with different tectono-metamorphic histories can link the upper and middle crust, also possibly connecting to fault systems at the Earth's surface (Ramsay, 1980). On a grain-scale deformation can stimulate mineral reactions driving metamorphism (White *et al.*, 1980; Wintsch *et al.*, 1995). As noted by many authors, the formation and role of shear zones in reworking the middle crust envelopes several mutually reinforcing processes, including deformation, fluid flow and metamorphic reactions (White *et al.*, 1980; Knipe, 1989; Ferry, 1994; Rumble, 1994; McCaig, 1997). As the development of shear zones depends on the rheological and tectonic environment, shearing may occur along reactivated pre-existing structures, either faults or shear zones, or along other planar heterogeneities, either lithological or structural, within the crust (Holdsworth *et al.*, 1997). Alternatively, shear zones can develop from random cracking within homogeneous rock (Ramsey, 1980). Within brittle-ductile shear zones, the brittle and ductile deformation histories can occur at different times during reworking (Passchier and Trouw, 1996). Once developed, the interplay between deformation, fluid flow and metamorphic reactions within shear zone systems enhances their permeability creating important fluid conduits through otherwise impermeable lithologies in the middle crust (Ferry, 1994; Rumble, 1994; McCaig, 1997).

Remembering that at an individual grain-scale deformation occurs by a variety of processes (Knipe, 1989), changes in rheology and the presence of fluid can effect the operative deformation mechanisms within a shear zone at any particular time. Thus during an extended period of shearing, deformation mechanisms may change from brittle to ductile through reaction-softening and fluid-assisted diffusional creep (Stewart *et al.*, 2000) or from ductile to brittle due to increased pore fluid pressures (Henderson and McCaig, 1996). The commonly multi-faceted nature of deformation and fluid flow regimes within shear zones preserves the reworking and exhumation history of the middle crust, and may indicate the conditions of reworking and the extent of material transfer through structural and geochemical analysis.

### 1.2.1 Shear zones as PTt indicators

The changes in pressure and temperature associated with exhumation of the middle crust during orogenic events are readily preserved as changes in mineralogy and chemistry (Dipple and Ferry, 1992a) and microstructures (Knipe, 1980) within shear zones. The combination of these features facilitates the construction of PTt (pressure-temperature-time) paths for the uplift of metamorphic terrains and aids the understanding of regional tectonic histories within multiply-deformed metamorphic blocks.

### 1.2.2 Shear zones as conduits for fluid flow

In the middle crust, shear zones typically contain assemblages that are more hydrous than their wall rocks, suggesting that they hosted substantial fluid flow (Dipple *et al.*, 1990; Dipple and Ferry, 1992a). The resulting material transport can be both upwards and downward within the crust (Passchier and Trouw, 1996).

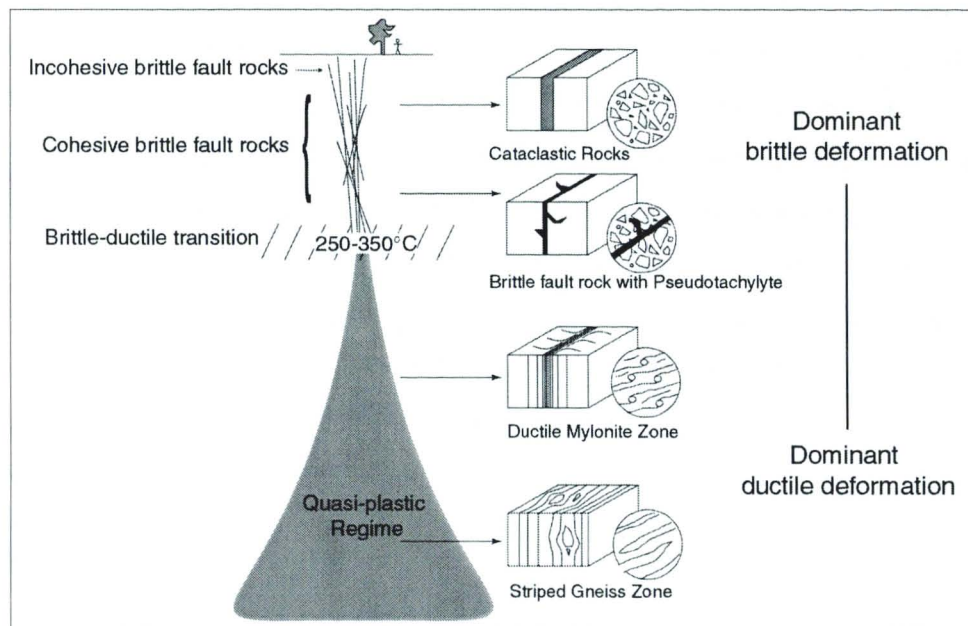


**Figure 1.1.** Schematic representation of main fault rock styles within major shear zones and associated fault rocks with increasing depth and metamorphic grade after Passchier and Trouw (1996).

Infiltrating fluids commonly cause major changes in rock chemistry via metasomatism and the re-equilibration of radiogenic and stable isotopes with respect to the wall rock composition (Beach, 1980; Dipple *et al.*, 1990; McCaig, 1997; Cartwright and Buick, 1999). Such changes are useful in interpreting tectonic processes, fluid budgets, fluid sources, the direction of fluid flow, and the timing of fluid movements within shear zones during reworking. Networks of shear zones throughout the crust are likely to be sufficiently permeable to transport fluids responsible for the re-hydration of higher-grade metamorphic rocks, in the middle and deep crust (Dipple and Ferry, 1992a) and may also be connected to the surface (Cartwright and Buick, 1999).

### **1.2.3. Hydration of middle crustal shear zones – what fluid source?**

The hydration and geochemical changes that occur in shear zones require the infiltration of large volumes of fluids (O'Hara, 1988; Selverstone *et al.*, 1991; Streit and Cox, 1998; Cartwright and Buick, 1999). As shearing commonly occurs at lower temperatures than the peak of regional metamorphism, either during retrogression or later lower-temperature metamorphic events, it is unlikely that dehydration of hydrous minerals within the wall rock assemblages would occur to any significant extent. In addition, within high-grade granitic or gneissic terrains, the lack of free water within the rock requires that fluid sources are likely to be great distances (>10 km) from the shear zones (Cartwright and Buick, 1999). Therefore, the source of the fluids required for hydration of the middle crust is unlikely to be local and this raises the question of where the fluid comes from.

As most retrogression reactions in metamorphic rocks are caused by the influx of fluid they will change the oxygen and hydrogen isotopic composition of the rock (Bowman and Willett, 1991; Jenkin *et al.*, 1994). Fluid infiltration will cause isotopic exchange between the rock and the fluid (Hoefs, 1997). In fluid-dominated systems the stable isotope values will tend to reflect those of the infiltrating fluids (Bowman *et al.*, 1994). As metamorphic, igneous and sedimentary rocks as well as magmatic, metamorphic and meteoric/formation waters can be distinguished on the basis of variation in  $\delta^{18}\text{O}$  and  $\delta\text{D}$  values (Fig. 1.2), stable isotope geochemistry of sheared rocks can identify the sources of fluids that infiltrated them during shearing (eg. McCaig, 1988; Dipple and Ferry, 1992b; McCaig *et al.*, 1990; Morrison, 1994; McCaig *et al.*, 1995; Cartwright and Buick, 1999; Barker *et al.*, 2000; Satir and Taubald, 2001). The extent of isotopic equilibration during fluid-rock interaction depends on: i) the rate of fluid infiltration; ii) the permeability and porosity of the rock; iii) the rate of isotope exchange; and iv) the mass ratio of the isotope in the rock and fluid (Bowman and Willett, 1991; Bowman *et al.*, 1994; McCaig, 1997). Several of these parameters are themselves governed by external factors, such as temperature, rock composition and deformation (Bowman and Willett, 1991).

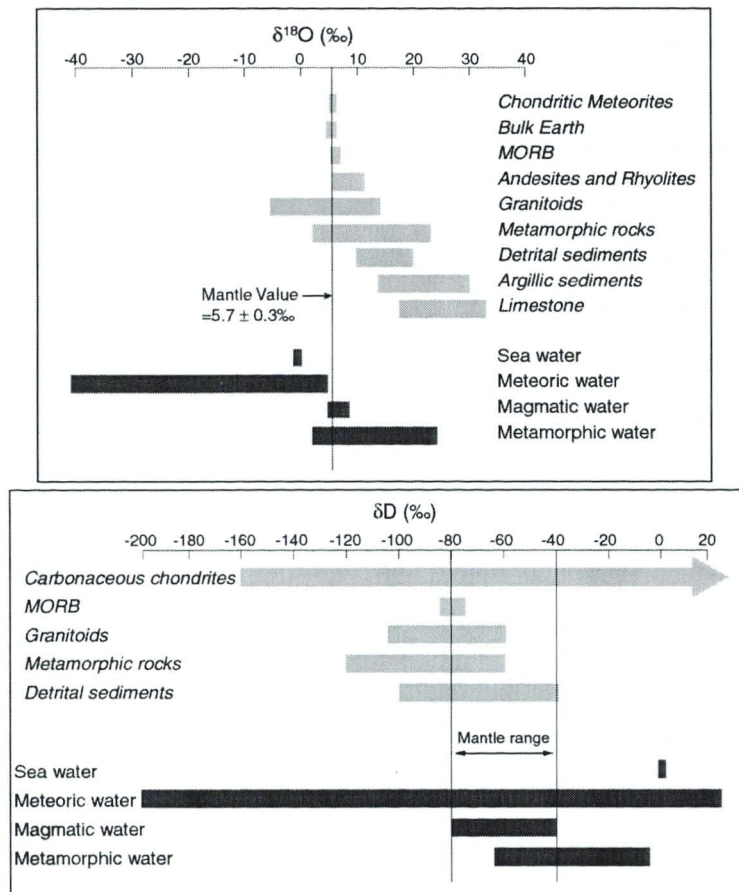


Figure 1.2. Ranges of  $\delta^{18}\text{O}$  and  $\delta\text{D}$  values from natural reservoirs, after Rollinson (1993) and Hoefs (1997).

*al.*, 1994; Cartwright and Oliver, 1994) and, although they are large contributors to the fluid budget within the middle crust, are typically absent during periods of low to medium-grade tectonic reworking. For surface reservoirs to be significant in middle crustal hydration, fluids need to move downwards into the ductile crust. As porosity and permeability in rocks is rapidly closed where fluid pressures are less than  $\sigma_3$  hydraulic head is not sustained and fluid flow is driven upwards through buoyancy. Thus downward fluid percolation should be mechanically constrained to the upper brittle crust, where closing and healing of fractures and porosity is slow. Examples from the Southern Alps, New Zealand and the Himalayas, suggest that large hydraulic heads created by elevated topography may drive fluids down steep thrust zones into mylonite zones at or near the brittle-ductile transition (Koons and Craw, 1991; Chamberlain *et al.*, 1995; Upton *et al.*, 1995). The existence of surface-derived fluids within ductile shear zones may also be explained by emplacement of water-rich sedimentary thrust sheets at depth (Lobato *et al.*, 1983; Selverstone *et al.*, 1991) and seismic pumping (McCaig, 1988; Cartwright and Buick, 1999). In addition, surface-derived fluid may infiltrate ductile shear zones during transient periods of brittle deformation and possibly relate to the displacement of the brittle-ductile transition downwards in shear zones.

Possible fluid sources include crystallising igneous rocks, the mantle, the surface and deep-seated metamorphic rocks (eg. Lobato *et al.*, 1983; McCaig, 1988; McCaig *et al.*, 1990; Selverstone *et al.*, 1991; Morrison, 1994; Upton *et al.*, 1995; Streit and Cox, 1998; Cartwright and Buick, 1999; Read and Cartwright, 2000).

Crystallising igneous rocks typically promote fluid flow during periods of high-temperature contact metamorphism (Cartwright and Valley, 1992; Buick *et al.*, 1994; Upton *et al.*, 1995; Streit and Cox, 1998; Cartwright and Buick, 1999; Read and Cartwright, 2000).

### **1.2.4 Timing of fluid flow and deformation**

In addition to the conditions of deformation and the source of fluids, analysis of the timing of fluid infiltration is necessary to understand the role of crustal fluid flow within the tectonic evolution of orogenic belts. The ages of minerals produced by metamorphic reactions that are driven by fluid infiltration can provide the age of the fluid flow (Ferry, 1994). Ionic diffusion rates are temperature sensitive and thus the movement of radiogenic isotopes through minerals can be dramatically effected by changes in temperature (Faure, 1986). This sensitivity of radioactive isotopes to temperature is the key to dating thermal events in metamorphic minerals. However, as illustrated by excess argon contamination within high-pressure rocks of the European Alps, fluids can play an important role in the distribution of isotopes during multiple metamorphic events (Arnaud and Kelley, 1995). Therefore, high-resolution dating techniques are necessary in the accurate assessment of fluid-dominated shear zone assemblages, as discussed in Chapter Seven.

## **1.3 RESEARCH AIMS**

Fluid flow is an important mechanism for crustal reworking, both mechanically during fluid-driven deformation processes, and chemically, as mass transfer of material occurs throughout the crust. As discussed above, the source, significance and mechanics of fluid flow throughout the crust are the focus of much research due to the recognition of the importance of fluid flow in the chemical and mechanical evolution of continental crust. This research aims to investigate the role of shear zones as fluid flow pathways through the middle crust. Geochemical and petrological techniques are used to distinguish between the competing mechanisms controlling fluid-rock interaction in order to illustrate the complexity of the coupling between fluid-driven deformation and geochemical alteration within shear zones. In addition, geochronological techniques are used to further the local debate over the extent and significance of the Devonian Alice Springs Orogeny within the Arunta Inlier by providing a more complete tectonic framework for shearing and fluid flow.

## **1.4 METHODOLOGY**

### **1.4.1 Suitability of study area**

The Arunta Inlier was selected for this study for four reasons.

- An extensive network of NW-SE oriented shear zones and faults cut 200,000km<sup>2</sup> of exposed Proterozoic polymetamorphic terrains (Fig. 1.3).

- A large number of the shear zones cut granitic terrains in which the homogenous nature of the host rocks provide an excellent opportunity to study chemical changes associated with fluid-rock interaction within the shear zones.
- A range of different sized shear zones, from microshears to crustal-scale features such as the Redbank High Strain Zone, provide an opportunity to study fluid-rock interaction at several scales.
- A variation in crustal depth of the shear zones, provides the opportunity to study ductile and brittle-ductile shear regimes.

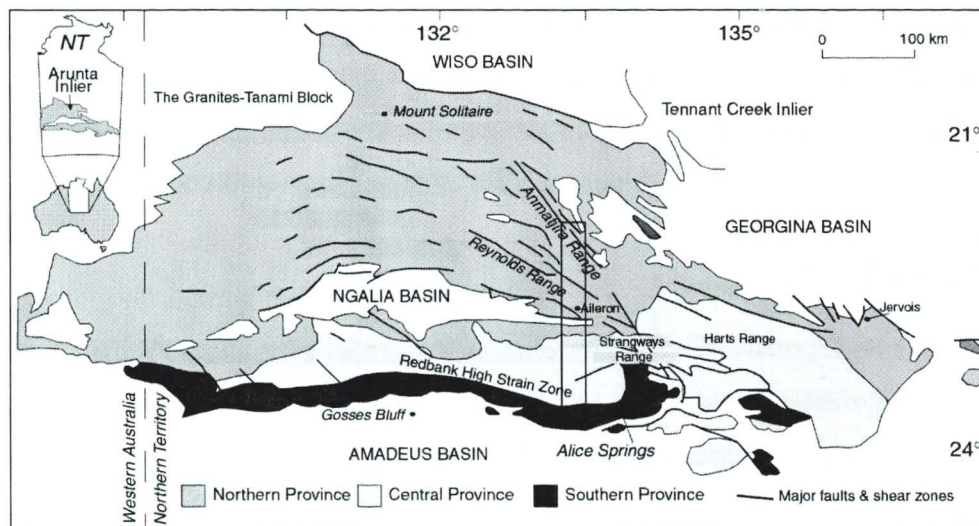


Figure 1.3. The Arunta Inlier, showing the tectonic provinces, major faults and shear zones and the surrounding Neoproterozoic basins. The rectangle indicates the location of the collection traverse across the central Arunta Inlier

### 1.4.2 Arunta Inlier sampling transect

Fieldwork was undertaken over a total of 13 weeks in central Australia between 1997 and 2000 in order to observe and record characteristics of shearing and fluid-rock interaction within poly-deformed high-grade terrains and to collect geochemical samples. Areas of investigation and sample collection include i) the SE Anmatjira Range, ii) the SE Reynolds Range, iii) the Wigley Zone of the Southern Province and iv) the eastern Redbank High Strain Zone (Fig 1.3). As the structural characteristics of the Arunta Inlier strike dominantly E-W the areas chosen for investigation form a traverse across the centre of the Arunta Inlier, representing a cross-section through the major structures (Fig. 1.3). In light of the lack of exposure within the flat lying areas of central Australia, the study leaves substantial sections unexplored, but structural interpretations of the northern central province indicate the dominant structural trends continue across the Arunta (Collins and Teyssier, 1989). The geology of these areas is discussed further in Chapter Two. Shear zones chosen for sampling include 100-500m wide, diffuse shear zones offsetting

lithological boundaries (Yalbadjandi Shear Zone, Redbank High Strain Zone) and smaller (5-100m wide) shear zones within granitic gneisses and paragneisses. Sampling of the shear zones was primarily carried out along transects oriented perpendicular to the mylonite foliation and shear zone boundaries. Samples were collected at metre-wide intervals, and/or at lithological changes in order to detect geochemical changes across the shear zones. Sets of samples from the shear zones were then thin-sectioned and prepared for geochemical analysis.

### **1.4.3 Analytical techniques**

The geochemical samples were crushed in a tungsten carbide mill that was cleaned with ethanol and quartz between each sample. Fractions of the samples were crushed to powder for whole rock analysis or dry sieved for mineral separates. Conventional magnetic separation, heavy liquid techniques and hand picking were used to obtain pure mineral separates.

#### *1.4.3.1 Oxygen isotopes*

Oxygen isotope ratios of silicate mineral separates and whole rock powders were analysed at Monash University, following the method of Clayton and Mayeda (1963), but using  $\text{ClF}_3$  as the oxidising reagent. The silicate minerals were separated by a combination of heavy liquid, magnetic separation and hand picking. Samples of 10mg heated at 500°C for 8 hours were converted to  $\text{CO}_2$  and isotope ratios were measured on the Finnigan MAT 252 mass spectrometer. Internal standards, BHQ and NBS-28, were run with the samples and yielded values within  $\pm 0.2\%$  of their expected values. The long-term average  $\delta^{18}\text{O}$  value of the standard quartz sand, BHQ, at Monash University, was  $10.44 \pm 0.19\%$  ( $1\sigma$ ) and NBS28 was  $9.55 \pm 0.18\%$  ( $1\sigma$ ).

Fifteen samples were analysed at the University of Cape Town (UCT), also following the method of Clayton and Mayeda (1963) and using  $\text{ClF}_3$  as the oxidising reagent. Samples were degassed under vacuum at 200°C for 2 hours prior to addition of  $\text{ClF}_3$ . The samples were then run overnight at 550°C. Sample sizes was generally sufficient to yield  $>100\text{mmol}$  of  $\text{CO}_2$ . Isotope ratios were measured on a Finnigan MAT 252 mass spectrometer in the Department of Archaeology (UCT). Two splits of the standard NBS-28 were run with a batch of eight samples. The NBS data was used to convert the raw data to the V-SMOW scale assuming an  $\delta^{18}\text{O}$  value for NBS-28 of 9.64%. The error on the values is measured by the variation in Murchison quartz (MQ) owing to the cessation of availability of NBS-28 and was  $\pm 0.16\%$ .

Oxygen isotope data are reported in the familiar  $\delta$  notation where  $\delta^{18}\text{O}$  is  $(R_{\text{sample}}/R_{\text{standard}}^{-1}) * 10^3$  and R is the ratio of  $^{18}\text{O}/^{16}\text{O}$ . The  $\delta^{18}\text{O}$  value is given in ‰ relative to V-SMOW.

#### 1.4.3.2 Hydrogen isotopes

Hydrogen isotopes were analysed at Monash University, by placing 200-300mg of whole rock or mineral separate into glass tubes that were melted under vacuum with an oxyacetylene torch to release all the volatiles from the sample. The water vapour was collected by freezing the gas into a glass tube and then defrosting it into liquid form. The water was then injected into a Finnigan MAT H/Device where reduction to  $\text{H}_2$  was achieved by reaction with chromium at  $850^\circ\text{C}$ . The results are given in ‰ relative to V-SMOW. Duplicate analyses indicate the error of this technique was  $\pm 5\%$ .

#### 1.4.3.3 Whole rock major and trace element geochemistry

Most of the whole rock major and trace element concentrations were analysed using X-ray fluorescence spectrometry at Melbourne University. Element compositions were determined on a Siemens SRS3000 sequential X-ray fluorescence spectrometer capable of measuring 38 elements to a 5ppm detection limit. Major and trace elements were measured from fused lithium metaborate glass disks. Fusion to  $1000^\circ\text{C}$  in platinum-gold crucibles was conducted in a Broadway furnace. Samples were weighed, loss on ignition calculated and remelted before final casting in graphite moulds. Standards were analysed concurrently with the sample runs. Samples from the Yalbadjandi Shear Zone transects were analysed at the University of New South Wales following similar methods.

#### 1.4.3.4 Mineral chemistry

Mineral chemistries were obtained by electron dispersion spectrometry (EDS) on the ARL SEMQ 2 microprobe at Monash University. Analyses were made of garnet, biotite, chlorite, epidote, muscovite, plagioclase, K-feldspar, and cordierite.

#### 1.4.3.5 Rb-Sr age determination analysis

Rb-Sr isotope analyses were undertaken at La Trobe University following methods described in Waight *et al.* (1997), with the exception of Sr purification which was done using Eichrom<sup>TM</sup> Sr.spec resin (Pin *et al.*, 1994). Mineral separates of biotite and muscovite were prepared at Monash University using conventional heavy liquid and magnetic techniques. Isotopic analyses were made on a Finnigan-MAT 262 multicollector mass spectrometer at La Trobe University.  $^{87}\text{Sr}/^{86}\text{Sr}$  ratios were reported relative to SRM987 = 0.71023. SRM607 K-feldspar gave:  $523.5 \pm 2.7$  ppm Rb,  $65.7 \pm 0.4$  ppm Sr,  $^{87}\text{Rb}/^{86}\text{Sr} = 24.128 \pm 0.051$ ,  $^{87}\text{Sr}/^{86}\text{Sr} = 1.20061 \pm 0.00062$  (all errors  $2\sigma$ ). For external

precision of isochron calculations, the following  $2\sigma$  input errors were used:  $\pm 0.5\%$  ( $^{87}\text{Rb}/^{86}\text{Sr}$ );  $\pm 0.01\%$  ( $^{87}\text{Sr}/^{86}\text{Sr}$ ).

#### 1.4.3.6 $^{40}\text{Ar}/^{39}\text{Ar}$ analysis by furnace step heating

$^{40}\text{Ar}/^{39}\text{Ar}$  step heating analyses were determined at the Australian National University (ANU) following the methods of McDougall and Harrison (1988). Mineral separates of biotite and muscovite were prepared at Monash University. The separates were purified at the ANU, using conventional magnetic separation and heavy liquid techniques. The resulting separates were mostly of  $\sim 99\%$  or higher purity. Approximately 5mg of mineral separate was wrapped in aluminium packets and placed into aluminium irradiation canister together with interspersed aliquots of the flux monitor GA1550 (Age = 98.8 Ma). Packets containing degassed potassium glass were placed at either end of the canister to monitor the  $^{40}\text{Ar}$  production from potassium. The irradiation canister was irradiated for 504 hours in position X34 of the ANSTO HIFAR reactor, Lucas Heights, New South Wales. The canister, which was lined with 0.2mm Cd to absorb thermal neutrons, was inverted three times during irradiation, which reduced neutron flux gradients to  $< 2\%$  along the length of the canister. After irradiation, the samples were removed from their packaging and 0.3 – 1.0 mg was loaded into tin foil packets for analysis. The samples were individually dropped into a Tantalum resistance furnace and heated to progressively higher temperatures, with temperatures maintained for fifteen minutes per step.  $^{40}\text{Ar}/^{39}\text{Ar}$  step-heating analyses were carried out on a VG3600 mass spectrometer using a Daly detector at the ANU. Mass discrimination was monitored by analyses of standard air volumes.

#### 1.4.3.7 $^{40}\text{Ar}/^{39}\text{Ar}$ laser probe analysis

Approximately 10 rock chips containing biotite and hornblende were selected for analysis. The chips were washed gently in distilled water and acetone prior to being shipped for irradiation. The chips were wrapped in an aluminium packet and placed into an aluminium irradiation canister together with aliquots of the flux monitor GA1550 (Age = 98.8). Packets containing degassed potassium glass were placed at either end of the canister to monitor the  $^{40}\text{Ar}$  production from potassium. The irradiation canister was irradiated for 504 hours in position X34 of the ANSTO, HIFAR reactor, Lucas Heights, New South Wales, Australia. The canister, lined with 0.2 mm Cd to absorb thermal neutrons, was inverted three times during the irradiation, which reduced neutron flux gradients to  $< 2\%$  along the length of the canister. After irradiation, the samples were removed from their packaging and several chips were loaded into a copper sample holder. Laser spot analyses were carried out on the biotite and hornblende using an argon-ion laser and an external shutter. Laser ablation pits were achieved using 20ms pulse durations.  $^{40}\text{Ar}/^{39}\text{Ar}$  analyses were

carried out on a VG3600 mass spectrometer using a Daly photo-multiplier detector. Mass discrimination was monitored by analyses of standard air volumes.

Correction factors for interfering reactions were as follows:  $(^{36}\text{Ar}/^{37}\text{Ar})\text{Ca} = 3.50(\pm 0.02) \times 10^{-4}$ ;  $(^{39}\text{Ar}/^{37}\text{Ar})\text{Ca} = 7.9(\pm 0.5) \times 10^{-4}$ ;  $(^{40}\text{Ar}/^{39}\text{Ar})\text{K} = 0.049(\pm 0.005)$  (Tetley *et al.*, 1980; McDougall and Harrison, 1999). K/Ca ratios were determined from the ANU laboratory hornblende standard 77-600 and were corrected for the system blanks, mass discrimination, reactor interferences, fluence gradients and atmospheric contamination. Errors associated with the age determinations are  $1\sigma$  uncertainties and exclude errors in the J-value estimates. The error on the J-value is 0.03 %, excluding the uncertainty in the age of GA1550 (which is ca. 1%). Decay constants were those of Steiger and Jäger (1977). Plateau portions of the age spectra for the step-heating analyses were defined as comprising at least three contiguous increments, with concordant ages (ie. ages that are within  $2\sigma$  of the mean age). In addition, this segment should contain a significant proportion of the total  $^{39}\text{Ar}$ -released (McDougall and Harrison, 1988).

## 1.5 LAYOUT OF THIS THESIS

This thesis is separated into 8 Chapters. Chapter Two provides an overview of the regional geology of the Arunta Inlier, including specific information on the areas focused on in this study. Chapters Three, Four and Five are individual studies of the shear zones in the Anmatjira and Reynolds Ranges of the northern Arunta Inlier. The shear zones sampled range in size from the 300m wide Yalbadjandi Shear Zone that forms the lithological boundary between high-grade granulites and orthogneiss in the SE Anmatjira Range to metre wide phyllonite-rich zones with undetermined offsets within granitic orthogneiss in the SE Reynolds Range. Chapter Three focuses on microstructural and geochemical alteration within the shear zones in order to explore the role of fluid in the evolution of compositional zonation. Chapter Four focuses on the source of fluids that infiltrated these shear zones using oxygen and hydrogen isotope geochemistry, in order to understand the scale of fluid flow possible throughout the crust. Chapter Five defines the timing of fluid infiltration using  $^{40}\text{Ar}/^{39}\text{Ar}$  and Rb-Sr data, providing more detail in the evolution of shearing during the Alice Springs Orogeny. Chapter Six and Seven contain studies of the southern Arunta Inlier including the Redbank High Strain Zone and Wigley Zone of the Southern Province. Chapter Six discusses the role of fluids within the crustal-scale Redbank High Strain Zone and smaller shear zones in the Southern Province based on the petrological and isotopic composition of the mylonites. Chapter Seven discusses the problems of resolution in dating mylonites in polydeformed terrains via conventional

mineral separate methods and the effects of open-system fluid exchange on isotopic compositions of mylonites. The results of  $^{40}\text{Ar}/^{39}\text{Ar}$  *in situ* laser probe analysis provide a new perspective on the thermal and fluid evolution of the Redbank High Strain Zone. The final discussion in Chapter Eight reviews the role of fluids in shear zones illustrated from the central Australian samples and discusses their implications for the understanding of fluid flow in crustal reworking.

## 1.6 NOMENCLATURE AND CLASSIFICATION OF SHEAR ZONE ROCKS

The nomenclature and classification of shear zone rocks used in this thesis is outlined below.

	Random fabric	Foliated
Incohesive	<b>Fault breccia</b> visible fragments > 30% rock mass	
	<b>Fault gouge</b> Visible fragments < 30 % rock mass	
Cohesive	<b>Pseudotachylyte</b>	
	Crush breccia Fine crush breccia Crush microbreccia	fragments >0.5cm 0.1cm < fragments < 0.5cm fragments < 0.1cm
	<b>Protocataclasite</b> 10-50% matrix	<b>Protomylonite</b> 10-50% matrix
	<b>Cataclasite</b> 50-90% matrix	<b>Mylonite/phyllonite</b> 50-90% matrix
	<b>Ultracataclasite</b> 90-100% matrix	<b>Ultramylonite</b> 90-100% matrix
		<b>Blastomylonite</b>

Figure 1.4. Fault rock classification scheme from Sibson, 1977, based on field observations.

1.4, protomylonites contain 0-50% matrix, mylonites contain around 50-90% and ultramylonites contain 90-100% (Sibson, 1977). The term phyllonite is applied to mylonites that contain abundant (90%) phyllosilicates, but are not necessarily derived from sediments (Yardley, 1989).

### 1.6.2 Other terms

Porphyroclast is used to describe large relics of pre-existing grains within a mylonitic matrix, (Passchier and Trouw, 1996). Augen is used to indicate porphyroclasts and

### 1.6.1 Mylonites

The term mylonite is used in this study to describe a rock occurring within a shear zone that is foliated and commonly lineated with extensive grain size reduction through dominantly ductile (crystal-plastic) deformation processes. This definition is derived as a combination of the terminology outlined in Snoke and Tullis (1996), Wise *et al.* (1984) and Mawer (1986).

Mylonites are divided into sub-groups related to the proportion of recrystallised matrix they contain. Following the classification scheme of Sibson (1977) represented in Figure

aggregates that have become elongated (“eye-shaped”) due to diffusive mass transfer processes along the grain boundary during shearing (Yardley, 1989).

### **1.6.3 Abbreviations**

The abbreviations used in this thesis are listed in Table 1.1.

**Table 1.1. Abbreviations used in this thesis**

ab	albite	ksp	K-feldspar
act	actinolite	ky	kyanite
amp	amphibole	mu	muscovite
an	anorthite	opq	undefined opaque mineral
ap	apatite	opx	orthopyroxene
blue am	blue amphibole	pl	plagioclast
bi	biotite	px	pyroxene
cd	cordierite	qz	quartz
chl	chlorite	sil	sillimanite
cpx	clinopyroxene	ti	titanite
cz	clinozoisite	tm	tourmaline
epi	epidote	zr	zircon
fsp	feldspar	PPL	plane polarised light
gnt	garnet	XPL	X-polarised light
hbl	hornblende	wr	whole rock
il	ilmenite		

## CHAPTER TWO

### GEOLOGY OF THE ARUNTA INLIER, CENTRAL AUSTRALIA

#### 2.1 INTRODUCTION

This chapter summarises the geology of central Australia, reviewing the timing and features of orogenic activity recorded within the Arunta Inlier and surrounding basins. The characteristics of the intracratonic Devonian-Carboniferous Alice Springs Orogeny are discussed, as this event represents the last major orogenic activity in central Australia and is discussed throughout the thesis. In addition, the characteristics of the local geology of specific areas within the Arunta Inlier that were examined and sampled during this study are reviewed.

#### 2.2 REGIONAL GEOLOGY OF CENTRAL AUSTRALIA

Across the Australian continent, there are several areas where middle- to lower-crustal rocks of Proterozoic and Archaean ages are exposed as orogenic provinces (Fig. 2.1). Typically, these provinces are bounded by large basins formed during continental tectonic activity including the break-up of Rodinia (Lindsay, 1999). In central Australia, the Arunta Inlier and Musgrave Block represent exposed mid-crustal rocks separated by the large, intracratonic, Amadeus Basin and surrounded by a number of correlated intracratonic basins including the Officer, Ngalia, Georgina and Wiso Basins (Shaw and Black, 1991; Warren and Shaw, 1995). The 200,000 km<sup>2</sup> Arunta Inlier is one of the largest Proterozoic provinces in Australia, approximately the same size as New Zealand. In common with other Australian Proterozoic provinces (Granites Tanami Block, Scrimgeour and Sandiford, 1993; Tennant Creek Inlier, Black, 1984; Mount Isa Block, Wyborn *et al.*, 1988; Broken Hill Block, Hobbs *et al.*, 1984), rocks within the Arunta Inlier record multiple high-temperature, low-pressure metamorphic events and the development of crustal-scale fault and shear zones. The central Australian mid-crustal rocks were deformed and metamorphosed during several tectonic events in the Proterozoic and Palaeozoic. Typically the Proterozoic orogenies are described as contractional events with abundant felsic magmatism representing melted continental crust. The development of the Centralian Superbasin from ~800 Ma indicates that central Australia was part of an intraplate

extensional setting at the end of the Proterozoic (Lindsay, 1999). Further high-grade metamorphism and deformation synchronous with the deposition of basinal sediments at ~470 Ma (Mawby *et al.*, 1999) suggests that mid-crustal reworking was associated with basin development during extensional tectonics in the Palaeozoic.

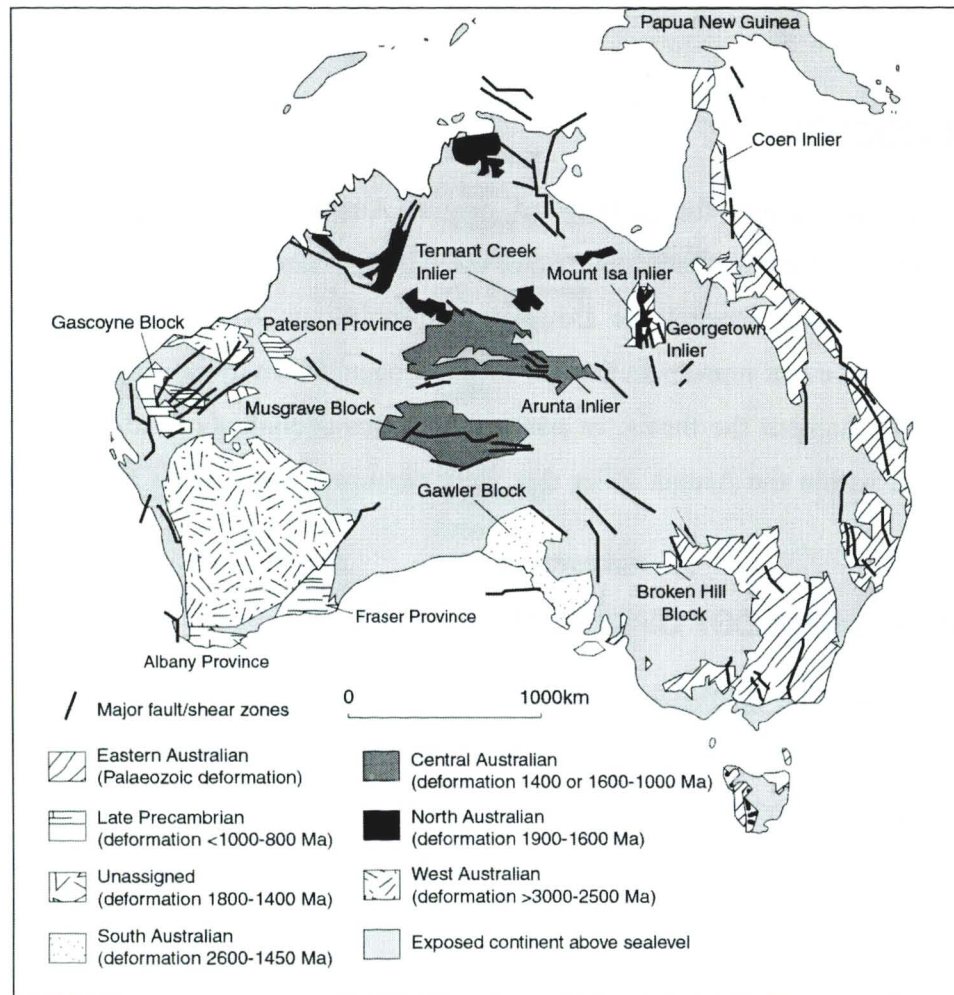


**Figure 2.1. Principle Australian orogenic provinces after Shaw and Black (1991).**

Major faults and shear zones within the Arunta Inlier, Musgrave Block and surrounding Neoproterozoic basins record episodes of crustal reworking and uplift during the Proterozoic and/or Palaeozoic (Allen and Black, 1979; Black *et al.*, 1983; Lambeck and Penny, 1984; Shaw *et al.*, 1984; Glikson, 1987; Collins and Teyssier, 1989; Goleby *et al.*, 1990; Wright *et al.*, 1990; Lambeck, 1991; Shaw and Black, 1991; Shaw *et al.*, 1992; Shaw *et al.*, 1995; Collins and Shaw, 1995; Korsch *et al.*, 1998; Scrimgeour and Close, 1999). Major periods of basement uplift in the region (including the Musgrave Block) were thought to have occurred at 1500-1400 Ma, (Shaw and Black, 1991), 560-520 Ma (Close *et al.*, 1999) and 300-400 Ma (Collins and Shaw, 1995). The youngest Paleozoic event recorded within central Australia is the Alice Springs Orogeny (400-300 Ma), which

determined the shape of the now exposed Arunta Inlier and the remnants of the Centralian Superbasin. The orientation and to a large extent kinematic behaviour of structures throughout central Australia during the Alice Springs Orogeny were contiguous with earlier shearing events, and possibly indicate that an already weakened lithosphere existed in central Australia during the Devonian-Carboniferous period. Tectonically, central Australia has been stable since the Carboniferous.

### 2.3 THE ARUNTA INLIER

The Arunta Inlier (Fig. 2.1 and 2.2) comprises exposed Proterozoic poly-deformed and metamorphosed mid-crustal rocks with some inherited detrital zircon populations indicating a crustal age of ~2500 Ma (Collins and Williams, 1995). The Inlier comprises greenschist to granulite-facies meta-sedimentary and meta-volcanic successions that have been intruded by differing generations of Proterozoic granitoids. Sediment provenance studies and interpretations of the magmatic history suggest that the Arunta Inlier is an ensialic mobile belt (Stewart *et al.*, 1984) with no recorded evidence of oceanic crust. The geochemistry of calc-alkaline to trondhjemitic granites within the southern Arunta Inlier (Zhao and McCulloch, 1995) and plate tectonic analogues to back-arc basin-style tectonics imply a plate margin setting is likely to have been present south of the Arunta Inlier at some time during the Proterozoic. It has been suggested that high-grade metamorphic events within the Arunta reflect back-arc basin processes where high-temperature metamorphism is stimulated by abundant plutonism and crustal thinning (Giles and Betts, in review). However, the observation that metamorphism was temporally unrelated to plutonism (Rubatto *et al.*, 2001 and Buick *et al.*, 1999b) within central Australia indicates that other geological processes are also likely to have contributed to orogenesis.

The Neoproterozoic Amadeus, Wiso, Ngalia and Georgina Basins unconformably overlie the Arunta Inlier and are largely undeformed except at their margins (Fig. 2.2). Correlations between the basal units indicate that these basins represent remnants of a superbasin that covered central Australia from 800 Ma (Collins and Teyssier, 1989; Walter *et al.*, 1995; Lindsay, 1999). Correlations have also been made with the basal units from the Adelaide Geosyncline, and the Officer Basin, indicating a large intracratonic setting during deposition (Webby, 1978; Walter *et al.*, 1995; Lindsay, 1999). The initiation of the superbasin as a giant sag basin at 800 Ma in central Australia coincides with the assembly and break-up of Rodinia and is thought to have developed on a peneplane surface during subsidence stimulated by deep mantle processes (Lindsay, 1999). Thus central Australia was located within a continental block from the Neoproterozoic onwards.

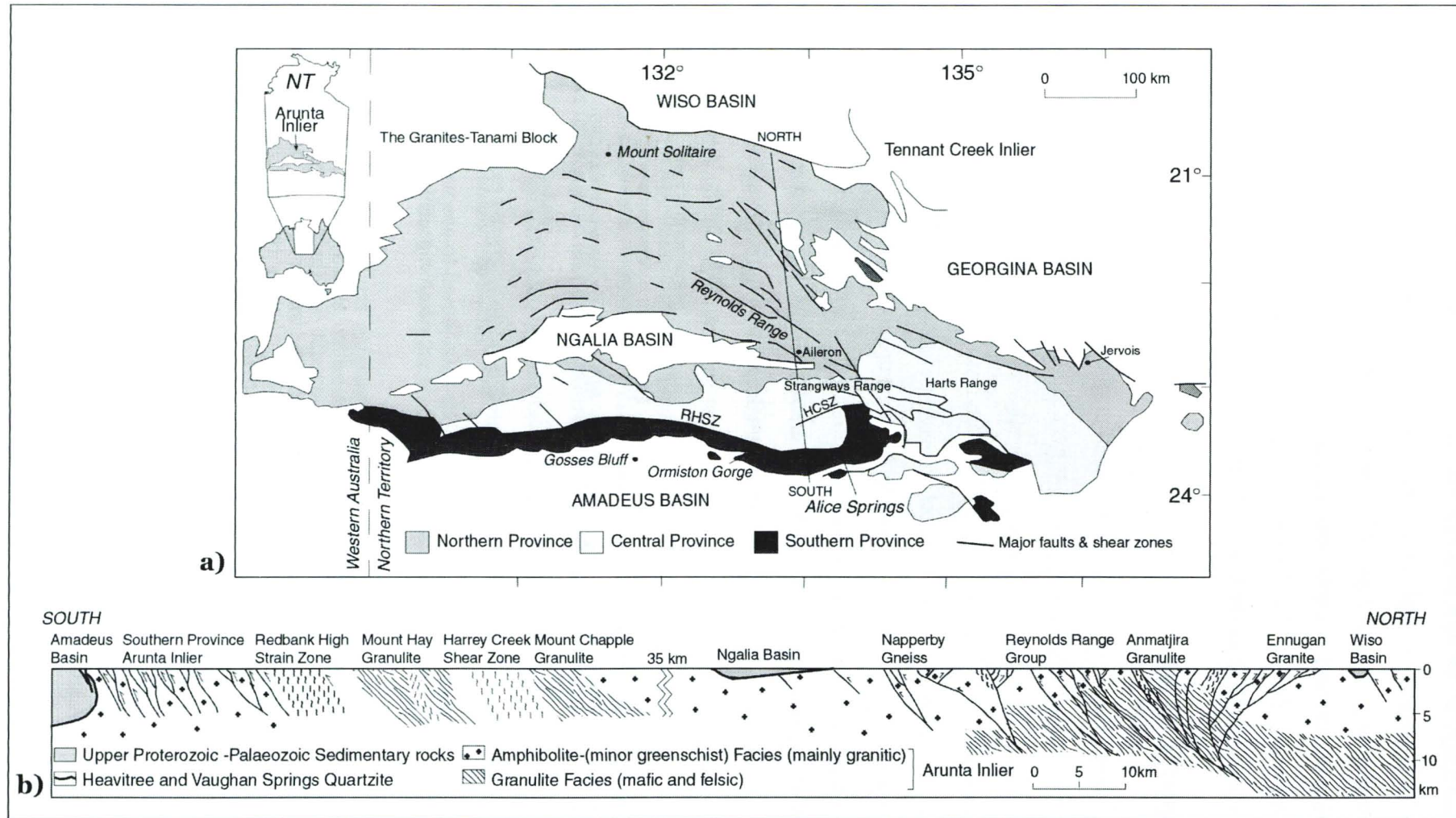


Figure 2.2. a) The Arunta Inlier, showing the tectonic provinces, major faults and shear zones and the surrounding Neoproterozoic basins (Ngalia, Amadeus, Wiso, Georgina). Abbreviations: RHSZ, Redbank High Strain Zone; HCSZ, Harry Creek Shear Zone. Showing approximate orientation of cross-section transect. b) Cross-section through the Arunta Inlier indicating the rock units and major structures, after Collins and Teysier (1989).

### **2.3.1 Rock nomenclature and divisions within the Arunta Inlier**

The Arunta Inlier is commonly divided into three provinces (Northern, Central and Southern, Fig. 2.2a), based on lithostratigraphic and structural correlations (Stewart *et al.*, 1984). The province names are now retained largely as geographical terms, due to re-evaluation of the tectonic complexities at the province boundaries, metamorphic age correlations, and structural relationships (Black and Shaw, 1992; Shaw *et al.*, 1992; Collins and Shaw 1995). The Northern Province is the largest of the three provinces and comprises greenschist- to granulite-facies paragneisses and orthogneisses. The Central Province comprises granulite-facies mafic and felsic rocks and is separated from the Southern Province, in the west, by the Redbank High Strain Zone. The Southern Province is dominated by granitic terrane with low-grade quartzite and calc-silicate cover sequences overthrusting the Amadeus Basin sediments to its south.

The rocks in the Inlier were also separated into three broad stratigraphic divisions (Divisions 1 to 3; Stewart *et al.*, 1984). Division 1 rocks occur dominantly within the Central Province and are mafic to felsic granulites of a bimodal metavolcanic origin, with interlayered meta-sediments. These rocks represent the initial sedimentation of the region. Division 2 rocks, occurring mainly within the Northern Province, are turbidite sequences that commonly contain amphibolite-facies assemblages. Division 3 rocks are platform-type deposits that comprise quartzite-shale-carbonate sequences. These rocks represent the latest period of sedimentation throughout the Inlier and unconformably overlie the other two divisions (Collins, 2000). Re-evaluation of the divisions following geochronological work produced inconsistencies and the use of the terminology is now rare. The Arunta Inlier rocks are now largely described and correlated in terms of regional metamorphic and structural events rather than by stratigraphic units. The deposition and correlation of regional units are presented on Table 2.1.

### **2.3.2 Tectonic and metamorphic history**

Multiple high-temperature, low-pressure metamorphism is prevalent throughout the Arunta Inlier (Warren 1983; Warren and Shaw, 1985; Clarke *et al.*, 1990; Norman and Clarke, 1990; Vernon *et al.*, 1990; Collins and Vernon, 1991; Dirks *et al.*, 1991; Arnold *et al.*, 1995; Vry *et al.*, 1996; Greenfield *et al.*, 1996; Miller *et al.*, 1997; Mawby *et al.*, 1999). The extent of individual tectonic events, however, remains controversial. Table 2.1 is a summary of the tectonothermal events documented from the Arunta Inlier.

### 2.3.2.1 Mount Stafford Event

The oldest metamorphism in the Arunta Inlier is known locally as D1/M1 or the Mount Stafford Event (Collins and Shaw, 1995 and references therein). It produced low-pressure (~2.5 kbar) greenschist-facies assemblages with locally developed high-temperature assemblages (Collins and Vernon 1991), N-S upright chevron folds, and an axial planar slaty cleavage of muscovite within the basement Lander Rock Beds of the Northern Province (Dirks and Wilson, 1990). High-temperature metamorphism in the Strangways Complex in the Central Province also occurred during this period (Buick *et al.*, 1999a).

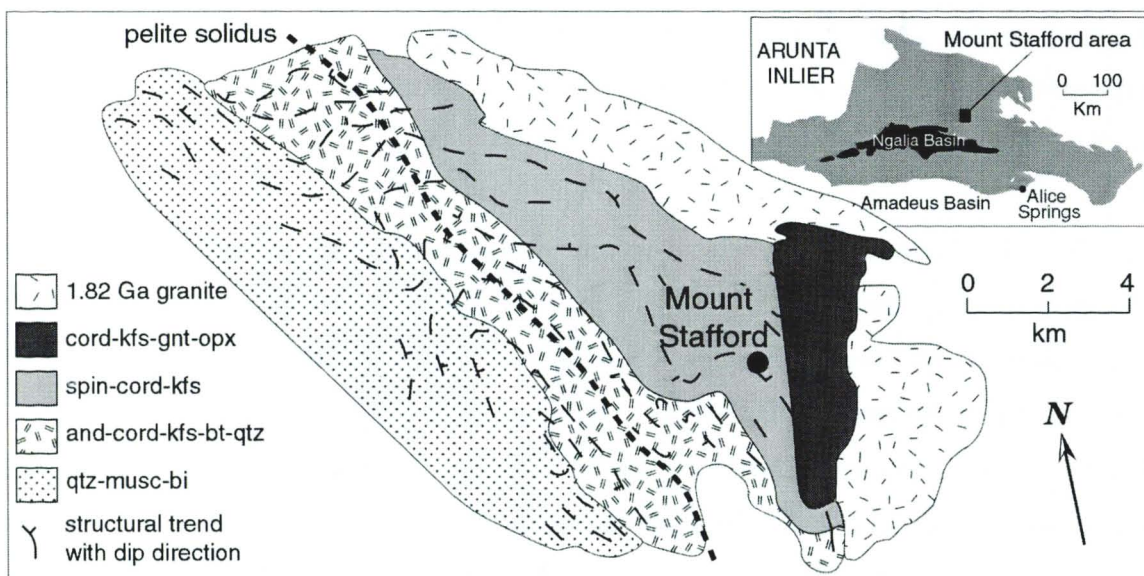


**Figure 2.3.** Metamorphic zones in the basement Lander Rock Beds, at Mount Stafford, Northern Province, after Greenfield *et al.* (1996). Bedding trends in the sediments and granites are also shown.

The high-temperature facies ( $>810^{\circ}\text{C}$  and  $2.5\pm 0.6$  kbar) in the Northern Province, reflect possible contact metamorphism in the vicinity of the Mount Stafford Granite and associated granitic rocks at 1820-1800 Ma (Greenfield *et al.*, 1996; Collins and Vernon, 1991; Vernon *et al.*, 1990). The contact aureole rocks can be divided into metamorphic zones of decreasing temperature over a distance of 10km (Fig. 2.3). D1/M1 affected only the basement sediments of the Northern Province occurring before the deposition of the cover sediments (~1800) and prior to the emplacement of voluminous felsic plutons at 1.78 Ga (Collins and Williams, 1995). An inherited detrital zircon population in basement sediments indicates that D1/M1 occurred after 1840 Ma (Vry *et al.*, 1996), and thus in the period between 1840 and ~1800 Ma.

### 2.3.2.2 Strangways Orogeny

The second tectonic event, the Strangways Orogeny, produced local HT/LP metamorphism in the Strangways Metamorphic Complex and widespread granitic magmatism over a 50

My period from 1780 Ma (Black *et al.*, 1983; Clarke *et al.*, 1990; Black and Shaw, 1992; Collins and Shaw, 1995; Buick *et al.*, 1999a). This second main period of magmatism at 1780 Ma contributed to the growth of the continental crust in the region (Foden *et al.*, 1995). However the association of metamorphism and deformation during this period remains contentious. The Strangways Orogeny is divided into early and late phases of 1780-1770 Ma and 1745-1730 Ma (Collins and Shaw, 1995) reflecting early magmatism and later deformation producing sheath-like folding and NW- to SW-directed overthrusting in the Strangways Metamorphic Complex (Collins and Shaw, 1995 after Gascombe, 1992). Recent geochronological research in the Strangways Metamorphic Complex indicates that the age of high-grade metamorphism is 1730-1715 Ma, suggesting that it may not be directly related to magmatism (Möller *et al.*, 1999). In the Northern Province, four phases of deformation produced reclined to upright and NW trending, locally isoclinal folding, associated with high-grade metamorphism. These four deformation phases are suggested by Collins *et al.* (1991) to have been coeval with granite emplacement at 1780 Ma, and reflect the early Strangways Orogeny. However, dating of zircons within the Anmatjira and Reynolds Ranges indicate inherited igneous ages of 1780 Ma and high-grade metamorphic overgrowths of 1590-1570 Ma (Rubatto *et al.*, 2001). Thus the extent of the Strangways Orogeny in the Northern Province is likely limited to magmatism, with local contact metamorphism and associated deformation.

#### 2.3.2.3 Argilke Event

Felsic magmatism, dominantly in the Southern Arunta at 1680-1650 Ma (Black and Shaw, 1992; Zhao and Bennett, 1995), has been labelled the Argilke Event (Collins and Shaw, 1995). This event may have caused extensive migmatisation and produced folding within basement gneisses of the Southern Province (Collins and Shaw, 1995). Continued magmatism is recorded to 1600 Ma (Collins *et al.*, 1995; Zhao and Bennett, 1995; Zhao and McCulloch, 1995).

#### 2.3.2.4 Chewings Orogeny

The last regional, low-pressure metamorphism of Proterozoic age occurred locally throughout the Northern, Central and Southern Provinces at 1560-1590 Ma (Black *et al.*, 1983; Collins *et al.*, 1995; Young *et al.*, 1995; Williams *et al.*, 1996; Vry *et al.*, 1996; Buick *et al.*, 1999b; Rubatto *et al.*, 2001). This event is known as the Chewings Orogeny or D2/M2 in the Northern Province. The Chewings Orogeny has been described as a deformation phase that produced N-directed overthrusting in the southern Arunta (Collins and Shaw, 1995, after Shaw *et al.*, 1984). Collins and Williams (1995) proposed that this

Table 2.1. Summary of the tectonothermal events in the Arunta Inlier (After Reed *et al.*, 1999). Sources of data and dating include Black *et al.*, 1983; Clarke *et al.*, 1996; Vernon *et al.*, 1996; Collins and Vernon, 1991; D'Arca *et al.*, 1991; Shaw and Black, 1991; Shaw *et al.*, 1991; Black and Shaw, 1992; Shaw *et al.*, 1992; Collins and Shaw, 1995; Collins and Williams, 1995; Doolan and Teyssier, 1995; Warren and Shaw, 1995; Young *et al.*, 1995; Mavly *et al.*, 1998; Miller *et al.*, 1998; Black *et al.*, 1999; Cartwright *et al.*, 1999; Collins, 2000; Rubatto *et al.*, 2001.

Age (Ma)	Nomenclature	Northern Province		Central Province			Southern Province	
		Western Arunta Mount Doreen	Reynolds-Anneke Ranges	Mount Chapple Mount Hay	Strangways Complex	Herb Range	Redbank-Wipje Zone	Chewings Zone
>1800-1840		Lander Rock Beds deposition			sedimentation ?			
>1818	Stafford Tectonic Event	Local HTLP metamorphism Felsic Magmatism (~1800 Ma)	Local HTLP metamorphism (>700°C at 3-4kbar) Felsic Magmatism (~1820 Ma)	Mafic/felsic magmatism?	Local HTMP metamorphism (850°C at 5-7kbar)			
1800		Reynolds Range Group deposition			sedimentation ?			
1780-1720	Strangways Orogeny early and late phases	Felsic Magmatism Low-mid grade metamorphism & deformation	felsic-mafic magmatism associated local HT metamorphism (700°C at 4kbar)	HTMP metamorphism (>800°C at 5-9kbar)	HTHP meta metamorphism (>800°C at 5kbar)	Felsic-mafic magmatism associated HT metamorphism	Felsic magmatism Upper-amphibolite-facies metamorphism S-deformation	
1700-1850	Aileron Event		amphibolite-facies metamorphism Felsic magmatism		felsic magmatism?	amphibolite-facies metamorphism & deformation felsic magmatism?	Felsic magmatism	Felsic magmatism
1670-1680	Argilla Tectonic Event	intermediate-mafic magmatism						
1610-1580					Manildra Metamorphic sediment deposition?	Isidra Supracrustal	Stimpsons Gap and Chewings Range sediment deposition and granitic magmatism	
1590-1570	Chewings Orogeny Weldon Tectonic Phase (D2/M2)	Volcanic felsic magmatism	HTLP Granulite-greenschist-facies metamorphism & SW-directed thrusting (750°C at 5-6kbar)	High-grade metamorphism (800°C at 7-8kbar)			Amphibolite-facies metamorphism N-directed thrusting	Amphibolite-facies metamorphism N-directed thrusting
1500-1400	Anneke Uplift Phase		shear zone development?	amphibolite-grade S-directed thrusting (RHSD)		S-directed thrusting		
1200-1100	Ormlion Event Taspoit Tectonometamorphic Event			pegmatite emplacement			Felsic-alkaline magmatism amphibolite-facies metamorphism & deformation	Felsic magmatism amphibolite-facies metamorphism & deformation
1050-900	Stuart Pass Dolerite Dyke Swarm		minor mafic dykes	N-S and E-W trending dykes	N-S and E-W trending dykes	assemblage deposition	N-S trending dolerite dykes	N-S and E-W trending dykes
-850		Onset of sedimentation of the Centralian Superbasin						
		Reactivation of Proterozoic faults in the Centralian Superbasin during extensional periods of basin formation						
470-450					granulite-facies metamorphism?	granulite to upper amphibolite facies metamorphism mafic magmatism		
450-400	Early Alice Springs Orogeny	S-directed shearing?		Greenschist-facies S-directed shearing	Amphibolite-facies metamorphism and S-directed shearing	Amphibolite-facies metamorphism and S-directed shearing	Greenschist-facies S-directed shearing	
400-300	Alice Springs Orogeny	Greenschist-facies S-directed shearing	Amphibolite-greenschist facies S-directed shearing	Greenschist-facies S-directed shearing	Amphibolite-greenschist facies S-directed shearing	Amphibolite-greenschist facies S-directed shearing	Greenschist-facies S-directed shearing	Greenschist-facies S-directed shearing

event was limited to pegmatite emplacement in the northern Arunta. However, it is now thought to have produced regional low-pressure metamorphism throughout the Arunta (Williams *et al.*, 1996; Vry *et al.*, 1996; Rubatto *et al.*, 2001). Amphibolite-facies metamorphism and the development of a regional foliation associated with isoclinal folding in the Southern Province occurred at 1586±69 Ma (Marjoribanks and Black, 1974) and was synchronous with extensive low-P regional metamorphism throughout the Northern Province at 1557-1587 Ma (Vry *et al.*, 1996; Rubatto *et al.*, 2001). This interpretation contrasts with suggestions that the D2/M2 metamorphism in the Northern Province was associated with extensive magmatic activity during the Strangways Orogeny (Collins and Vernon, 1991; Black and Shaw, 1992; Collins and Shaw, 1995; Collins and Williams, 1995).

Models for high geothermal gradients caused by heat production from buried granites have been suggested to account for HT/LP metamorphism in Proterozoic terranes throughout Australia (Sandiford and Hand, 1998a). Granitic gneisses from the Northern Province had a calculated heat production of c.  $8\mu\text{Wm}^{-3}$  during pervasive regional low-pressure metamorphism (~1.6 Ga) (Sandiford and Hand, 1998a). This suggests that a conductive high-geothermal gradient was likely to be responsible for the high-temperature mineral growth over ~30Ma during the Chewings Orogeny (Cartwright *et al.*, 1997; Sandiford and

Hand, 1998a; Rubatto *et al.*, 2001). Interpretation of the coeval deformation and other episodes of deformation remain highly contentious.

#### 2.3.2.5 Anmatjira Uplift Event

The Anmatjira Uplift Event (1400-1500 Ma), also described as the “Proterozoic Reworking”, is recognised from deformed granite in the Anmatjira Range (Black *et al.*, 1983), and from mylonites along the Redbank High Strain Zone (Shaw and Black, 1991). The event is also recognised within mylonites in the eastern Arunta Inlier, in the Strangways Range (Iyer *et al.*, 1976; Gascombe, 1992) and the Harts Range (Foden *et al.*, 1995). Though little described, the Anmatjira Uplift Event has been attributed to major amphibolite-facies reworking and south-directed thrusting throughout the Arunta Inlier (Collins and Shaw, 1995).

#### 2.3.2.6 Dyke Swarm

Minor mafic dyke emplacement across the southern central Arunta Inlier at  $1076 \pm 33$  Ma to 900 Ma has been used to constrain deformation events and to infer reactivation of Proterozoic structures (Black *et al.*, 1980; Collins and Shaw, 1995). Possible correlations to other dyke swarms in the area have been suggested (Collins and Shaw, 1995).

#### 2.3.2.7 Larapinta Event

The Larapinta Event is a recently identified Palaeozoic tectonic episode from the eastern Arunta Inlier, where pervasive medium to high-pressure granulite-facies metamorphism ( $\sim 800^\circ\text{C}$  and 8 to 10 kbar) (Fig. 2.4) occurred during the Mid-Ordovician (480 to 460 Ma) (Mawby *et al.*, 1998; Miller *et al.*, 1998; Hand *et al.*, 1999; Mawby *et al.*, 1999; Buick *et al.*, 2001). The metamorphic event is characterised by extensive fluid-absent partial melting at  $476 \pm 14$  Ma, followed by 4 kbar of near isothermal decompression at  $475 \pm 4$  to  $469 \pm 7$  Ma (Fig 2.4; Mawby *et al.*, 1999). A regional sub-horizontal foliation and some mylonitization developed during decompression, suggesting an extensional tectonic setting (Mawby *et al.*, 1999; Buick *et al.*, 2001). Metamorphism in the middle- to deep-crust

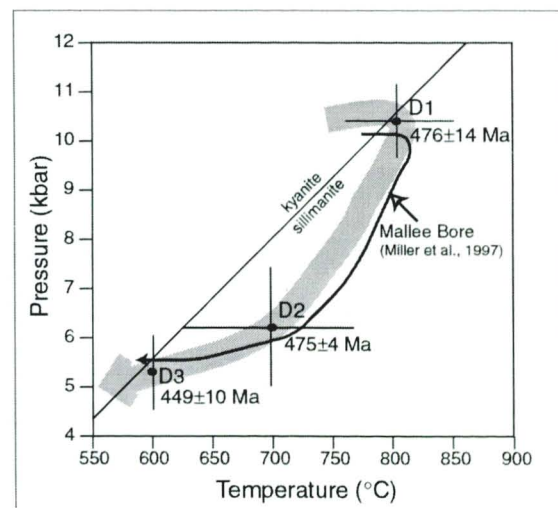


**Figure 2.4.** Proposed PTt path (thick grey line) for the Early to Mid-Ordovician Larapinta Event in the Harts Range after Mawby *et al.* (1999). The P-T estimates have errors of  $\pm 2\sigma$ . The thin black line represents the P-T path proposed for rocks from Mallee Bore (north of the Harts Range) from Miller *et al.* (1997) that are contemporary in age (Miller *et al.*, 1999).

Metamorphism in the middle- to deep-crust

during the Larapinta Event was synchronous with the deposition of the Larapinta Group into a subsiding basin above the now exposed Arunta Inlier (Mawby *et al.*, 1999). This event is the only recognised high-grade metamorphism during the Palaeozoic within the Arunta Inlier that occurred within an extensional intraplate setting synchronous with basinal sedimentation within the Larapinta Rift (Hand *et al.*, 1999). Detrital zircon populations within the granulites mimic those of the upper Amadeus Basin sediments and suggest that a new sediment source developed within central Australia during the Ordovician, possibly relating to the sedimentation of the east coast of Australia. The Larapinta Rift, depicted by negative gravity anomalies along the north-eastern margin of the Arunta Inlier, is likely to have formed a sea-way connected to the east (Webby, 1978; Fig 2.5). Further analysis of the Harts Range units is underway to document this sedimentation and high-grade metamorphic event.

#### 2.3.2.8 Alice Springs Orogeny

Neoproterozoic basin deposition, associated with the uplift and erosion of the Arunta Inlier, began at ~800 Ma and records deformation associated with the Alice Springs Orogeny (400 to 300 Ma) (Collins and Shaw, 1995; Lindsay, 1999; Table 2.1). Crustal reworking within the Arunta Inlier during the Palaeozoic produced movement across E-W and NW-SE oriented compressional fault systems. The shear and fault zones specific to this study are associated with the Alice Springs Orogeny, as either reactivated Proterozoic structures or newly-developed shear zones.

## 2.4 THE ALICE SPRINGS OROGENY

The Alice Springs Orogeny was a Devonian-Carboniferous intraplate orogenic event that produced predominantly north-south contractional tectonism (Forman and Shaw, 1973; Shaw *et al.*, 1984; Teyssier, 1985; Spikings *et al.*, 2001; Walter and Veevers, 1997) that followed a period of N-S extension at ~490 Ma (Hand *et al.*, 1999; Hand and Buick, 2001). The effects are widely recorded throughout central Australia as well as to the south in the Flinders Range (Mitchell *et al.*, 1998) and Officer Basin (Walter *et al.*, 1995; Walter and Veevers, 1997), to the north in the Mount Isa Inlier (Spikings *et al.*, 1997), and to the west in the Canning Basin, Western Australia (Shaw *et al.*, 1984). Geochronological studies of mylonites and reworked rocks of the Arunta Inlier indicate that metamorphism and deformation associated with compressive tectonics continued sporadically between 400 to 300 Ma in central Australia (Shaw and Black, 1991; Shaw *et al.*, 1992; Cartwright *et al.*, 1999). Extensional tectonics of the same age are recorded in the Canning Basin, north Western Australia (Shaw *et al.*, 1984). Substantial gravity anomalies in central Australia

were formed during the Alice Springs Orogeny, and represent some of the largest crustal gravity anomalies in the world.

#### **2.4.1 An intraplate orogeny**

The Alice Springs Orogeny is thought to have occurred in an intraplate setting. The evidence supporting this includes:

- 1) Correlation of the Neoproterozoic Centralian Superbasin remnants (the Officer, Amadeus, Ngalia, Georgina and Savory Basins) indicates that central and southern Australia were joined prior to 800 Ma (Walter and Veevers, 1997; Lindsay, 1999).
- 2) Depositional and erosive effects of the Delamerian Orogeny are recorded in basins throughout the Australian continent including the Georgina and Officer Basins, during the Cambrian-Early Ordovician period (Fig. 2.5; Webby, 1978).
- 3) The close proximity of the paleomagnetic poles from central and southern Australia during the Mid-Cambrian indicate that the two continental blocks were adjacent at this time (Klootwijk, 1980).
- 4) There are no recorded examples of preserved oceanic crust in central Australia, or other features indicative of intercontinental collision during the Palaeozoic, such as high-pressure low-temperature subduction style metamorphism or arc-related volcanism and plutonism (Forman and Shaw, 1973; Shaw *et al.*, 1984).

#### **2.4.2 The Centralian Superbasin**

The Centralian Superbasin, initiated during sagging in response to the break-up of Rodinia at 800 Ma (Walter and Veevers, 1997; Lindsay, 1999), contains intracratonic sediments stretching over several hundred kilometres and spanning the Neoproterozoic to the Mid-Palaeozoic (Walter *et al.*, 1995). Depositional and erosive effects of the late Cambrian-Early Ordovician Delamerian Orogeny can be traced through the Superbasin stratigraphy (Webby, 1978) with the development of the Larapintine Sea (Fig. 2.5). Sedimentation was disrupted internally by the onset of the Cambrian Petermann Orogeny (560-520 Ma; Scrimgeour and Close, 1999), the Ordovician Larapinta Event (490 to 460 Ma; Mawby *et al.*, 1999; Buick *et al.*, 2001) and the Devonian-Carboniferous Alice Springs Orogeny (300 to 400 Ma; Shaw and Black, 1991). The opening of the Larapintine Seaway during the Larapinta Event (~490 Ma) relates to a period of extension prior to the onset of the compressional Alice Springs Orogeny, and is likely to be a continuation of the same tectonic event ending at around 300 Ma (Hand and Buick, 2001). The effects of basement exhumation during these orogenies formed the structural basins now present in central Australia (Fig. 2.6; Collins and Shaw, 1995; Walter and Veevers, 1997). There is no

evidence of sedimentation in the Amadeus Basin after the late Devonian, suggesting the Alice Springs Orogeny was the last tectonic event, in this region, to produce sufficient topography to feed sedimentation systems (Shaw *et al.*, 1984). Intracratonic deformation

within the Amadeus Basin is attributed to both the Petermann and the Alice Springs Orogenies (Flöttmann *et al.*, 1999). Timing of deformation within the basin is indicated predominantly

by the disruption of the Larapintine Sea linking the Canning, Georgina and Amadeus basins at this time.

post-Cambrian (post-Petermann Orogeny) sediments (Shaw *et al.*, 1992). The Alice Springs Orogeny produced thin-skinned style shortening including fold-thrust belts, originally identified as “Alpine-style” nappes along the northern margin of the Amadeus Basin (Teyssier, 1985; Collins and Teyssier, 1989).

Recent seismic data indicate that much less shortening took place at the northern margin of the Amadeus basin than that implied by Alpine-style nappe formation and has thus lead to a re-evaluation of the structures at the basin margins (Flöttmann and Hand, 1999). Shortening at the basin margin was produced through the propagation of a foreland facing wedge, comprising Arunta basement and the two lower units of the Amadeus Basin sequence (Flöttmann and Hand, 1999). Seismic data indicate that this thrust system is linked to the Redbank High Strain Zone at depth (Shaw *et al.*, 1991). The rotating basement wedge model indicates around 19 km of shortening, comparable with the seismic data (Flöttmann and Hand, 1999).

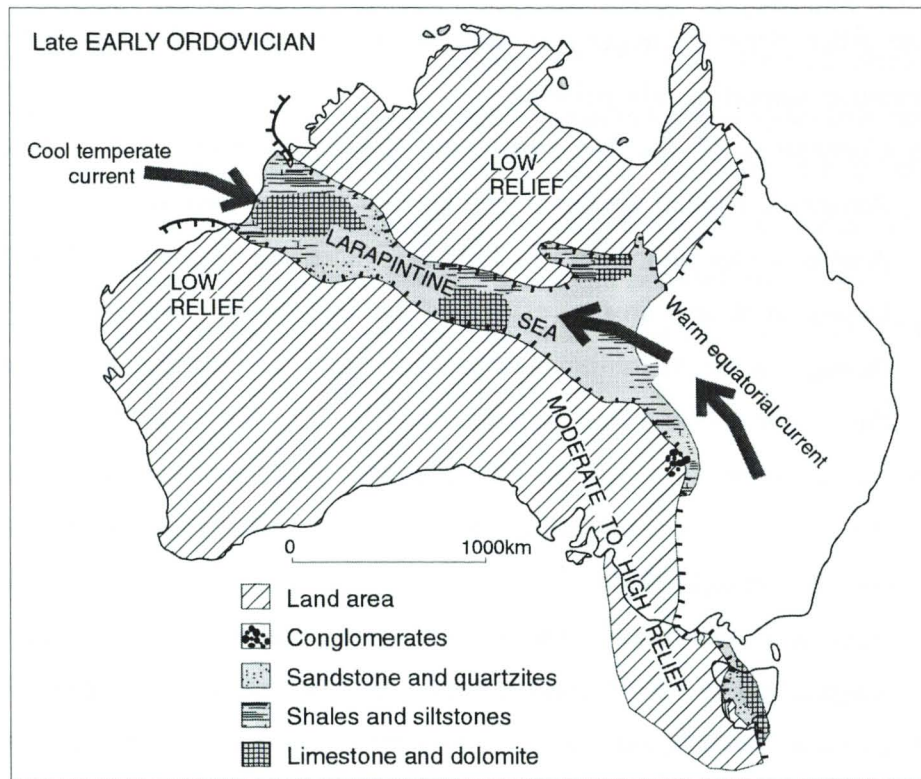


**Figure 2.5. Early Ordovician palaeogeography of the Australian Craton after Webby (1978) showing the formation of the Larapintine Sea linking the Canning, Georgina and Amadeus basins at this time.**

Palaeozoic deformation is also recorded away from the basins margins. Within the Amadeus Basin, synorogenic sedimentation occurred during the Alice Springs Orogeny and is spatially associated with major faults. The synorogenic sedimentation is thickest between the Gardiner Thrust and the MacDonnell Homocline (Shaw *et al.*, 1991), where seismic data indicates 6km of N-directed thrusting across the Gardiner Thrust. In addition large N-S and NE-SW-trending anticlines throughout the Amadeus Basin are inferred from the seismic data (Fig. 2.6; Shaw *et al.*, 1991). The complex nature of the basement-basin boundaries in central Australia indicates that some coupling between the cover and basement occurred during the Alice Springs Orogeny (Sandiford and Hand, 1998b).

#### **2.4.3 Effects of the Alice Springs Orogeny within the Arunta Inlier**

Crustal reworking during the Alice Springs Orogeny is predominantly confined to narrow shear zones containing plentiful hydration reactions within middle crustal metamorphic provinces.  $^{39}\text{Ar}$ - $^{40}\text{Ar}$ , Rb-Sr and Sm-Nd mineral ages from sheared rocks throughout the Arunta Inlier yield many Paleozoic ages (Allen and Black, 1979; Black *et al.*, 1983; Windrim and McCulloch, 1986; Cooper *et al.*, 1988; Shaw and Black, 1991; Collins and Shaw, 1995; Bendall *et al.*, 1998; Cartwright *et al.*, 1999; Ballèvre *et al.*, 2000) that are consistent with the Alice Springs Orogeny. The Redbank High Strain Zone, a major crustal fault zone separating the Central and Southern Provinces, yields Rb-Sr mineral and whole rock ages that indicate re-activation occurred between 350-400 Ma (Shaw and Black, 1991). Sm-Nd analyses of amphibolite facies shear zones in the eastern Arunta indicate ages of 380 Ma (Ballèvre *et al.*, 2000). Similarly,  $^{39}\text{Ar}$ - $^{40}\text{Ar}$  and Rb-Sr mineral ages from the Northern Province indicate shearing occurred from 300-350 Ma (Cartwright *et al.*, 1999; this study). There is local disparity in ages of Alice Springs Orogeny structures within the Arunta Inlier. In the southern Arunta Inlier shear zones apparently decrease in age gradationally in a southward direction (Bendall *et al.*, 1998). Whereas in the northern Arunta Inlier shear zone ages decrease in age towards the north (Chapter Five). Initial interpretation of the extent of Alice Springs age deformation within the Arunta Inlier was controversial. Collins and Teyssier (1989) proposed that the event caused major movement and developed a network of shear zones throughout the Arunta Inlier at greenschist- to amphibolite-facies conditions. They suggest that all shear zones have Alice Springs age movement, either as reactivated older structures or as primary Alice Springs structures. By contrast Dirks and Wilson (1990) and Shaw *et al.* (1992) proposed that the event was of minor significance, forming only greenschist-facies retrogression zones with little vertical displacement. These authors suggest that the higher-grade shear zones in the region record Proterozoic movement, forming during the ~1400 Ma Anmatjira Uplift Phase at the end of

the Chewings Orogeny (Dirks and Wilson, 1990). Other research indicates however, that Alice Springs Orogeny ages occur throughout shear zones of different metamorphic conditions, including kyanite-bearing and amphibolite-facies shear zones (Dunlap and Teyssier, 1995; Bendall *et al.*, 1998; Cartwright *et al.*, 1999; Ballèvre *et al.*, 2000). Estimates of 20km of exhumation during the Alice Springs Orogeny have been suggested from the eastern Arunta Inlier (Mawby *et al.*, 1998). This research suggests that the Alice Springs Orogeny was a major uplift event that led to the exposure of a large amount of the Arunta Inlier basement and reached temperatures of at least amphibolite-facies conditions. Estimates from the Redbank High Strain Zone suggest that crustal shortening in the order of 20-30% occurred during the Alice Springs Orogeny (Shaw *et al.*, 1992) at a slower rate (0.6-3km/Ma) than proposed for continent-continent collision.

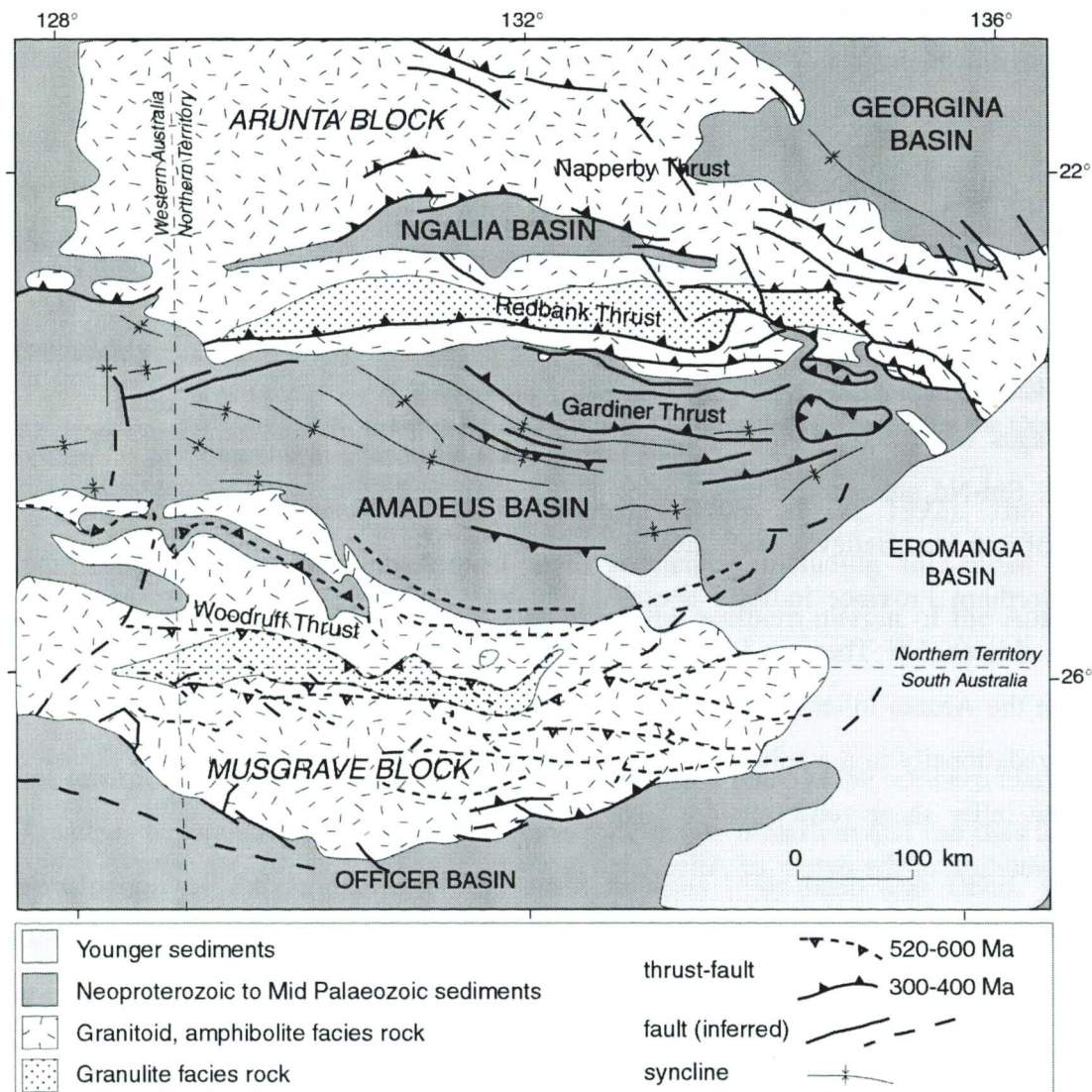


Figure 2.6. Regional map of central Australia, including the Arunta Inlier, Amadeus, Ngalia and southern Georgina Basins, the Musgrave Block and the northern margin of the Officer Basin. Thrust systems active during the Petermann Orogeny (520 to 600 Ma) and Alice Springs Orogeny (300 to 400 Ma) are shown in dashed and full lines respectively (map after Shaw *et al.*, 1991, Sandiford and Hand, 1998b and Read *et al.*, 1999).

In contrast to earlier interpretations of low heat flow during the Alice Springs Orogeny, Sandiford and Hand (1998b) suggest that the crust was heated to significant temperatures (>500°C for over 70 Ma) during the Alice Springs Orogeny. This is consistent with the higher-grade sheared assemblages with Alice Springs ages in the northern and eastern Arunta Inlier. Sandiford and Hand (1998b) suggest that locally the depth of the Centralian Superbasin was spatially associated with the location of reactivation during the two main Palaeozoic orogenies in central Australia. Specifically, in the south during the Petermann Orogeny and in the north during the Alice Springs Orogeny.

The presence of high heat producing granites in central Australia and the depth of the basins contributed to the thermal weakening of the central Australian crust and thus caused reactivation along discrete Proterozoic structures during the Palaeozoic orogenies (Sandiford and Hand, 1998b). The fault and shear zones throughout the western Arunta Inlier (Figs. 2.2, 2.6) have regional W-E and NW-SE orientations and variable dip. The shear zones range in width from centimetres to greater than 100 metres and can be traced for tens to hundreds of kilometres along strike. The shear zone assemblages are consistently lower grade and more hydrous than their host rocks, indicating that fluid flow occurred during shearing. Typically, greenschist-facies shear zones cut amphibolite-facies terrains and amphibolite-facies shear zones cut granulite terrains. For example the granulite complexes of the Mount Chapple - Mount Hay region are cut by upper amphibolite-facies shear zone assemblages (Collins, 2000) and the upper amphibolite-facies gneisses of the Redbank High Strain Zone are cut by amphibolite- to greenschist-facies shear zones (Shaw and Black, 1991). In the Northern Province, the grade of the shear zones varies along the length of the Reynolds and Anmatjira Ranges recording a temperature increase towards the SE. This mirrors the regional ~1.6 Ga low-pressure metamorphic conditions. The sheared rocks generally have mylonitic fabrics, with S-C mylonites and extensive mineral lineations (Collins and Teyssier, 1989, this study). Heterogenous strain and anastomosing fabrics are dominant within the larger shear zones (Shaw and Black, 1991). Evidence of initial brittle deformation and reworking during the Alice Springs Orogeny is common, though typically masked by pervasive recrystallisation. The development of pseudotaclytes is also recorded from the Redbank High Strain Zone (Shaw and Black, 1991) and the Harry Creek Shear Zone (Allen and Black, 1979).

#### **2.4.4 Summary**

The Alice Springs Orogeny produced detachment-style structures along the northern margin of the Amadeus Basin and crustal-scale thick-skinned thrusting throughout the

Arunta Inlier, indicating compressive failure of the whole crust in central Australia (Goleby *et al.*, 1989; Shaw *et al.*, 1992). Thrusting during the Alice Springs Orogeny is interpreted to be episodic due to the spread of mineral ages in the Redbank High Strain Zone and across the Northern Province (Shaw *et al.*, 1992; Chapter Seven). Possible problems with geochronology of the Redbank High Strain Zone will be further described in Chapter Six. However, it is clear that major uplift and retrogression within the Arunta Inlier occurred between 300 and 400 Ma, causing the formation and reactivation of crustal scale fault and shear systems.

## **2.5 LOCAL GEOLOGY**

Within the Arunta Inlier, four separate regions were sampled for this study. They include the SE Anmatjira Range and SE Reynolds Range within the Northern Province, the eastern Redbank High Strain Zone, separating the central and Southern Provinces and the Wigley Zone in the NE Southern Province. A discussion of the local geology of each region follows.

## **2.6 NORTHERN PROVINCE**

The Northern Province is the largest of the three provinces within the Arunta Inlier (Fig. 2.7). It comprises predominantly of a local basement of Mesoproterozoic turbidite sequences variably intruded by K-feldspar megacrystic granites (Stewart *et al.*, 1984; Collins *et al.*, 1991). Calc-silicate and meta-sedimentary units unconformably overly the basement turbidities, and all were intruded by 1.78Ga granites (Collins and Shaw, 1995; Collins and Williams, 1995). Major NW-SE trending faults and reverse-sense shear zones disrupt the regional E-W-trending contractional fabrics throughout the ranges. Some of the larger shear zones extend into the deep crust (Lambeck *et al.*, 1988; Goleby *et al.*, 1990), and have juxtaposed rocks from different crustal depths (Dirks *et al.*, 1991; Collins and Shaw, 1995). The paragneiss and orthogneiss lithologies that host shear zones in the Northern Province are outlined below.

### **2.6.1 Paragneisses of the Northern Province**

The widespread, fairly homogenous layered pelitic and psammitic Lander Rock Beds (Fig. 2.7) form the Mesoproterozoic basement unit throughout much of the Northern Province.

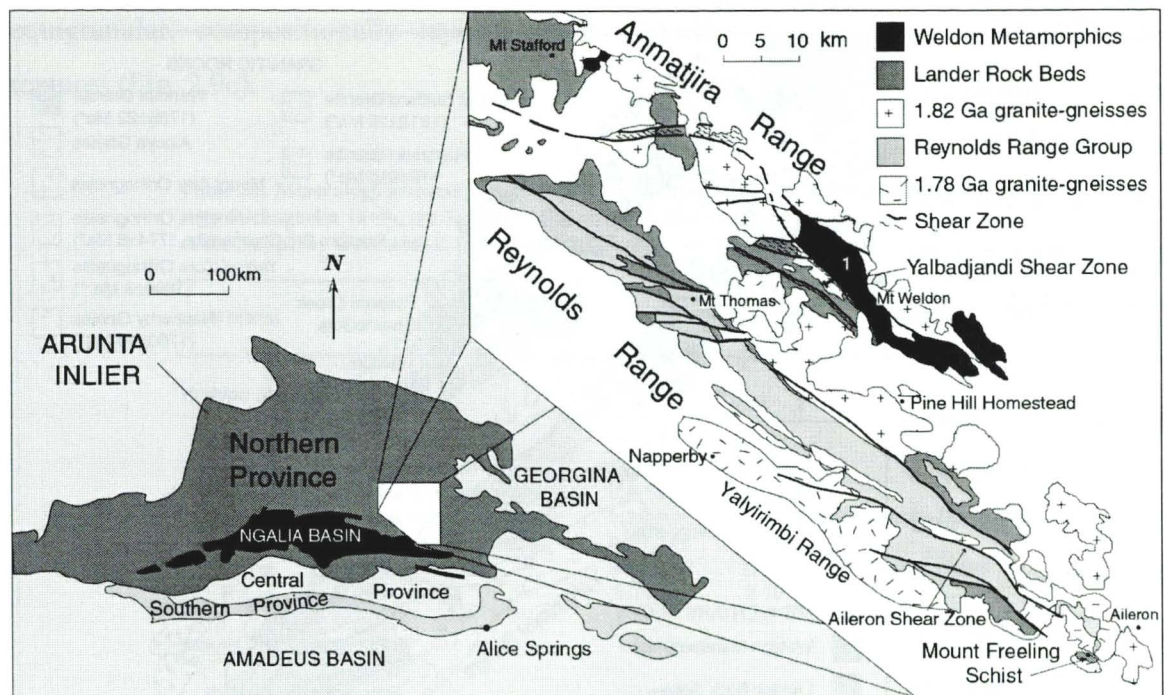


**Figure 2.7.** Geology of the Reynolds and Anmatjira Ranges, Northern Province, Arunta Inlier, including major shear zones, metamorphic grade and locations referred to in text.

Relic bouma sequences indicate that the Lander Rock Beds formed in a high-energy turbidite deposition system. Limited U-Pb analyses from detrital zircons suggests that deposition occurred until at least 1838 Ma (Vry *et al.*, 1996). The Lander Rock Beds are intruded by ~1.82Ga granites and show evidence of contact and regional low-pressure metamorphism (Stewart, 1981; Collins and Williams, 1995; Williams *et al.*, 1996; Vry *et al.*, 1996). The Weldon Metamorphics crop out in the central and SE Anmatjira Range (Fig. 2.7), separated from the Lander Rock Beds to the south by the Yalbadjandi Shear Zone. The Weldon Metamorphics are thought to be high-grade equivalents of the Lander Rock Beds (Collins and Shaw, 1995). They are intruded generally by ~1.82 Ga granites and locally by the ~1.78 Ga Possum Creek Charnockite (Fig. 2.8; Collins and Williams, 1995). Similarly, the Mount Freeling Schist (Fig. 2.7) is likely to represent a high-grade equivalent of the Lander Rock Beds in the SE Reynolds Range (Collins and Shaw, 1995), though no geochronological work has been undertaken. The Reynolds Range Group forms the cover sequence along the Reynolds Range, overlying the Lander Rock Beds with local angular unconformities (Dirks *et al.*, 1991). The Reynolds Range Group comprises quartzite, pelite, marl and marble (Stewart *et al.*, 1984; Cartwright *et al.*, 1999), which have been divided into units. The first deposited are the 500-600m thick Basal Quartzite Unit and laterally equivalent Lower Calcsilicate Unit (Buick *et al.*, 1999b). These are overlain by the 500-600m thick Pelitic Unit, which contains 300-350m thick lenses of calc-silicate known as the Upper Calc-silicate Unit (Cartwright *et al.*, 1996; Buick *et al.*, 1999b). Sedimentation of these units began around 1.8 Ga following the first granitic

magmatic event and associated metamorphism in the region and had ceased prior to 1.78 Ga when the second granite magmatism began (Cartwright *et al.*, 1996; Collins and Williams, 1995). The following section summarises the Proterozoic granulite-facies

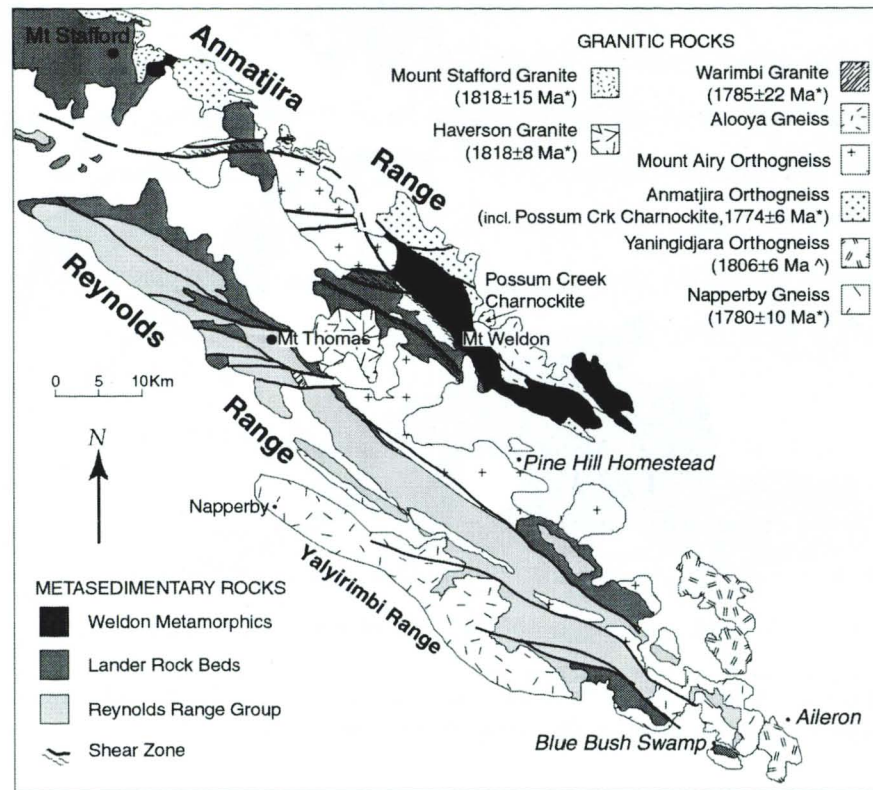


**Figure 2.8. Simplified geological map of the Anmatjira and Reynolds Ranges showing the location of the main granitic rocks with emplacement ages from Collins and Williams (1995)\* and Vry *et al.* (1996)^.**

paragneisses that host shear zones analysed in this study.

#### 2.6.1.1 The Weldon Metamorphics

The Weldon Metamorphics are exposed in the SE Anmatjira Ranges (Fig. 2.7). They comprise layered migmatitic paragneisses of pelitic and psammitic composition with minor interlayers of cordierite-rich granofels. The felsic melt segregations are concordant with, and locally cut the compositional layering (Fig. 2.9a). Deformation associated with metamorphism at 1.6 Ga produced regional NW-SE trending folds with a well-developed axial planar foliation. Pyroxene-bearing mafic granulite bodies within the pelites have sub-parallel fabric and granulite-facies metamorphic textures, indicating their incorporation into the sediments prior to regional metamorphism probably as mafic intrusions. The Weldon Metamorphics are coarse-grained (1 to 5mm) and contain variable K-feldspar, cordierite, plagioclase, sillimanite, garnet, biotite and quartz (Table 2.2). Within the pelitic layers, the foliation is clearly defined by aligned blocky sillimanite and biotite grains (Fig. 2.9b). The leucosomes comprise coarse-grained (5 to 10mm) K-feldspar, plagioclase, cordierite, quartz and embayed garnet. Layers of blocky sillimanite form a weak foliation. The mafic bodies that intrude the paragneiss contain assemblages of hornblende, augite, orthopyroxene, plagioclase, biotite and locally quartz. They form coarse-grained (~1mm),

equigranular, compositionally layered mafic granulite with well-developed polygonal textures (Fig. 2.9c).

**Table 2.2. Mineralogy summary of the Weldon Metamorphics (n=4) and the Mount Airy Orthogneiss (n=4), the Napperby Gneiss (N=3) and a biotite-rich variation of the Napperby Gneiss (n=1) from the SE Anmatjira and Reynolds Ranges.**

Mineral	Shape	Size	%	Inclusions
<b>Weldon Metamorphics</b>				
K-feldspar	anhedral-euhedral	1-2 mm	25-35	
Plagioclase	anhedral-euhedral	0.5-1mm	10-20	
Quartz	strain-free irregular subgrains	0.5-1mm	ca. 30	
Cordierite	anhedral-subhedral	0.5-1mm	3-10	sillimanite + biotite
Sillimanite	blocky clusters and needles	5-10 mm	5-15	
Garnet	elongate embayed	2-10 mm	ca. 5	sillimanite + biotite
Biotite	subhedral sheets	0.2 mm	2-10	
<b>Mount Airy Orthogneiss</b>				
K-feldspar	subhedral	~2 mm	30-35	
Plagioclase	subhedral	1-2 mm	25-30	
Quartz	euhedral, sub-grained	1-3 mm	25-30	
Biotite	anhedral sheets	0.1 mm	5-10	
<b>Alooya Gneiss</b>				
K-feldspar	subhedral porphyroclasts	1-2 cm	35	
Plagioclase	subhedral	1-2 mm	20-25	
Quartz	euhedral, sub-grained	1-3 mm	25-30	
Biotite	anhedral sheets	0.1 mm	5-10	
<b>Napperby Gneiss</b>				
Quartz	strain-free subgrains	1-5 mm	30-55	
K-feldspar	euhedral (embayed)	1-2 mm	25-30	
Plagioclase	subhedral (embayed)	0.5-1 mm	15-25	
Biotite	euhedral	0.1 mm	5-10	
Muscovite	fine accicular masses	0.005 mm	0-9	
Titanite	subhedral	0.05 mm	0-1	
<b>Biotite-rich Napperby Gneiss</b>				
Cordierite	anhedral	0.5-1 mm	10	
Quartz	anhedral	1-5 mm	30	
K-feldspar	euhedral-subhedral	1-2 mm	15	
Plagioclase	subhedral	0.5-1 mm	20	
Biotite	anhedral sheets	0.1 mm	20	
Titanite	subhedral	0.05 mm	3	
Epidote	subhedral	0.05 mm	2	

#### 2.6.1.2 P-T conditions

Using THERMOCALC v2.5 (Holland and Powell, 1998) P-T conditions are calculated from sample CR97AR1 (Transect 1, Fig. 2.7) for the assemblage garnet + cordierite + plagioclase + K-feldspar + biotite giving an estimate of  $T = 696 \pm 34^\circ\text{C}$  and  $P = 4.9 \pm 0.4$  kbar (mineral composition data in Table 2.3). Estimates based on the assemblage cordierite + spinel + garnet + ilmenite by Collins and Vernon (1991) for Weldon Domain granulites to the north are  $T > 750^\circ\text{C}$  and  $P = 5.5 \pm 1$  kbar.

**Table 2.3. Mineral Compositions of biotite, cordierite, plagioclase, K-feldspar and garnet from the Weldon Metamorphics (CR97AR1). Concentrations of oxides in wt%.**

<i>Biotite</i>										<i>Cordierite</i>				
<i>Analysis</i>	1	2	3	4	5	6	7	8	9	1	2	3	4	5
SiO <sub>2</sub>	37.84	35.36	35.14	35.55	35.76	35.16	34.34	35.64	34.53	47.78	47.96	47.47	47.43	47.62
TiO <sub>2</sub>	4.06	2.50	3.60	4.59	4.68	2.02	2.13	2.33	4.30					
Al <sub>2</sub> O <sub>3</sub>	16.21	17.03	17.46	16.88	17.33	17.26	18.45	17.14	16.75	33.30	33.55	33.01	33.39	33.56
FeO	18.69	18.20	19.31	18.30	18.22	17.60	18.68	17.25	20.79	8.82	9.73	9.34	8.45	8.49
MnO	0.12	0.00	0.07	0.05	0.16	0.10	0.00	0.00	0.08					
MgO	9.82	12.26	10.88	10.74	10.75	12.72	11.97	12.94	9.03	9.59	9.00	8.91	9.69	9.70
CaO														
Na <sub>2</sub> O														
K <sub>2</sub> O	9.17	9.75	9.91	9.74	9.77	9.56	9.00	9.39	9.64					
Total	95.92	95.10	96.39	95.87	96.68	94.43	94.58	94.70	95.37	99.51	100.25	98.74	98.98	99.37
#O	22	22	22	22	22	22	22	22	22	18	18	18	18	18
Si	5.68	5.39	5.32	5.38	5.36	5.38	5.26	5.42	5.30	4.88	4.88	4.90	4.87	4.87
Ti	0.46	0.29	0.41	0.52	0.53	0.23	0.25	0.27	0.50					
Al	2.87	3.06	3.12	3.01	3.06	3.11	3.33	3.07	3.03	4.01	4.03	4.02	4.04	4.05
Fe	2.34	2.32	2.44	2.31	2.28	2.25	2.39	2.19	2.67	0.75	0.83	0.81	0.73	0.73
Mn	0.02	0.00	0.01	0.01	0.02	0.01	0.00	0.00	0.01					
Mg	2.19	2.78	2.46	2.42	2.40	2.90	2.73	2.93	2.25	1.46	1.37	1.37	1.48	1.48
Ca														
Na														
K	1.75	1.90	1.91	1.88	1.87	1.87	1.76	1.82	1.89					
Total	15.31	15.74	15.67	15.53	15.52	15.75	15.72	15.70	15.65	11.10	11.11	11.10	11.12	11.13

<i>Plagioclase</i>			<i>K-feldspar</i>						<i>Garnet</i>				
<i>Analysis</i>	1	2	3	1	2	3	4	5	6	1	2	3	4
SiO <sub>2</sub>	58.79	58.88	58.53	62.62	63.64	62.42	63.74	62.54	62.97	36.39	36.29	36.47	36.62
TiO <sub>2</sub>										0.19	0.15	0.10	0.16
Al <sub>2</sub> O <sub>3</sub>	26.03	25.80	25.63	19.30	19.55	19.21	19.93	19.27	19.96	21.80	21.65	21.91	22.02
FeO	0.00	0.04	0.11	0.08	0.03	0.25	0.00	0.05	0.13	36.70	36.21	36.48	35.26
MnO										0.64	0.51	0.62	0.48
MgO	1.21	1.14	1.20	1.11	1.02	0.87	1.17	0.85	1.16	4.42	4.59	4.65	5.62
CaO	6.88	6.91	6.68	0.37	0.61	0.52	0.55	0.42	0.91	0.91	1.02	0.94	1.00
Na <sub>2</sub> O	7.00	7.49	7.61	1.45	1.36	1.09	1.93	1.14	1.86				
K <sub>2</sub> O	0.15	0.17	0.32	15.15	15.51	15.46	14.15	14.31	13.37				
Total	100.06	100.44	100.07	100.09	101.73	99.83	101.48	98.58	100.37	101.05	100.42	101.18	101.18
#O	8	8	8	8	8	8	8	8	8	12	12	12	12
Si	2.62	2.62	2.62	2.90	2.91	2.91	2.90	2.92	2.89	2.90	2.91	2.90	2.90
Ti										0.01	0.01	0.01	0.01
Al	1.37	1.35	1.35	1.05	1.05	1.05	1.07	1.06	1.08	2.05	2.05	2.05	2.05
Fe	0.00	0.00	0.00	0.00	0.00	0.01	0.00	0.00	0.00	2.45	2.43	2.43	2.33
Mn										0.04	0.03	0.04	0.03
Mg	0.08	0.08	0.08	0.08	0.07	0.06	0.08	0.06	0.08	0.53	0.55	0.55	0.66
Ca	0.33	0.33	0.32	0.02	0.03	0.03	0.03	0.02	0.04	0.08	0.09	0.08	0.08
Na	0.60	0.65	0.66	0.13	0.12	0.10	0.17	0.10	0.17				
K	0.01	0.01	0.02	0.90	0.90	0.92	0.82	0.85	0.78				
Total	5.01	5.04	5.05	5.08	5.08	5.08	5.07	5.01	5.04	8.06	8.07	8.06	8.06

The pressures and temperatures for the Mount Weldon rocks compared to the more northern granulites could suggest some down-temperature resetting following peak metamorphism, reflected in the mineral assemblage. However, both estimates indicate the SE Anmatjira Range gneisses underwent low-pressure granulite-facies metamorphism.

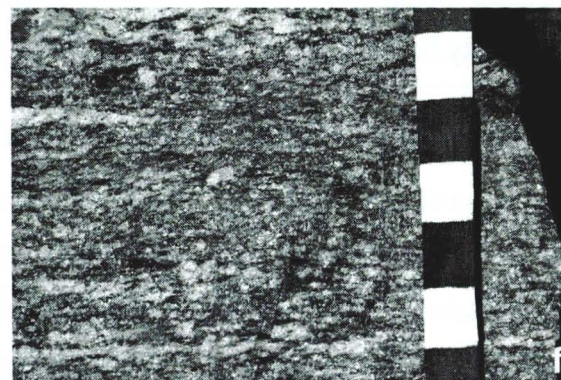
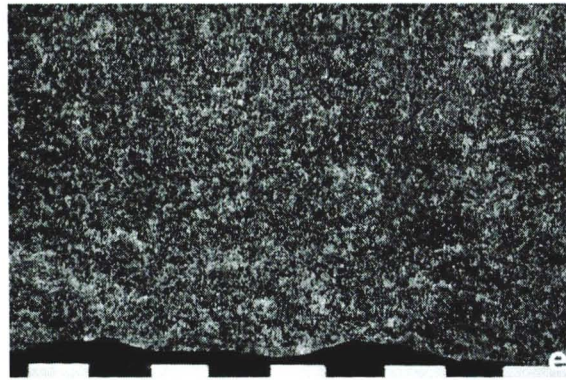
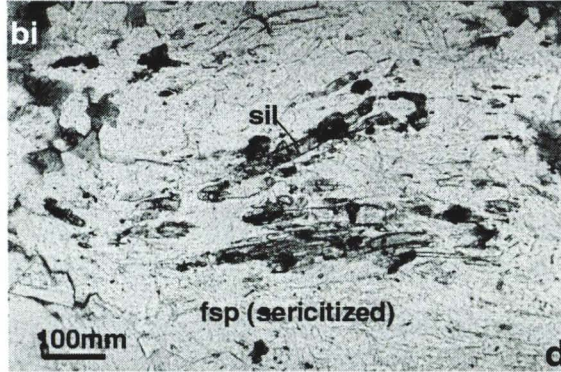
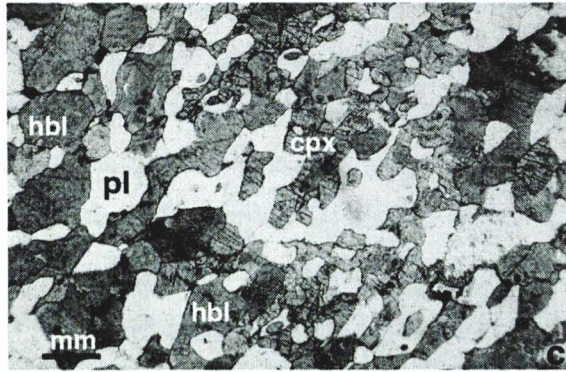
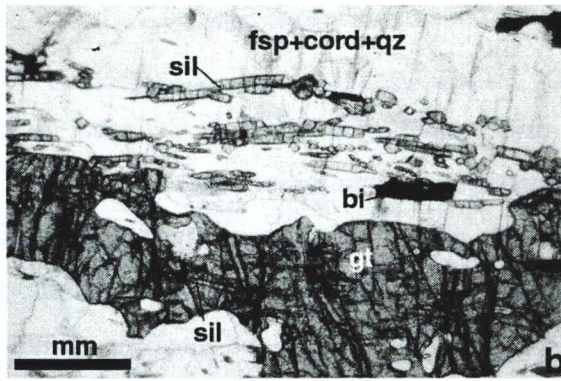
### 2.6.1.3 The Mount Freeling Schist

The Mount Freeling Schist is exposed in the southern Reynolds Range (Fig. 2.7) and is equivalent to the Lander Rock Beds that forms the basement meta-sedimentary sequence in the northern Arunta Inlier (Collins and Shaw, 1995). The Mount Freeling Schist comprises medium-grained interlayered quartzofeldspathic and sillimanite-bearing pelitic schists that are commonly retrogressed to chlorite-muscovite assemblages. The Mount Freeling Schist also includes granofels and gneisses containing variable quantities of quartz, microcline, cordierite, biotite and sillimanite, which formed during upper amphibolite-facies metamorphism (Stewart, 1981). At Blue Bush Swamp, the Mount Freeling Schist has been pervasively retrogressed from sillimanite-bearing high-grade schist to a medium-grained biotite plus quartz-rich schist, containing the assemblage: quartz, biotite, muscovite, titanite and locally sillimanite (Table 2.2). Sillimanite inclusions are present within the cores of altered feldspars (Fig. 2.9d). The northern exposure of the shear zone at Blue Bush Swamp shows a 1.78Ga intrusive contact with the Napperby Gneiss and pegmatites. The intrusive contact is partially sheared, forming protomylonites, and the pegmatites are commonly boudinaged.

### 2.6.2 Orthogneisses of the Northern Province

Two generations of granitic activity are recorded in the Anmatjira and Reynolds Ranges (Table 2.1). Early magmatism involved the emplacement of the precursors to the Anmatjira Orthogneiss (including the Mount Stafford Granite), the Haverson Granite and possibly the Mount Airy Orthogneiss at ~1820 Ma (Collins and Williams, 1995; Vry *et al.*, 1996). This was followed by the Yaningidjara Orthogneiss precursor granitoid at 1806 Ma (Vry *et al.*, 1996). The Napperby Gneiss granitic precursor, the Warimbi Granite, the Possum Creek Charnockite and the Coniston Granite intruded at ~1.78 Ga (Collins and Williams, 1995). Local amphibolite-facies contact metamorphism and minor deformation immediately followed the magmatism, causing andalusite and cordierite growth associated with a weak foliation (Collins and Williams, 1995).

The 1.82 Ga granites typically contain large K-feldspar megacrysts and show S-type chemical affinities (Collins and Williams, 1995). The 1.78 Ga granites have a much broader distribution with synchronous ages obtained from elsewhere in the Central (Black and Shaw, 1992; Zhao and Bennett, 1995; Cooper *et al.*, 1998) and Northern (Young *et al.*, 1995) Provinces of the Arunta Inlier. The Napperby Gneiss underlies and locally intrudes basal units of the Reynolds Range Group and has emplacement age of  $1780 \pm 10$  Ma (Collins and Williams, 1995).



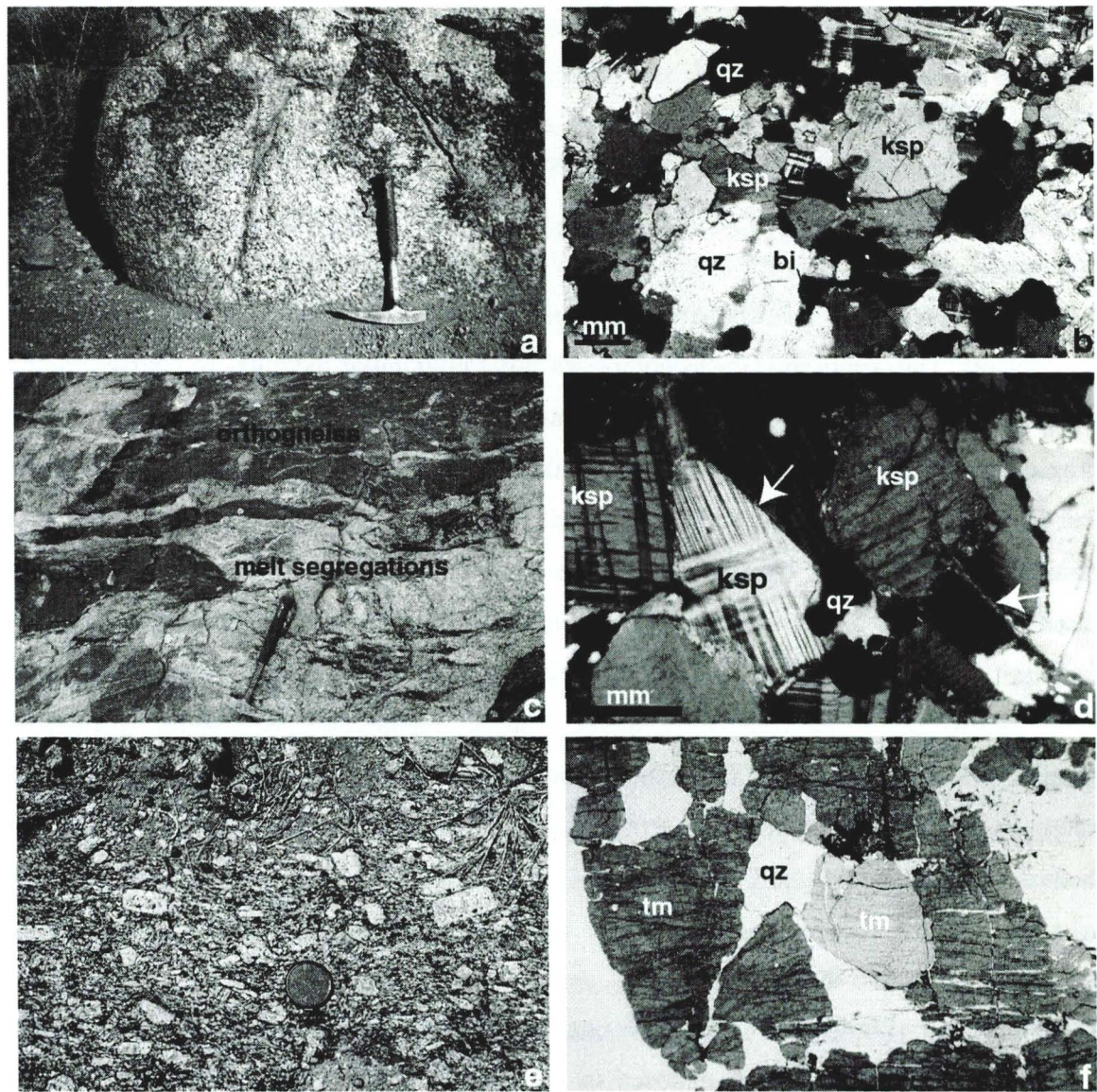


Figure 2.10. a) Coarse-grained granitic Napperby Gneiss, SE Reynolds Range, with foliation defined by biotite. b) equigranular medium-grained Napperby Gneiss (CR98NG17) XPL. c) Mount Airy Orthogneiss near Mount Weldon, with extensive melt segregations. d) equigranular K-feldspar rich Mount Airy Orthogneiss with extensive deformation twins and recrystallisation at grain edges, XPL. e) Alooja Gneiss, SE Anmatjira Ranges with abundant undeformed K-feldspar porphyroclasts. f) Fractured and recrystallised tourmaline and quartz vein within the Alooja Gneiss, PPL. Abbreviations in Table 1.1 (Chapter One).

Figure 2.9. (opposite page) a) Weldon Metamorphics at Mount Weldon, SE Anmatjira Range, granulite-facies paragneiss with abundant cross cutting and layer parallel melt segregations. b) Blocky sillimanite, garnet and biotite defining gneissic foliation, PPL. c) Mafic granulite, Mount Weldon, with equigranular hornblende, clinopyroxene and plagioclase defining a foliation top right to bottom left, PPL. d) Blocky sillimanite aligned within sericitized K-feldspar porphyroclasts of the Mount Freeling Schist at Blue Bush Swamp (CR98BBS40). e) medium-grained mafic granulite at Mount Hay, Central Province, scale in centimetres f) intermediate granulite at Mount Hay, Central Province with minor leucosomes, scale in centimetres g) Folded, migmatitic quartzofeldspathic gneiss of the Madderns Yard Metamorphic Complex, south of Littlers Yard, Southern Province. h) Quartzofeldspathic gneiss of the Ellery Granitic Complex, Littlers Yard, Southern Province

### 2.6.2.1 The Napperby Gneiss

The Napperby Gneiss occurs along the southern flank of the Reynolds Range, forming the low-lying Yalyirimbi Range (Fig. 2.8). It is a large homogenous body of granitic orthogneiss (Fig. 2.10a) with a regional NW-trending upright foliation (Hand and Dirks, 1992) associated with the Chewings Orogeny and is cut by numerous NW-SE-oriented shear zones. The Napperby Gneiss comprises sub-equigranular medium- to coarse-grained (1-5mm) K-feldspar, plagioclase, quartz, muscovite and biotite with minor Fe-oxides (Table 2.2; Fig. 2.10b). Gneissic layering is defined by aligned mica and elongated quartz and feldspar layers that are locally cut by felsic melt patches, likely representing melting associated with the ~1.6 Ga granulite- to upper-amphibolite facies regional metamorphism (Dirks *et al.*, 1991; Vry *et al.*, 1996; Rubatto *et al.*, 2001). In places the Napperby Gneiss is porphyritic with large K-feldspar augens. Entrained within the granitic orthogneiss is a more biotite-rich rock, comprising quartz, biotite, plagioclase, K-feldspar, cordierite, titanite and epidote (Table 2.2). These rocks contain similar high-grade deformation microstructures and probably represent pods of pelitic xenolith material. Shear zones cut these cordierite-bearing gneisses.

### 2.6.2.2 The Mount Airy Orthogneiss

The Mount Airy Orthogneiss is a coarse-grained foliated granitoid with minor partial melt segregations (Fig. 2.10c). It is exposed in the Hanson River Valley, along the northern edge of the Reynolds Range and the southern edge of the central Anmatjira Range (Fig. 2.8). The Mount Airy Orthogneiss is coarse-grained (1 to 2mm), comprising quartz, K-feldspar, plagioclase and biotite. Aligned, randomly distributed grains of biotite and aligned long axes of feldspar and quartz grains define a weak foliation. The large igneous K-feldspar and plagioclase grains show deformation twinning. Some recrystallisation occurs along feldspar grain boundaries often forming replacement myrmekite textures. Deformation lamellae and perthitic intergrowths are common within the large feldspar clasts (Fig. 2.10d).

### 2.6.2.3 The Alooja Gneiss

The Alooja Gneiss crops out along the northern edge of the SE Anmatjira Range (Fig. 2.8). It is well foliated and comprises coarse- to medium-grained (0.4 to 1mm) granitic assemblages of quartz, plagioclase, K-feldspar, biotite and muscovite (Table 2.2). The gneiss contains strain-free polygonal quartz and aligned micas defining a weak foliation that trends NW-SE, consistent with the 1.6 Ga peak metamorphic fabric that is well

developed elsewhere (Dirks *et al.*, 1991). Predominantly undeformed igneous phenocrysts of sanidine and antiperthitic plagioclase are common (Fig. 2.10e). In addition abundant quartz and tourmaline-bearing veins and pegmatites cut the gneissic foliation and are themselves deformed (Fig. 2.10f). In Tyson Creek the augen-rich, well-foliated, Aloooya Gneiss contains melt segregations that are folded and show normal shear sense.

### 2.6.3 Tectonic evolution of the Anmatjira and Reynolds Ranges

Three major orogenic episodes, the Mount Stafford Event, the Strangways Orogeny and the Chewings Orogeny have affected the Northern Province. Controversy remains over the extent of deformation and metamorphism related to the Strangways Orogeny in this region. The Strangways Orogeny is limited to felsic magmatism and minor contact metamorphism and deformation in the Reynolds Range with the main period of low-pressure regional metamorphism and E-W fabric development occurring during the ~1.6 Ga Chewings Orogeny. Regional low-pressure metamorphism occurred at 1557 to 1587 Ma (Vry *et al.*, 1996; Rubatto *et al.*, 2001) causing greenschist (400°C) to granulite-facies (680 to 720°C) assemblages from NW to SE along the length of the Anmatjira and Reynolds Ranges (Dirks and Wilson, 1990; Clarke and Powell, 1991; Dirks *et al.*, 1991; Buick *et al.*, 1998; Rubatto *et al.*, 2001) (Fig. 2.11). Due to a stable high geothermal regime the growth of accessory phases continued over a 30 Ma period (Rubatto *et al.*, 2001), indicating metamorphism was long lived. M2 metamorphism was associated with tight to isoclinal NW-SE trending upright folding (F2) and the development of a penetrative, subvertical

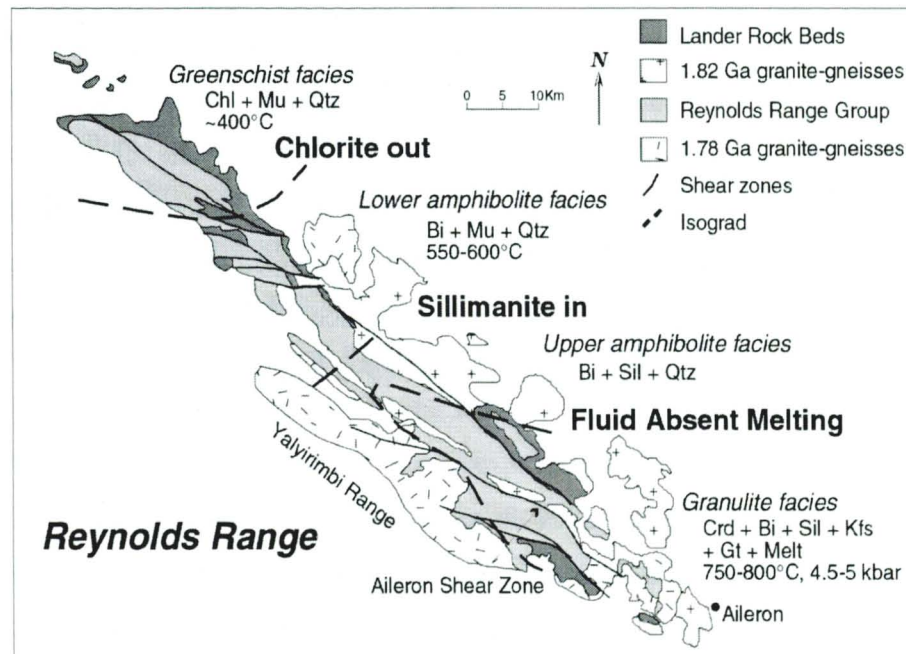
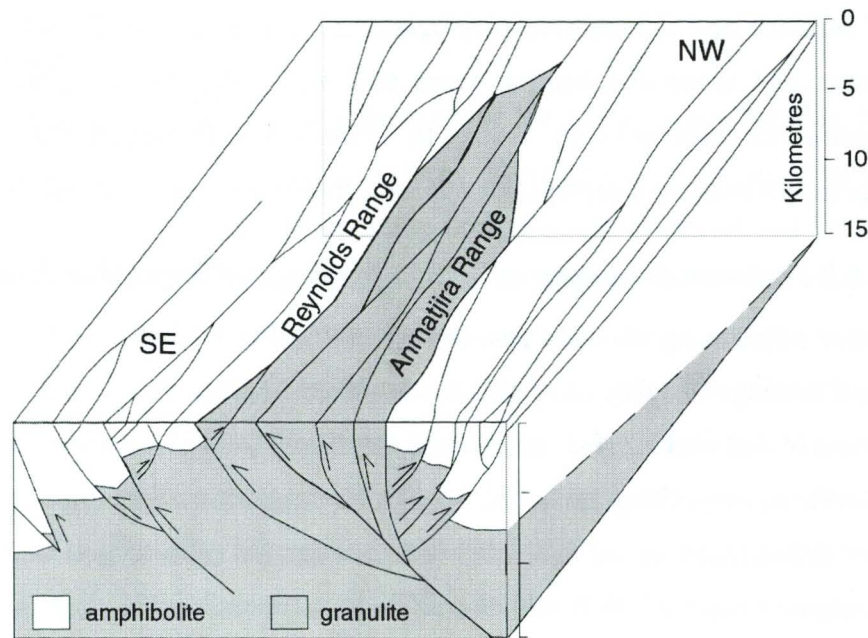


Figure 2.11. Isograds and metamorphic assemblages for the Reynolds Range after Rubatto *et al.* (2001).

foliation (S2) (Dirks *et al.*, 1991; Buick *et al.*, 1999b). Shear and crenulation bands, and local partial melt patches with retrogressive halos, represent retrogression following peak metamorphism

(Buick *et al.*, 1999). High-temperature (650-700°C and 560-625°C) hydrothermal quartz veins within the Reynolds Range Group (Cartwright *et al.*, 1996; Buick *et al.*, 1998) contain newly formed monazites and zircons with



**Figure 2.12.** Schematic block diagram representation of the proposed crustal pop-up structure that operated in the Northern Province, exposing the deep crustal granulites of the Anmatjira and Reynolds Ranges.

metamorphic overgrowths of  $1586 \pm 5$  Ma and  $1568 \pm 4$  Ma (Williams *et al.*, 1996), and  $\sim 1576 \pm 3$  Ma garnet (Buick *et al.*, 1999). The veins indicate fluid flow causing retrogression of granulite-facies rocks, following peak metamorphism. Epidote within the high-temperature quartz veins record ages of  $1454 \pm 34$  Ma and  $1469 \pm 26$  Ma (Buick *et al.*, 1999b). Multiple periods of fluid flow during slow cooling ( $\sim 3^\circ\text{CMy}^{-1}$ ) following M2 peak metamorphism is suggested by Buick *et al.* (1999b) to account for the large age difference. It is likely that the extensive  $\sim 1.81$  Ga and  $\sim 1.78$  Ga high heat-producing granites (high in Th, U and K), in the Anmatjira and Reynolds Ranges produced enough heat, over tens of millions of years, to create a high conductive geothermal gradient. An abundance of granite in the SE Anmatjira and Reynolds Ranges may account for the change in geothermal gradient along their length. The Chewings Orogeny is synchronous with contractional deformation elsewhere in the Arunta Inlier associated with high-grade metamorphism in the Mount Hay region of the Central Province and amphibolite-facies metamorphism in the Southern Province (Collins and Shaw, 1995 and references therein).

#### **2.6.4 Shearing and fluid flow**

A network of major NW-SE and W-E oriented N-dipping reverse-sense shear zones cut all the earlier structures within the Northern Province. They contain lower grade amphibolite- to greenschist-facies assemblages with local kyanite-bearing pelitic schists. Dirks and Wilson (1990) describe two distinct deformation phases in the greenschist-facies shear zones within the Reynolds Range, earlier south-directed reverse movement and later

dextral strike slip (Dirks and Wilson, 1990). To date the shear zones of the Reynolds Range have yielded only Alice Spring ages (Cartwright *et al.*, 1999), with no earlier Anmatjira Uplift Phase ages, as are reported from elsewhere in central Australia (Collins and Shaw, 1995; Shaw and Black, 1991). Collins and Teyssier (1989) propose that a crustal scale pop-up structure operated in the Northern Province (Fig. 2.12). Relative movement across N- and S-facing shear zones have uplifted granulite-facies rocks along the Anmatjira and Reynolds Ranges during a contractional regime (Collins and Teyssier, 1989). These crustal-scale shear zones allow the examination of fluid-flow processes throughout the crust. The shear zones examined for this study occur within the southeastern Anmatjira (Chapter Three) and Reynolds Ranges (Chapter Four), where amphibolite-facies shear zones disrupt granulite-facies poly-metamorphic terrains.

## 2.7 CENTRAL PROVINCE

The Central Province is a narrow elongate sequence of dominantly high-grade mafic and felsic rocks. The western Central Province is relevant to this study because its southern margin is the hanging wall of the Redbank High Strain Zone (Fig. 2.13). To the east, the Central Province includes the Strangways Metamorphic Complex and the Harts Range region. Both these regions are currently the focus of more geochronological and structural interpretation due to the recent dating of granulites that record Palaeozoic high-grade metamorphism during the Larapinta Event (Miller *et al.*, 1998; Hand *et al.*, 1999; Mawby *et al.*, 1999; Buick *et al.*, 2001).

### 2.7.1 Lithologies

The Central Province comprises felsic and mafic granulites, probably of volcanic origin, with minor quartzofeldspathic gneisses and calc-silicate rocks, similar to those in the Northern Province (Stewart *et al.*, 1984; Warren and Shaw, 1995). The metamorphic grade across the Central Province ranges from granulite-facies in the west to amphibolite-facies in the east. Unlike the Northern and Southern Provinces there are relatively few granite bodies within the Central Province (Stewart *et al.*, 1984; Glikson, 1987). The Narwietooma Metamorphic Complex forms the basement of the Central Province and is intruded by the Mount Zeil Granite, the Forty-five Augen Gneiss and the Anburla Anorthosite. The basement units that make up the Palaeoproterozoic Narwietooma Metamorphic Complex include the Mount Chapple Metamorphics, the Mount Hay Granulite and the Bunghara Metamorphics. Although the ages of the igneous parent lithologies are unknown, all the units within the Narwietooma Metamorphic Complex underwent high-grade, regional metamorphism and associated deformation and magmatic activity during the Strangways

Orogeny (1780 to 1720 Ma; Black and Shaw, 1992) and the 1.6 Ga Chewings Orogeny (Collins, 2000).

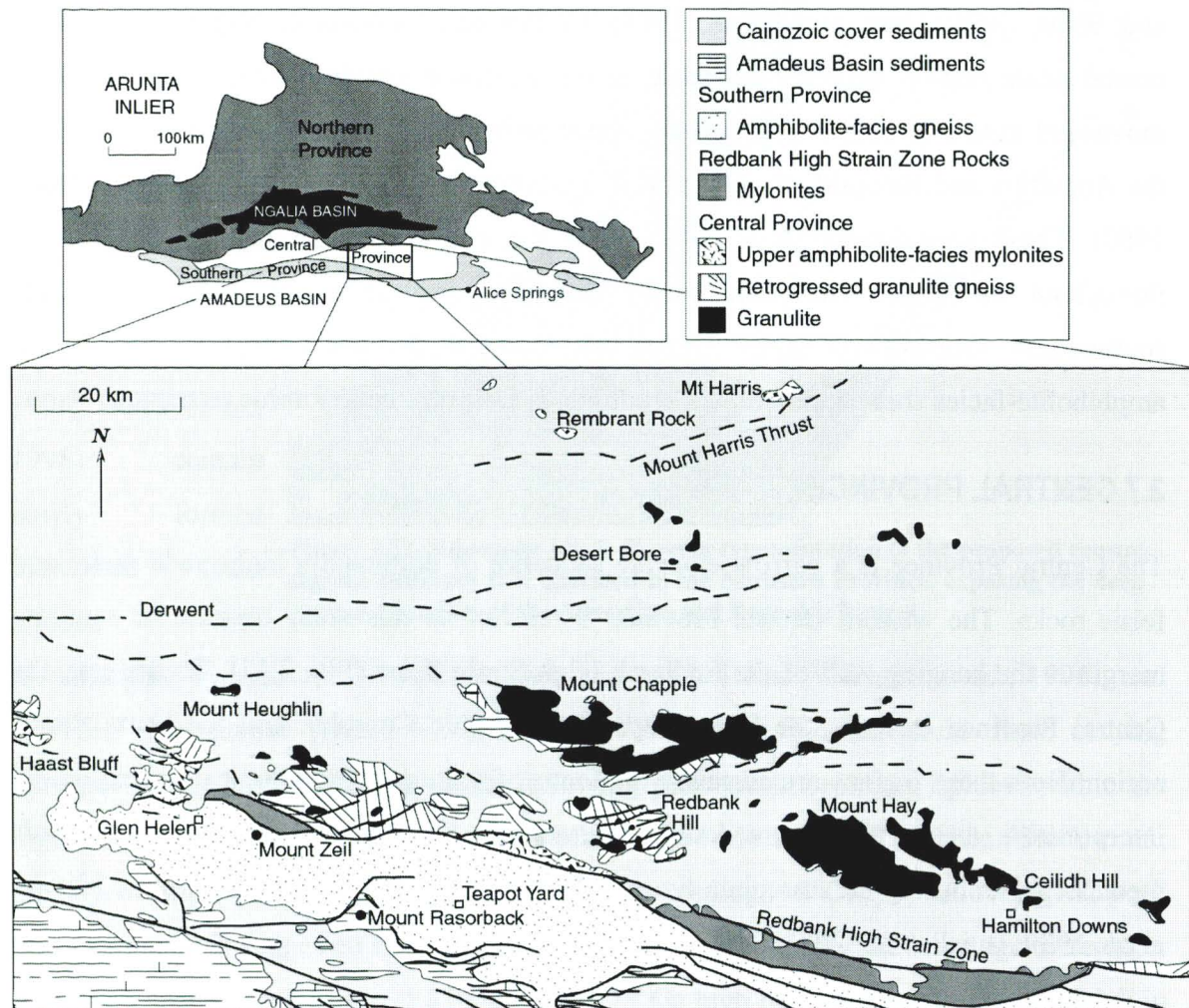


Figure 2.13. Geological map of the western Central Province, Redbank High Strain Zone, Southern Province and Amadeus Basin, after Shaw and Black (1991).

Overall, the Narwietooma Metamorphic Complex has a WNW-oriented gneissic fabric, which dips to the north (Glikson, 1987), and is parallel to the regional tectonic fabric. Felsic and intermediate gneisses of the Rendall Peak Metamorphics, to the east, are chemically similar to the Narwietooma Metamorphic Complex felsic and intermediate rocks (Warren and Shaw, 1995) and are dated at 1770 Ma (Zhao *et al.*, 1992). However, stratigraphic interpretation to the north suggests that the Narwietooma Metamorphic Complex might underlie the ~1880 Ma Lander Rock Beds (Young *et al.*, 1995). It is clear that the Narwietooma Metamorphic Complex forms the Palaeoproterozoic basement of the western Central Province, but, more detailed data is required to determine the stratigraphic position and relative age of the Complex within the Arunta Inlier.

The Mount Chapple Metamorphics, exposed at Mount Chapple and the low hills to the east (Fig. 2.13), are dominantly felsic, with intermediate and felsic granulites commonly forming migmatites. The area is also intruded by granite pods and veins and contains some metasediments (Glikson, 1987). The Mount Hay Granulite (Mount Hay Massif) is exposed at Mount Hay and Ceilidh Hill (Fig. 2.13). It comprises dominantly mafic granulite (Fig. 2.9e) containing numerous bands of intermediate (leucogabbro-anorthosite) and felsic (tonalitic-granodioritic) gneisses (Fig. 2.9f) with minor intercalated paragneiss layers (Glikson, 1987; Warren and Shaw, 1995). The Mount Hay Granulite appears to grade into the Mount Chapple Metamorphics to the west (Warren and Shaw, 1995). The Bungbara Metamorphics are exposed at Mount Heughlin and along the northern edge of the RHSZ (Fig. 2.13). The unit comprises meta-igneous gneisses of mafic to intermediate composition with minor meta-sediments containing granulite-facies assemblages and minor melt segregations (Warren and Shaw, 1995).

### **2.7.2 Tectonic history**

The earliest identified metamorphism and deformation from the Central Province occurred at ~1880 Ma (Young *et al.*, 1995) predominantly to the west of the study area. Inferences of two granulite-facies events from corona textures in the Mount Hay-Mount Chapple region have been recently supported by SHRIMP dating of zircons from granulites and megacrystic granites (Collins, 2000). The first regional granulite-facies metamorphism occurred at ~1770 Ma (The Strangways Orogeny) and the second at ~1600 Ma (The Chewings Orogeny; Collins, 2000). The Strangways Event (1780 to 1730 Ma) caused widespread high-temperature and moderate-pressure granulite-facies metamorphism (850°C and 6 to 9kbar) with associated dehydration melting producing migmatites (Warren and Shaw, 1995; Collins and Shaw, 1995). Felsic magmatism followed the Strangways Event (Iyer *et al.*, 1976; Black *et al.*, 1983; Shaw *et al.*, 1984; Black and Shaw, 1992). Deformation associated with the granulite-facies metamorphism produced sheath-like folds coaxial about an extensive NE-plunging mineral lineation (Black and Shaw, 1992; Collins and Sawyer, 1996; Collins, 2000) and a layer-parallel fabric within the Narwietooma Metamorphic Complex (Warren and Shaw, 1995). The Chewings Orogeny at ~1600 is the first major tectonic event recorded from both the Central and Southern Provinces. Granulite-facies (700 to 800°C and 7 to 8kbar) metamorphism of the Chewings Orogeny was associated with up-right folding in the Mount-Hay and Mount Chapple region (Collins, 2000). Undeformed E-W dykes in the Redbank Hill area reached granulite-facies conditions (Warren and Shaw, 1995) during this event.

### **2.7.3 Crustal reworking**

Along the eastern end of the northern MacDonnell Ranges, the Bunghara Metamorphics are foliated, folded, and strongly lineated, suggesting they have been entrained in the Redbank High Strain Zone (Warren and Shaw, 1995). The development of a strong mylonitic foliation is associated with garnet, plagioclase and hornblende decompression reactions in mafic mylonite gneisses (Read *et al.*, 1999; Chapter Six). Mylonite zones also occur along the southern edge of the Central Province throughout the Mount Hay Granulite and the Mount Chapple and Bunghara Metamorphic Complexes.  $^{40}\text{Ar}$ - $^{39}\text{Ar}$  cooling ages of biotite of  $435 \pm 4$  Ma within the Mount Hay Granulite suggest that these shear zones represent Alice Springs age movement on the Redbank High Strain Zone (Shaw *et al.*, 1992). Uplift of Central Province rocks along the Redbank High Strain Zone is indicated by the change in peak pressure estimates across the Redbank High Strain Zone in the order of 20km vertical distance (Shaw and Black, 1991). This uplift is thought to have occurred during both the Anmatjira Uplift Event and the Alice Springs Orogeny (Shaw and Black, 1991) and is reviewed with new geochronological data in Chapter Seven.

In summary, the Central Province forms a dominantly high-grade, meta-igneous polydeformed metamorphic province, with pressure conditions estimated at a maximum of 8 kbars suggesting these are exhumed deep-crustal rocks. Shear zones that were active during the Alice Springs Orogeny cut the granulites.

## **2.8 REDBANK HIGH STRAIN ZONE**

The Redbank High Strain Zone forms a 400 kilometre long boundary between the Central and Southern Provinces in the southern Arunta Inlier (Fig. 2.2). Varying from a few hundred metres up to 20 kilometres in width, the Redbank High Strain Zone comprises a range of brittle and ductile deformation zones associated with steeply north-dipping, south-verging, imbricate thrust movement. The high strain zone is proposed to either juxtapose two different vertical depth sections of the same age or to separate two terranes of different ages (Glikson, 1987).

### **2.8.1 Deep structure of the Redbank High Strain Zone**

Geophysical studies over the last two decades within central Australia, especially concentrating on the Redbank High Strain Zone, have been stimulated by the substantial anomalies in crustal structure in the region (Lambeck and Penney, 1984; Goleby *et al.*, 1990; Wright *et al.*, 1990; Lambeck, 1991; Shaw *et al.*, 1991; Shaw, 1991; Korsch *et al.*, 1998).

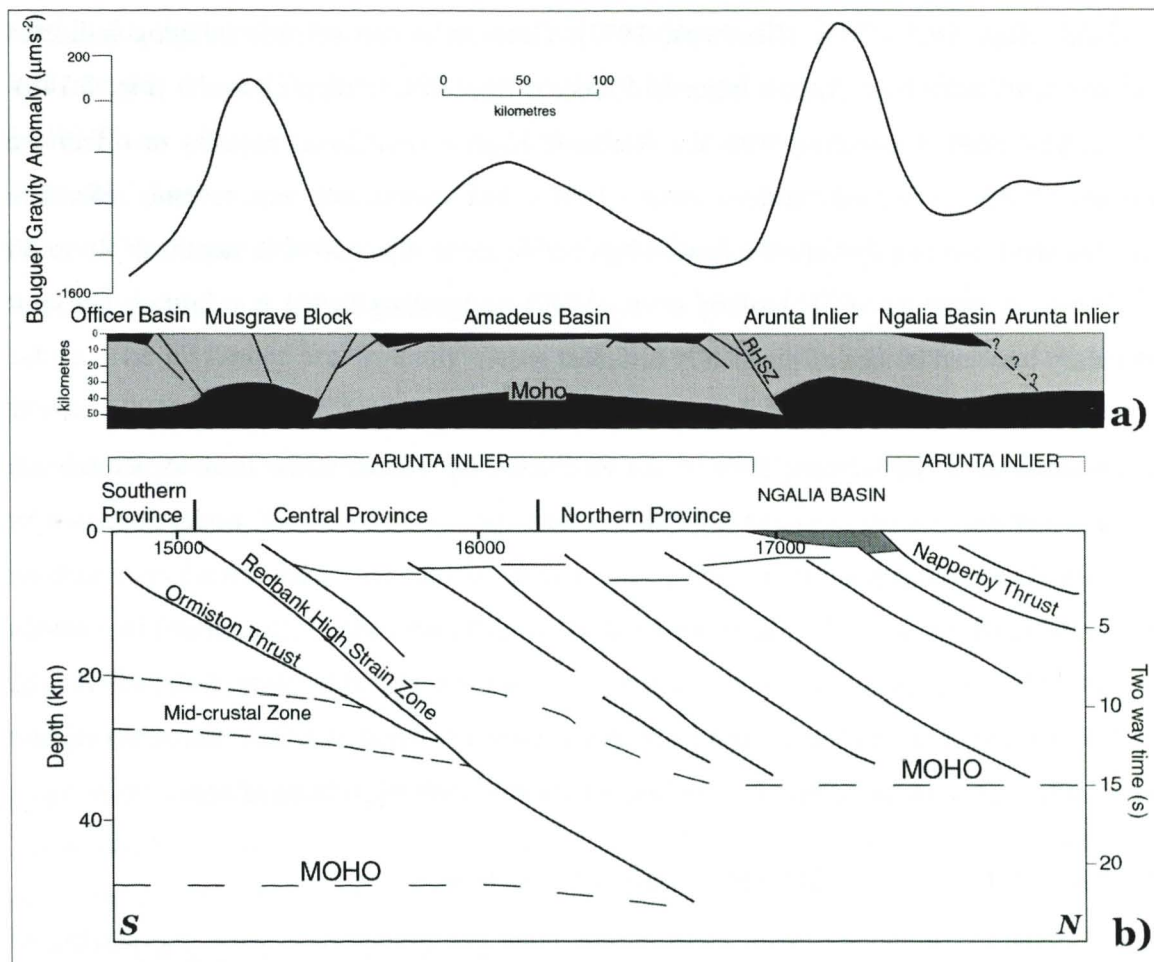


**Figure 2.14.** a) Bouguer gravity anomaly across the Arunta Inlier, after Goleby *et al.* (1990) and Shaw *et al.* (1991) with an associated cross section showing the major structures across central Australia. b) Structural interpretation following deep reflection seismic imaging across the Redbank High Strain Zone, after Goleby *et al.* (1990), Lambeck (1991) and Korsch *et al.* (1998).

Large linear positive Bouguer anomalies are associated with the exposed basement in the southern Arunta Inlier and Musgrave Block (Fig. 2.14a). These gravity anomalies are significant on a world scale with change in the Bouguer gravity of  $\sim 1400 \mu\text{ms}^{-2}$  across the Arunta Inlier, and have been interpreted as imaging major discontinuities within the crust (Shaw *et al.*, 1991; Goleby *et al.*, 1990). The largest changes in Bouguer gravity occur across the Redbank High Strain Zone where the strongly negative anomalies within the Amadeus Basin change to strongly positive anomalies where the basement is exposed to the north (Shaw *et al.*, 1991). It has been suggested that rapid cooling, stimulated by the removal of the basinal sediments during erosion, may have caused the freezing of these large gravity anomalies into the central Australian crust during the denudation caused by the Palaeozoic Petermann and Alice Springs Orogenies (Sandiford and Hand, 1998b). E-W trending teleseismic travel-time anomalies have also been recorded in the Amadeus Basin and Arunta Inlier. An abrupt change occurs from relatively low-velocity material in the

south to relatively high-velocity material in the north coinciding approximately with the Redbank High Strain Zone (Lambeck, 1991). Deep reflection seismic imaging indicates that the crust across the Arunta Inlier is dissected by similarly dipping faults (Fig. 2.14b). The largest fault, coinciding with the Redbank High Strain Zone, appears to offset the Moho by ~15 kilometres (Goleby *et al.*, 1990). The teleseismic and seismic reflection imaging data indicate that the Redbank High Strain Zone dips 45° N to depths of 40 to 50 kilometres (Lambeck, 1991; Goleby *et al.*, 1990), suggesting that it is a large-scale fault boundary between blocks of physically different crust.

Interpretations of the tectonic style of the Redbank High Strain Zone from structural and geophysical data include thin and thick-skinned models. A thin-skinned model proposed by Teyssier (1985), suggests that the steep thrust structures in the upper crust join a shallow dipping sole thrust at depth. The more popular thick-skinned models, proposed by Forman and Shaw (1973), Lambeck (1991) Shaw *et al.* (1984, 1991) and Korsch *et al.* (1998) (Fig. 2.14b) suggest that the fault zones are deep structures that displace the crust-mantle boundary, as seen in the reflection profiling of the Redbank High Strain Zone.

### **2.8.2 Mylonites of the Redbank High Strain Zone**

The boundaries of the Redbank High Strain Zone are gradational, with interleaving of shear zone mylonites and unsheared host rock (Glikson, 1987; Fliervoet *et al.*, 1997). The gneisses are commonly migmatitic and locally contain feldspar augen. The sheared rocks within the Redbank High Strain Zone are thought to be equivalents to these units. They are commonly quartzofeldspathic, some containing garnet and/or amphibole, and are typically of amphibolite-facies metamorphic grade with some greenschist-facies overprinting associated with shearing (Obée and White, 1985; Shaw and Black 1991). They commonly occur as protomylonite, mylonite, ultramylonite and phyllonite formed in a heterogeneous shear regime (Glikson, 1987; Warren and Shaw, 1995).

### **2.8.3 Tectonic history**

Rocks of the southern Arunta Inlier, in the vicinity of the Redbank High Strain Zone, record several tectonic events, ranging from the Palaeoproterozoic through to the Devonian (Table 2.1; Marjoribanks and Black, 1974; Shaw *et al.*, 1984; Shaw and Black, 1991; Black and Shaw, 1992; Shaw *et al.*, 1992; Zhao *et al.*, 1992; Collins *et al.*, 1995; Collins and Shaw, 1995). The early high-grade metamorphic histories of the provinces that are now juxtaposed by the RHSZ are described in the Central and Southern Province sections (2.7 and 2.9).

Dating of amphibolite-facies, south-directed shearing of the Redbank High Strain Zone indicate that the earliest preserved ages are 1450 Ma, and developed during the Anmatjira Uplift Phase (Shaw and Black, 1991). This event is recorded in shear zone north of the Redbank Thrust within the Central Province. To date, no Anmatjira Uplift Phase ages are recorded from the Southern Province. The Anmatjira Uplift phase produced wide E-NE trending shear zones containing amphibolite-facies (550 to 600°C) mylonites with gneissic fabric. The mylonites are typically augen rich and form L and L-S tectonites (Shaw and Black, 1991). Abundant asymmetric folding and rotated porphyroclasts indicate reverse movement across individual shear zones. Felsic magmatism occurred throughout the Southern Province and Redbank High Strain Zone during the Teapot Tectonomagmatic Event (1200 to 1150 Ma; Shaw and Black, 1991; Black and Shaw, 1992; Shaw *et al.*, 1992), indicating that the Central and Southern Provinces were juxtaposed by Mesoproterozoic time. The Teapot Tectonomagmatic Event also produced pegmatite dykes and local migmatisation that intrude mylonite zones throughout the Southern Province. No migmatisation or pegmatite formation occurred after the Teapot Tectonomagmatic Event. Therefore the shear zones that are intruded by pegmatites and/or melt segregations are older than 1200 Ma. These shear zones are likely to be related to the Anmatjira Uplift Event (Shaw and Black, 1991). A later thermal pulse that produced the Stuart Pass Dolerite Dyke Swarm (~1050-900 Ma; Zhao and McCulloch, 1993) in the Southern Province is likely to have produced the N-S oriented mafic dykes that also cut the early mylonite zones in the Redbank High Strain Zone. The dolerite dykes are subsequently offset by shearing during the Alice Springs Orogeny (Collins and Shaw, 1995). Mylonites formed during the Alice Springs Orogeny typically occur in narrow E-SE trending zones, have a schistose fabric, and form LS and S tectonites. They contain greenschist-facies minerals (350 to 450°C) with a matrix texture indicative of dynamic recrystallisation (Shaw and Black, 1991). SC fabrics, shear bands and rotated porphyroclasts indicate predominantly reverse movement across the Alice Springs Orogeny shear zones of the Redbank High Strain Zone, with a lesser component of dextral strike slip. During shearing, deformation was focussed along pre-existing structures creating an overall anastomosing E-W foliation (dipping 40°N) and lineation (steeply plunging NE) across the entire zone.

## 2.9 SOUTHERN PROVINCE

The Southern Province forms a narrow, E-W oriented, complexly-deformed metamorphic terrain, overlain by the Amadeus Basin sediments to the south and fault bounded against the Central Province to the north by the Redbank High Strain Zone. The Southern Province

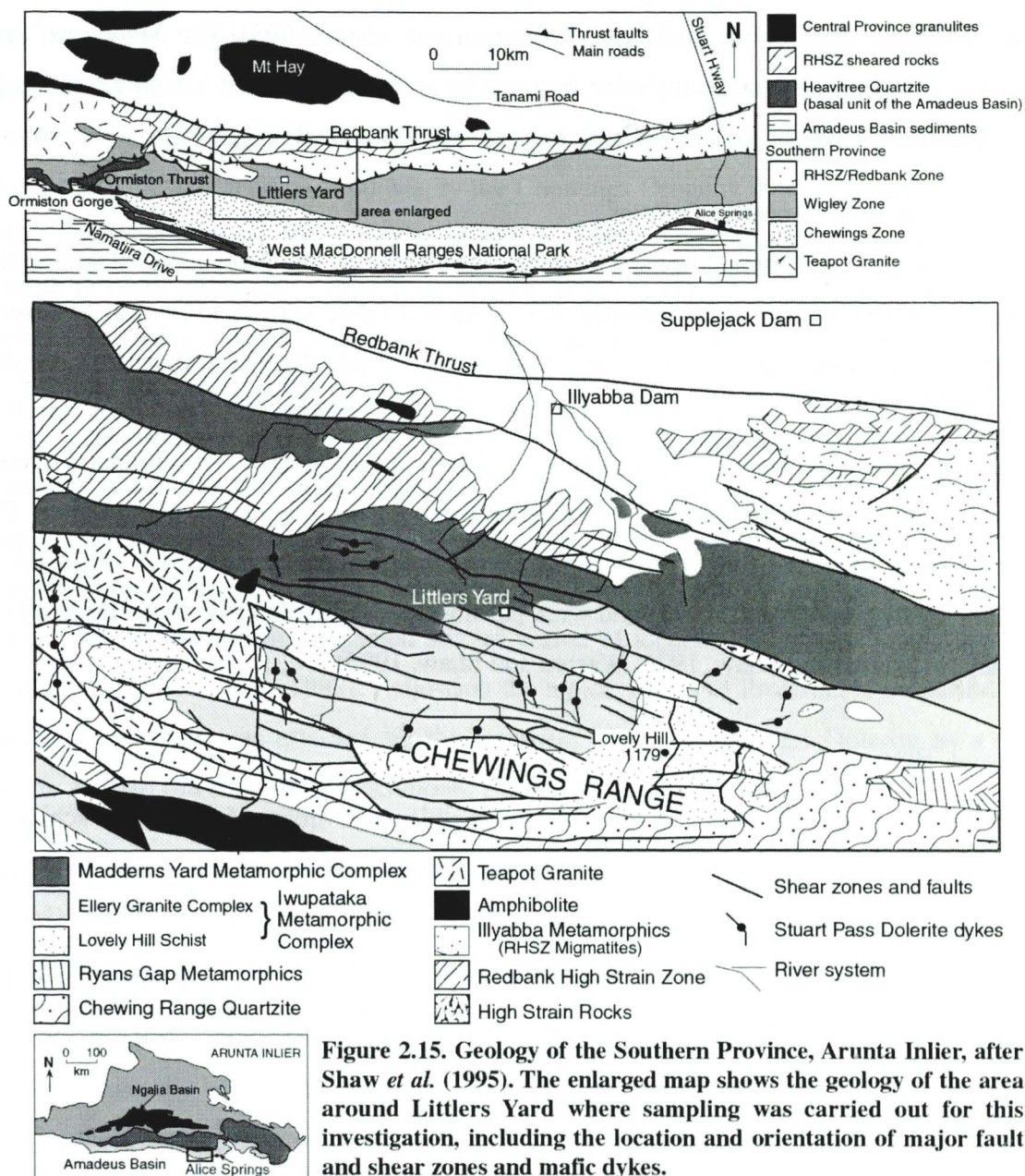
has been divided into three structural and lithological zones: the Redbank, Wigley, and Chewings Zones (Fig. 2.15). The Redbank Zone, in the north of the province, comprises highly mylonitized rocks. The Wigley Zone, in the centre, contains mainly migmatite gneisses of the Madderns Yard Metamorphic Complex, and the Chewings Zone, in the southeast, comprises meta-volcanic rocks and schists of the Simpsons Assemblage (Collins and Shaw, 1995). The Chewings and Wigley Zones are fault-bounded by the Palaeozoic Ormiston Thrust Zone (Shaw *et al.*, 1992) and prior to its development, the two zones were likely to have been continuous (Collins and Shaw, 1995).

Rocks of the Southern Province are generally composed of banded quartzofeldspathic and granitic gneiss, unconformably overlain by silicic and aluminous meta-sedimentary rocks (Black and Shaw, 1992) regionally metamorphosed to amphibolite-facies conditions during the Proterozoic Chewings Orogeny (~1.6Ga) (Black and Shaw, 1992). Abundant granitic magmatism occurred throughout the Proterozoic during the Strangways Orogeny and Argilke Event (Table 2.1, Black and Shaw, 1992), with less voluminous mafic igneous intrusives including the Stuart Pass Dolerite Dyke Swarm (~1080 Ma, Zhao and McCulloch, 1993). The Southern Province is cut by numerous E-W trending, steeply north (45 to 80°) dipping faults and shear zones (Fig. 2.15). They predominantly have N to NE plunging lineations that show southward reverse movement ranging in size from centimetre-scale shear bands to the crustal-scale Ormiston Thrust (Teyssier, 1985). The fault zones are characterised by a northward change in dominant deformation mechanisms from cataclastic to progressively more mylonitic (Teyssier, 1985). Lower greenschist-facies assemblages of chlorite, green biotite and muscovite define the mylonitic fabric of the northern shear zones within the Wigley Zone (Collins and Teyssier, 1989).

### **2.9.1 The Wigley Zone**

Shear zones hosted by the Madderns Yard Metamorphic Complex and the Iwupataka Metamorphic Complex within the Wigley Zone were sampled during this investigation. All of which have undergone amphibolite-facies metamorphism during the Chewings Orogeny (Collins and Shaw, 1995). The rocks that form the base of the Iwupataka Metamorphic Complex have intercalated felsic to mafic volcanic and sedimentary protoliths (Warren and Shaw, 1995). The Stuart Pass Dolerite Swarm form approximately north-south oriented dykes that range from 1 to 50m in width and show variable offsetting across shear zones (Warren and Shaw, 1995). The shear zones that disrupt the dolerite dykes imply they were re-activated during the Alice Springs Orogeny. The shear zones that are cut by intact dykes indicate no post ~1050 Ma shearing. Amphibolite-facies shear zone assemblages are

considered to indicate Proterozoic shearing, with greenschist-facies shear assemblages indicating Alice Springs ages.



### 2.9.1.1 Madderns Yard Metamorphic Complex

The Madderns Yard Metamorphic Complex forms the basement and comprises migmatized quartzofeldspathic gneisses representing intercalated sediments and mafic to felsic volcanics (Warren and Shaw, 1995). Both high-Y, low-Sr intracrustal and high-Sr and low-Y sub-crustal melting signatures are recorded from gneisses of the Madderns Yard Metamorphic Complex, suggesting variation in the ages of melting (Warren and Shaw, 1995). The migmatitic quartzofeldspathic and garnet biotite gneisses that form the

dominant lithology of the Madderns Yard Metamorphic Complex are intensely folded in the Littlers Yard area (Fig. 2.9g). The gneisses show at least two generations of migmatite, probably formed during upper amphibolite-facies metamorphism of the Chewing Orogeny and the Teapot Tectonomagmatic Event (Warren and Shaw, 1995). The Madderns Yard Metamorphic Complex migmatites are intruded by the Ellery Granitic Complex, although most of the exposed contacts in the Littlers Yard area are faulted (Fig. 2.15).

#### *2.9.1.2 Iwupataka Metamorphic Complex*

The Madderns Yard Metamorphic Complex is overlain by the Iwupataka Metamorphic Complex, which comprises intercalated sediments and felsic volcanics, as well as several granites (Warren and Shaw, 1995). The granitic units include the Ellery Granites Complex (Warren and Shaw, 1995), and the Ormiston Pound Granite that contained the first recorded Chewings Orogeny ages (1.6 Ma, Collins *et al.*, 1995). The Teapot Granitic Complex forms a large complex of quartzofeldspathic gneiss, migmatites and granites. The granites were produced during the Teapot Tectonomagmatic Event (1.2-1.1 Ga Black *et al.*, 1983; Shaw and Black, 1991) and were possibly derived from extensively migmatized volcanics (Collins and Shaw, 1995; Warren and Shaw, 1995).

#### *The Lovely Hill Schist*

The Lovely Hill Schist forms interlayered pelitic and quartzofeldspathic schist of amphibolite-facies metamorphic grade. A fine- to medium-grained and finely laminated muscovite and biotite-schist is exposed at the foot of the Chewing Range. Ellery Granite Complex granites SW of Littlers Yard intrude the Lovely Hill Schist, however, commonly it overlies the granite gneiss.

#### *The Ellery Granitic Complex.*

The Ellery Granite Complex consists of several different granitic gneisses that occur to the north and south of the Chewings Range. The presence of large K-feldspar porphyroclasts suggests the gneiss originated as a S-type granite. In the Littlers Yard area the Ellery Granitic Complex occurs as layered leucocratic augen gneiss and granitic gneiss (Fig. 2.9h). Melt segregations within the gneisses imply that upper amphibolite-facies conditions were reached during regional metamorphism. Aligned biotite and compositional layering define an E-W-oriented gneissic foliation.

### **2.9.2 Tectonic and metamorphic history**

All three tectonic zones of the Southern Province have been subjected to three major regional metamorphic events, namely the Argilke Tectonic Event, the Chewings Orogeny and the Teapot Tectonomagmatic Event (Table 2.1). The oldest event is the Argilke Tectonic Event at 1680 to 1650 Ma (Collins *et al.*, 1995; Collins and Shaw, 1995) which caused pervasive amphibolite-facies assemblages throughout the Southern Province. This event was followed at 1610-1600 Ma by the Chewings Orogeny (Marjoribanks and Black, 1974; Zhao and Bennett, 1995; Collins and Shaw, 1995). The Chewings Orogeny produced a north to south gradation of upper amphibolite-facies to greenschist-facies assemblages in association with the development of an intense regional W-E-trending schistosity and tight to isoclinal folding (Collins and Teyssier, 1989; Collins *et al.*, 1995; Collins and Shaw, 1995). Chewings-age tectonism also produced widespread migmatisation of the Madderns Yard Metamorphic Complex followed by the development of retrogressive north-directed high strain zones during cooling (Teyssier *et al.*, 1988; Collins and Shaw, 1995). The Teapot Tectonomagmatic Event occurred at 1200-1100 Ma. It produced voluminous granitic intrusions and an associated second period of localised migmatisation (Black and Shaw, 1992; Shaw *et al.*, 1992). Following the major phases of Proterozoic orogenesis the Southern Province was affected by the intrusion of the Stuart Pass Dolerite as a dyke swarm at 1080 Ma (Zhao and McCulloch, 1993).

The Anmatjira Uplift Phase is thought to have produced mylonitization north of the Redbank Zone at 1400 to 1500 Ma (Shaw *et al.*, 1991). However, it is unclear how much affect the event had within the Southern Province. Mineral ages and structural evidence are sparse, possibly due to re-equilibration of isotopic ratios during the Teapot Tectonomagmatic Event. The effects of the Alice Springs Orogeny are inferred throughout the Southern Province through sheared offsets of the dolerite dykes and the presence of greenschist-facies assemblages within narrow reactivated and primary shear zones. Little geochronological data is available south of the Redbank Zone.

### **2.10 SUMMARY**

The Arunta Inlier, preserves evidence of multiple orogenic activities throughout the Proterozoic and Palaeozoic. It forms a distinctive metamorphic province surrounded by correlated Neoproterozoic basins. Tectonic activity during the Alice Springs Orogeny segmented the Centralian Superbasin and represents the last orogen within the region. The abundance of shear zones within diverse lithologies and of a variety of sizes throughout the Arunta Inlier provides an excellent opportunity to study fluid-rock interaction in the middle

crust. The continental setting of the Alice Springs Orogeny also provides a basis for studying crustal-scale fluid flow during intraplate orogeny.

## CHAPTER THREE

# THE ROLE OF FLUIDS IN CHEMICAL AND MECHANICAL PARTITIONING WITHIN SHEAR ZONES OF THE NORTHERN ARUNTA INLIER, CENTRAL AUSTRALIA

### **Abstract**

A NW-SE-oriented network of anastomosing shear zones in the northern Arunta Inlier cuts both granitic orthogneisses and paragneisses of the Proterozoic basement. Many of the shear zones that cut granitic orthogneisses are substantially compositionally zoned, with predominantly siliceous orthoschists and protomylonites alternating with narrow phyllonite and less commonly, foliated cataclasite domains. The presence of annealed cataclasite in bands within the Yalbadjandi Shear Zone indicates that heterogeneous brittle deformation occurred early during shearing. The cataclasites were subsequently partially recrystallised during shearing. Hydrous reactions stimulated by fluid channelling may have led to the development of some of the phyllonite zones from cataclasites. The ductile shear zones throughout the northern Arunta Inlier contain silica-poor phyllonite domains and silica-rich orthoschist and protomylonite domains. The development of compositional domains within the ductile shear zones is the result of strain partitioning, hydration reactions, and silica dissolution and precipitation via fluid transfer at upper greenschist-facies conditions. The extensive lateral silica redistribution suggests that within the whole shear zone system strain gradients and pressure changes may effect the dissolution and precipitation of silica to a greater extent than temperature changes along the flow path. Fluid-rock interaction may be significantly affected by the mechanics of fluid-assisted mass transfer, and any attempts to use geochemical changes to quantify the direction of fluid flow or fluid fluxes must take this into account.

### **3.1 INTRODUCTION**

Fluid flow in the middle crust can be recognised through the formation of hydrous minerals and chemical alteration of rocks (e.g. Beach, 1980; Dipple *et al.*, 1990; Selverstone *et al.*, 1991; McCaig, 1997; Cartwright and Buick, 1999). This is especially obvious where fluid has been channelled through rocks with low water contents, such as granites and high-grade metamorphic rocks (O'Hara 1988; Selverstone *et al.*, 1991; Streit and Cox, 1998, Cartwright and Buick, 1999). During large-scale fluid flow, fluids typically become channelled within fractures and shear zones where permeability maybe orders of magnitude greater than in the adjacent wall rock (e.g. Ferry, 1994; Rumble, 1994; Henderson and McCaig, 1997). Indeed, within rocks of low static permeability, such as those in the middle crust, fluid may be relatively immobile without deformation. (Upton, 1998). Deformation enhanced permeability in fault zones is typically a transient property, being created and destroyed during progressive shearing. Thus, the conditions of shearing,

mechanisms of fluid movement, and volume of fluid that infiltrates shear zones control the degree of fluid-rock interaction. The growth of hydrous minerals within shear zones during fluid-rock interaction promotes strain accommodation, which in turn locally creates high permeability and thus promotes further fluid infiltration (Ferry, 1994; Rumble, 1994; Wintsch *et al.*, 1995; McCaig, 1997). Continued fluid flow through zones of high strain leads to chemical and mechanical changes that promote increased ductility and strain accommodation. Clearly, fluid-rock interaction during shearing is intimately involved in the mechanical and chemical changes that take place within shear zones.

This chapter discusses fluid flow through shear zones in the northern Arunta Inlier that preserve the crustal response to intercontinental compression. Microstructural and chemical characteristics of the shear zones are used to infer mechanisms of fluid-rock interaction and shear zone development. An understanding of the mechanisms of chemical transfer are important as these shear zones contribute to the overall chemical recycling that occurs within the crust.

### 3.2 GEOLOGICAL SETTING

A detailed discussion of central Australian geology is presented in Chapter Two, with a review of the northern Arunta Inlier, including the Anmatjira and Reynolds Ranges. Only a brief review of the main geological features is presented here, in order to establish the geological setting of the shear zones.

The NW-SE-trending Anmatjira and Reynolds Ranges, in the northern Arunta Inlier, expose a series of Proterozoic multiply-metamorphosed and deformed rocks of both sedimentary and igneous origin (Fig. 3.1). The Palaeoproterozoic turbidite basement was intruded by voluminous granitoid bodies at 1.81 and 1.78 Ga (Collins and Williams, 1995; Vry *et al.*, 1996) during major crustal building events. At ~1.59 Ga the Chewings Orogeny locally produced low-pressure metamorphism (Vry *et al.*, 1996; Williams *et al.*, 1996; Rubatto *et al.*, 2001) accompanied by tight to isoclinal upright folding and the development of a NW-SE oriented foliation (Collins and Shaw, 1991). The Chewings Orogeny is recognised throughout the Arunta Inlier as a period of compression associated with regional fabric development, though the tectonic environment remains unclear. Metamorphism reached granulite facies in the SE Anmatjira and Reynolds Ranges (~750°C and ~5kbar) and greenschist-facies (~400°C and 4-5kbar) in the NW (Clarke *et al.*, 1990; Fig. 3.1).

The high-grade gneisses of the SE Anmatjira and Reynolds Ranges form the core of a crustal pop-up structure, where reverse movement across a network of sub-parallel NW-SE-oriented N- and S-dipping shear zones juxtapose slices of mid-crustal rocks (Fig. 3.1b; Collins and Teyssier, 1989). The shear zones cut all earlier structures within the Proterozoic metamorphic province and were most likely to have been active during

the Alice Springs Orogeny as part of the inversion process that exposed the Arunta Inlier. The geochronology and tectonic history of the shear zone network formation in the northern Arunta Inlier is further discussed in Chapter Five.

The shear zones range in size from centimetres to hundreds of metres wide and metres to kilometres long, creating an interlinking network of large NW-SE-oriented and smaller W-E-oriented shear zones. The NW-oriented Aileron Shear Zone, on the southern flank of the Reynolds Range, is a steeply NE-dipping crustal-scale structure that cuts the moHo (Lambeck *et al.*, 1988) and separates granulite-facies assemblages to the north from upper

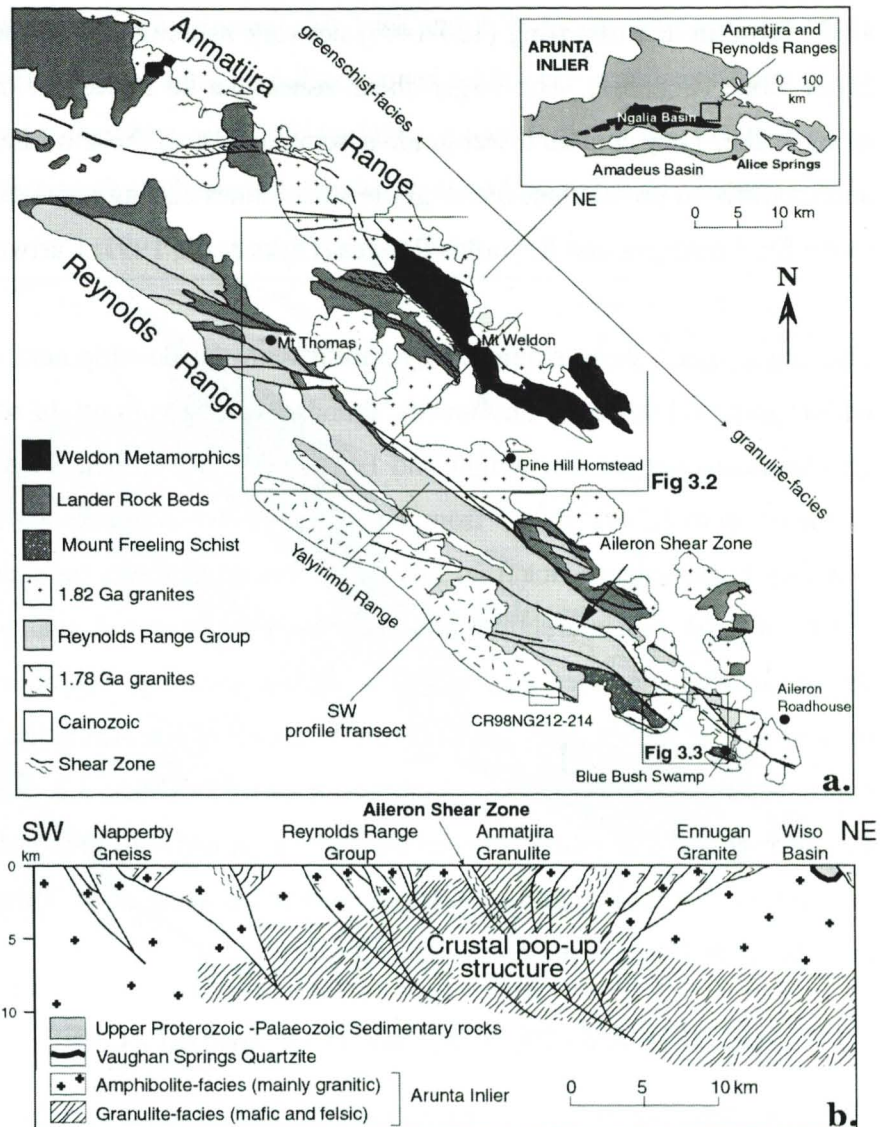


**Figure 3.1.** a) General geological map of the Anmatjira and Reynolds Ranges, Northern Province, Arunta Inlier, showing the location of major shear and fault zones. The boxes indicate the areas under investigation detailed in Figs. 3.2 and 3.3. b) Cross section SW to NE across the Reynolds and Anmatjira Ranges (after Collins and Teyssier, 1989) showing the geometry of shear zones associated with a crustal pop-up structure.

amphibolite-facies assemblages to the south (Fig. 3.1). The shear zones examined in this study form an anastomosing (120-140°) network associated with the crustal-scale Aileron Shear Zone (Fig. 3.1). The larger shear zones can be traced for hundreds of kilometres along strike. They contain lower grade assemblages than those of their host lithologies with amphibolite- to greenschist-facies grade shear zones cutting areas of granulite-facies rocks in the SE Anmatjira and Reynolds Ranges (Dirks *et al.*, 1991; Cartwright *et al.*, 1999).

The shear zones show extensive hydration with the development of phyllonite domains within granitic lithologies and locally abundant quartz veining. In addition, on the basis of geochemical changes Cartwright and Buick (1999) document large time-integrated fluid fluxes of up to  $4.2 \times 10^5 \text{ m}^3 \text{ m}^{-2}$  from some shear zones in the SE Reynolds Range, implying that they hosted significant fluid flow. This chapter assesses the mechanical and chemical affects of fluid-rock interaction throughout both the large and small shear zones, in order to determine characteristics of fluid flow during shearing. Specifically, this investigation focuses on the higher-grade shear zones in the SE of the Anmatjira and Reynolds Ranges that cut granulite- to upper amphibolite-facies rocks (Figs. 3.2, 3.3). In the higher-grade shear zones, the distinction between the shear zone and wall rock is easily recognisable due to changes in grain size and mineralogy within the shear zone. Petrological summaries of the host granulites are found in Chapter Two.

### 3.3 STRUCTURE AND PETROGRAPHY OF SHEAR ZONES

The shear zones in the SE Anmatjira and Reynolds Ranges vary in width from millimetres to hundreds of metres and contain an anastomosing steeply north-dipping (Fig. 3.4a) mylonitic foliation and a down-dip stretching lineation (Fig. 3.4b). SC fabrics, asymmetric folds (Fig. 3.4c) and rotated porphyroclasts are abundant, indicating predominantly reverse sense of movement, with some crenulation cleavage indicating a component of strike slip.

#### 3.3.1 Sample Collection

In order to identify regional fluid flow characteristics, thirteen shear zones were sampled in the northern Arunta Inlier. These shear zones are part of an interconnected network of many different sized structures (Fig. 3.1). The Yalbadjandi Shear Zone and six smaller shear zones were sampled in the Anmatjira Range region (Fig. 3.2). In addition, a shear zone cutting the pelitic Mount Freeling Schist at Blue Bush Swamp and five shear zones cutting the Napperby Gneiss were sampled in the SE Reynolds Range (Fig. 3.3). Twenty samples of country rock at these locations were also collected for comparative analysis.

Apart from the Yalbadjandi Shear Zone and the samples from Blue Bush Swamp, the shear zones discussed in this study predominantly cut 1.81 and 1.78 Ga granitic orthogneisses (Figs. 3.2, 3.3). The preference in sampling shear zones within the granitic orthogneiss is due to the homogeneous chemistry and low-variance mineralogy of the orthogneisses, which are ideal for assessing the subsequent geochemical and petrological changes due to fluid infiltration.

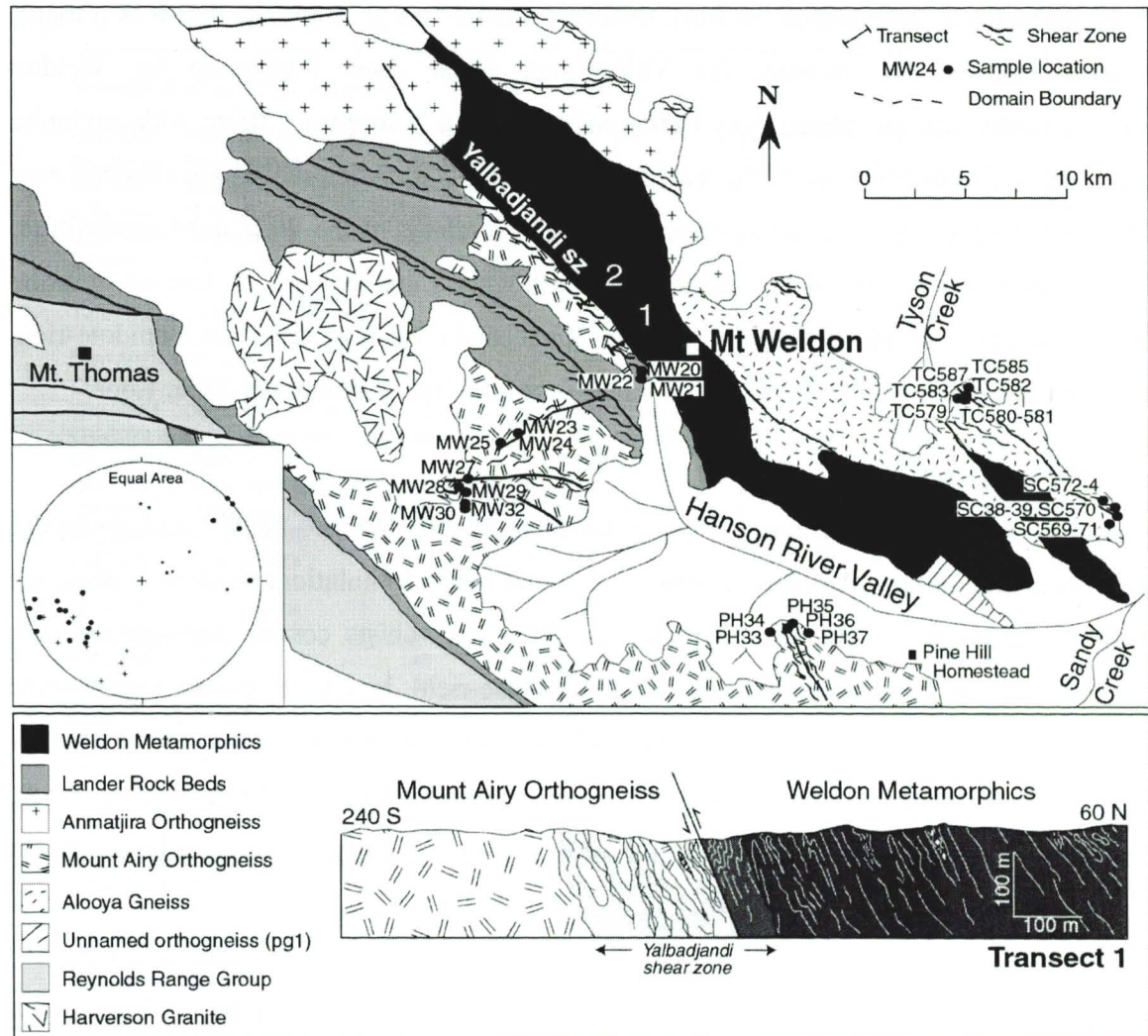


**Figure 3.2.** Geology of the SE Anmatjira Range, central Australia, after Stewart, 1981). Data discussed in the text are from transects across the Yalbadjandi Shear Zone, marked 1 and 2 east of Mount Weldon and from sample sites as located by reference number. Cross-section through Transect 1 shows basic features of the Yalbadjandi Shear Zone, including large unsheared blocks of orthogneiss and multiple narrow high-strain zones in the footwall, as well as increasing abundance of crenulations and microfolding in the hangingwall near the thrust surface. Lower hemisphere equal area projection of poles to the mylonitic foliation within the Yalbadjandi Shear Zone (circles,  $n=19$ ), other shear zones within the SE Anmatjira Range (crosses,  $n=11$ ) and elongation lineations (stars,  $n=10$ ), showing predominantly steeply N-dipping shear zone foliations with down-dip lineation direction.

The Yalbadjandi Shear Zone was sampled in two transects perpendicular to the shear zone foliation (Fig. 3.2) in order to identify any lateral discontinuity across the zone, and along strike. Sampling of the smaller shear zones was also done in traverses where possible. Samples were collected where lithological changes occurred and at regular distances ( $\sim 1$ m)

in the absence of changes. Sample preparation and whole rock major and trace element concentrations followed the analytical techniques outlined in Chapter One.

### **3.3.2 The Yalbadjandi Shear Zone, Anmatjira Range**

The Yalbadjandi Shear Zone forms the boundary between the Lander Rock Beds and the Weldon Metamorphics (Collins and Shaw, 1995). Movement across the Yalbadjandi Shear Zone juxtaposed meta-sediments from different crustal levels, implying that it is a major structure. At Mount Weldon, the Yalbadjandi Shear Zone juxtaposes the Weldon Metamorphics and the Mount Airy Orthogneiss across a N-dipping ~300m wide mylonite zone with a 138-160°/40-86°NE oriented foliation (Fig. 3.2). Mica schists are exposed over ~100m in the hangingwall and represent sheared equivalents of the Weldon Metamorphics. The sheared equivalents of the Mount Airy Orthogneiss are exposed as layered, granitic protomylonites containing narrow (0.5 to 2m) bands of phyllonite and epidote-rich, annealed cataclasite in the 150 to 200m wide footwall of the Yalbadjandi Shear Zone.

#### **3.3.2.1 Mica Schists**

The mica schists have an anastomosing foliation of 140-166°/40-80°NE and down-dip stretching lineations. Parasitic asymmetric folds and crenulations become abundant towards the centre of the shear zone (Fig. 3.4c). The schists contain strongly-foliated, metre-scale, quartzofeldspathic and phyllosilicate-rich layers, and millimetre-scale compositional layers. The shear zone assemblage comprises variable abundances of fine-grained (10 to 50µm) quartz, muscovite, feldspar, biotite and titanite (Table 3.1, Fig. 3.4d). Cordierite, sillimanite and garnet, all present in the host granulites, are completely absent from the sheared rocks.

Quartz is completely recrystallised and sub-grained, and forms augen-shaped lenses with irregular sub-grain boundaries, and minor undulose extinction (Fig. 3.4e). K-feldspar and plagioclase porphyroclasts (50 to 30µm) are significantly smaller than in the protolith and are commonly embayed or altered to muscovite (Fig. 3.4d). Muscovite grains form pressure fringes along K-feldspar clasts parallel to the shear fabric (Fig. 3.4d) and also occur as shear bands. Muscovite also forms small (15µm) prismatic needles overprinting biotite and commonly occurs in association with ilmenite. Opaque minerals form very thin seams along edges of porphyroclasts parallel to the foliation (Fig. 3.4f).

## 3.3.2.2 Protomylonites

The protomylonites have an anastomosing 140-166°/62-86°NE oriented fabric with extensive down-dip stretching lineation. They contain boudinaged and offset pegmatites, quartz veins

Table 3.1. Estimated modal mineral proportions (%) for sheared rocks from the SE Anmatjira Range, central Aus

Sample	Rock Type	qz	fsp	ksp	pl	mu	bi	ti	epi	others
<b>Yalbadjandi Shear Zone Hangingwall</b>										
CR97AR9	Protomylonite (felsic)	75	10	-	-	5	10	0	0	0
CR98MMt4	Protomylonite	45	-	15	15	15	10	0	0	0
CR97AR8	Mica schist	55	15	-	-	15	15	0	0	0
CR98MMt5	Mica schist	50	15	-	-	15	20	0	0	0
CR97AR10	Mica schist	50	10	-	-	25	15	0	0	0
CR98MMt6	Phyllonite	15	5	-	-	60	20	0	0	0
<b>Yalbadjandi Shear Zone footwall</b>										
CR97AR23	Orthogneiss (felsic)	35	-	35	20	0	10	0	0	0
CR97AR28	Deforming orthogneiss	25	-	40	25	0	10	0	0	0
CR97AR34	Deforming orthogneiss	30	-	40	20	0	10	0	0	0
CR98MMt14	Deforming orthogneiss	35	-	33	20	0	10	0	2	0
CR98MMt10	Protomylonite	50	-	24	10	1	13	0	2	0
CR98MMt12	Protomylonite	40	-	30	10	2	14	0	4	0
CR98MMt13	Protomylonite (mafic)	30	-	17	13	0	30	1	7	2 il
CR98MMt16	Protomylonite	30	-	30	20	5	7	0	8	0
CR98MMt18	Protomylonite	40	-	30	10	0	15	0	5	0
CR97AR20	Protomylonite	40	-	30	15	5	10	0	0	0
CR97AR21	Protomylonite	30	-	35	20	0	15	0	0	0
CR97AR24	Protomylonite	40	-	25	15	0	15	0	5	0
CR97AR26	Protomylonite	40	-	25	15	0	15	0	5	0
CR97AR32	Protomylonite	30	-	35	20	0	15	0	0	0
CR97AR16	Phyllonite	25	15	-	-	0	35	1	24	0
CR97AR35	Phyllonite	10	-	10	5	0	55	5	15	0
CR97AR36	Cataclasite	25	-	35	20	0	15	0	5	0
<b>Upper Hanson River Valley</b>										
CR98MM22	Protomylonite (mafic)	25	45	-	-	0	28	0	0	2 ap
CR98MM24	Protomylonite	35	40	-	-	15	10	0	0	0
CR98MM27	Protomylonite (felsic)	40	45	-	-	10	5	0	0	0
CR98MM21	Mylonite	53	35	-	-	2	7	0	3	0
CR98MM20	Phyllonite	30	-	35	20	0	15	0	0	0
CR98PH34	Phyllonite	10	10	-	-	10	70	0	0	0
CR98PH35	Phyllonite	5	0	-	-	15	80	0	0	0
<b>SE tip of the Anmatjira Range</b>										
CR98SC572	Deforming orthogneiss	40	-	30	15	2	10	0	0	3 il
CR98SC574	Protomylonite	40	-	35	5	5	15	0	0	0
CR98SC38	Protomylonite	30	-	35	10	2	15	0	0	3 cd
CR98SC39	Protomylonite	30	-	35	10	2	15	0	0	8 cd
CR98SC570	Schist	52	5	0	0	38	5	0	0	0
<b>Tyson Creek</b>										
CR98TC585	Orthogneiss	35	-	30	20	3	12	0	0	0
CR98TC579	Protomylonite	50	-	25	10	5	10	0	0	0
CR98TC580	Schist	40	25	-	-	20	15	0	0	0
CR98TC582	Mica Schist	45	0	-	-	0	30	5	0	20 chl
CR98TC583	Mica Schist	40	5	-	-	0	50	5	0	0
CR98TC587	Phyllonite	40	0	-	-	10	50	0	0	0

and large elongate blocks of orthogneiss that visually appear unaffected by shearing. The protomylonite layers vary in abundance of quartz, K-feldspar, plagioclase, biotite and

epidote, and locally contain muscovite and chlorite (Table 3.1). Titanite is the predominant accessory phase. The protomylonites have a weak fabric, defined predominantly by biotite and some aligned epidote. They contain large angular to rounded feldspar porphyroclasts with eroded edges in a matrix of dynamically recrystallised quartz (0.5 to 1mm) and finer feldspar (0.3mm) (Fig. 3.5a). Biotite forms shear bands that anastomose around smaller feldspar porphyroclasts. Some K-feldspar porphyroclasts are sericitized and fibrous biotite occurs along porphyroclast edges and in pressure shadows. The larger porphyroclasts contain abundant deformation lamellae and exsolution textures. In the lowest strain protomylonites, domains of recrystallised quartz with undulose extinction and elongate sub-grains pass laterally into domains of small, dynamically recrystallised grains.

#### 3.3.2.3 *Phyllonites*

The phyllonite zones oriented 152-168°/60-80°NE anastomose around blocks of protomylonite or unsheared orthogneiss. They have planar edges and are typically dark green-brown in outcrop. The phyllonites contain variable quantities of biotite, epidote, quartz and feldspar locally with muscovite (Table 3.1, Fig. 3.5b). More felsic domains comprise muscovite, quartz, epidote and fine biotite. Some biotite phyllonites are nearly monomineralic and are commonly crenulated (Fig. 3.5b). The phyllonites typically have completely recrystallised fabrics, but some feldspar porphyroclasts with sharp angular edges occur within the more epidote rich phyllonites. Epidote grains are typically subhedral aligned within the foliation in bands.

#### 3.3.2.4 *Foliated cataclasites*

Narrow (<1m wide) quartzofeldspathic domains within the protomylonites contain variable sized angular feldspar fragments, within a recrystallised matrix of feldspar, quartz, epidote and biotite. There is a weak foliation defined predominantly by the alignment of fragmented feldspar and biotite shear bands (Fig. 3.5c). Feldspar porphyroclasts contain microshears and faults that show both antithetic and synthetic movement. Epidote abundance is highly variable and the feldspar fragments commonly show signs of recrystallisation along fragment boundaries (Fig. 3.5d). Quartz sub-grains have irregular boundaries and undulose extinction, often present along feldspar fractures and in between fragmented clasts (Fig. 3.5e). Fibrous overgrowths of biotite and epidote, and fine seams of opaque material are common (Fig. 3.5e).

### 3.3.3 Blue Bush Swamp Shear Zone, Reynolds Range

#### 3.3.3.1 Sheared Mount Freeling Schist

The 400 metre-wide shear zone that cuts the Mount Freeling Schist at Blue Bush Swamp (Fig. 3.3, 3.6a) contains kyanite-bearing assemblages, similar to those at Mount Boothby to the SE (Dirks *et al.*, 1991). The shear zone dips steeply to the north with a mylonitic foliation of  $100\text{-}130^\circ/60\text{-}80^\circ\text{N}$  (Fig. 3.3). Quartz-rich layers are rodded with strong down-dip lineations. Kyanite-quartz veins are abundant, with clear, recrystallised quartz and large splays of kyanite that are commonly bent, folded and boudinaged with some recrystallisation (Fig. 3.6b). Narrow (~5 to 20cm wide) biotite-rich bands also occur, associated with quartz veining.

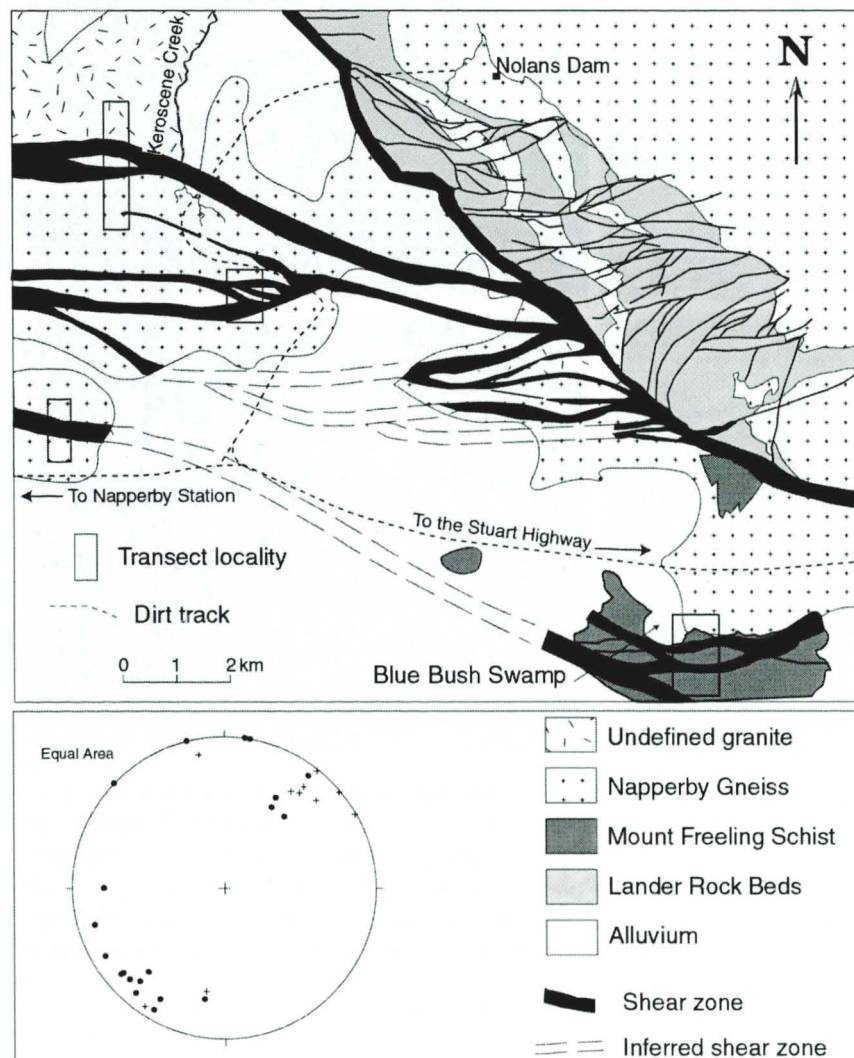


Figure 3.3. Location, orientation and approximate size of faults and shear zones within the anastomosing shear zone network of the SE Reynolds Range data from Dirks *et al.* (1991). Transect localities discussed in the text are denoted by boxes. Lower-hemisphere equal-area projection of poles to the mylonitic foliation of the sheared Napperby Gneiss (circles,  $n=20$ ) and the sheared Mount Freeling Schist at Blue Bush Swamp (crosses,  $n=10$ ). Showing anastomosing steeply NE- and SW-dipping foliations.

The schists are fine grained and characterised by compositional layering comprising biotite-muscovite, muscovite-chlorite, chlorite-rich and quartz-rich layers. The layering varies in thickness from 1 to 10mm. The major mineral assemblage comprises (50 to  $200\mu\text{m}$ ) quartz, biotite, muscovite, chlorite, and kyanite (Table 3.2). Accessory phases include titanite, ilmenite and clinzoisite, ranging in size from 10 to  $500\mu\text{m}$ .

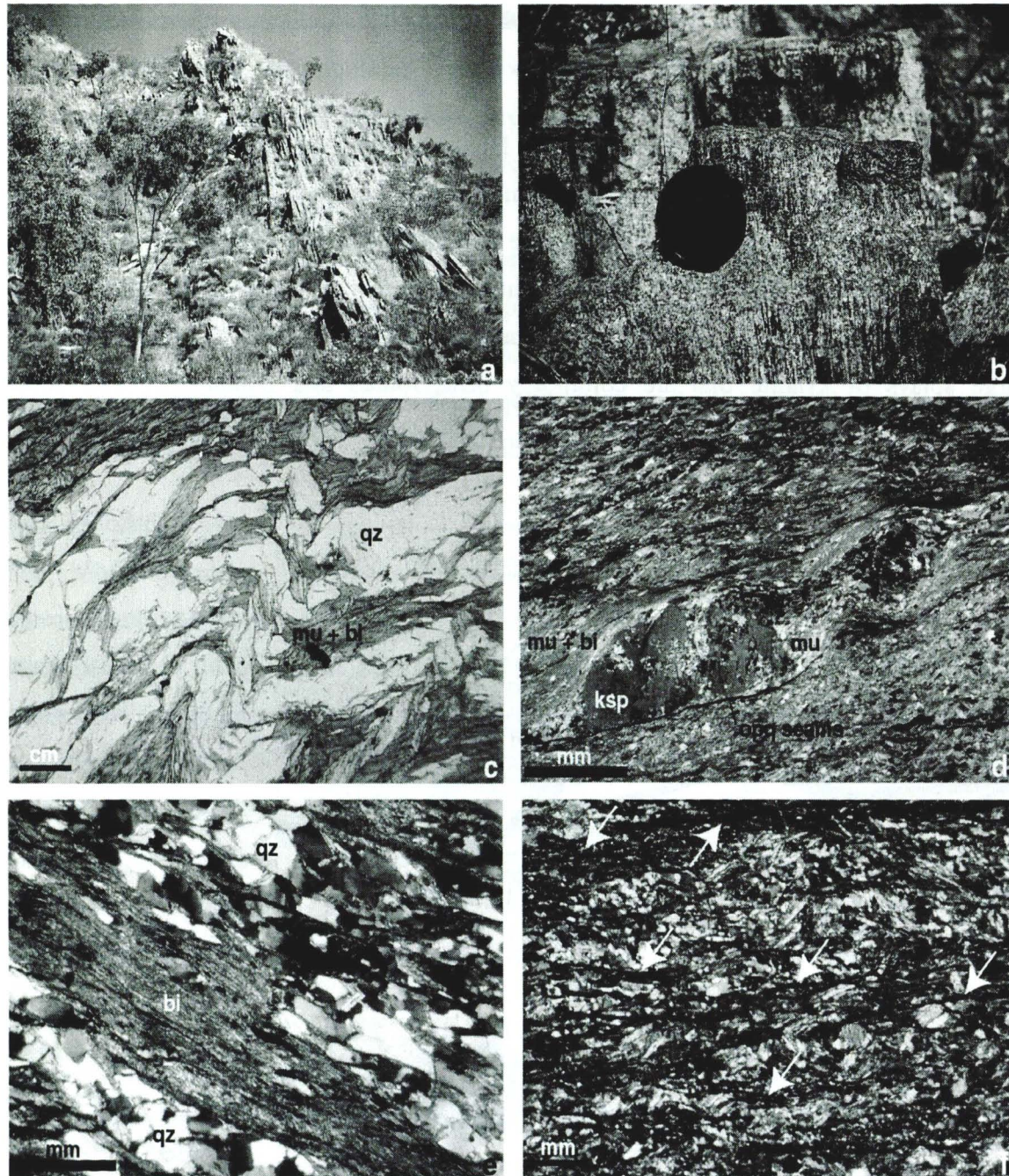


Figure 3.4. a) Looking west along strike of a steeply north dipping shear zone off Nolan Dam Track, SE Reynolds Range. b) Down dip lineations on sheared orthogneiss, SE Anmatjira Range. c) Parasitic folds in mica schist from the hangingwall of the Yalbadjani Shear Zone at Mount Weldon, showing reverse sense of shear, PPL. d) K-feldspar porphyroclasts in predominantly muscovite mica schist, showing the breakdown of K-feldspar to muscovite and mica fringes at the edges of the porphyroclast, XPL. e) biotite-rich mica schist with undulose quartz, XPL. f) Fine-grained mica schist with abundant dissolution seams (arrows) of opaque material, XPL.

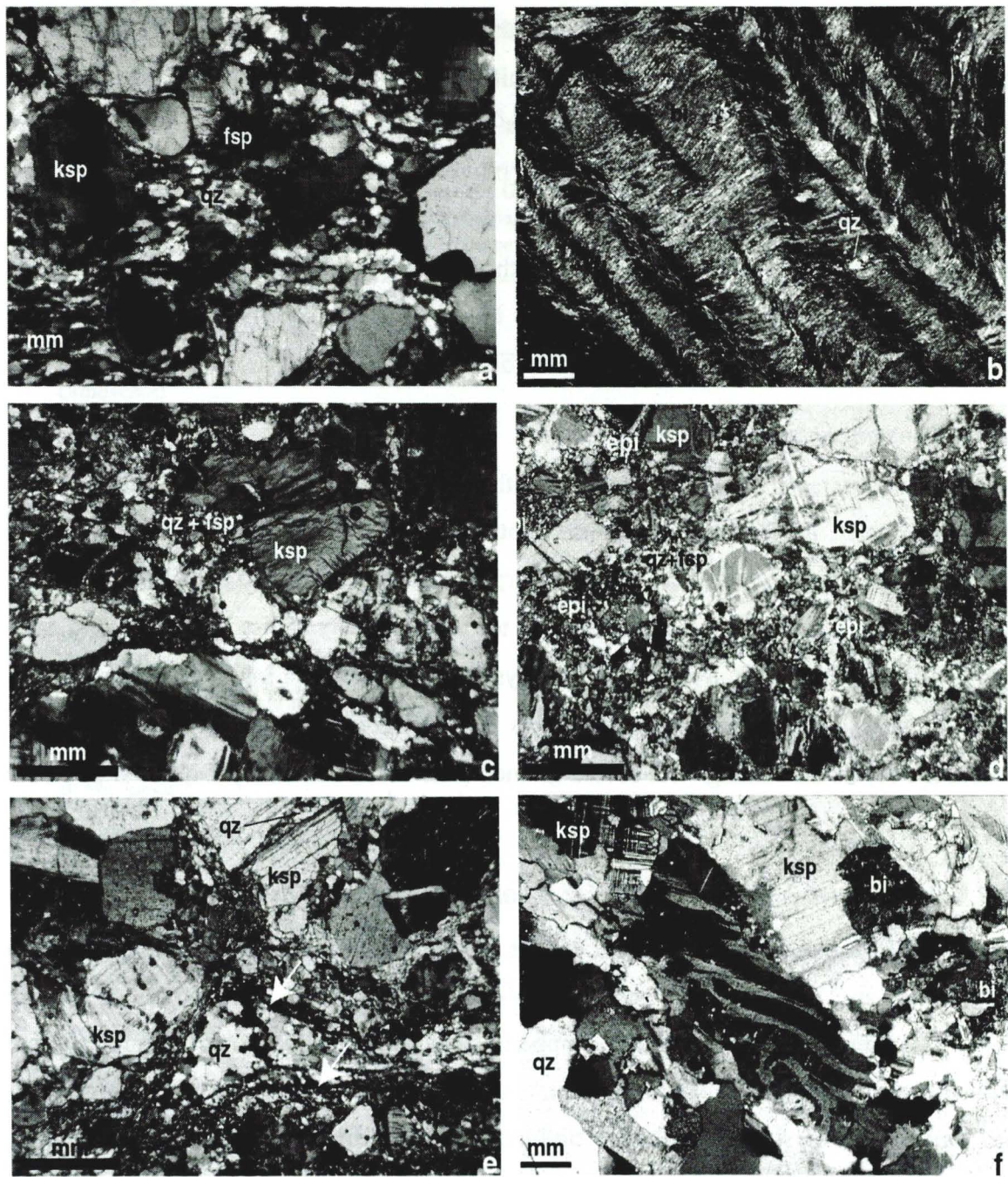


Figure 3.5. Sheared rocks from the footwall of the Yalbadjandi Shear Zone, Mount Weldon, SE Anmatjira Range a) Protomylonite, with large K-feldspar porphyroclasts surrounded by a recrystallised matrix of quartz, feldspar and some fine biotite, XPL. b) biotite phyllonite (CR97AR16), with abundant crenulations and minor elongated quartz lenses, XPL. c) Foliated cataclasite with fine annealed quartz and feldspar matrix surrounding aligned angular feldspar clasts. d) annealed cataclasite with abundant epidote, XPL. e) Annealed cataclasite with dissolution seams and quartz growth within fractured feldspar, XPL. f) Protomylonite at the northern edge of the shear zone at Blue Bush Swamp, SE Reynolds Range.

Kyanite typically occurs as fine-grained squat needles rimming partially altered biotite grains (Fig. 3.6c) and is associated with titanite crystallisation. In addition, kyanite occurs as large deformed grains within quartz veins. Quartz occurs predominantly as strain-free grains with near-polygonal texture with a minor undulose grains with irregular grain boundaries. Biotite and muscovite commonly form an anastomosing foliation around sub-grained quartz lenses. Biotite locally forms thin (50 $\mu$ m) shear bands, in which kyanite is present as small needles. Chlorite replaces biotite in distinct layers (Fig. 3.6d). Some chlorite occurs in blocky needles cutting the foliation.

#### 3.3.3.2 *Sheared orthogneiss and pegmatites*

The protomylonites at the sheared contact with the Napperby Gneiss at Blue Bush Swamp comprise quartz, K-feldspar, plagioclase, biotite with some opaque minerals (Table 3.2). Large (20mm) plagioclase and K-feldspar porphyroclasts are wrapped in a weak mylonitic fabric defined by biotite, fine-grained (50 to 100 $\mu$ m) recrystallised feldspar and sub-grained quartz (Fig. 3.5f). Mica and quartz systematically replace fractured porphyroclasts of K-feldspar. The sheared pegmatite veins contain medium-grained (~250 $\mu$ m) quartz-muscovite layers alternating with coarse-grained (5 to 10mm) K-feldspar-quartz-muscovite layers.

### 3.3.4 *Shear Zones in the Napperby Gneiss, Reynolds Range*

The NW-SE-oriented shear zones that cut the Napperby Gneiss range in width from 5m to 100m and are predominantly steeply SW-dipping (52-82°S) with strong down-dip lineations (Fig. 3.6e). The sheared Napperby Gneiss typically shows major grainsize reduction and a dramatic increase in mica abundance within the shear zones compared to the wall rock. The sheared rocks are divided into three distinct compositional domains, orthoschists (Fig. 3.7a), muscovite-chlorite phyllonites (Fig. 3.7b), and biotite phyllonites (Fig. 3.7c). There are typically multiple narrow (1 to 5m wide) phyllonite domains within the shear zones; however, the bulk of the shear zone is orthoschist, which contains abundant folded quartz boudins and pure quartz bands (Fig. 3.6f). The boundaries of compositional domains are gradational, with quartz decreasing and phyllosilicate increasing towards phyllonite domains.

#### 3.3.4.1 *Orthoschist*

The orthoschists contain variable abundances of quartz, feldspar, and muscovite, locally with chlorite and biotite (Table 3.4). They form equigranular fine- to medium-grained (20 to 300 $\mu$ m), strongly foliated, white mica- and chlorite-rich schist commonly with well-

developed crenulations in the phyllosilicate-rich layers and pale green hue in outcrop. Quartz boudins within the orthoschist (Fig. 3.6f) are completely recrystallised, showing crystallographic preferred orientation aligned parallel to the shear zone foliation.

**Table 3.2. Modal mineral proportions of shear zone rocks from the SE Reynolds Range. Orthoschist, p and bi-phylionite are derived from the Napperby Gneiss. The pelitic schist is derived from the Mount I Schist and the pegmatite and protomylonite that intrude the Mount Freeling Schist at Blue Bush Swan derived from the Napperby Gneiss. \*bi-rich Napperby Gneiss.**

Sample	qz	fsp	ksp	pl	mu	bi	chl	ti	epi	ky
<b>Orthoschist</b>										
CR98NG165	50	5	-	-	10	20	15	0	0	0
CR98NG168	50	0	-	-	15	0	35	0	0	0
CR98NG190	35	-	35	18	2	10	0	0	0	0
CR98NG214	55	0	-	-	35	0	10	0	0	0
CR99NG26	50	10	-	-	20	20	0	0	0	0
CR99NG32	45	1	-	-	34	0	20	0	0	0
* CR98NG218	55	2	-	-	25	0	15	2	1	0
* CR98NG177	40	10	-	-	29	0	20	1	0	0
<b>Phyllonite</b>										
CR99NG30	10	0	-	-	70	0	20	0	0	0
CR99NG33	19	1	-	-	5	15	59	1	<1	0
CR99NG34	5	1	-	-	74	0	20	<1	0	0
* CR98NG217	13	0	-	-	42	0	43	2	<1	0
<b>Bi Phyllonite</b>										
CR98NG173	14	0	-	-	5	80	0	1	0	0
CR99NG29	10	0	-	-	5	85	0	0	0	0
<b>pelitic schist</b>										
CR98BBS40	60	5	-	-	15	20	0	0	0	0
CR98BBS50	45	5	-	-	30	20	0	0	0	0
CR98BBS55	55	10	-	-	0	35	0	0	0	0
CR98BBS79	60	5	-	-	20	0	15	0	0	0
CR98BBS82	55	10	-	-	2	20	3	0	0	10
CR98BBS84	60	5	-	-	5	15	7.5	0	0	7.5
CR98BBS87	60	15	-	-	0	15	10	0	0	0
CR98BBS111	50	5	-	-	10	15	5	0	0	15
CR98BBS126	60	15	-	-	10	15	0	0	0	0
CR98BBS138	50	10	-	-	20	20	0	0	0	0
<b>Pegmatite</b>										
CR98BBS45	50	-	40	0	10	0	0	0	0	0
<b>Protomylonite</b>										
CR98BBS128	60	25	-	-	0	15	0	0	0	0

Typically the orthoschist contains an anastomosing fabric of white mica, biotite and locally chlorite around quartz lenses (Fig. 3.7d) and feldspar porphyroclasts (Fig. 3.7e). Muscovite is the dominant mica and forms euhedral fine- to medium-sized (20 to 100µm) grains that commonly form shear bands and pressure fringes around porphyroclasts (Fig. 3.7e). Biotite, when present, occurs as aligned medium-sized (~300µm) grains, and is commonly partly pseudomorphed by muscovite. Chlorite typically forms aligned fine-grained acicular

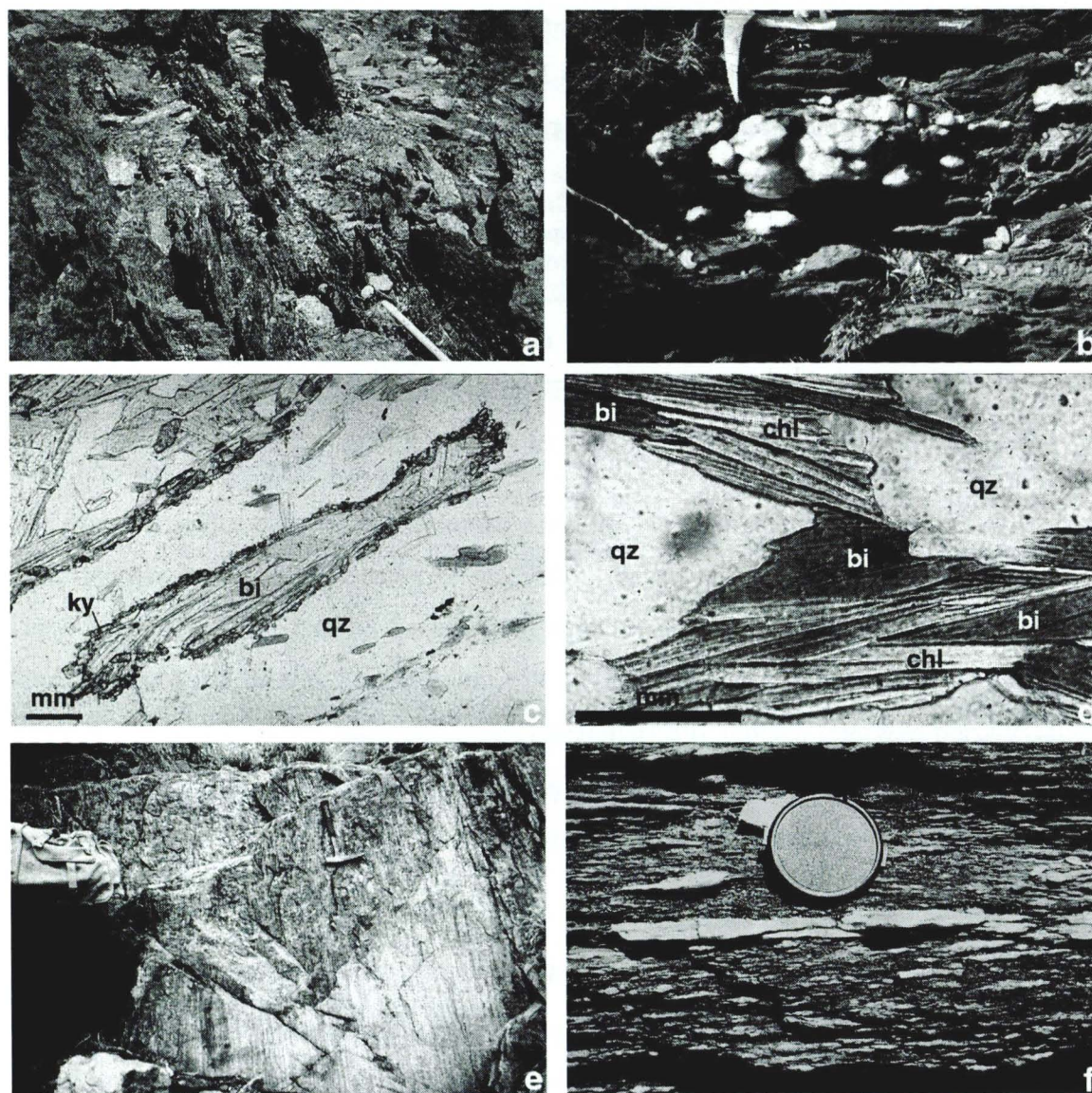
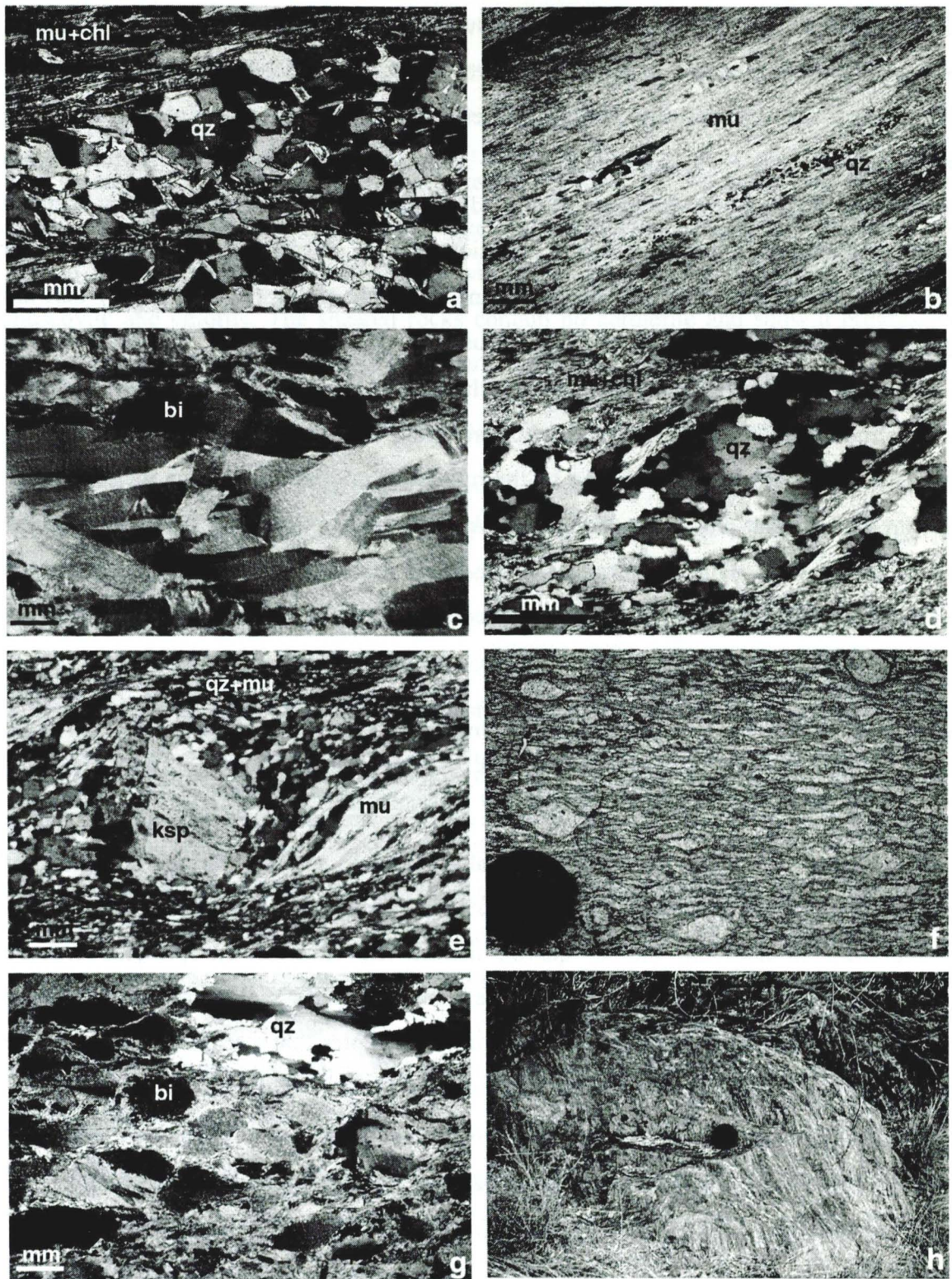


Figure 3.6. a) North-dipping shear zone at Blue Bush Swamp. b) Boudinaged quartz vein in the shear zone at Blue Bush Swamp. c) Fine blocky kyanite rimming recrystallised biotite in a kyanite-biotite schist at Blue Bush Swamp, PPL. d) Chlorite pseudomorphous replacement of biotite in chlorite-biotite schist at Blue Bush Swamp, PPL. e) Down-dip lineation in sheared Napperby Gneiss, SE Reynolds Range. f) Quartz lenses in orthoschist from a Napperby Gneiss-hosted shear zone off Nolans Dam Track, SE Reynolds Range.

Figure 3.7 (opposite page) a) Typical orthoschist with strain-free subgrained quartz with aligned muscovite and chlorite, XPL. b) Muscovite phyllonite with strong planar foliation and stretched quartz lenses, SE Reynolds Range, XPL. c) Biotite-phyllonite with evidence of reworking of the large grains, XPL. d) Quartz lens within orthoschist with serrated sub-grain boundaries and undulose extinction, rimmed by fibrous muscovite and chlorite, XPL. e) Orthoschist from the SE Reynolds Range, showing fibrous muscovite tail around a K-feldspar porphyroclast with a recrystallized quartz pressure shadow showing sinistral sense of shear, XPL. f) Large K-feldspar porphyroclasts aligned within a strong mylonitic fabric, Sandy Creek, SE Anmatjira Range. g) Reworked biotite phyllonite, Upper Hansen River Valley, SE Anmatjira Range. h) Sheared Aloooya Gneiss in the SE Anmatjira Range with a well developed down-dip lineation.



masses, and is also present in pressure shadows at the edges of porphyroclasts and quartz lenses (Fig. 3.7d). The asymmetry of these pressure shadows indicates reverse shear sense (Fig. 3.7d, e). Quartz typically occurs as lenses of strain-free grains with polygonal texture and interfacial angles of  $\sim 120^\circ$  (Fig. 3.7a). However, some quartz has serrated grain boundaries and undulose extinction (Fig. 3.7d). Feldspar porphyroclasts typically occur as corroded grains that contain muscovite inclusions and are surrounded by quartz. Titanite is the most abundant accessory phase occurring as small grains (10 to 100 $\mu\text{m}$ ) that are typically entrained in the anastomosing muscovite shear bands and along dissolution seams. Other phases of minor abundance include clinozoisite and small (20 $\mu\text{m}$ ), euhedral tourmaline grains occurring in clusters aligned with the shear fabric. In the progressively more mica-rich orthoschist, the size of the muscovite and chlorite grains increase up to 500 $\mu\text{m}$ . Some larger muscovite grains are kinked and rotated within the fabric. Small shear bands of fine muscovite truncate the lattice-preferred orientation, forming shear bands within the orthoschist. Chlorite commonly occurs in the centre of the shear bands.

#### 3.3.4.2 *Muscovite – Chlorite Phyllonite*

Muscovite-chlorite phyllonite occurs in 1 to 5m wide domains within the shear zones in the Napperby Gneiss. The muscovite-chlorite phyllonites comprise fine- to medium-grained micaceous minerals with elongated, flattened quartz lenses and exhibit an intense foliation parallel to the shear zone walls. The mineral assemblage contains variable quantities of muscovite (up to 74%) and chlorite (up to 60%) in muscovite-rich and chlorite-rich layers (Table 3.2). In addition, biotite, quartz, titanite and ilmenite are present. Chlorite commonly pseudomorphs muscovite. Very few feldspar porphyroclasts remain within the phyllonite and these are commonly present only in samples that also contain biotite. The muscovite-rich phyllonite typically has lepidoblastic texture, with very few quartz lenses, and is almost monomineralic (Fig. 3.7c). Quartz lenses contain equigranular, strain-free recrystallised grains with straight, elongate, grain boundaries, locally freckled with small titanite grains. New grains of titanite are also aligned within millimetre-sized layers of the phyllonite.

#### 3.3.4.3 *Biotite Phyllonites*

Biotite phyllonite occurs in narrow (10 to 50 cm wide) bands within the shear zones, typically at the edge of muscovite phyllonite domains. Biotite represents up to  $\sim 83\%$  of the phyllonite with some more quartz-rich and some muscovite-bearing variants (Table 3.4). The biotite grains are coarse (2mm diameter), elongated parallel to the shear zone boundary and homoclastic (Fig. 3.7d). Some recrystallised muscovite is present in pressure

shadows at the ends of augen-shaped grains. Quartz occurs in polycrystalline lenses, which display irregular sub-grain boundaries and undulose extinction.

#### *3.3.4.4. Xenolith-hosted shear zone rocks*

The shear zone that cuts the biotite-rich xenolith within the Napperby Gneiss contains similar mica schist and phyllonite assemblages to their neighbouring shear zones. They are fine to medium grained (20 to 100 $\mu$ m) with shear zone-parallel foliations defined by muscovite and chlorite. The sheared rocks contain no cordierite and show a progressive loss in feldspar (Table 3.2). Titanite is a common accessory mineral.

### **3.3.5 Shear zones in the Mount Airy Orthogneiss, Anmatjira Range**

Narrow shear zones (up to 20 m wide) that cut the Mount Airy Orthogneiss south of Mount Weldon contain coarse-grained (~0.8mm) protomylonites (e.g. samples CR97MW1, CR97MW2) of granitic composition. The protomylonites show major grain size reduction of the feldspar porphyroclasts by fracturing and dynamic recrystallisation, in association with the growth of new biotite and muscovite. Where the shearing is more intense, quartzofeldspathic mylonites and orthoschists occur with a variably fine-grained (<20 $\mu$ m to 2mm) shear matrix and large (5 to 6mm) feldspar porphyroclasts or aggregates of feldspars (Fig. 3.7f). Some brittle fracturing within feldspar porphyroclasts occurs in these mylonites, but typically they contain equant, sub-grained strain-free quartz and feldspar with aligned, elongate mica grains. The shear assemblages contain variable amounts of quartz, biotite, muscovite, epidote and titanite (Table 3.2). Bands of biotite-rich phyllonites are common in the area (CR98MW20, CR98PH34, CR98PH35) and have a strong fabric cut by later micro-shears (Fig. 3.7g). The phyllonites comprise 70-90% biotite, are medium grained (0.5 to 2mm), with large feldspar augens, wrapped by deformed biotite and finer grained plagioclase and K-feldspar.

### **3.3.6 Shear zones in the Alooya Gneiss, Anmatjira Range**

Shear zones that cut the Alooya Gneiss in Sandy Creek and Tyson Creek (Fig. 3.2) vary from several metres to hundreds of metres in width. They comprise heterogeneous anastomosing bands of highly sheared and less sheared rocks with well-developed down-dip lineations (Fig. 3.7h). Quartzofeldspathic mylonites (CR98SC38, CR98SC39, CR98SC574, CR98TC579, CR98TC580) have relic grains of feldspar in a matrix of fine-grained (500 $\mu$ m) recrystallised quartz and biotite. Centimetre-wide compositional bands of quartz-feldspar and biotite-rich layers form a strong foliation. Major grain size reduction and the recrystallisation of quartz and feldspar are common, with shear fabrics wrapping

aggregates and porphyroclasts of relic feldspar. Myrmekite textures occur typically at the edges of feldspars in cusped lobes common in blastomylonitic textures (Passchier and Trouw, 1996). Muscovite schists (CR98SC570, CR98TC582, CR98TC583) and a biotite phyllonite (CR98TC857) are also present. They comprise fine-grained (100 to 200µm) muscovite, quartz, biotite and locally chlorite (Table 3.1). Abundant shear bands of coarse biotite and muscovite truncate the predominant foliation of both the mylonites and mica schists, indicating that continued deformation occurred within the shear zones during metamorphism and hydration.

### 3.4 CHARACTERISTICS OF DEFORMATION

In general, the shear zones throughout the Anmatjira and Reynolds Ranges are laterally heterogeneous with compositional domains, variable strain intensity and recrystallisation from protomylonite fabrics to totally recrystallised phyllonites. The sheared rocks contain abundant dynamic recrystallisation microstructures such as sub-grained quartz with distinctive transitional rotation recrystallisation from undulose to strain-free polygonal textures as well as aligned micas and pressure shadow development. In addition, there are abundant indicators of fluid-assisted mass-transfer such as phyllosilicate fringes and truncated edges around feldspar grains, dissolution seams and linear accumulations of opaque minerals (Passchier and Trow, 1996; Imber *et al.*, 1997). There are also variably abundant cataclasis and microfaulting, suggesting brittle deformation processes were locally operational during shearing. As quartz always shows ductile deformation, even in the cataclastic zones, shearing must have occurred above ~350°C (O'Hara, 1988) throughout all of the shear zones. In addition, the mineralogy, comprising assemblages of kyanite-biotite, biotite-muscovite, and muscovite-chlorite support amphibolite- to greenschist-facies conditions during shearing.

The different compositional domains within the shear zones contain variable deformation features. The high-strain phyllonite domains contain a planar, shear zone-parallel foliation, and extensive dynamic crystal-plastic microstructures. The lower strain rocks, including protomylonites and schists, contain abundant quartz bands and transposition textures, indicating continual reworking during shearing. The variation of microstructures within the protomylonites indicates a heterogeneous strain regime throughout the shear zones. Myrmekite textures, common in amphibolite-facies mylonites (Simpson and Wintsch, 1989) occur throughout the SE Anmatjira Range, whereas kinked micas, abundant within the phyllonite bands, are typical of greenschist-facies conditions (Passchier and Trouw,

1996). Coarse perthite textures, as observed in the microcline of protomylonites and deforming orthogneiss, may result from the influence of fluid during exsolution (Deer *et al.*, 1992). Abundant truncating shear bands, fibrous overgrowths and pressure solution seams common within the phyllonites suggest that fluid movement throughout the shear zones became highly focussed and continued throughout shearing.

The microstructures of the different rocks within the shear zones suggest that a combination of strain-assisted, fluid assisted and temperature-dependant processes occurred throughout the development of the shear zones. The lower strain rocks contain higher temperature microstructures, whereas the higher strain zones are more fully recrystallised, contain more altered assemblages and lower temperature minerals, such as chlorite. These features suggest that as strain partitioned within the shear zones, fluid became increasingly channelled and deformation and retrogression continued during cooling after the compressional event.

#### **3.4.1 Yalbadjandi Shear Zone**

The preservation of annealed cataclasite, phyllonite and protomylonite within the Yalbadjandi Shear Zone indicates heterogeneous deformation and strain partitioning during shearing. The extensive dynamic recrystallisation of quartz, internal deformation and some brittle failure of large feldspar grains and the fibrous growth of biotite and epidote in strain shadows and along grain boundaries within the protomylonites represent low strain brittle deformation overprinted by fluid-assisted ductile deformation microstructures. The narrow cataclasite and phyllonite zones represent focussed high-strain domains. As the phyllonites contain angular clasts of feldspar this suggests they also formed initially as a result of cataclasis. Most likely fluid infiltration into the highly permeable cataclasite zones drove reaction weakening, producing phyllosilicates and thus developing ductile phyllonites (White and Knipe, 1978; White *et al.*, 1980). In addition, fibrous overgrowths of biotite and epidote within the cataclasites indicate fluid-driven mass transfer was also important during shearing. The transformation of cataclasite to phyllonite indicates that initial high-strain deformation within the Yalbadjandi Shear Zone was brittle and became progressively ductile as fluid-rock interaction occurred. This type of brittle to ductile transition is documented from the Great Glen Fault Zone (Stewart *et al.*, 2000; Holdsworth *et al.*, 2001), and Outer Hebrides Fault Zone (Imber *et al.*, 1997) Scotland. The smaller shear zones in the SE Anmatjira Range show completely recrystallised fabrics and extensive phyllonite development and ductile textures. Fabrics of mylonites in Hansen River Valley show dynamic recrystallisation followed by recovery.

### **3.4.2 Napperby Gneiss-hosted shear zones**

The intensity of mylonitic fabric within the different domains of the Napperby Gneiss shear zones is a feature of both their composition and the partitioning of strain. The quartz and feldspar-bearing orthoschists contain an anastomosing fabrics defined by mica shear bands and augen-shaped aggregates of quartz and feldspar, while the phyllonites have a very planar, shear zone-parallel foliation. The folded quartz boudins and layers within the orthoschists form transposition textures (Tobisch and Paterson, 1988; Gray and Foster, 1998). Owing to the lack of larger quartz porphyroclasts or quartz veins within the Napperby Gneiss the boudins are suggested to represent quartz veining associated with shearing.

The dominance of strain-free recrystallised quartz grains within the orthoschist and phyllonites indicates abundant recovery in quartz which is typical during deformation at  $>400^{\circ}\text{C}$  (Passchier and Trouw, 1996). The presence of an interstitial fluid, however, may have stimulated recovery processes in quartz at lower temperatures. This is a likely scenario in the light of abundant transitional sub-grain rotation recrystallisation observed in the lower strain samples where irregular sub-grain boundaries within quartz lenses is associated with intercrystalline deformation and undulose extinction (Passchier and Trouw, 1996). Transitional sub-grain rotation recrystallisation suggests lower temperatures of  $300\text{--}400^{\circ}\text{C}$  during deformation (Passchier and Trouw, 1996). Kinking of large muscovite grains and the development of small shear bands with chlorite centres also indicates continued deformation and retrogression during shearing, and are consistent with the macroscopic transposition textures. The orthoschists, therefore, reflect progressive dynamic recrystallisation textures while the phyllonites have completely recrystallised fabrics, implying higher strain intensity within the phyllonites. Abundant foliation-parallel straight boundaries of quartz lenses and feldspar porphyroclasts within both the orthoschists and phyllonites and the growth of phyllosilicate fringes represent fluid-assisted diffusive mass transfer processes. Dissolution seams, common throughout the orthoschist, and muscovite and chlorite shear bands imply solution transfer processes. In addition, clusters of small euhedral tourmaline and fine titanite grains indicate dissolution seams where insoluble material has accumulated. These observations suggest that fluid played a significant role in the deformation of the shear zones. The narrow domains of biotite phyllonite probably remain as remnant precursors to the muscovite and chlorite phyllonites at the edges of the phyllonite zones and indicate that retrogressive mineral growth continued during deformation.

### **3.4.3 Blue Bush Swamp Shear Zone**

The development of veins within the Blue Bush Swamp Shear Zone indicates substantial fluid activity during reworking of the Mount Freeling Schist. Bent kyanite grains and the crystallographic preferred orientation within boudinaged veins indicates that deformation outlasted vein formation and produced transposition textures. Strain-free quartz and euhedral mica and chlorite crystals indicate moderate temperatures during recrystallisation in a high-strain, fluid-present environment (Passchier and Trouw, 1996). The presence of biotite seams along the boundaries of quartz veins suggests that mass transfer processes operated during shearing.

### **3.4.4 Summary**

Many of the different sized shear zones examined in the SE Anmatjira and Reynolds Range comprise compositionally distinct, narrow phyllonite and wide orthoschist and protomylonite domains. Strain is partitioned into the weaker phyllonite zones, where reworking of the shear zone-parallel fabrics is common. The development of these domains may be related to the brittle failure of the host gneiss, allowing the infiltration of fluid, and thus driving reaction weakening, as suggested in the Yalbadjandi Shear Zone. However the complete recrystallisation of the smaller ductile shear zones in both the Anmatjira and Reynolds Ranges has masked any indication of the early history. The microstructures indicate a range from greenschist- to amphibolite-facies conditions during deformation that lasted for enough time to create transposition textures and reworked mylonitic fabrics, typical of shear zones. The influence of fluid is significant in the deformation of the shear zones, with diffusive mass transfer/pressure solution, reaction weakening and dynamic recrystallisation representing the dominant deformation mechanisms preserved. Annealing following cataclasis is also enhanced by the presence of fluid. The textures of the shear zone rocks suggest a fluid dominated brittle-ductile to ductile deformation regime with extensive strain partitioning and channelled fluid infiltration.

## **3.5 HYDRATION AND METAMORPHIC REACTIONS**

As described above, the infiltration of fluid throughout the shear zones in the northern Arunta Inlier was heterogenous and typically channelled into phyllonite zones. The hydrous nature of the sheared rocks and the presence of extensive quartz lenses and veins indicate that fluid played a significant role in the development of the shear zones. The metamorphic reactions associated within fluid-rock interaction produced the compositional zoning, creating mechanically weak, phyllosilicate-rich domains that progressively

accommodated strain. The extensive mineralogical changes observed within the shear zones, particularly in the development of phyllonites suggest fluid flow was fundamental in the development of the shear zones.

### 3.5.1 Orthogneiss-hosted shear zones

Assemblages of K-feldspar, plagioclase, quartz, biotite and ilmenite (Table 3.2) of the

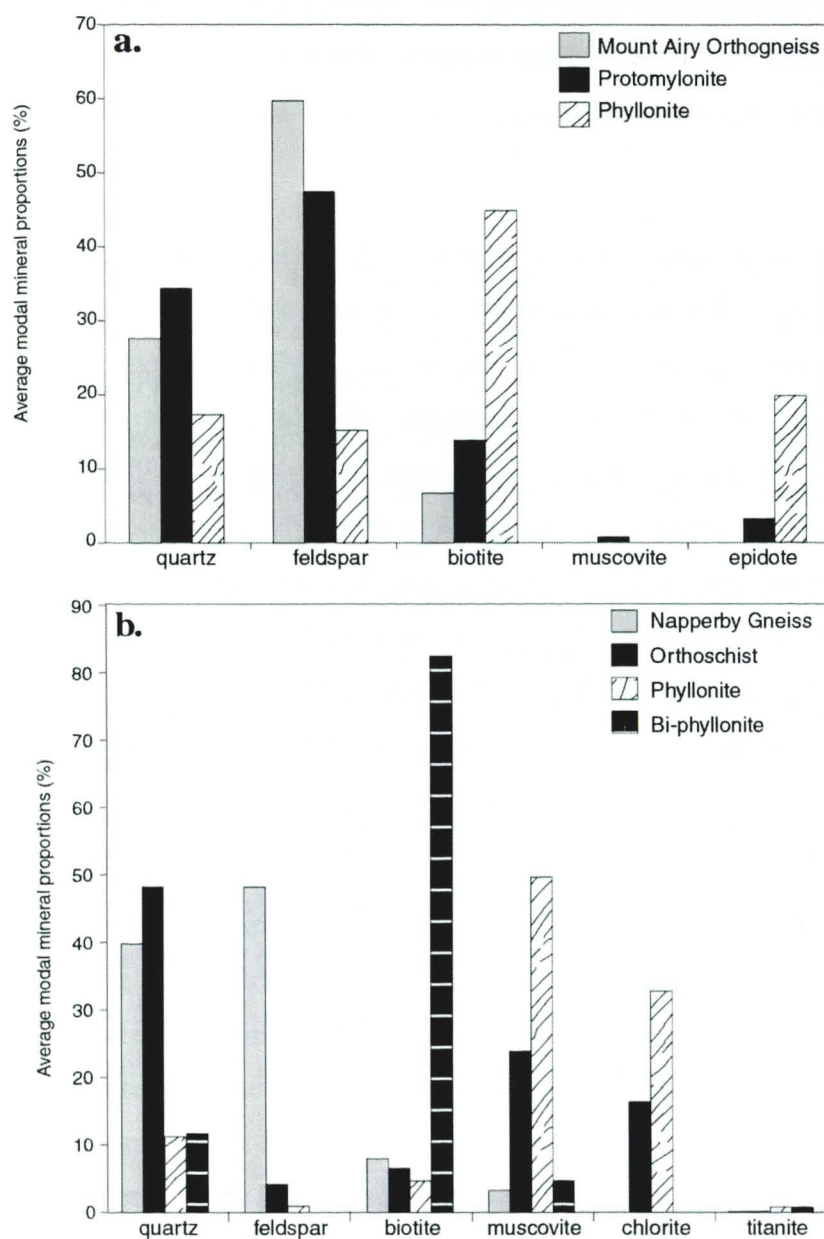


**Figure 3.8.** Comparison of average modal mineral abundances (%) for unshered and sheared rocks in the northern Arunta Inlier from a) the Yalbadjandi Shear Zone in the Anmatjira Range and b) Napperby Gneiss hosted shear zones in the Reynolds Range. The graphs indicate significant increase in phyllosilicates at the expense of feldspar. Quartz increased in the low-strain protomylonites and orthoschists and decreased in the high-strain phyllonites.

granitic orthogneiss host rocks are predominantly altered to variable volumes of quartz, biotite, muscovite, chlorite, epidote, albite, microcline and titanite within the shear zones. Changes in composition across the shear zones are substantial. The average changes in modal mineral abundances with respect to the Napperby Gneiss and Mount Airy Orthogneiss (Fig. 3.8) indicate that both the protomylonites and the orthoschists gained quartz during shearing, while the phyllonites lost quartz. K-feldspar and plagioclase are lost from all the lithologies. Biotite increases in abundance within the

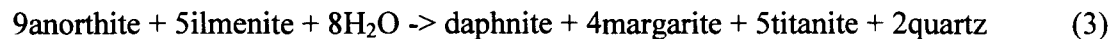
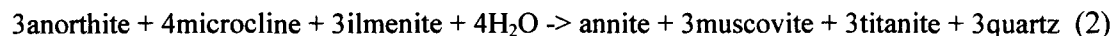
lower strain protomylonites and orthoschists, and is the dominant mineral (up to 90%), in the high strain phyllonites of the SE Anmatjira Range. In the Napperby Gneiss, biotite-

phylionites are replaced by chlorite-muscovite assemblages, suggesting that retrogression occurred, likely towards the end of shearing. Chlorite replacement of biotite is typically associated with greenschist-facies retrogression (Deer *et al.*, 1992). In order to produce the assemblages of the shear zone rocks substantial metasomatism associated with metamorphism is required. The disproportionate abundance of chlorite and muscovite in the sheared rocks relative to their unsheared precursors suggest that metasomatism occurred during fluid flow through the shear zones in the Napperby Gneiss. Epidote is variably abundant in the protomylonites and phylionites in the footwall of the Yalbadjandi Shear Zone (Table 3.1). Plagioclase breakdown during hydration may stimulate the growth of epidote by providing Ca and Fe. However, modal mineralogy changes indicate that the proportion of epidote within some sheared samples requires that the host rocks provide more Fe and Ca than. Titanite commonly occurs rimming ilmenite, suggesting that the mobilisation of Ca also stimulated the production of titanite from ilmenite.

The breakdown of cordierite, garnet, sillimanite, plagioclase and K-feldspar to create mica schists in the hangingwall of the Yalbadjandi Shear Zone suggests losses of Na, Ca, Mg and Fe during shearing. The quartz-biotite-K-feldspar mylonites of the footwall protomylonites suggest the loss of Na through the breakdown of plagioclase. In addition, the presence of pure quartz bands and lenses within the Napperby Gneiss-hosted shear zones indicate the SiO<sub>2</sub> was also mobilised, likely via a fluid phase. These mineralogical changes suggest that SiO<sub>2</sub>, K<sub>2</sub>O and H<sub>2</sub>O have been gained during shearing at the expense of NaO<sub>2</sub> and CaO, except where epidote is abundant. Similar trends have been noted in other Reynolds Range Shear Zones (Cartwright and Buick, 1999). Open system reactions that represent the changes seen within the shear zones of the northern Arunta Inlier such as:

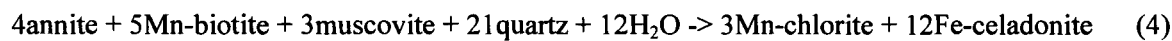


reflect the breakdown of plagioclase and the growth of muscovite. Modelled closed system reactions that may also reflect the mineralogical changes seen within the shear zones include:



(mineral compositions in Table 3.5). These reactions are between end-member compositions and thus no metamorphic conditions can be ascertained, however they are reactions that are typical of greenschist-facies conditions.

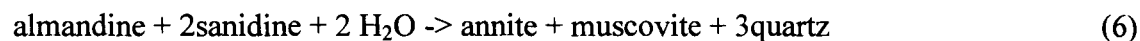
In the Napperby Gneiss, the decreasing abundance of feldspar and increasing proportions of mica and chlorite (Fig. 3.8, Table 3.2) also indicate that substantial hydration occurred during shearing. Mica increases in abundance by a factor of up to three, from 29% in the Napperby Gneiss to 90% in the phyllonites. In addition, the growth of chlorite represents up to 35% of the orthoschist and up to 59% of the phyllonite. The growth of chlorite appears to occur later in the shearing history than the growth of biotite and muscovite, and therefore likely reflects reactions involving the newly-formed biotite and muscovite such as:



Reaction (2) doubles the biotite contents, while breaking down plagioclase and K-feldspar, and may be relevant to the production of biotite phyllonite. The presence of deformed quartz boundins within the orthoschists suggests some silica was released into an aqueous fluid and precipitated into veins within the shear zone.

### 3.5.2 Pelite-hosted shear zones

Relative to the Weldon Metamorphics granulite protolith, the pelitic mica schists contain approximately twice the modal mica and quartz contents. End-member hydration reactions (using THERMOCALC v2.5) describing the transition from pelitic granulite (containing garnet, sillimanite, cordierite, K-feldspar, plagioclase quartz and biotite as end-member compositions) to mica schist (containing quartz, feldspar, biotite and muscovite) include:



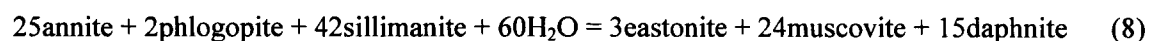
(mineral compositions listed in Table 3.5). Reactions 5 and 6 produce abundant quartz; however, the very large observed quartz abundances within the schists suggest that metasomatism also occurred during shearing.

The sheared Mt Freeling Schist at Blue Bush Swamp preserves evidence of retrogressive metamorphic reactions where biotite is replaced by chlorite, producing biotite-muscovite schists, biotite-muscovite-chlorite schists and muscovite-chlorite schists. The replacement is typically pseudomorphous, and the presence of chlorite indicates greenschist-facies shearing conditions ( $\sim 400^\circ\text{C}$ ; Deer *et al.*, 1992).

Possible reactions involved in the hydration of the Mount Freeling Schist to produce these assemblages include:

**Table 3.3. Chemical formulae of minerals in reactions listed in text, from Powell and Holland (1998).**

Mineral	Abbreviation	Chemical formula
K-feldspar	ksp	$\text{KAlSi}_3\text{O}_8$
anorthite	an	$\text{CaAl}_2\text{Si}_2\text{O}_8$
albite	ab	$\text{NaAlSi}_3\text{O}_8$
quartz	qz	$\text{SiO}_2$
cordierite	crd	$\text{Mg}_2\text{Al}_4\text{Si}_5\text{O}_{18}$
almandine	alm	$\text{Fe}_3\text{Al}_2\text{Si}_3\text{O}_{12}$
annite	ann	$\text{KFe}_3\text{AlSi}_3\text{O}_{10}(\text{OH})_2$
phlogopite	phlog	$\text{KMg}_3\text{AlSi}_3\text{O}_{10}(\text{OH})_2$
eastonite	east	$\text{KMg}_2\text{Al}_3\text{Si}_2\text{O}_{10}(\text{OH})_2$
Na-phlogopite	naph	$\text{NaMg}_3\text{AlSi}_3\text{O}_{10}(\text{OH})_2$
Mn-biotite	mnbi	$\text{KMn}_3\text{AlSi}_3\text{O}_{10}(\text{OH})_2$
margarite	ma	$\text{CaAl}_4\text{Si}_2\text{O}_{10}(\text{OH})_2$
muscovite	mu	$\text{KAl}_3\text{Si}_3\text{O}_{10}(\text{OH})_2$
Fe-celadonite	fecel	$\text{KFeAlSi}_4\text{O}_{10}(\text{OH})_2$
Mn-chlorite	mnchl	$\text{Mn}_5\text{Al}_2\text{Si}_3\text{O}_{10}(\text{OH})_4$
daphnite	daph	$\text{Fe}_5\text{Al}_2\text{Si}_3\text{O}_{10}(\text{OH})_4$
clinozoisite	cz	$\text{Ca}_2\text{Al}_3\text{Si}_3\text{O}_{12}(\text{OH})$
titanite	ti	$\text{CaTiSiO}_5$



(mineral compositions listed in Table 3.5). Kyanite and titanite are observed to have nucleated around the edges of altering biotite grains, indicating that the reactions took place within the kyanite stability field at maximum temperatures of  $\sim 513^\circ$  at 4 kbar or  $\sim 560$  at 5 kbar (Holland and Powell, 1998).

### 3.6 MAJOR ELEMENT GEOCHEMISTRY

The variably high proportions of biotite, muscovite chlorite and/or epidote within the protomylonites, orthoschists and phyllonites that make up the shear zones of the northern Arunta Inlier suggests that changes to the whole rock composition occurred during shearing. These changes can be quantified by comparing the whole-rock composition of the host gneiss with the shear zone rocks. Whole rock compositions of unaltered host

lithologies and altered shear zone rocks from the Yalbadjandi Shear Zone and the Napperby Gneiss hosted shear zones are listed in Table 3.5, 3.6 and 3.7 respectively.

**Table 3.4. Major element and selected trace element data from the Weldon Metamorphics pelitic granulites (WMG) and the Mount Airy Orthogneiss (MAO) from the northern Arunta Inlier. CR97AR1 & CR97AR2 are leucocratic layers within the layered granulite, CR97AR7 is a biotite-rich pelitic layer. Standard deviations of the Mount Airy Orthogneiss indicate homogeneity of the granitic gneiss.**

	CR97AR1 WMG	CR97AR2 WMG	AVERAGE WMG	STD DEV WMG	CR97AR7 WMG	CR97AR18 MAO	CR97AR19 MAO	CR97AR29 MAO	CR97AR34 MAO	AVERAGE MAO	STD DEV MAO
<i>Major element oxides (wt%)</i>											
SiO <sub>2</sub>	69.46	76.06	72.76	4.67	46.95	73.79	74.71	73.28	73.45	73.81	0.64
TiO <sub>2</sub>	0.57	0.16	0.37	0.29	1.23	0.11	0.09	0.22	0.15	0.14	0.06
Al <sub>2</sub> O <sub>3</sub>	15.34	13.56	14.45	1.25	31.98	14.30	13.83	15.14	14.79	14.51	0.57
Fe <sub>2</sub> O <sub>3</sub> *	6.01	1.43	3.72	3.24	10.99	1.71	1.04	1.86	1.51	1.53	0.36
MnO	0.06	0.02	0.04	0.03	0.05	0.03	0.01	0.02	0.02	0.02	0.01
MgO	1.72	0.27	1.00	1.03	4.21	0.35	0.34	0.44	0.34	0.37	0.05
CaO	0.61	0.82	0.71	0.14	0.17	1.85	1.12	2.38	2.30	1.91	0.58
Na <sub>2</sub> O	1.09	2.29	1.69	0.85	0.70	3.43	3.23	3.52	3.93	3.53	0.30
K <sub>2</sub> O	3.74	5.22	4.48	1.04	3.61	4.05	4.05	3.41	2.38	3.47	0.79
P <sub>2</sub> O <sub>5</sub>	0.07	0.11	0.09	0.02	0.06	0.03	0.05	0.06	0.02	0.04	0.02
SO <sub>3</sub>											
LOI	0.31	0.44	0.38	0.09	0.75	0.30	0.75	0.76	0.64	0.61	0.22
Total	98.98	100.38	99.68	0.99	100.70	99.93	99.36	101.08	99.53	99.98	0.77
<i>Selected trace elements (ppm)</i>											
V	87	136	112	35	193	24	21	31	23	25	4
Cr	83	109	96	18	213						
Co	56	58	57	1	46	50	61	44	39	49	9
Ni	30	44	37	10	73	4	4	8	6	5	2
Cu	16	14	15	2	13	10	11	15	12	12	2
Zn	75	110	92	25	200	29	9	27	23	22	9
Ga	20	32	26	8	49	16	14	16	17	16	1
Ba	987	1750	1368	539	885	474	821	619	706	655	146
La											
Ce	78	102	90	17	204	51	40	37	30	40	8
Nd											
Nb	11	15	13	3	28	7	3	7	6	6	1
Zr	179	135	157	31	186	102	93	125	134	114	19
Y	28	31	29	2	44	17	8	6	4	9	6
Sr	121	173	147	37	85	126	169	207	269	193	61
Rb	174	206	190	23	239	178	105	159	108	137	37
U	4	3	3	0	5	2.8	0.9	0.7	1.1	1	1
Pb	21	35	28	10	22	24	15	26	24	22	5
Th	16	26	21	7	44	12	6	5	10	8	3
As						1.2	0.7	1.2	0.1	1	1

### 3.6.1 Variability within the host gneisses

The compositions of the Napperby Gneiss and Mount Airy Orthogneiss are typical of siliceous granitic gneiss (Table 3.5). The small standard deviations of the major elements indicate chemical homogeneity of both units and, therefore, average compositions are

appropriate for comparison with the altered shear zone rocks. Alkalis and MgO show some variability within the Napperby Gneiss. Sample CR98NG215, the biotite-rich xenolith rock within the Napperby Gneiss, has a more mafic composition, particularly high in MgO and Al<sub>2</sub>O<sub>3</sub>, indicating a likely pelitic origin.

**Table 3.4 cont. Major element and selected trace element data from the Napperby Gneiss. Sample CR98NG215 is a biotite-rich xenolith within the granite. The standard deviation indicates the average values are a good approximation of the Napperby Gneiss, with the exception of MgO and the alkalis.**

	CR99NG17 NG	CR99NG28 NG	CR99NG31 NG	CR98NG153 NG	AVERAGE NG	STD DEV NG	CR98NG215 NG
<i>Major element oxides (wt%)</i>							
SiO <sub>2</sub>	76.97	76.80	77.04	77.03	76.96	0.11	50.83
TiO <sub>2</sub>	0.11	0.06	0.20	0.15	0.13	0.06	0.92
Al <sub>2</sub> O <sub>3</sub>	12.70	12.38	12.83	12.43	12.59	0.22	20.08
Fe <sub>2</sub> O <sub>3</sub> <sup>+</sup>	0.60	0.94	0.73	0.79	0.77	0.14	3.28
MnO	0.00	0.01	0.00	0.02	0.01	0.01	0.02
MgO	0.16	0.02	1.49	3.56	1.31	1.64	15.10
CaO	0.62	0.82	0.54	0.11	0.52	0.30	0.06
Na <sub>2</sub> O	3.94	3.36	4.83	0.15	3.07	2.04	0.17
K <sub>2</sub> O	4.24	4.55	1.73	3.34	3.47	1.27	2.66
P <sub>2</sub> O <sub>5</sub>	0.07	0.00	0.09	0.04	0.05	0.04	0.00
SO <sub>3</sub>	0.00	0.00	0.00	0.00	0.00	0.00	0.00
LOI	0.60	0.54	1.06	2.55	1.19	0.94	7.01
Total	100.14	99.58	100.64	100.27	100.16	0.44	100.24
<i>Selected trace elements (ppm)</i>							
V	2	5	44	9	15	20	47
Cr	56	127	93	121	99	33	98
Co	23	18	57	20	30	18	21
Ni	3	6	4	2	4	2	9
Cu	36	15	24	50	31	15	35
Zn	11	12	7	18	12	5	29
Ga	13	18	18	13	16	3	17
Ba	124	14	228	91	114	89	1068
La	55	39	69	37	50	15	46
Ce	128	48	112	70	90	37	71
Nd	42	21	46	30	35	11	35
Nb	17	25	11	20	18	6	10
Zr	135	86	203	120	136	49	194
Y	67	25	25	65	46	24	37
Sr	56	40	358	48	125	155	334
Rb	356	339	83	100	220	148	182
U	31	19	9	14	18	9	7
Pb	6	4	0	51	15	24	4
Th	62	36	36	32	42	14	36
Sc	8	6	6	0	5	3	11
F (%)	0	0	0	0	0	0	0
Cl	61	67	75	93	74	14	83
As							

Due to the small number of Weldon Metamorphics samples analysed the average geochemical data of these granulites may not be totally representative. Large changes in silica are observed between the pelitic and psammitic layers. Due to the large silica content of the mica schists the average value of the two psammitic samples (CR97AR1 and CR97AR2) are compared, excluding the pelitic sample (CR97AR7) in order to show the minimum changes during metasomatism.

**Table 3.5. Major and selected trace element data from sheared rocks within the Yalbadjandi Shear Zone, Mount Weldon, SE Anmatjira Range (Transect 1, Fig. 3.2). CR97AR3, CR97AR9 & CR97AR10 are sheared equivalents of the Weldon Metamorphics. The other samples are sheared equivalents of the Mount Airy Orthogneiss (descriptions in Table 3.3).**

	CR97AR3 Schist	CR97AR9 Protomylonite	CR97AR10 Schist	CR97AR21 Protomylonite	CR97AR24 Protomylonite	CR97AR27 Mylonite	CR97AR32 Protomylonite	CR97AR35 Phyllonite	CR97AR36 Cataclasite
<i>Major element oxides (wt%)</i>									
SiO <sub>2</sub>	59.07	91.97	81.86	66.25	72.56	69.90	71.49	46.06	62.05
TiO <sub>2</sub>	0.78	0.25	0.40	1.39	0.23	0.74	0.68	1.94	0.28
Al <sub>2</sub> O <sub>3</sub>	23.81	4.06	8.81	12.95	15.26	13.76	13.29	16.18	19.38
Fe <sub>2</sub> O <sub>3</sub> *	7.88	1.08	3.03	7.39	2.60	5.54	3.08	14.85	2.54
MnO	0.07	0.01	0.04	0.09	0.05	0.07	0.05	0.17	0.03
MgO	2.58	0.40	0.79	1.35	0.58	1.15	0.52	3.84	0.53
CaO	0.24	0.48	0.30	3.48	3.31	2.50	1.41	8.63	2.31
Na <sub>2</sub> O	0.82	0.45	0.50	2.21	4.11	2.53	2.26	1.33	5.50
K <sub>2</sub> O	5.06	1.08	2.65	3.22	1.67	3.24	5.29	3.50	6.19
P <sub>2</sub> O <sub>5</sub>	0.08	0.02	0.05	0.28	0.06	0.13	0.13	0.37	0.15
LOI	0.56	0.44	1.21	0.83	0.38	0.76	0.60	2.68	0.55
Total	100.95	100.21	99.65	99.44	100.80	100.32	98.77	99.56	99.51
<i>Selected trace elements (ppm)</i>									
Mo	1	3	2	3	1	1	2	2	1
Nb	8	5	8	21	6	13	13	12	7
Zr	87	282	247	397	114	192	519	195	64
Y	23	8	16	62	13	34	47	59	19
Sr	52	49	69	85	194	104	123	220	149
U	5	3	3	4	0	8	6	3	3
Rb	307	64	110	201	115	237	273	525	209
Th	10	15	19	31	7	33	61	13	0
Pb	40	10	11	27	20	21	36	26	25
As				1	1	1	1	0	0
Ga	16	6	11	19	19	18	16	24	15
Zn1	42	29	45	86	37	62	40	146	33
Cu	26	18	13	35	10	24	15	11	18
Ni	3	8	16	4	5	9	1	15	8
Co	62	109	60	85	40	39	44	34	25
Cr	7	22	36	44	10	36	11	57	3
Ce	31	66	30	181	50	67	153	70	1
V	26	45	61	148	35	105	59	298	49
Ba	234	319	1239	635	197	584	582	178	1508

Using the method of Grant (1986) graphical representation of elemental changes between unaltered and altered rocks is presented in Figures 3.9, 3.10, 3.11 and 3.12 for Mount Airy Orthogneiss, the Weldon Metamorphics, Napperby Gneiss and Napperby Gneiss Xenolith

hosted shear zones. The elements Al, Ti, Zr, Y and Nb are commonly accepted to be immobile during shearing (e.g. Grant 1986; Dipple *et al.*, 1990; Glazner and Bartley, 1991; Selverstone *et al.*, 1991; Tobisch *et al.*, 1991, Dipple and Ferry 1992a; Marquer and Buckhard, 1992; Streit and Cox, 1998; Cartwright and Buick, 1999). If these elements are immobile during fluid-rock interaction, they will lie on an isocon that intersects the origin on the elemental composition plots (Grant, 1986). However, there is considerable variation

**Table 3.6. Major and trace element data for orthoschists and phyllonites from shear zones within the Napperby Gneiss. CR98BG177, CR98NG217 and CR98NG218 are sheared equivalents of the biotite-rich xenolith, CR98NG215.**

	CR99NG26	CR99NG32	CR99NG33	CR99NG34	CR98NG173	CR98NG178	CR98NG190	CR98NG214	CR98NG177	CR98NG217	CR98NG218
<i>Major element oxides (wt%)</i>											
SiO <sub>2</sub>	68.01	67.12	48.28	77.38	74.70	69.98	77.36	66.29	39.76	39.61	39.79
TiO <sub>2</sub>	0.45	0.42	2.14	0.23	0.11	0.49	0.03	0.56	0.50	1.04	1.05
Al <sub>2</sub> O <sub>3</sub>	15.99	15.47	15.10	12.03	13.70	14.19	12.78	16.36	26.81	28.44	28.64
Fe <sub>2</sub> O <sub>3</sub>	3.33	3.73	10.64	1.24	1.49	1.45	1.41	0.91	2.81	3.27	3.28
MnO	0.01	0.05	0.04	0.00	0.01	0.01	0.00	0.00	0.02	0.02	0.02
MgO	1.31	1.12	12.46	3.46	2.95	6.42	1.87	7.69	16.55	13.31	13.43
CaO	3.52	2.72	0.12	0.07	0.14	0.23	0.38	0.26	0.37	0.06	0.06
Na <sub>2</sub> O	4.52	2.99	0.33	0.28	0.10	0.13	1.27	0.18	0.27	0.41	0.39
K <sub>2</sub> O	1.21	4.43	7.58	2.44	3.89	3.02	3.21	3.16	5.11	6.09	6.16
P <sub>2</sub> O <sub>5</sub>	0.12	0.15	0.12	0.03	0.09	0.21	0.18	0.14	0.32	0.01	0.02
SO <sub>3</sub>	0.00	0.00	0.00	0.00	0.00	0.00	0.00	0.00	0.00	0.00	0.00
LOI	0.90	1.10	1.78	2.60	2.81	3.80	1.77	4.61	7.82	7.22	7.24
Total	99.52	99.54	100.15	99.86	100.10	100.02	100.34	100.30	100.45	99.63	100.22
<i>selected trace elements (ppm)</i>											
V	3	53	67	87	129	0	6	12	15	73	41
Cr	63	200	57	24	157	83	113	104	140	13	164
Co	11	5	10	11	28	18	17	9	20	7	15
Ni	0	3	8	3	144	9	5	14	0	6	10
Cu	13	203	9	11	35	23	15	26	15	10	10
Zn	13	100	19	13	27	7	11	12	9	14	8
Ga	31	12	14	27	52	12	12	16	17	22	15
Ba	115	187	129	222	189	136	146	220	105	169	84
La	17	0	19	63	174	26	17	34	37	3	0
Ce	3	25	29	185	673	58	74	18	72	58	34
Nd	5	15	16	68	229	35	27	17	38	19	9
Nb	26	20	24	33	117	9	16	11	21	15	17
Zr	68	253	434	370	499	92	126	111	177	322	234
Y	35	30	18	36	124	80	59	38	56	20	18
Sr	27	33	30	41	20	109	29	32	36	30	28
Rb	289	95	82	178	1153	76	230	290	119	226	119
U	13	12	8	8	39	16	13	2	7	8	8
Pb	0	0	0	0	0	4	0	0	0	0	0
Th	31	38	59	43	177	30	35	34	47	53	39
Sc	4	8	10	19	73	5	8	0	3	9	13
F (%)	0	0	0	0	2	0	0	0	0	0	0
Cl	78	67	60	64	329	78	63	67	79	56	79
Sn	0	0	0	0	300	0	0	0	0	0	0

in Y and minor variation in Ti within the Mount Airy Orthogneiss and the Napperby Gneiss, as well as variation in Ti and Zr concentrations within the psammitic granulites of the Weldon Metamorphics (Table 3.5). These compositional variations within the host rocks may cause discrepancies within the geochemical analysis not related to shearing,

therefore Y and Ti are not used to define an isocon in the orthogneiss analyses and Ti and Zr are not considered in the Weldon Metamorphics analysis.

Although Nb and Zr for the Mount Airy Orthogneiss (Fig. 3.9) and Al and Nb commonly define an isocon for the Napperby Gneiss (Figs. 3.11, 3.12) there are no isocons defined by all three immobile elements. This indicates that there is no set of unambiguous immobile elements. As the unaltered Napperby Gneiss and Mount Airy Orthogneiss are homogenous, the mobility of these typically incompatible elements suggests that the shear zones experienced extensive metasomatism. In order to broadly define the chemical changes that occurred during metasomatism Al, Nb and Zr are used to define a wedge-shaped shaded area that cuts the origin. Each wedge denotes an area in which the extent of element mobility can be constrained. The elements that plot to the left of the wedge, indicating gains and those to the right, indicating losses, during shearing. Where the wedge is narrow there is good precision on the data, where the wedge is wide the data cannot precisely constrain elemental changes. In addition, a dashed line is drawn that defines the constant volume isocon. The position of the wedge relative to the constant volume isocon predicts a gain or loss of volume of the sheared sample, with loss of volume indicated by the wedge occurring to the right of the constant volume isocon and a gain to the left. If the wedge is narrow the inverse of the slope of the wedge will indicate the actual volume change that occurred during shearing, as the concentration of the unsheared immobile elements/concentration of the sheared immobile elements.

### **3.6.2. The Yalbadjandi Shear Zone**

#### *3.6.2.1 Mount Airy Orthogneiss*

The footwall of the Yalbadjandi Shear Zone comprises the sheared equivalents of the Mount Airy Orthogneiss. The element concentration plots (Fig. 3.9) indicate variability of the immobile element concentrations that suggests fluid-rock interaction was heterogenous throughout the shear zone. The wedges indicate slight gains in volume within the protomylonite CR97AR24 and phyllonite CR97AR35 during shearing but are inconclusive for the other samples. SiO<sub>2</sub> is consistently lost and Na<sub>2</sub>O is lost from all the samples except CR97AR24 and CR97AR36, reflecting the loss of feldspar. The two samples that gained Na<sub>2</sub>O may indicate the growth of albite heterogeneously within the shear zone. Ba and Sr are consistently lost, also likely reflecting the loss of feldspar. CaO is typically heterogenous in concentration, being gained in the samples with high epidote contents.

Fe<sub>2</sub>O<sub>3</sub> and TiO<sub>2</sub> are consistently gained within the protomylonites and cataclasite, and substantially gained in the epidote-biotite rich phyllonite (CR97AR35).

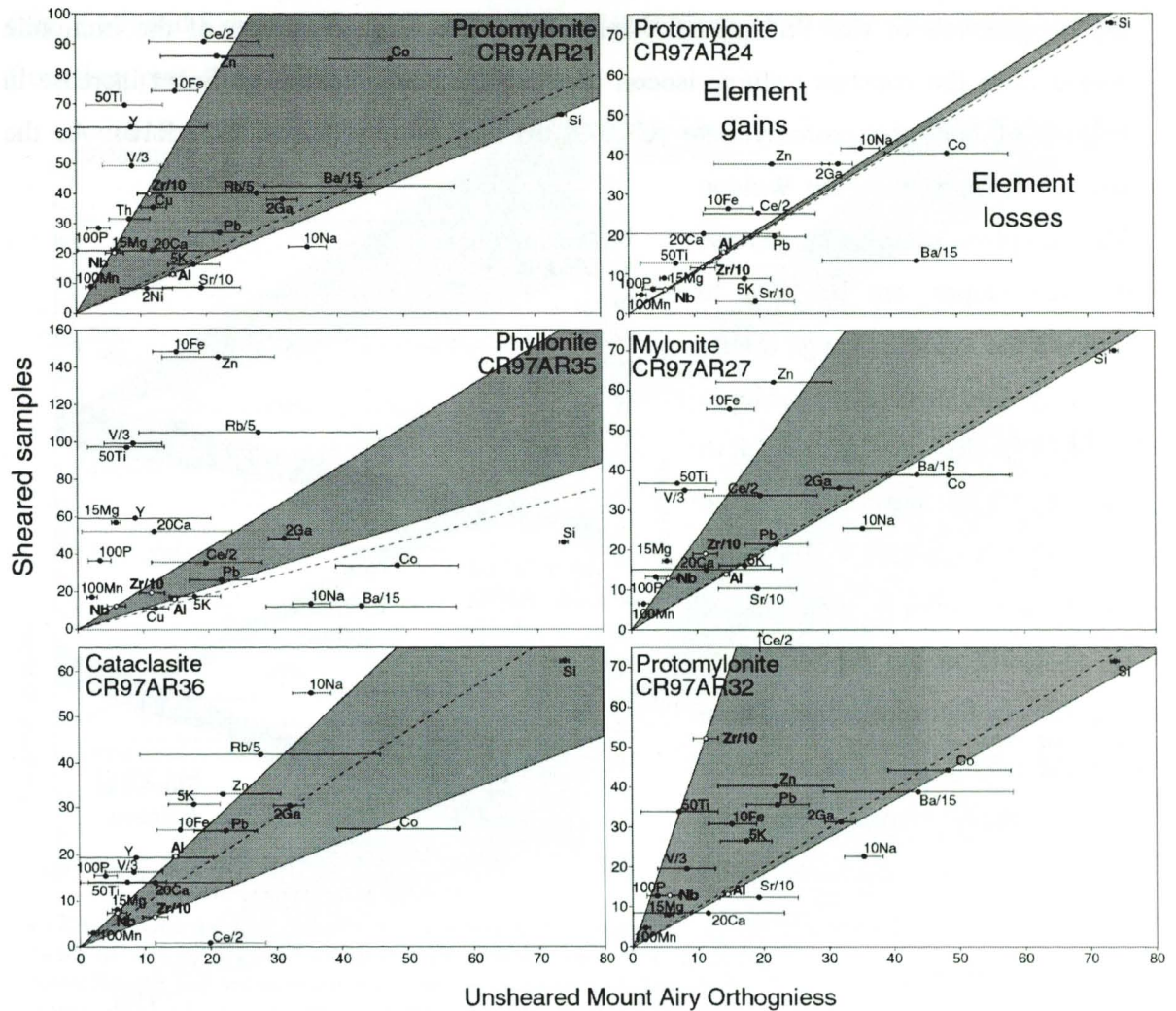


Figure 3.9. Differences in element concentrations between unshared Mount Airy Orthogneiss (average of 4 samples) versus 6 individual sheared samples from the Yalbadjandi Shear Zone. Rock descriptions in Table 3.1. Elemental concentrations are scaled to the factors shown. Open symbols denote probable immobile elements that define a shaded wedge from the origin, representing the area of undefinable element mobility. The elements to the left of the wedge were gained during metamorphism, the elements to the right were lost. The dashed line denotes the constant volume isocon. Error bars define 1 $\sigma$  variation in the unshared Mount Airy Orthogneiss composition (data on Table 3.4).

These elemental changes are consistent with the established loss of feldspar and quartz within the protomylonites and the gain in biotite and epidote (Fig. 3.8). The extensive loss of silica from the phyllonite is consistent with the mineralogy and indicates loss of quartz into a fluid phase during metamorphism. The significant increases in abundance of epidote and titanite within the phyllonite domains of the Yalbadjandi Shear Zone are reflected in substantial increases in CaO, Fe<sub>2</sub>O<sub>3</sub> and TiO<sub>2</sub> within the phyllonite sample (CR97AR35). K<sub>2</sub>O abundance throughout the samples is ambiguous. Within the Mount Airy Orthogneiss Si is lost from the system and Fe<sub>2</sub>O<sub>3</sub> and TiO<sub>2</sub> are gained. The other elements appear to have concentrated spatially into the different samples reflecting the growth of phyllosilicates and epidote.

## 3.6.2.2 Weldon Metamorphics

Immobile element wedges join Al, Y and Nb for the Weldon Metamorphics (Fig. 3.10) in the hangingwall of the Yalbadjandi Shear Zone. The large deviation of the immobile wedge from the constant volume isocon (dashed line) indicates a significant increase in volume of both the protomylonite (CR97AR9) and mica schist (CR97AR10). As the wedges are narrow for the Weldon

Metamorphics samples the inverse of their slopes can be used to indicate the volume change during shearing. The inverse of the slopes for CR97AR9 and CR97AR10 (3.6 to 2.6 and 1.8 to 1.6 respectively) indicates that they experienced volume increases of up to 260% in the protomylonite and 80% in the mica schist. These implied volume changes are much larger than those generally recorded in shear zones, typically 10 to 20% (e.g. Dipple and Ferry, 1992a; Cartwright and Buick, 1999) but locally up to 60% (Streit and Cox, 1998). While such large volume changes are possible (and agree with the broad mineralogical changes), they would be unusual, thus the results should be regarded with some caution.

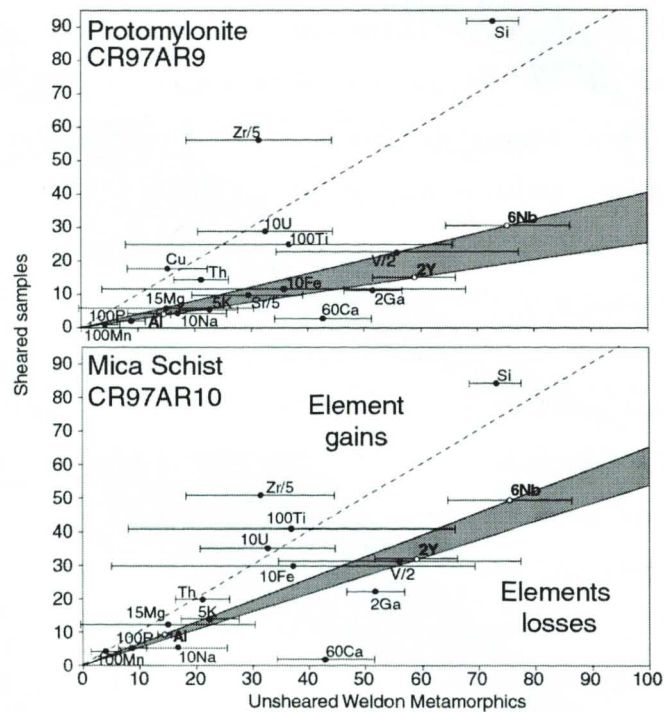


**Figure 3.10.** Differences in element concentrations between unsheared Weldon Metamorphics (average of two samples) versus 2 individual sheared samples from the Yalbadjandi Shear Zone. Sample descriptions on Table 3.1. Elemental concentrations are scaled to the factors shown. Open symbols denote probable immobile elements that define a shaded wedge, representing the area of undefinable element mobility. The elements to the left of the wedge were gained during metasomatism, the elements to the right were lost. The dashed line defines the constant volume isocon. Error bars define 1 $\sigma$  variation in the unsheared Weldon Metamorphics composition (data on Table 3.5).

Figure 3.10 shows that that CR97AR9 & CR97AR10 gained mainly SiO<sub>2</sub> during metasomatism. This trend is consistent within the observed mineralogy. The loss of Na<sub>2</sub>O and CaO from both the protomylonite and the mica schist is consistent with the loss of plagioclase and garnet (e.g. O'Hara, 1988). The other major element oxides indicate very minor changes that may be spurious due to the large standard deviation of the elements within the protolith granulite. The loss of cordierite, garnet and K-feldspar and the growth of muscovite, biotite and addition of quartz are consistent with the substantial gain in SiO<sub>2</sub>

and loss in Na<sub>2</sub>O and CaO. The results indicate that silica metasomatism occurred during shearing. The changes in elemental concentration of the sheared rocks in the hangingwall (Fig. 3.10) and footwall (Fig. 3.9) of the Yalbadjandi Shear Zone show extensive alteration from their protolith compositions is extensive.

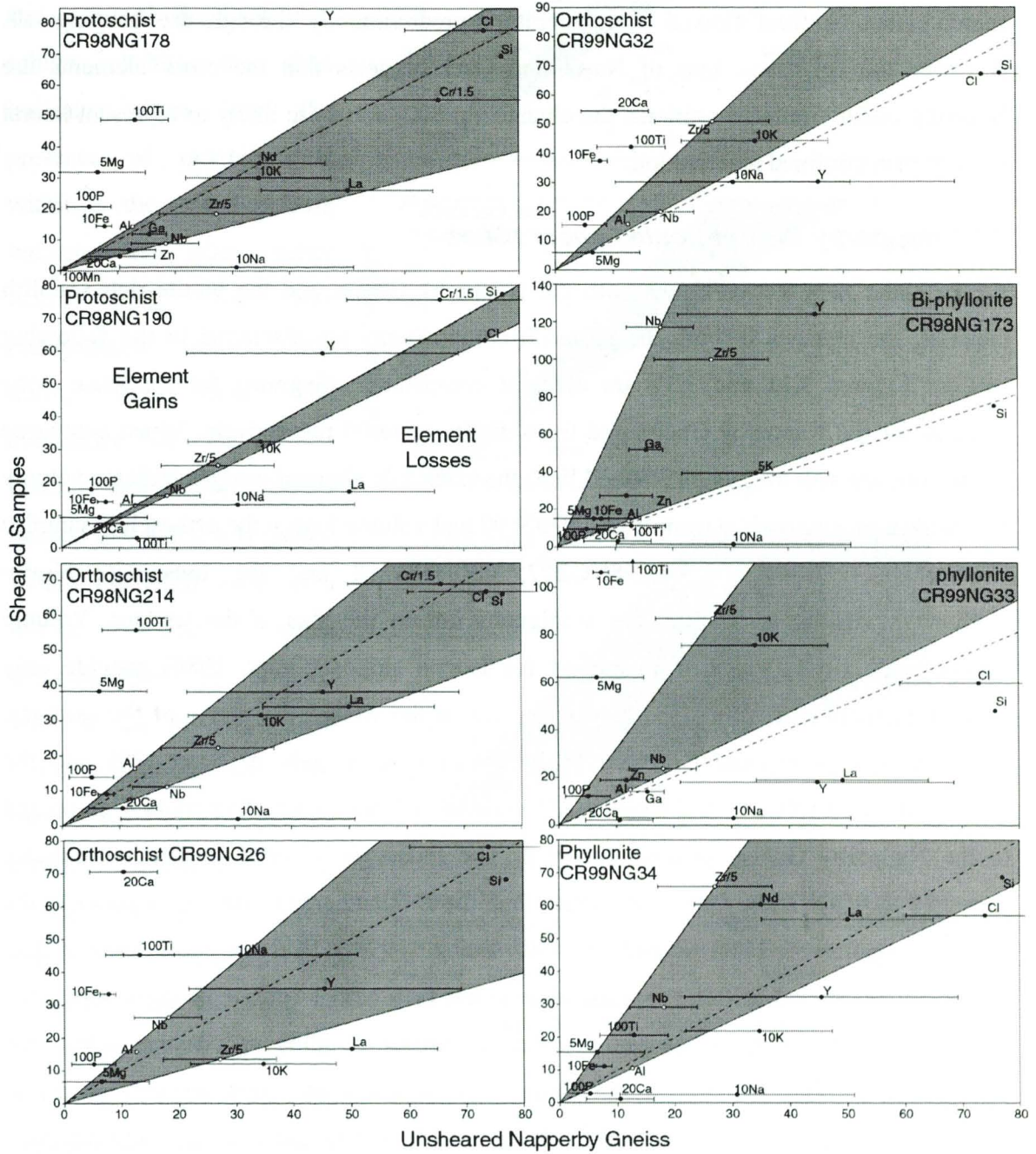


Figure 3.11. Differences in elemental concentration between the unsheared Napperby Gneiss (average of 5 samples) and individual orthoschist, muscovite-chlorite phyllonite and a biotite phyllonite from the SE Reynolds Range (Tables 3.2, 3.6). Error bars are shown for 1 $\sigma$  variation for the average Napperby Gneiss (Table 3.4). Major elements are plotted as wt% oxides and trace elements as ppm with the scaling factors listed on the diagrams. The dashed line denotes a constant volume isocon. Open symbols denote probable immobile elements that define a shaded wedge, representing the area of undefinable element mobility. The elements to the left of the wedge were gained during metasomatism, the elements to the right were lost.

They also show opposite trends of silica metasomatism and volume change during shearing, with small losses of silica and volume in the footwall and major gains of both in

the hangingwall. The gain and loss of silica suggests that either some lateral exchange has occurred across the shear zone redistributing silica or that different parts of the shear zone were active under different fluid flow regimes. For example the shear zone may have lost silica through down-temperature fluid flow concentrated in the footwall, and subsequently gained silica as fluid flowed up-temperature predominantly through the hangingwall. However the consistent loss of Na<sub>2</sub>O and CaO suggests that the other elements are behaving under similar conditions, the changes in SiO<sub>2</sub> are more likely to represent lateral transfer than confined reactivation.

### 3.6.3 Napperby Gneiss-hosted shear zones

As the shear zone network cuts both the Napperby Gneiss and the biotite-rich xenolith material, the changes in both the protolith compositions are discussed in the following section. Figures 3.11 and 3.12 are element composition diagrams for the shear zone samples for the Napperby Gneiss and the xenolith material respectively. When compared to the constant volume isocon (dashed line) the immobile element wedges indicate volume gain within the orthoschist sample CR98NG190 and volume loss in the orthoschist samples CR99NG32, CR98NG177, CR98NG217, CR98NG218 and the muscovite-chlorite phyllonites. The other samples are ambiguous due to the size of the wedges. Volume changes calculated from the inverse of the isocon slopes (Grant, 1986) provide only general estimations for the data due to the size of the wedges for many of the samples. However, the protoschist CR98NG190 indicates volume gain of 5 to 12% and the orthoschists CR98NG218 and CR99NG32 indicate volume losses of 15 to 49% compared to the Napperby Gneiss xenolith material. The muscovite-chlorite phyllonites indicate losses 26 to 42%. These values are larger than those documented from shear zones to the south of (gains of 11%; Cartwright and Buick, 1999), likely because they reflect compositional zoning within the shear zone rather than actual volume changes across the entire shear zone. The presence of abundant quartz boudins and layers within the orthoschist domains indicates a significant gain in silica and thus suggests an actual volume gain within the shear zone as a whole. Further on site measurements and sampling would need to be undertaken in order to use mass balance calculations to verify this. The overall volume change is not necessarily represented by individual samples within a zoned shear zone, as is also indicated by Selverstone *et al.* (1991) for the zoned aluminous schist of the Tauern Window in the Eastern Alps. This is significant in that estimations of volume changes across shear zones with compositional zoning can be erroneous if they are not considered within the entire shear zone composition.

Silica is predominantly lost from the schist samples, except the orthoschist CR98NG190.

The loss of silica is consistent with the reduction in quartz in the phyllonites and more phyllosilicate-rich schists. While the data indicates silica loss, the presence of quartz veins within the orthoschists indicates that silica, rather than being lost was redistributed into veins during fluid flow. The abundance of the quartz boudins and lenses suggests instead that silica was gained within the shear zone as a whole. The silica metasomatism is coupled with losses in Na<sub>2</sub>O and CaO, consistent with the breakdown of plagioclase during hydration (e.g. O'Hara, 1988). K<sub>2</sub>O content does not differ markedly as it transfers from K-felspar to muscovite. MgO varies, but is gained in the chlorite-rich orthoschists and phyllonites.

Shear zones without compositional domains in the Sandy Creek area of the Reynolds Range documented by Cartwright and Buick (1999) gain Si and K and lose Ca and Na, suggesting fluid flowed down-temperature during shearing. Assuming a normal geotherm, this reflects upward fluid flow. Up-temperature fluid flow is also likely in the shear zones sampled in this study, although internal variations in the shear zone composition has

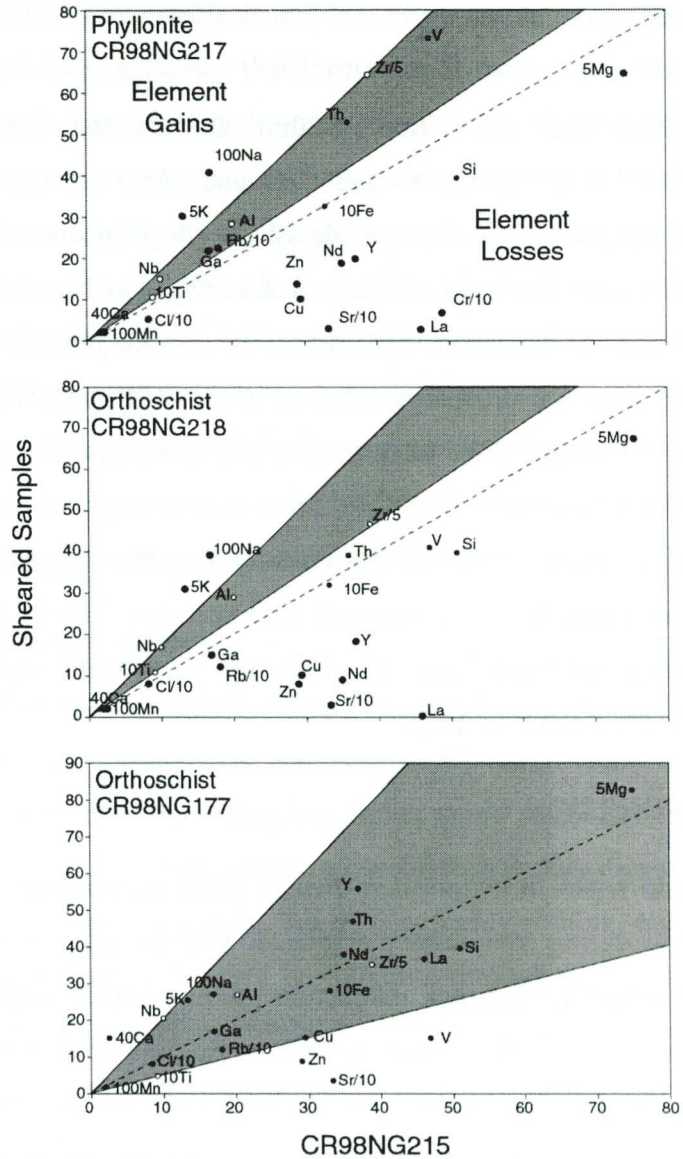


Figure 3.12. Differences in element concentrations between unsheared Napperby Gneiss Xenolith rock (CR98NG215) versus 3 individual sheared samples from the Shear Zone on the road to Napperby Station (Fig. 3.3, Tables 3.4 and 3.6). Elemental concentrations are scaled to the factors shown. Open symbols denote probable immobile elements that define a shaded wedge, representing the area of undefinable element mobility. The elements to the left of the wedge were gained during metasomatism, the elements to the right were lost. The dashed line defines the constant volume isocon.

limited the opportunity to calculate the extent of silica metasomatism and thus also the time integrated fluid fluxes.

Na<sub>2</sub>O and K<sub>2</sub>O are gained within the sheared xenolith samples (CR98NG177, CR98NG217, CR98NG218) and CaO and MgO are lost. The increase in Na<sub>2</sub>O likely reflects the growth of albite, while all the Ca-plagioclase has broken down and CaO has been removed. The relatively large loss of MgO, and less significant loss of Fe<sub>2</sub>O<sub>3</sub> reflects the removal of cordierite. The loss of Sr and Rb reflects the loss in feldspar. The trace elements also show consistent losses in the REE's Y, Nd, Th and La, all of which are commonly thought to be incompatible elements, typically not altering significantly during fluid-rock interaction. Therefore, these results suggest that the effect of extensive fluid flow within shear zones can dramatically alter the composition of rocks, and indicate that the shear zones hosted substantial fluid volumes. This is consistent within the estimated time integrated fluid fluxes of  $\sim 10^4 \text{m}^3 \text{m}^{-2}$  (Cartwright and Buick, 1999) for other shear zones in the Reynolds Range.

### 3.7 DISCUSSION

The shear zones in the northern Arunta Inlier record a period of focused deformation and fluid flow during compression associated with the late reworking of the Proterozoic middle crust. Extensive fluid-rock interaction produced schist and phyllonite assemblages within the granitic rocks. The shear zones are fluid-dominated systems that were dynamically recrystallised during internal rotation associated with reverse sense shearing. Importantly, the shear zones provide an opportunity to assess the response to compression and the effect of fluid infiltration within the central Australian middle crust.

#### 3.7.1 Development of the shear zones

The long-term weakening effects of fluids on fault zones, as discussed by Holdsworth *et al.*, (2001) and Wintsch *et al.*, (1995), suggests that fluid infiltration and subsequent metamorphic reactions producing hydrous phyllosilicates create interlinked networks of high strain throughout fault zones and caused overall weakening. This heterogeneous fluid infiltration and subsequent strain partitioning is preserved within the shear zones of the northern Arunta Inlier as narrow bands of intensely altered and deformed rocks. The shear zones likely developed as a network of anastomosing fluid flow pathways through cataclastic fracturing and dynamic recrystallisation of the granite at approximately greenschist-facies conditions. The presence of brittle fractures within feldspars, crystal-plastic deformation of quartz and the occurrence of hydrous phyllosilicates indicate a

possible temperature range of 300 to 500°C for shearing. Experimental studies indicate that microstructures of fault rocks formed by cataclasis and pressure solution accompanied by some dislocation creep may look like mylonites that formed by dynamic recrystallisation (Bos and Spiers, 2001). The brittle fracturing of the orthogneiss in the Yalbadjandi Shear Zone likely reflect an early response to compressive forces that through continued strain and fluid-rock interaction became ductile and developed into phyllonite, similar to that described by Stewart *et al.* (2000) and Holdsworth *et al.* (2001) in the Great Glen Fault Zone, Scotland. Progressive channelling of fluid and partitioning of strain into the phyllonite zones is likely to have occurred through reaction weakening processes, reducing quartz and feldspar abundance and producing shear zone parallel fabrics defined by phyllosilicates. The presence of quartz veins within the less strained orthoschists suggests that they behaved as a sink for the silica dissolved from the phyllonite zones.

### **3.7.2 SiO<sub>2</sub> redistribution during fluid flow**

The mineralogical domains within the Yalbadjandi Shear Zone and the shear zones that cut the Napperby Gneiss, Mount Airy Orthogneiss and Alooya Gneiss preserve striking variations in composition. The loss of silica within the higher strain phyllonites and the abundance of quartz boudins within the lower strain orthoschists infer significant lateral changes in silica abundance across the shear zone. As SiO<sub>2</sub> is highly soluble, movement via a fluid is likely. Assuming the fluid is flowing up-foliation, through the shear zones, driven by buoyancy created by increased permeability, the lateral changes in silica composition are normal to the dominant flow direction, and therefore silica redistribution via temperature differences along the flow path can be ruled out as a means of transfer. Chemical potential gradients are also unlikely to substantially affect the distribution of silica within shear zones in a silica over-saturated granitic province. Therefore mechanical processes of element redistribution are the most likely mechanism by which the compositional domains formed within the shear zones.

The fully-recrystallised fabrics and abundance of phyllosilicate minerals within the phyllonite domains suggests that strain and fluid flow were partitioned into narrow domains. The presence of dissolution seams and quartz veins within the orthoschists indicate that solution mass transfer processes operated during shearing. Quartz is more soluble than phyllosilicates (Passchier and Trouw, 1996) and will therefore be preferentially dissolved during fluid-rock interaction. The preferred dissolution of quartz at quartz-mica contacts under high normal stress (Bos and Spiers, 2001) and the removal of silica through diffusional transfer and fluid flow to areas of lower normal stress may

therefore have occurred within the shear zones (Fig. 3.13). Constraining major element metasomatism in the shear zones is complicated by the substantial lateral changes but generally results in the net gain of silica, and loss of  $\text{Na}_2\text{O}$  and  $\text{CaO}$  during metasomatism. This trend represents the upward flow of fluid (Dipple and Ferry, 1992a; Cartwright and Buick, 1999), typical within the ductile crust.

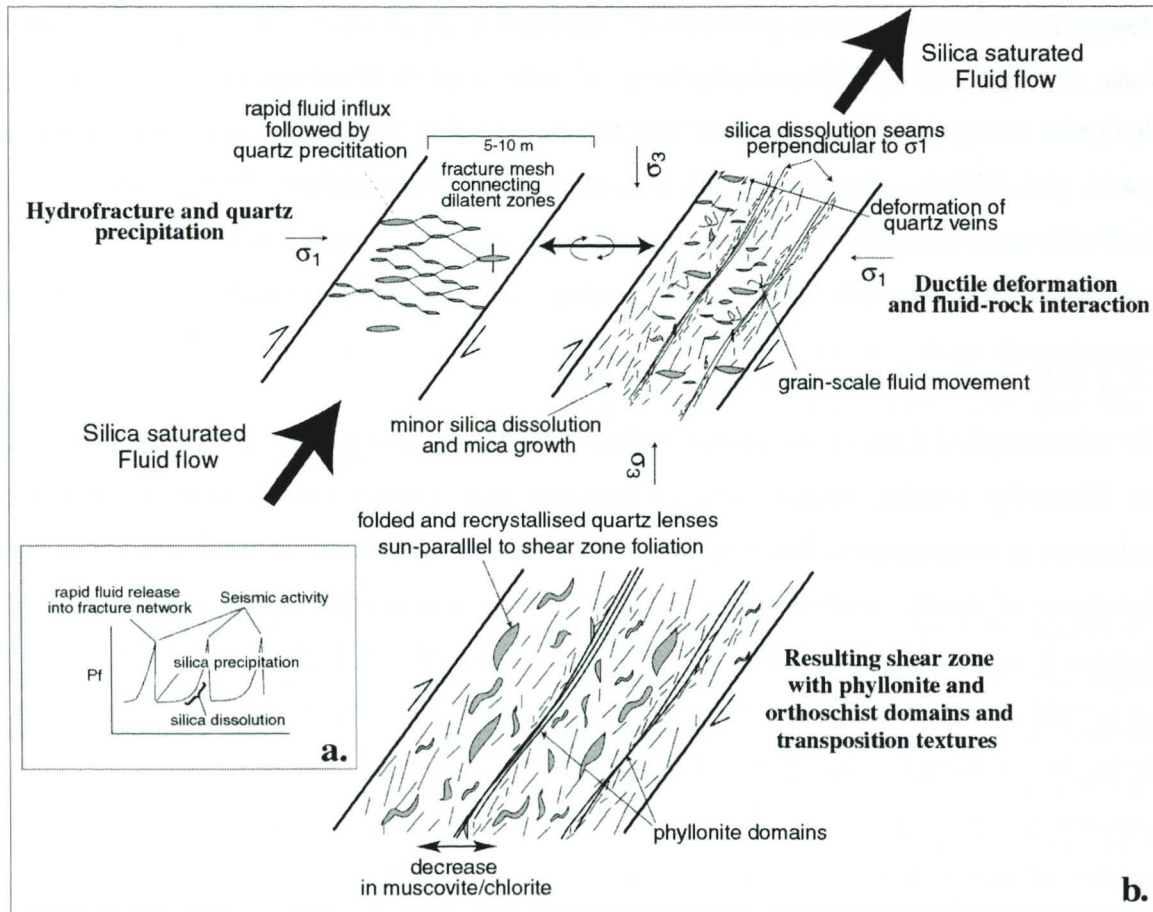


**Figure 3.13.** a) Fault valve model (after Sibson, 1990) showing cycles of seismicity with associated changes in fluid pressure, reflecting cycles of silica precipitation and dissolution. b) Fluid flow model for the formation of compositional domains in the reverse-sense shear zones of the northern Arunta Inlier. Repeated episodes of seismic-induced hydrofracture stimulate fluid flow and quartz precipitation in a connected fracture mesh perpendicular to  $\sigma_3$  (adapted from Sibson, 1996 and 1998), followed by recrystallisation and deformation of the quartz veins as a consequence of rotation within the shear zone during continued movement. In addition, preferential silica dissolution occurs in seams perpendicular to  $\sigma_1$  during periods of fluid pressure increases (a) causing the development of mica-rich, silica-poor, compositional domains. The resulting silica over-saturated fluids flow upwards through the shear zones, depositing their silica loads during periods of dilatation associated with hydrofracture events.

The mechanisms controlling fluid flow through the shear zones and responsible for the dissolution, transportation and precipitation of silica may involve fluid flow via mobile hydrofracturing associated with fault valving. The cycle of fluid flow that causes the compositional changes across the shear zones may be intimately linked with earthquake activity (Henderson and McCaig, 1997) and pore fluid pressure (Miller and Nur, 2000). Periods of transient dilatancy within the shear zones immediately following earthquakes,

and possibly in response to the rotation of the shear zone under compression may create fractures within the shear zones. These fractures cause massive rises in permeability and fluid flows upward into the fracture networks (Boullier *et al.*, 1994). The sudden drop in fluid pressure within the fractures stimulates localised quartz precipitation (Fig. 3.13a) (e.g. Oliver and Bons, 2001). As the fractures close the fluid pressure drops and fluid-rock interaction is again controlled by metamorphic reactions in the ductile shear zone. As permeability is low during high stress the fluid-pressure begins to rise and fluids gradually dissolve quartz pervasively across the shear zones. Over time preferential dissolution of quartz within the high strain (phylionite) domains occurs due to the coupling of metamorphic reactions and the preferred dissolution of quartz under high normal stress (Bos and Spiers, 2001). The evolution of the internal network then determines the chemical changes within the shear zone system. This cycle of silica redistribution continued throughout deformation, removing the bulk of the quartz from the phylionite domains and depositing as veins within the orthoschists above. The upward redistribution of silica through fluid flow occurs over large distances and produces compositional layers within the shear zones over time (Fig. 3.13b). The whole system is driven by pressure changes during periodic fracturing of the shear zone combined with the dissolution through strain-assisted metamorphic reactions during fluid-rock interaction.

### 3.8 CONCLUSIONS

The petrographic and geochemical analysis of shear zones in the northern Arunta Inlier demonstrate that the combination of hydrofracturing, strain partitioning, rotational deformation, fluid flow and hydration reactions can lead to the development of compositional domains within shear zones. Structural and microstructural processes within the shear zones are mutually important in the process of fluid flow and shear zone development and must be considered in combination with geochemical alteration. Though temperature controls the solubility of quartz, fluid pressure changes may have more control on the transport of silica through shear zone systems. Therefore, assumptions of temperature-dependant metasomatic alteration within the deforming crust are insufficient to describe the complexity of fluid-rock interaction. The heterogeneity within the shear zones of the northern Arunta Inlier clearly demonstrates the difficulty in assessing fluid flow through shear zones using geochemical changes, and illustrates the need for comprehensive analysis within individual shear zones where compositional domains may mask the actual geochemical trends.

**3.8.1 Problems with quantifying time-integrated fluid fluxes**

This research illustrates some of the problems in quantifying time-integrated fluid fluxes and even determining the direction of fluid flow in shear zones. Failure to recognise that lateral redistribution of elements has occurred may result in erroneous conclusions if only one type of compositional domain was sampled. To quantify fluid flow accurately in these shear zones would require the precise integration of the chemistry of the different domains.

**3.8.2 Implications for how fluids migrate through shear zones**

The dynamic recrystallisation and transition between brittle and ductile structures in these shear zones will govern the fluid transport. Permeability will be a transient property varying laterally and also changing between grain boundary and fracture hosted. Understanding the dynamics of recrystallisation and deformation is important to documenting how fluids migrate through shear zones. Given the data presented in this chapter, shear zones cannot be considered to have a typical permeability.

## CHAPTER FOUR

# THE INFILTRATION OF SURFACE-DERIVED FLUIDS INTO MIDDLE CRUSTAL SHEAR ZONES IN THE NORTHERN ARUNTA INLIER

### **Abstract**

O and H-isotope analyses of protomylonites, orthoschists, phyllonites, mica schists and quartz veins in the northern Arunta Inlier indicate that low  $^{18}\text{O}$  fluids infiltrated shear zones during predominantly ductile shearing at 335°C to 550°C. Estimated  $\delta^{18}\text{O}_{\text{fluid}}$  values as low as  $-7.1$  and  $\delta\text{D}_{\text{fluid}}$  values of  $-55$  to  $9.8$  indicate that the shear zones were infiltrated by a surface-derived fluid. The fluid is likely to have originated from the Centralian Superbasin forming above the Proterozoic crust from 900 to 300 Ma. The infiltration of fluid down through the crust to depths of at least 15km must have occurred through shear-related permeability connecting the upper crust with the middle crust. The preservation of the meteoric signature of the fluids indicates that extensive volumes of fluid infiltrated these shear zones, with little fluid-rock interaction along their flow path. This suggests that the creation of the fluid flow networks during shearing were rapid and that fluid was highly channelled into the middle crust. Some preserved brittle deformation within the Yalbadjandi Shear Zone indicates that brittle processes were involved in the infiltration of the fluid locally, and is consistent with fluid flow through the brittle-ductile transition.

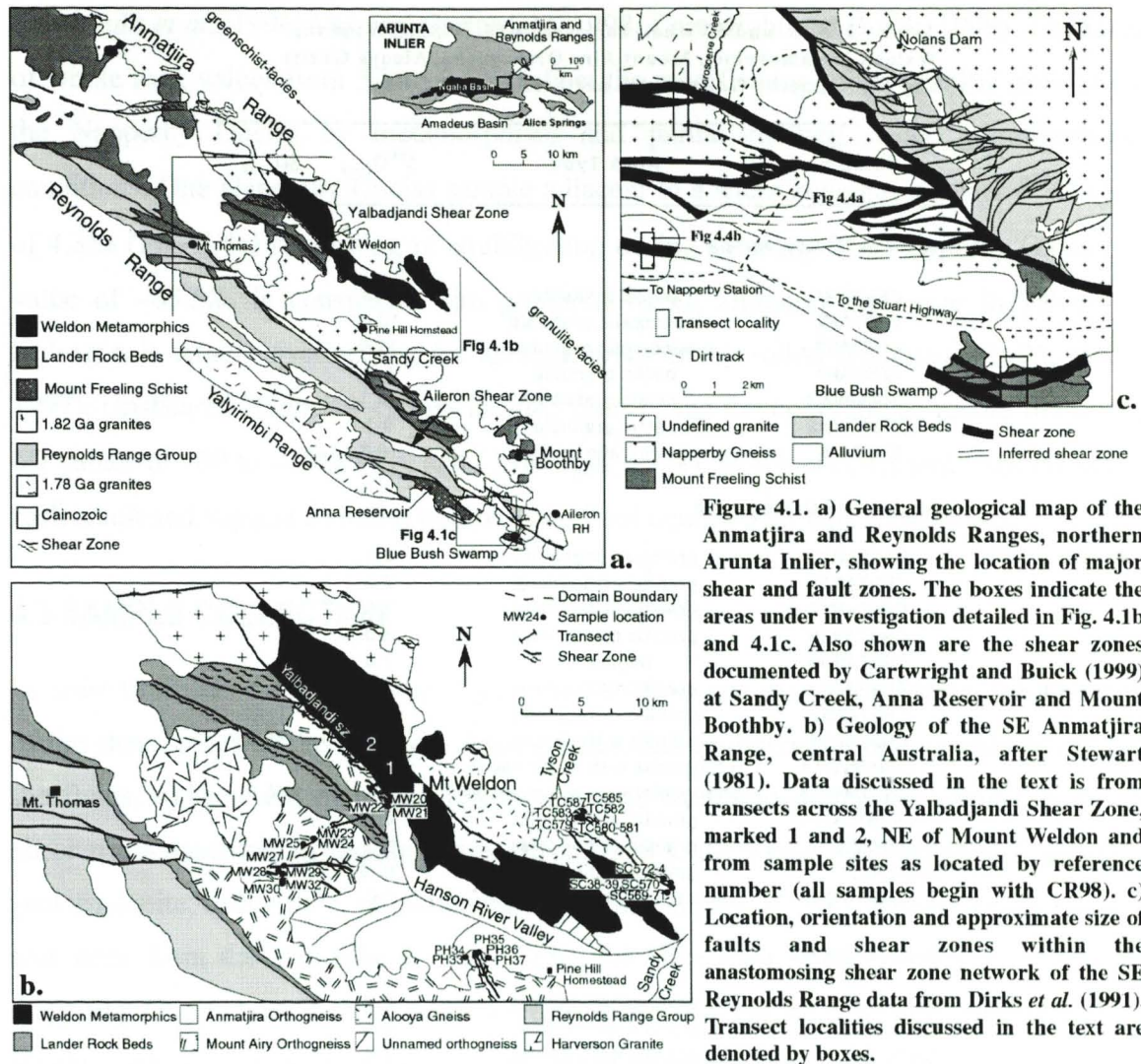
### **4.1 INTRODUCTION**

Where shear zones form after the peak of high-grade metamorphism, dehydration of the local country rocks is unlikely to produce significant volumes of fluid as the mineral assemblages are stable to higher temperatures than those of shearing. Shear zones with mineral assemblages more hydrous than those of their wall rocks require the infiltration of locally exotic fluids to drive hydration reactions. Within high-grade granitic or gneissic terranes, fluid sources are likely to originate at great distances ( $>10$  km) from the shear zones as the immediate country rocks will have little free fluid available. In the Arunta Inlier, central Australia, intra-continental thrusting is preserved within amphibolite- and greenschist-facies shear zones that cut  $\text{H}_2\text{O}$ -poor granulite-facies metamorphic rocks. The aim of this study is to identify the sources of the fluids that infiltrated the shear zones in order to understand the large scale fluid flow networks operating in the central Australian middle crust during shear zone development. This in turn will provide further information on possible sources of fluids that hydrate high-grade metamorphic terranes worldwide.

As shear zones are typically fluid-dominated systems, oxygen and hydrogen isotopes are ideal for determining fluid flow as they track the fluid themselves. In fluid-dominated systems, stable isotopes can identify the origins of the last fluids to have interacted with the rocks as well as estimate the temperature of re-equilibration (Sheppard, 1986; Hoefs, 1997). Possible fluid sources include crystallising igneous rocks, the mantle, the surface and deep-seated metamorphic rocks (e.g. Lobato *et al.*, 1983; McCaig, 1988; McCaig *et al.*, 1990, Morrison 1994; Upton *et al.*, 1995; Streit and Cox, 1998). To date, stable isotope analyses of some shear zones within the Reynolds Range have identified surface reservoirs as a likely source for fluids that hydrated the middle crust (Cartwright and Buick, 1999). However, it has not been established whether this is a local or widespread phenomenon. The aim of this chapter is to: (1) further establish characteristics of fluid-rock interaction within the shear zones discussed in Chapter Three and; (2) to determine the source of fluids that hydrated these shear zones in the northern Arunta Inlier in order to provide a regional interpretation of fluid flow through the northern Arunta Inlier during shearing.

## **4.2 GEOLOGICAL SETTING**

As discussed in Chapters Two and Three, multiple anastomosing shear zones cut the Proterozoic basement lithologies of the northern Arunta Inlier (Fig. 4.1). These shear zones underwent significant fluid-rock interaction and metasomatism during shearing. The shear zones in the SE Anmatjira and Reynolds Ranges contain predominantly protomylonite and orthoschist rocks with narrow phyllonite and rarely cataclastic domains. Quartz veins are abundant in the Napperby Gneiss-hosted shear zones and throughout the sheared orthogneisses of the Hansen River Valley. Petrological analysis indicates that shearing was associated with a substantial loss of feldspar, the growth of muscovite, biotite and chlorite and the redistribution of quartz. This suggests that significant fluid flow occurred at middle crustal conditions (Chapter Three). Geochemical analyses indicate a gain of Si and a loss of Na and Ca occurs consistently throughout the shear zones (Chapter Three). In addition, a gain of Si and K and the loss of Na and Ca are documented from other shear zones in the region (Cartwright and Buick, 1999). These geochemical trends suggest that fluid flowed down-temperature through the shear zones. Assuming a normal geothermal gradient, this corresponds to fluid flow toward the surface.



### 4.2.1 Host rocks

O- and H-isotope ratios of the host rocks to the shear zones were established in order to provide a framework in which to assess fluid-rock interaction within the shear zones.

#### 4.2.1.1. Weldon Metamorphics

The unsheared Weldon Metamorphics have  $\delta^{18}\text{O}$  values of 15.1 to 9.1‰ (Fig. 4.2, Table 4.1). The higher  $\delta^{18}\text{O}$  values are indicative of meta-sedimentary rocks; however, the values around 9‰ are relatively low for meta-sedimentary rocks (Hoefs, 1997). These low  $\delta^{18}\text{O}$  values probably reflect interaction with a crustal fluid associated with contact metamorphism around the Anmatjira Orthogneiss at 1.82Ga. Isotopic re-equilibration through contact metamorphic fluid flow has been documented around other granites in the region (Vry and Cartwright, 1998).

**Table 4.1.  $\delta^{18}\text{O}$  and  $\delta\text{D}$  whole rock values (‰ V-SMOW) of the Weldon Metamorphics, Mount Airy Orthogneiss, Aloooya Gneiss and the Napperby Gneiss in the northern Arunta Inlier.**

Sample	Rock Type	$\delta^{18}\text{O}_{(\text{wr})}$	$\delta\text{D}_{(\text{wr})}$
<b>Weldon Metamorphics</b>			
CR97AR1	pelitic granulite	11.7	
CR97AR2	leucocratic granulite	10.6	
CR97AR3	leucocratic granulite	10.0	
CR97AR7	pelitic granulite	9.7	
CR98MWt1	pelitic granulite	15.1	
CR98MWt2	pelitic granulite	9.1	
CR97AR9	leucocratic gneiss	10.7	
<b>Mount Airy Orthogneiss</b>			
CR97AR17	qtz-fspar pegmatite	8.1	
CR97AR18	granitic orthogneiss	7.3	
CR97AR19	granitic orthogneiss	7.8	
CR97AR29	granitic orthogneiss	8.0	
CR97AR30	pegmatite	7.8	
CR97AR31	granitic orthogneiss	7.3	
CR97AR32	granitic orthogneiss	8.2	
CR97AR34	granitic orthogneiss	7.3	-85.6
CR98MWt14	orthogneiss with shear bands	6.6	
CR98MWt18	orthogneiss with shear bands	6.6	-76.5
CR98MWt19	granitic orthogneiss	6.7	
CR98PH33	granitic orthogneiss	10.1	
CR98PH37	granitic orthogneiss	10.6	
CR97AR22	quartz vein in orthogneiss	8.6	
<b>Aloooya Gneiss</b>			
CR98SC572	granitic orthogneiss	9.2	
CR98SC573	granitic orthogneiss	8.1	
CR98TC585	granitic orthogneiss	7.9	
<b>Napperby Gneiss</b>			
CR98NG153	granitic orthogneiss	5.7	
CR98NG215	granitic orthogneiss	6.7	
CR99NG17	granitic orthogneiss	7.3	-65.5
CR99NG28	granitic orthogneiss	5.7	
CR99NG31	orthogneiss with shear bands	4.3	

#### 4.2.1.2. Mount Airy Orthogneiss

The unsheared Mount Airy Orthogneiss has  $\delta^{18}\text{O}$  values ranging from 8.2 to 6.6‰ (Fig. 4.2, Table 4.1), which is typical of granitic rocks (Taylor and Sheppard, 1986) and similar to granite gneisses elsewhere in the region (Buick *et al.*, 1994; Cartwright *et al.*, 1996; Vry and Cartwright, 1998, Cartwright and Buick, 1999). The Mount Airy Orthogneiss near the Yalbadjandi Shear Zone has  $\delta\text{D}$  values of -85.6‰ and -76.5‰.

#### 4.2.1.3 Napperby Gneiss

Locally, the samples of Napperby Gneiss not immediately adjacent to shear zones range in  $\delta^{18}\text{O}$  values from 5.7 to 7.3‰ (Table 4.1). These values are similar to Napperby Gneiss elsewhere in the region (6.1 to 9.5‰; Buick *et al.* 1994; Buick and Cartwright, 1996;

Cartwright *et al.*, 1996; Vry and Cartwright, 1998; Cartwright and Buick, 1999). The range of whole rock values from 5.7 to 9.5‰ reflect the modification of the granitic protolith of the Napperby Gneiss by metamorphism and partial melting under granulite-facies conditions. One Napperby Gneiss sample adjacent to a shear zone has a lower  $\delta^{18}\text{O}$  value of 4.3‰ (Fig. 4.4a) suggesting re-equilibration during shearing. The Napperby Gneiss  $\delta\text{D}$  value of -65.5‰ is consistent with granitoid rocks, although the range in values for hydrogen is largely overlapping for all rock types at this value (Rollinson, 1993; Hoefs, 1997). Unsheared Napperby Gneiss in other parts of the Reynolds Range record muscovite  $\delta\text{D}$  values of -60 to -75‰ (Vry and Cartwright, 1998), which is consistent with the whole rock result and suggest a similar composition fluid equilibrated with these rocks.

### 4.3 SAMPLE COLLECTION

In order to further understand the effects of fluid flow and the crystallisation temperatures of the shear zones of the Northern Arunta Inlier, and to determine the possible sources of the fluids, oxygen and hydrogen isotope analysis were undertaken on samples from the shear zones described in Chapter Three. In addition to the whole rock samples of granulite, protomylonite, orthoschist, phyllonite and schists, samples of quartz bands, quartz boudins and veins from the Yalbadjandi Shear Zone, the Blue Bush Swamp Shear Zone and the Napperby Gneiss hosted shear zones were collected and analysed. Sample preparation and whole rock and mineral separate concentrations were done following the analytical techniques outlined in Chapter One.

## 4.4 O AND H ISOTOPE RESULTS

### 4.4.1 Yalbadjandi Shear Zone

Within the Yalbadjandi Shear Zone there is substantial variation in the oxygen isotopic composition of the rocks (Table 4.2, Fig. 4.2). Five samples of sheared Mount Airy Orthogneiss (CR97AR35, CR97AR36, CR97AR37, CR98WMt16, CR98MWt17, CR98MWt20), one sample of sheared Weldon Metamorphics (CR98MWt6) and a quartz vein (CR98MWt15) have very low  $\delta^{18}\text{O}$  values ranging from -6.4 to 4.2‰ (Fig. 4.2, Table 4.2). The rest of the samples have values similar to those of the unsheared rocks, ranging from 8.5 to 10.8‰ for the sheared granulites and 6.1 to 8.2‰ for the sheared orthogneiss (Fig. 4.2). All the low  $\delta^{18}\text{O}$  rocks occur within the shear zone, suggesting that oxygen isotope re-equilibration occurred during shearing. The sheared orthogneiss samples have  $\delta\text{D}$  values of -63.1 to 97.4‰ and the pelitic mica schist preserves a  $\delta\text{D}$  value of -90.5‰.

As lower volumes of H<sub>2</sub>O-rich fluids are required to reset the hydrogen isotopes compared to oxygen (Bickle and Mackenzie, 1987) it is likely that the sheared rocks preserve  $\delta D$  values of the infiltrating fluid, rather than the protolith.

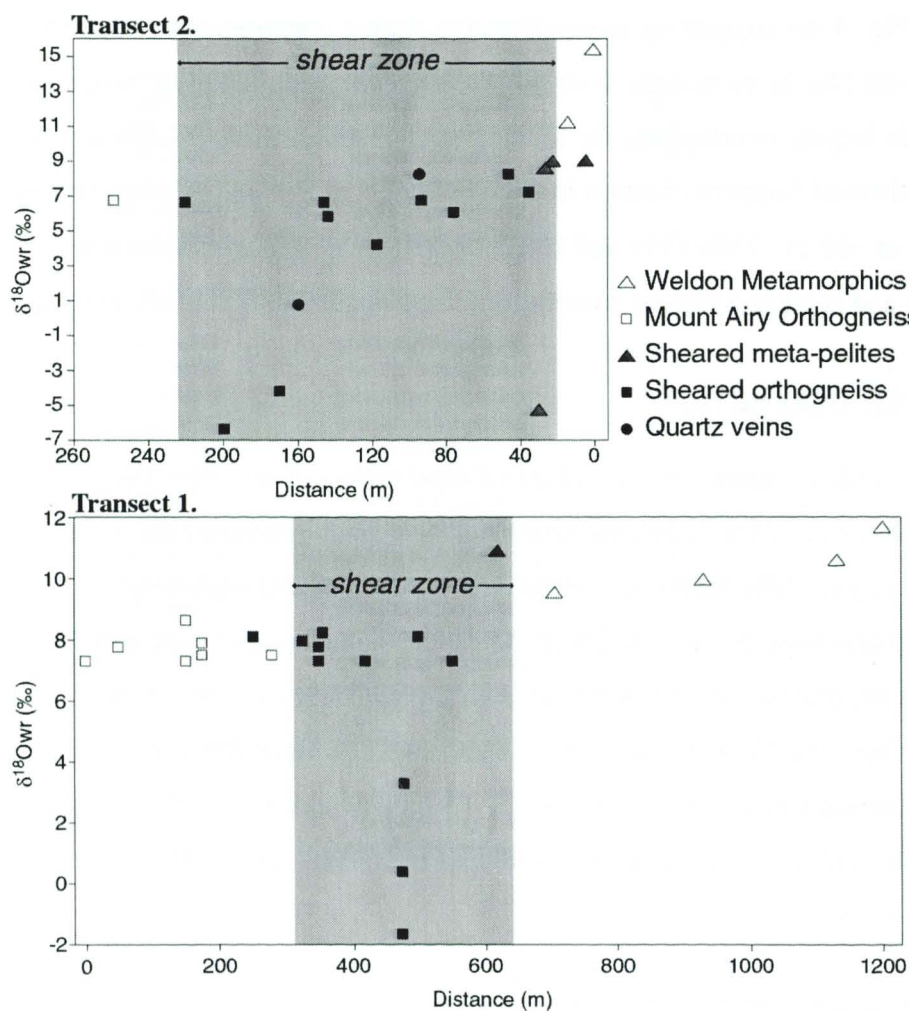


**Figure 4.2.** Oxygen isotope profiles across the Yalbadjandi Shear Zone at Transect 1 and 2 (Fig. 4.1b) showing the  $\delta^{18}O$  composition of the unsheared Mount Airy Orthogneiss (open squares) and Weldon Metamorphics (open triangles) compared to sheared equivalent rocks (closed symbols) and associated quartz veins.  $\delta^{18}O$  values within the shear zone are generally consistent with those of the host rocks, except in narrow bands where the  $\delta^{18}O$  values are dramatically reduced.

#### 4.4.2 Orthogneiss-hosted shear zones, SE Anmatjira Range

Many of the samples from the narrow shear zones throughout the SE Anmatjira Ranges and Hansen River Valley have  $\delta^{18}O$  values of 7-10‰, similar to those of their unsheared protoliths, the Alooja Gneiss and Mount Airy Orthogneiss (Table 4.2, Fig. 4.3). One sample from a narrow (5m wide) shear zone south of Mount Weldon has a very low  $\delta^{18}O$  value (2.7‰), similar to the low values in the Yalbadjandi Shear Zone to the north (Fig. 4.1b).

**Table 4.2.  $\delta^{18}\text{O}$  and  $\delta\text{D}$  whole rock values (‰ V-SMOW) of the sheared samples from the Yalbadjandi Shear Zone, shear zones in Sandy Creek, Tyson Creek and the Upper Hanson River Valley in the SE Anmatjira Range.  $\delta^{18}\text{O}_{\text{fluid}}$  values are presented for samples with mineral proportion data (Table 3.4) and mineral-water fractionations factors of Chacko *et al.* (1999), Zheng, (1993a, b) and Suzuoki and Epstein (1976) for shearing at 550°C.**

Sample	Rock Type	$\delta^{18}\text{O}_{(\text{wr})}$	$\delta^{18}\text{O}_{(\text{fluid})}$	$\delta\text{D}_{(\text{wr})}$	$\delta\text{D}_{(\text{fluid})}$
<b>Yalbadjandi Shear Zone</b>					
CR97AR10	muscovite schist	10.7	10.0		
CR98MW3	muscovite schist	10.8			
CR98MW4	protomylonite	9.0	8.2		
CR98MW5	muscovite schist	8.5	7.8		
CR98MW6	mica schist	-5.2	-2.9	-90.5	-71.8
CR97AR21	protomylonite	7.3	6.7		
CR97AR24	orthogneiss with shear bands	7.5	6.8		
CR97AR25	protomylonite	7.9			
CR97AR26	protomylonite	8.1	7.4		
CR97AR27	mylonite	7.5			
CR97AR35	phylionite	-1.7	-0.3	-88.1	-50.9
CR97AR36	foliated cataclasite	0.4	-0.04	-74.0	-36.3
CR97AR37	protomylonite	3.3	2.6	-97.4	-62.0
CR98AR16	phylionite	-4.2	-5.1	-95.1	-55.2
CR98MW7	mylonite	7.2			
CR98MW8	ultramylonite	8.2			
CR98MW9	mylonite	6.1			
CR98MW10	protomylonite	6.7	5.6		
CR98MW12	protomylonite	4.2	3.3	-97.0	-62.0
CR98MW13	protomylonite	5.8	5.9		
CR98MW14	protomylonite				
CR98MW17	protomylonite	-6.4	-7.1	-63.1	-27.7
CR98MW11	quartz vein	8.2	5.7		
CR98MW15	quartz vein	0.7	-1.8		
<b>Upper Hanson River Valley</b>					
CR98MW20	phylionite	-2.7	-3.4		
CR98MW21	mylonite	4.8			
CR98MW22	mylonite	4.0	3.9		
CR98MW23	protomylonite	7.7			
CR98MW24	protomylonite	6.6	5.9		
CR98MW25	quartz vein	6.0	3.5		
CR98MW27	protomylonite	7.1	6.2		
CR98MW28	quartz vein	6.6	4.1		
CR98MW29	quartz vein	4.3	1.8		
CR98MW30	protomylonite	9.5			
CR98MW32	mylonite	14.2			
CR98PH34	phylite	6.8	8.4		
CR98PH35	mylonite	5.7	7.8		
CR98PH36	bt-rich mylonite	6.8			
<b>Sandy Creek / Hanson River</b>					
CR98SC38	QFL Protomylonite	9.2	8.6		
CR98SC39	QFL mylonite	9.8	9.3		
CR98SC569	chl-musc schist	8.7			
CR98SC570	musc schist	5.3	4.5		
CR98SC571	qtz-tourm vein	8.1			
CR98SC574	protomylonite	7.3	6.4		
<b>Tyson Creek</b>					
CR98TC579	protomylonite	5.2	4.1		
CR98TC580	QFL mylonite	6.2	5.7		
CR98TC581	quartzite	6.8			
CR98TC582	mica-schist	5.7	5.6		
CR98TC583	mica-schist	5.6	6.0		
CR98TC587	bt-schist	6.8	7.1		

**Table 4.3. Whole rock  $\delta^{18}\text{O}$  and  $\delta\text{D}$  data (‰ V-SMOW) for orthogneiss, orthoschist and phyllonite from shear zones in the Napperby Gneiss and the calculated fluid  $\delta^{18}\text{O}$  &  $\delta\text{D}$  values based on mineral- $\text{H}_2\text{O}$  fractionation factors at temperatures of 335°C from Chacko *et al.* (1999), Cole and Ripley (1998), Zheng (1993a,b, 1991), Graham *et al.* (1984), and Suzuoki and Epstein (1976) and mineral proportions (Table 3.4).**

Sample	Rock Type	$\delta^{18}\text{O}_{(\text{wr})}$	$\delta^{18}\text{O}_{(\text{fluid})}$	$\delta\text{D}_{(\text{wr})}$	$\delta\text{D}_{(\text{fluid})}$
<b>Orthoschist</b>					
CR98NG159	orthoschist	3.9			
CR98NG165	bi-chl-mu orthoschist	5.6	2.7		
CR98NG168	chl-mu orthoschist	6.1	3.1		
CR98NG177	mu-chl orthoschist	5.3	2.2		
CR98NG178	orthoschist	5.8			
CR98NG190	bi-orthoschist	5.8	2.3		
CR98NG213	orthoschist	4.5			
CR98NG214	mu-orthoschist	2.2	-1.3	-92.6	-53.4
CR98NG218	mu-chl orthoschist	2.9	-0.5		
CR99NG26	mu-bi orthoschist	6.6	3.4	-66.0	-15.5
CR99NG26	mu-bi orthoschist			-66.9	-16.4
CR99NG32	mu-orthoschist	3.4	0.4	-71.1	-33.0
<b>Phyllonite</b>					
CR98NG217	chl-phyllonite	2.0	1.1	-56.9	-19.6
CR99NG30	mu-chl phyllonite	1.9	0.8	-80.4	-41.3
CR99NG33	chl-bi phyllonite	2.9	1.8	-107.3	-67.9
CR99NG34	mu-phyllonite	1.4	0.5	-94.6	-68.0
CR99NG34	mu-phyllonite			-107.3	-55.4
<b>Biotite Phyllonite</b>					
CR98NG173	bi phyllonite	3.4	3.8	-49.4	9.8
CR99NG29	bi phyllonite	1.7	2.4	-80.7	-21.4

Several quartzofeldspathic protomylonites (CR98TC579, CR98MW21, CR98MW22) and quartz veins (CR98MW25, CR98MW28, CR98MW29) have lower  $\delta^{18}\text{O}$  values of 4.0 to 4.8‰ and 4.3 to 6.6‰ respectively. Thus, as with the Yalbadjandi Shear Zone, the 8 smaller shear zones in the SE Anmatjira Range and Hansen River Valley contain rocks with lower  $\delta^{18}\text{O}$  values compared to the host Alooya Gneiss and Mount Airy Orthogneiss.

#### 4.4.3 Napperby Gneiss-hosted shear zones

The orthoschists and phyllonites from Napperby Gneiss-hosted shear zones in the SE Reynolds Range have whole rock  $\delta^{18}\text{O}$  values of 1.4 to 6.6‰ (Table 4.3, Fig. 4.4a). The unshered Napperby Gneiss varies in  $\delta^{18}\text{O}$  value from 5.7 to 7.3‰. Thus the data indicate a general lowering of  $\delta^{18}\text{O}$  values within or immediately adjacent (<1m) to the shear zones (Fig. 4.4a) implying that re-equilibration is associated with shearing throughout the area. Mount Airy Orthogneiss- and Napperby Gneiss-hosted shear zones in Sandy Creek and Anna Reservoir (Fig. 4.1a) are documented as having whole rock  $\delta^{18}\text{O}$  values as low as 0‰ (Cartwright and Buick, 1999), consistent with the significant depletion of  $^{18}\text{O}$  during

shearing. Hydrogen isotope ratios for the Napperby Gneiss and associated sheared rocks (Table 4.3)

Table 4.4. Whole rock and mineral  $\delta^{18}\text{O}$  values (‰ V-SMOW) for the Mount Freeling Schist at Blue Bush Swamp.

Sample	Rock Type	Transect (m)	$\delta^{18}\text{O}$	$\delta^{18}\text{O}_{(\text{qz})}$	$\delta^{18}\text{O}_{(\text{bi})}$	$\delta^{18}\text{O}_{(\text{ky})}$	$\delta^{18}\text{O}_{(\text{mu})}$	$\delta^{18}\text{O}_{(\text{chl})}$
CR98BBS40	Schist	0	10.1					
CR98BBS50	Schist	45		9.8	4.7			
CR98BBS51	Qtz-ky vein	52		9.1		3.7		
CR98BBS55	Schist	80	7.9					
CR98BBS66	Bi-schist	114			3.8			
CR98BBS70	Qtz-ky vein	134		7.0		4.5		
CR98BBS71	Schist	135			4.0	7.3		
CR98BBS72	Qtz-bi vein	140		8.8	3.1			
CR98BBS76	Schist	161					6.1	2.2
CR98BBS79	Schist	189	5.3					
CR98BBS80	Qt-bt vein	192		7.3				
CR98BBS82	Ky-schist	195	12.0					
CR98BBS84	Ky-schist	210	7.1					
CR98BBS87	Schist	251	7.7	8.2	3.9			
CR98BBS91	Schist	266	6.6					
CR98BBS111	Schist	360		6.2	0.2	2.7		
CR98BBS113	Qtz-bi-ky vein	370		6.4	1.8	2.2		
CR98BBS123	Qtz-bi-ky vein	417		5.4	2.6			
CR98BBS126	Schist	435	7.5					
CR98BBS140	Schist	500	4.7					
CR98BBS143	Pegmatite	516	4.5					
CR98BBS148	Schist	538	5.6					
CR98BBS150	Quartz boudin	550	8.8					

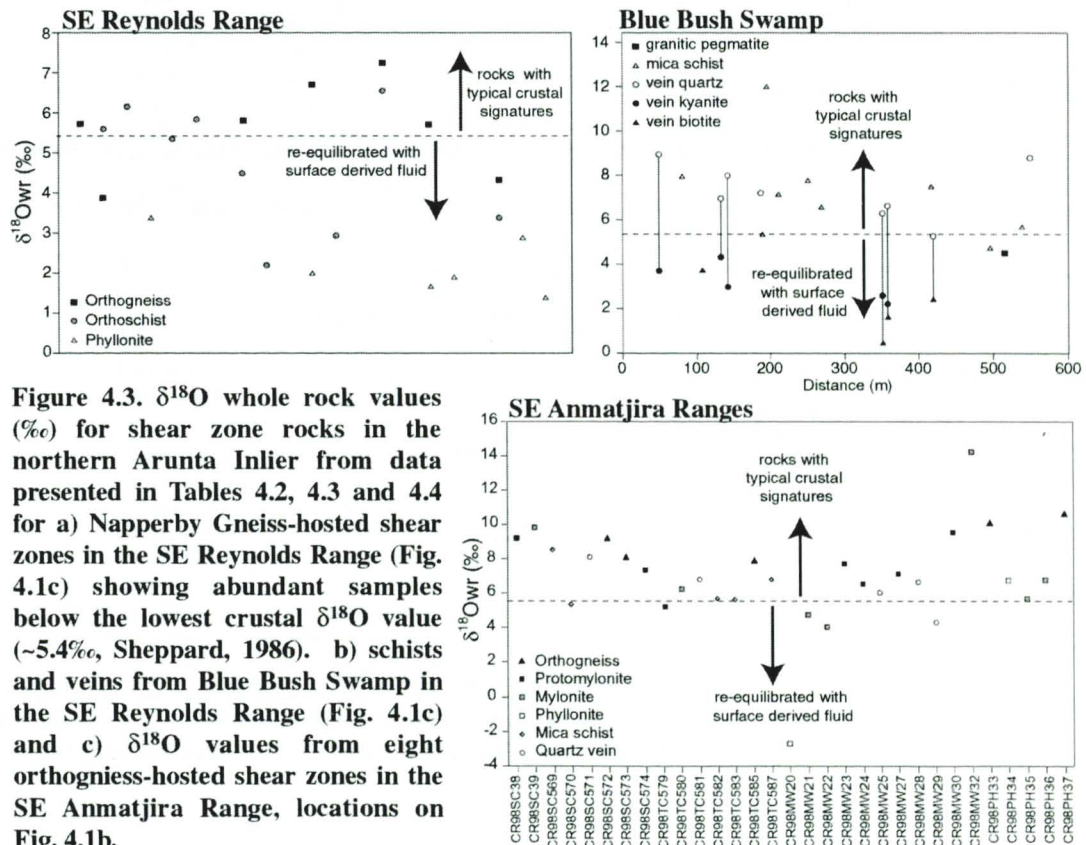


Figure 4.3.  $\delta^{18}\text{O}$  whole rock values (‰) for shear zone rocks in the northern Arunta Inlier from data presented in Tables 4.2, 4.3 and 4.4 for a) Napperby Gneiss-hosted shear zones in the SE Reynolds Range (Fig. 4.1c) showing abundant samples below the lowest crustal  $\delta^{18}\text{O}$  value (~5.4‰, Sheppard, 1986). b) schists and veins from Blue Bush Swamp in the SE Reynolds Range (Fig. 4.1c) and c)  $\delta^{18}\text{O}$  values from eight orthogneiss-hosted shear zones in the SE Anmatjira Range, locations on Fig. 4.1b.



(CR98BBS140 & CR98BBS148) record the lowest  $\delta^{18}\text{O}$  values for schist within the shear zone (4.7‰ & 5.6‰) with the exception of CR98BBS79, a chlorite-rich schist from the middle of the shear zone. The low  $\delta^{18}\text{O}$  values of the pegmatite and surrounding schist within the Blue Bush Swamp Shear Zone are very similar in value to those documented by Cartwright *et al.* (1996) and interpreted to reflect the early contact metamorphic fluid flow. This may suggest that some lowering of  $\delta^{18}\text{O}$  values occurred before shearing, as the pegmatite is unlikely to have been infiltrated by fluids during shearing, due to low permeability. However, there is a general trend of reduction in  $\delta^{18}\text{O}$  values of 3 to 5‰ during shearing at Blue Bush Swamp (Table 4.4, Fig. 4.4b), consistent with the regional trend of lower  $\delta^{18}\text{O}$  values within shear zones. In addition, the  $\delta^{18}\text{O}$  values of quartz-kyanite veins are typically lower than the whole rock values (Fig. 4.4b) indicating that the fluid that formed the veins had lower  $^{18}\text{O}$  than the Mount Freeling Schist.

Table 4.5. Mineral  $\delta^{18}\text{O}$  values (in ‰ V-SMOW) for samples of the Yalbadjandi Shear Zone, orthoschist and phyllonite in the Napperby Gneiss and schist and vein samples in the Mount Freeling Schist at Blue Bush Swamp. Temperature estimates calculated from qz-bi and qz-mu fractionation factors of Zheng (1992) and Chacko *et al.* (1996).

Sample	Rock Type	$\delta^{18}\text{O}_{(\text{qz})}$	$\delta^{18}\text{O}_{(\text{bi})}$	$\delta^{18}\text{O}_{(\text{mu})}$	$\Delta(\text{qz-bi})$	$\Delta(\text{qz-mu})$	T (°C)
<b>Yalbadjandi Shear Zone samples</b>							
CR98MM1	pelitic granulite	9.6	2.0		7.5		288
CR98MM19	granitic orthogneiss	4.3	1.5		2.8		758
CR97AR35	bt-epi phyllonite	0.8	-3.4		4.2		541
CR97AR36	foliated cataclasite	0.4	-2.1		2.5		824
CR97AR37	protomylonite	4.2	0.9		3.3		667
CR98MM12	protomylonite	5.3	4.7		0.6		> 850
CR98MM13	protomylonite	8.8	4.8		4.0		566
CR98MM14	protomylonite	7.4	1.9		5.5		414
CR98MM17	protomylonite	-5.1	-9.3		4.2		541
<b>Napperby Gneiss shear zones samples</b>							
CR98NG214	orthoschist	4.1		0.3		3.8	335
CR99NG26	orthoschist	8.2		4.3		3.9	335
CR99NG34	phyllonite	4.2		0.1		4.1	312
CR98NG173	bi-phyllonite	5.3	4.6		0.7		> 750
<b>Blue Bush Swamp Shear Zone samples</b>							
CR98BBS50	Schist	9.8	4.7		5.1		450
CR98BBS87	Schist	8.2	3.9		4.3		529
CR98BBS111	Schist	6.2	0.2		6.0		397
CR98BBS72	Qtz-bi vein	8.8	3.1		5.7		400
CR98BBS113	Qtz-bi-ky vein	6.4	1.8		4.6		500
CR98BBS123	Qtz-bi-ky vein	5.4	2.6		2.8		750

## 4.5. TEMPERATURE OF SHEARING

As discussed in Chapter Three, the shear zones of the SE Anmatjira and Reynolds Ranges contain fine- to medium-grained protomylonites, schists, phyllonites and quartz veins. The schists contain variably abundant biotite, muscovite and chlorite that have grown at the expense of feldspar, cordierite and garnet. Given that the breakdown of K-feldspar to muscovite is of little importance below 300°C (O'Hara, 1988), and the breakdown of biotite to chlorite is common within greenschist-facies conditions (O'Hara, 1988; Deer *et al.*, 1992) the grade of shearing in the SE Anmatjira and Reynolds Ranges is broadly constrained as being greenschist-facies (300-550°C). However, in order to calculate the composition of the fluid that infiltrated the shear zones, a more accurate estimate of the re-equilibration temperature is necessary. Two minerals that have equilibrated with the same oxygen reservoir will have a systematic variation in their  $\delta^{18}\text{O}$  values as a function of temperature by the relationship:

$$\Delta^{18}\text{O}_{\text{A-B}} = 1000 \ln \alpha_{\text{A-B}} = D \cdot (10^6)/T^2 + E \cdot (10^3)/T + F$$

(e.g. Zheng, 1993a,b) where the  $\Delta^{18}\text{O}_{\text{A-B}}$  is the difference in  $\delta^{18}\text{O}$  of the two minerals (A and B), for example quartz and biotite,  $\alpha_{\text{A-B}}$  is the fractionation of mineral A to mineral B, D, E and F are standards and T is time. Thus, mineral  $\delta^{18}\text{O}$  data are compared in order to constrain the temperatures of shearing. As the relationship depends on complete re-equilibration, variability in the results often occurs where minerals are isotopically zoned or contain internal isotopic heterogeneity, due to lack of complete re-equilibration. Additionally the mixing of re-equilibrated and relict grains in mineral separates may produce scattered results. Cartwright *et al.* (1993) describes such differential resetting in shear zones. Difficulties in obtaining pure mineral separates from the sheared rocks, owing to the intergrowth of biotite with epidote during shearing, and the difficulty in separating feldspar and quartz, may also produce some scatter in the results.

A quartz and biotite mineral pair from the unshered pelitic granulite in the hangingwall of the Yalbadjandi Shear Zone has  $\Delta^{18}\text{O}(\text{qz-bi})$  value of 7.5‰, while the unshered Mount Airy Orthogneiss in the footwall records  $\Delta^{18}\text{O}(\text{qz-bi})$  value 2.8‰. Sheared Mount Airy Orthogneiss in the Yalbadjandi Shear Zone has  $\Delta^{18}\text{O}(\text{qz-bi})$  values that range from 0.65 to 5.53‰ (Table 4.5). Using mineral fractionations from Zheng (1993b), the calculated crystallisation temperature of the Weldon Metamorphics that corresponds to  $\Delta^{18}\text{O}(\text{qz-bi})$  of 7.5‰ is 288°C. The quartz  $\delta^{18}\text{O}$  value (9.6‰) of the Weldon Metamorphics sample (CR98MWt1) is much lower than would be expected (~16‰) given the whole rock  $\delta^{18}\text{O}$

value of 15.1‰. In addition, the estimated temperature of crystallisation (288°C) is not consistent with the granulite texture, suggesting that the two minerals are not in equilibrium within the rock. Low temperature O-isotope resetting of the quartz during minimal fluid-rock interaction associated with the later shearing event is possibly the reason for disequilibrium.

The Mount Airy Orthogneiss (CR98MWt19) preserves a mineral equilibrium temperature of 758°C and likely reflects no later oxygen isotopic re-equilibration following high temperature metamorphism.

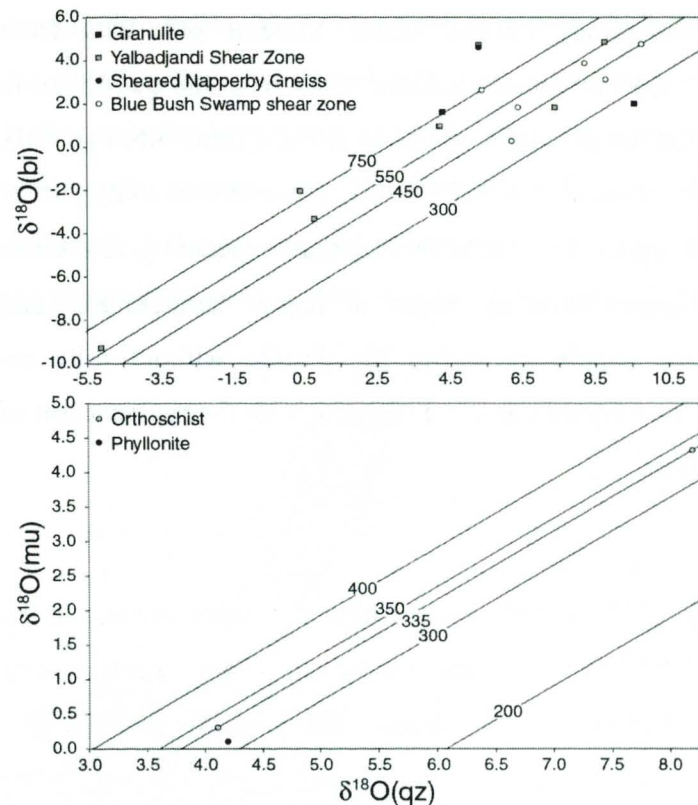


**Figure 4.6.**  $\delta^{18}\text{O}$  values (‰) of a) quartz and biotite for the sheared and unsheared rocks of the Yalbadjandi Shear Zone, sheared Napperby Gneiss and Mount Freeling Schist. b) quartz and muscovite from orthoschist and a phyllonite in shear zones hosted by the Napperby Gneiss. Lines represent the expected fractionation at different temperatures as denoted (°C). Data from Table 4.5. The higher temperature bi-phyllonite sample CR98NG173 likely reflects disequilibrium between the quartz and biotite, while the other sheared rocks indicate mineral growth at ~335°C during shearing. Mineral fractionations are from Zheng (1993a,b). Scatter of the data is discussed in the text.

The corresponding temperatures of the quartz and biotite mineral pairs from the sheared rocks are also scattered, ranging from 414°C to >850°C (Table 4.5, Fig. 4.6). The biotite-epidote phyllonite is the most deformed and hydrated rock within the Yalbadjandi Shear Zone, and therefore is most likely to be completely re-equilibrated. As the phyllonite sample plots with two protomylonites around ~550°C, one of which contains low  $\delta^{18}\text{O}$  values (Table 4.5)

indicating it has been reset by an external fluid, it is likely that temperatures of 541 to 566°C reflect the conditions during shearing. This temperature range is consistent with the grain size and hydrous mineralogy of the sheared rocks

and suggests that fluid infiltration in the Yalbadjandi Shear Zone occurred at lower amphibolite-facies to upper greenschist-facies conditions. The large scatter of the results is consistent with the heterogeneity of the protomylonite recrystallisation textures and the whole rock isotope data.

Quartz and biotite mineral pairs from the Mount Freeling Schist at Blue Bush Swamp have  $\Delta^{18}\text{O}(\text{qz-bi})$  values of 2.8 to 6.0‰. The corresponding mineral fractionation temperatures range from 397 to 750 °C, clustering around 400 to 500°C (Table 4.5, Fig. 4.6). Only one sample (CR98BB123) shows substantial disequilibrium between the quartz and biotite. The minor variation within the other samples is most likely due to either the intergrowth of chlorite and magnetite within the biotite, in schist sample CR98BB87, and muscovite and chlorite replacement of biotite in sample CR98BBS111, or the lack of complete re-equilibration throughout the samples during shearing. Greenschist-facies conditions (400 to 500°C) are consistent with the mineralogy of the schist. Mineral pair data from orthoschists and a phyllonite in the Napperby Gneiss indicate muscovite and quartz are in equilibrium and preserve crystallisation temperatures of 312 to 335°C (Table 4.5, Fig. 4.6). Quartz and biotite in the biotite-phyllonite sample CR99NG173 are substantially out of equilibrium, with the biotite having a higher  $\delta^{18}\text{O}$  value (4.6‰) than expected given whole rock values of 3.4‰. The data suggest shearing began at higher temperatures and continued to lower greenschist-facies conditions within the granite without fully re-equilibrating the biotite phyllonite. This interpretation is consistent with the replacement of biotite with chlorite during retrogression.

#### **4.5.1 Shearing characteristics**

The mineral equilibrium temperatures (335 to 566°C) are similar to other estimates in the region: ~580°C and 400MPa for andalusite- and staurolite-bearing shear zones cutting pelitic granulites in the SE Anmatjira Range (Hand and Buick, 2001); 425 to 535°C at 400 to 650MPa for shear zones within Mount Airy Orthogneiss at Sandy Creek (Cartwright and Buick, 1999); and 550 to 600°C at 500 to 600MPa for shear zones within the Lander Rock Beds (Dirks and Wilson, 1990; Dirks *et al.*, 1991). High geothermal gradients are predicted in central Australia due to the abundance of high heat-producing granites that form the bulk of the Proterozoic basement (Sandiford and Hand, 1998a). Modern-day thermal gradients as high as 35°Ckm<sup>-1</sup> locally are recorded from the Amadeus Basin to the south of the Arunta Inlier (Sandiford and Hand, 1998b). Shear zones in the Reynolds Range (Dirks *et al.*, 1991; Cartwright and Buick, 1999), have geothermal gradients of 25 to 32°Ckm<sup>-1</sup>, and in the Anmatjira Range are calculated to be ~44°Ckm<sup>-1</sup> (Hand and Buick, 2001). Given that a possible locus for shearing is the thermal instability caused by the depth of the overlying sedimentary basins (Sandiford and Hand, 1998b; Hand and Sandiford, 1999), higher geotherms, as predicted by the data, would be expected during shear zone formation. Shearing of the Napperby Gneiss, Blue Bush Swamp and Yalbadjandi Shear

Zones would occur at approximately 12, 16 and 13km depth given geotherms of  $28.5^{\circ}\text{Ckm}^{-1}$  in the Reynolds Range (Cartwright and Buick, 1999) and  $44^{\circ}\text{Ckm}^{-1}$  in the Anmatjira Range (Hand and Buick, 2001). Depths of  $\sim 12$  to 16km for the Reynolds Range shear zones are consistent with the observed ductile deformation and presence of kyanite within the pelitic schists. The Yalbadjandi Shear Zone contains ductile and cataclastic deformation and thus a depth of 13km is consistent with the brittle-ductile transition. Further geobarometry is required to determine the actual pressures during shearing.

The differences in conditions of shearing recorded in the shear zones, from greenschist- to amphibolite-facies, likely represent exposure of shearing at different crustal depths along the thrust system associated with the crustal pop-up structure of Collins and Teyssier (1989). Shallower depths are exposed to the south of the Aileron Thrust, deepening northwards towards the SE Anmatjira Ranges (Fig. 4.7). The relative timing of deformation during the Alice Springs Orogeny may also control the crystallisation within the shear zones and is further discussed in Chapter Five.

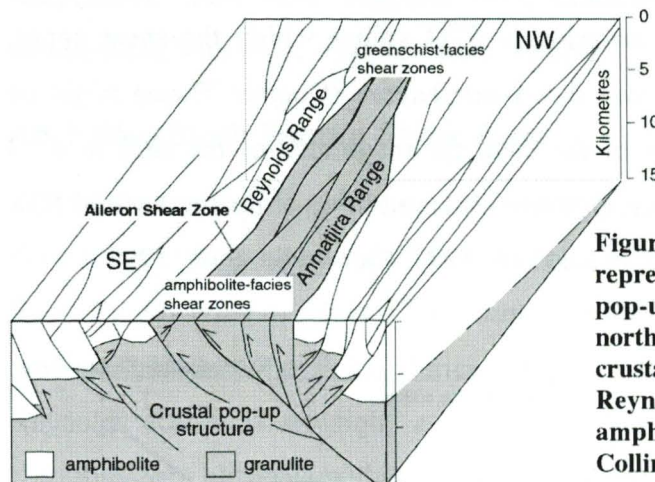


**Figure 4.7.** Schematic block diagram representation of the proposed crustal pop-up structure that operated in the northern Arunta Inlier, exposing the deep crustal granulites of the Anmatjira and Reynolds Ranges along greenschist to amphibolite-facies shear zones (after Collins and Teyssier, 1989).

## 4.6 FLUID-ROCK INTERACTION

Lowering of whole rock  $\delta^{18}\text{O}$  values within the SE Anmatjira and Reynolds Ranges is widespread, occurring in both the small and large shear zones. Within the Yalbadjandi Shear Zone the depletion of  $^{18}\text{O}$  in the sheared rocks is substantial, ranging from a maximum of 13‰ in the footwall to  $\sim 16\%$  in the hangingwall. The Napperby Gneiss shear zones preserve  $^{18}\text{O}$  depletions of up to 6‰, while the orthogneiss hosted shear zones in the SE Anmatjira Ranges preserve  $\delta^{18}\text{O}$  values lowered by  $\sim 3\%$  in Tyson Creek,  $\sim 4\%$  in Sandy Creek and up to  $\sim 7\%$  in the Hansen River Valley (Table 4.2, Fig. 4.4). The range of  $\delta^{18}\text{O}$  values preserved in the rocks reflects heterogeneity in the extent of fluid-rock

interaction consistent with the petrological and geochemical trends discussed in Chapter Three. The fluid-rock interaction that led to the depletion in  $^{18}\text{O}$  within the shear zone rocks, and the identification of the source of the fluid that infiltrated the shear zones, can be assessed by the combination of rock composition analysis, the temperature of shearing and the fractionation of oxygen isotopes.

Lowering of  $\delta^{18}\text{O}$  values during fluid-rock interaction can be achieved by a combination of: (1) infiltration of an exotic, low- $\delta^{18}\text{O}$  fluid; (2) up-temperature equilibrium fluid flow and; (3) compositional changes caused by metasomatism (McCaig, *et al.*, 1990; Dipple and Ferry, 1992b; Bowman *et al.*, 1994; Barker *et al.*, 2000; Cartwright *et al.*, 2001). Geochemical trends in the shear zones from this study (discussed in Chapter Three), and for similar shear zones documented by Cartwright and Buick (1999), indicate that fluid flowed down-temperature, rather than up-temperature in the SE Reynolds and Anmatjira Ranges. Down-temperature fluid flow typically leads to  $^{18}\text{O}$  enrichment and D depletion (Dipple and Ferry, 1992b), suggesting that temperature changes along the fluid flow path were not responsible for the observed lowering in  $\delta^{18}\text{O}$  values within the shear zones. While the interpretation that fluid flow was down-temperature (Chapter Three) might be open to question due to the complexity of the data, the magnitude of the shift in  $\delta^{18}\text{O}$  values (up to 16‰) is far greater than that typically observed in up-temperature fluid flow systems (1-2‰: Chamberlain *et al.*, 1990; Stern *et al.*, 1992; Cartwright *et al.*, 1995).

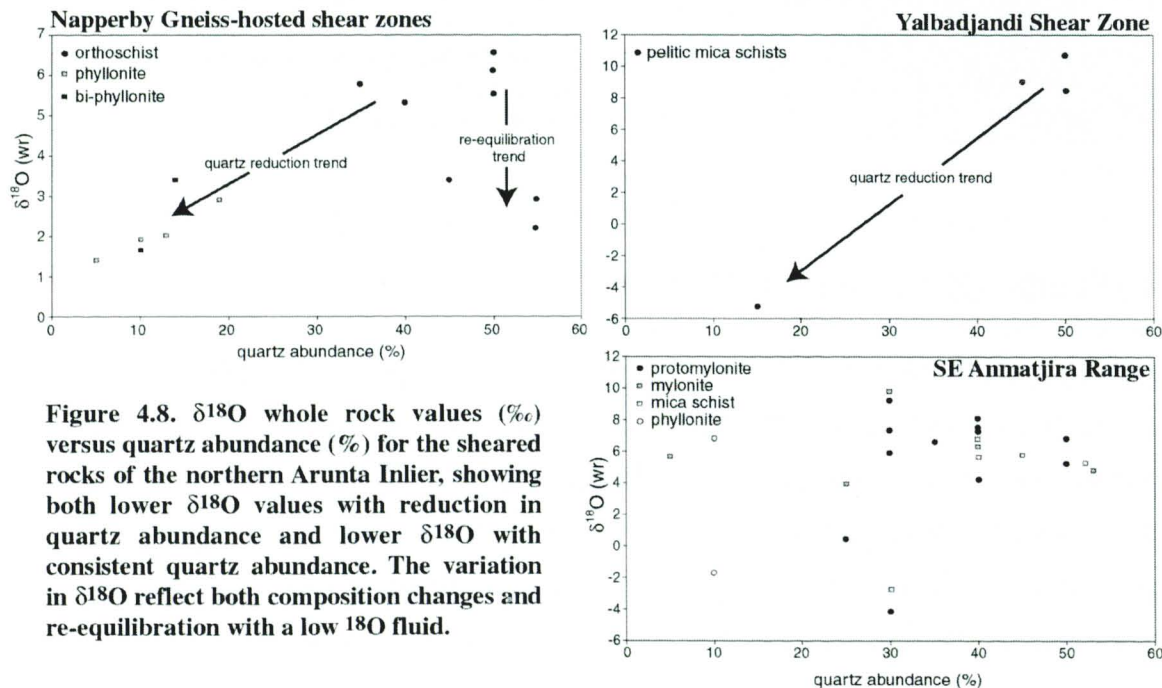


**Figure 4.8.**  $\delta^{18}\text{O}$  whole rock values (‰) versus quartz abundance (%) for the sheared rocks of the northern Arunta Inlier, showing both lower  $\delta^{18}\text{O}$  values with reduction in quartz abundance and lower  $\delta^{18}\text{O}$  with consistent quartz abundance. The variation in  $\delta^{18}\text{O}$  reflect both composition changes and re-equilibration with a low  $^{18}\text{O}$  fluid.

The composition of the domains within the shear zone rocks will also affect the whole rock  $\delta^{18}\text{O}$  values. As  $^{18}\text{O}$  has an observed tendency to accumulate in quartz (Faure, 1986), the quartz-poor phyllonites will have lower  $\delta^{18}\text{O}$  values compared to the quartz-rich protomylonites and orthoschists if they equilibrated with the same oxygen reservoir. Although this trend occurs in some samples (Fig. 4.8), several quartz-rich protomylonites and orthoschists also have lower  $\delta^{18}\text{O}$  values. For example, some orthoschists (CR98NG214, CR98NG218, CR99NG32) in the Napperby Gneiss are lower by more than 4‰ than others of similar composition (Fig. 4.8a). The data from shear zones in the Anmatjira Range indicate similar heterogeneity in isotopic resetting during fluid infiltration (Fig. 4.8c). The Mount Airy Orthogneiss has an  $\delta^{18}\text{O}$  value of  $\sim 7.5\%$  in the Mount Weldon area and  $\sim 10.4\%$  in the Pine Hill area, while the protomylonites with similar composition have  $\delta^{18}\text{O}$  values as low as 4.0‰. In addition to this, compositional changes do not produce changes in  $\delta^{18}\text{O}$  values of this magnitude (Dipple and Ferry, 1992b). Thus the lowering of  $\delta^{18}\text{O}$  values within entire shear zones during down-temperature fluid flow suggests re-equilibration with an exotic low  $^{18}\text{O}$  fluid, in combination with some compositional changes.

#### **4.6.1 Blue Bush Swamp Shear Zone**

The similarity in  $\delta^{18}\text{O}$  values of the Napperby Gneiss and the schist in the shear zone at Blue Bush Swamp may be the result of re-equilibration during contact metamorphic fluid flow. The lowering of schist  $\delta^{18}\text{O}$  values to as low as 4‰ adjacent to granites by combined igneous and meteoric fluids during contact metamorphism is well documented in the Reynolds Range (Cartwright *et al.*, 1996; Vry and Cartwright, 1998). The minimal metasomatism observed within the pelites and the low variance mineral assemblages in the sheared rocks may explain why  $\delta^{18}\text{O}$  values associated with Proterozoic contact metamorphic fluid flow are preserved within the shear zone. The low values of the vein materials suggest that the fluid associated with vein formation within the shear zone at Blue Bush Swamp was derived from the exotic fluid source. Due to the high fluid content of the Mount Freeling Schists the mixing of local fluid and low  $^{18}\text{O}$  fluid may have led to the higher recorded whole rock values in the shear zone at Blue Bush Swamp.

## 4.7 FLUID COMPOSITION

### 4.7.1 Oxygen isotopes

The composition of an infiltrating fluid can be determined if a rock (or a specific mineral therein) has been re-equilibrated to the isotopic composition of the fluid. For a mineral-fluid pair the  $\delta$ -values and fractionation factor ( $\alpha$ ) are related by:

$$\delta^{18}\text{O}_{\text{mineral}} - \delta^{18}\text{O}_{\text{fluid}} = \Delta^{18}\text{O}_{\text{mineral-fluid}} \approx 1000 \ln \alpha_{\text{mineral-fluid}}$$

(Hoefs, 1997). Thus, given the  $\delta$ -value of the mineral and the calibrated  $1000 \ln \alpha_{\text{mineral-fluid}}$  at the temperature of infiltration, the  $\delta$ -value of the infiltrating fluid can be calculated as;

$$\delta^{18}\text{O}_{\text{fluid}} = \delta^{18}\text{O}_{\text{mineral}} - 1000 \ln \alpha_{\text{mineral-fluid}}$$

The infiltration temperatures used here are 550°C for the shear zones in the SE Anmatjira Range, including the Yalbadjandi Shear Zone, 400-500°C for the Blue Bush Swamp Shear Zone and 335°C for the shear zones in the Napperby Gneiss, as calculated in section 4.6. In addition, whole rock  $\delta^{18}\text{O}$  data can provide an estimate of the fluid composition by calculating the combined mineral-water fractionations for all the phases within the rocks using the modal mineral proportions determined in Chapter Three (Table 3.4). This method assumes the mineral assemblages are in equilibrium. This is unlikely to be the case within all the shear zone rocks and, therefore, these results are used with caution.

**Table 4.6. Fluid  $\delta^{18}\text{O}$  composition from samples within the Yalbadjandi Shear Zone calculated from quartz and biotite fractionation with water at 550°C. Fractionation factors from Zheng (1993a, b).**

Sample	$\delta^{18}\text{O}_{(\text{qz})}$	$\delta^{18}\text{O}_{(\text{fluid})}$	$\delta^{18}\text{O}_{(\text{bi})}$	$\delta^{18}\text{O}_{(\text{fluid})}$
	$1000 \ln \alpha$	2.53		-2.51
CR97AR35	0.4	-2.1	-2.1	0.4
CR97AR36	4.2	1.7	0.9	3.4
CR97AR37	8.8	6.3	4.8	7.3
CR98MWt13	0.8	-1.7	-3.4	-0.9
CR98MWt17	-5.1	-7.6	-9.3	-6.8
CR98MWt14	7.4	4.9	1.9	4.4

Within the Yalbadjandi Shear Zone, quartz and biotite from the samples CR97AR35, CR98MWt13 and CR98MWt17 provided crystallisation temperatures near 550°C and are thus likely to contain minerals in mutual equilibrium. The quartz-water and biotite-water fractionation factors ( $\Delta^{18}\text{O}_{\text{qz-}}$

$\text{H}_2\text{O}$ ,  $\Delta^{18}\text{O}_{\text{bi-H}_2\text{O}}$ ) at 550°C are 2.53 and -2.51 respectively (Zheng, 1993a,b). The estimated  $\delta^{18}\text{O}_{\text{fluid}}$  value from the quartz and biotite samples for each rock give a range in fluid values of -7.6 to 4.9‰, excluding CR97AR37, which records values of 6.3 to 7.3‰ (Table 4.6). The  $\delta^{18}\text{O}_{\text{fluid}}$  values are significantly lower than those that would have been in equilibrium with the Mount Airy Orthogneiss, indicating that they are exotic to the area. The shear zones in the SE Anmatjira Range, including the Yalbadjandi Shear Zone,

preserve a range in  $\delta^{18}\text{O}_{\text{fluid}}$  values estimated from whole rock compositions of 10.0 to  $-7.1\text{‰}$  (Table 4.2). The range indicates that low  $^{18}\text{O}$  fluids have infiltrated the shear zones, and is consistent with the compositions estimated from the quartz and biotite data. The sheared samples that have oxygen isotopic values similar to those of the wall rocks may have retained their initial isotopic signature due to interaction with lower volumes of low  $^{18}\text{O}$  fluid that had partially equilibrated with the wall rocks.

**Table 4.7.  $\delta^{18}\text{O}$  of quartz boudins and lenses within orthoschist in Napperby Gneiss shear zones in the SE Reynolds Range.  $\delta^{18}\text{O}_{\text{fluid}}$  values are calculated from qz-H<sub>2</sub>O fractionation factor of Zheng (1993a) at 335°C.**

Sample	$\delta^{18}\text{O}_{(\text{qz})}$	$\delta^{18}\text{O}_{(\text{fluid})}$
CR98NG155	6.6	0.6
CR98NG160	7.2	1.3
CR98NG180	7.0	1.0
CR98NG182	7.4	1.4
CR98NG182	7.2	1.2
CR98NG188	7.6	1.6
CR98NG199	7.4	1.4
CR98NG200	6.9	0.9
CR98NG200	7.4	1.4
CR98NG201	7.4	1.4
CR98NG201	7.4	1.4
CR98NG203	7.1	1.1
CR98NG205	6.0	0.0
CR98NG205	6.3	0.3
CR98NG207	4.4	-1.6
CR98NG209	6.9	1.0

Abundant quartz boudins and lenses that formed initially as veins within the orthoschist of the Napperby Gneiss hosted shear zones have  $\delta^{18}\text{O}_{\text{quartz}}$  values of 7.9 to 4.4‰ (Table 4.7). As the quartz-water fractionation factor ( $\Delta^{18}\text{O}_{\text{qz-H}_2\text{O}}$ ) at 335°C is 5.98 (Zheng, 1993a) the quartz records a range in  $\delta^{18}\text{O}_{\text{fluid}}$  values of  $-1.6$  to  $1.6\text{‰}$ , significantly lower than fluids that would have been in equilibrium with the Napperby Gneiss. The orthoschists and phyllonites preserve a range in  $\delta^{18}\text{O}_{\text{fluid}}$  values of  $-1.3$  to  $3.4\text{‰}$  at 335°C (Table 4.3), consistent with the quartz lenses.

The low  $\delta^{18}\text{O}$  values of the fluid that infiltrated the shear zones in both the SE Anmatjira and Reynolds Ranges is consistent with a fluid of meteoric or formation-water origin (Sheppard, 1986; Hoefs, 1997). The consistent surface-derived fluid  $^{18}\text{O}$ -signatures throughout the rocks suggests that fluid flowed through the shear zones during ductile shearing at 335 to 550°C and that, at least locally, fluid volumes were sufficient to preserve the isotopic signature over long distances.

#### 4.7.2 Hydrogen isotopes

The  $\delta\text{D}$  value of the fluid is calculated from biotite and whole rock samples of the Yalbadjandi Shear Zone and the Napperby Gneiss shear zone rocks in a similar way to the  $\delta^{18}\text{O}$  values. At temperatures of 550°C the  $\delta\text{D}_{\text{fluid}}$  values for the Yalbadjandi Shear Zone range from  $-71.8$  to  $-27.7\text{‰}$ . In the Napperby Gneiss, the fluid that infiltrated the shear zones during shearing at 335°C had estimated  $\delta\text{D}_{\text{fluid}}$  values of  $-68.0$  to  $9.8\text{‰}$ . Both, but particularly the Napperby Gneiss shear zones, indicate possible mixing of waters of different origins. The biotite phyllonite (CR98NG173) yields a positive  $\delta\text{D}_{\text{fluid}}$  value,

substantially higher than metamorphic fluids (-20 to -60‰), indicating a meteoric water influence. However the overlap of  $\delta D$  values for metamorphic fluids and meteoric fluids is large (Hoefs, 1997) restricting the ability for the  $\delta D$  data to constrain the fluid origin alone.

## 4.8 FLUID ORIGIN

Fluid origins can be discriminated by combining the  $\delta D$  and  $\delta^{18}O$  fluid values (Fig. 4.9). The samples from the shear zones in the northern Arunta Inlier plot within the range of formation waters on Figure 4.9, with a clear variation in hydrogen isotopes. The data likely represents the re-equilibration of surface fluids towards rock values during fluid-rock interaction, showing a consistent trend away from the meteoric water line.

This isotopic data suggests that the fluids that infiltrated the shear zones of the SE Anmatjira and Reynolds Ranges were derived from a surface reservoir, penetrating the middle crust during greenschist- to amphibolite-facies metamorphism.

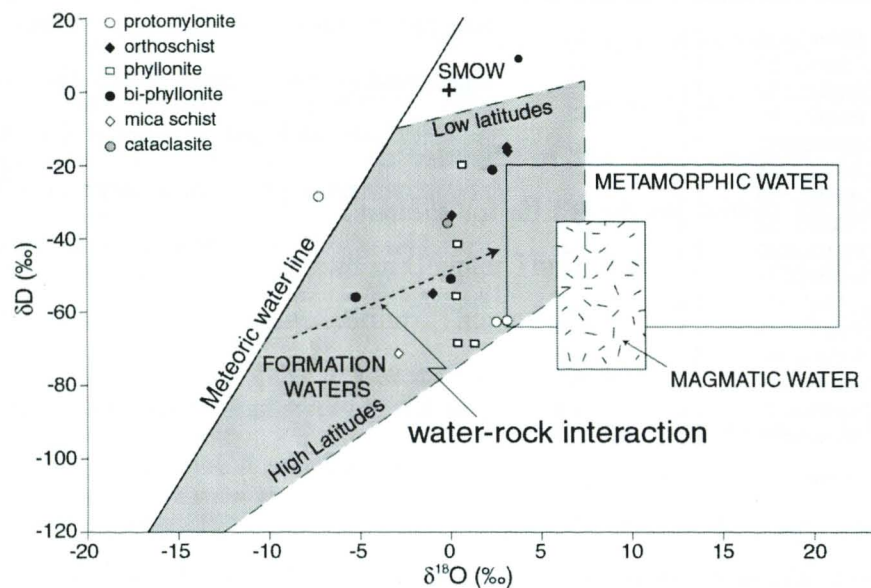


**Figure 4.9.**  $\delta D_{\text{fluid}}$  and  $\delta^{18}O_{\text{fluid}}$  values for the shear zone rocks of the SE Anmatjira and Reynolds Range (data in Tables 4.2 and 4.3) indicating a formation water origin. Formation water, metamorphic water and magmatic water fields after Rollinson, 1993 from data of Taylor, 1974 and Sheppard, 1986. There is a spread of hydrogen values indicating mixing of different fluids during shearing.

There is no clear indication of either high or low latitude formation waters, however. As central Australia moved from low to high latitudes during the Alice Springs Orogeny (300 to 400Ma), the time the shear zones formed (Chapter Five), influences of both may occur within the data. As the Proterozoic crust of the Arunta Inlier was covered with sediments of the Centralian Superbasin from 900Ma the formation water that infiltrated the shear zones is likely to have originated from the overlying sediments. The latitude during deposition of the Basin ranges from 15°N to 64°S from 600 to 245Ma (Veevers, 1984) and is therefore beyond the definition of the data.

## 4.9 CHARACTERISTICS OF FLUID FLOW

### 4.9.1 Yalbadjandi Shear Zone

Both profiles (Fig. 4.2) across the Yalbadjandi Shear Zone have only narrow areas of the low  $\delta^{18}\text{O}$  values. There is often substantially more biotite and epidote in the rocks with low  $\delta^{18}\text{O}$  values (such as samples CR97AR35, CR97AR37, CR98MWt13 and CR98MWt16), indicating an increase in fluid flux through these parts of the shear zone. The discrete zones of low  $\delta^{18}\text{O}$  values likely represent a variation in the volume of fluids becoming focused through structurally-controlled networks within the shear zone. Low  $\delta^{18}\text{O}$  values also occur within samples of protomylonites that preserve brittle deformation characteristics (CR97AR36, CR97AR34). This may suggest that the infiltration of the low  $\delta^{18}\text{O}$  fluid into the Yalbadjandi Shear Zone was facilitated by cataclasis, or hydraulic fracturing, that drove reaction weakening and lead to the development of the biotite- and epidote-rich phyllonite zones. The heterogeneity of strain, and therefore permeability, throughout the shear zone is most likely responsible for the large variation of  $\delta^{18}\text{O}$  values. Due to the lack of local fluid available from the granulite host rocks the higher  $\delta^{18}\text{O}_{\text{fluid}}$  values recorded in the shear zone are likely to represent partial re-equilibration and/or little fluid-rock interaction with the host rocks.

### 4.9.2 Blue Bush Swamp Shear Zone

The variation in values of the schists and veins in the sheared Mount Freeling Schist also indicates variation in the effects of fluid-rock interaction at Blue Bush Swamp. Minimal fluid-rock interaction and/or the mobilisation of local fluids during retrogressive reactions may account of the higher  $\delta^{18}\text{O}$  values recorded within the sheared Mount Freeling Schist compared to the sheared orthogneiss samples. The abundance of large veins and preservation of protolith  $\delta^{18}\text{O}$  values suggest that fluids were substantially focused within the shear zone. Boudinage, kinking and folding of the veins during shearing indicates that deformation continued within the shear zone following initial fluid infiltration, and may have led to partial re-equilibration with the wall rocks.

### 4.9.3 Napperby Gneiss-hosted shear zones

The narrow (5-10m wide) shear zones within the Napperby Gneiss contain extensive compositional domains reflecting strain partitioning and fluid-assisted silica redistribution over metre scales (Chapter Three). The preservation of low  $\delta^{18}\text{O}_{\text{fluid}}$  values and the extensive chemical changes within the shear zones suggest that they hosted significant

fluid flow during shearing. The partially complete retrogressive reactions observed within the phyllonites indicate that fluid flow was substantial throughout shearing. The phyllosilicate-rich shear zones in the Napperby Gneiss would have been significantly weaker than the granitic orthogneiss thus focusing the strain within the interlocking network of shear zones. The permeability generated from metamorphic reactions and deformation within the orthoschists and phyllonites would have been significant, creating effective fluid conduits through the impermeable Napperby Gneiss.

#### 4.10 FORMATION WATERS IN THE MIDDLE CRUST

Shearing within the SE Anmatjira Range occurred under greenschist- to lower amphibolite-facies conditions of 335 to 550°C at depths of 12 to 17km. The shear zone  $\delta^{18}\text{O}_{\text{fluid}}$  values indicate that fluid from a surface reservoir infiltrated the shear zones at or near the brittle-ductile transition. The formation water signature of the fluids indicates that the Centralian Superbasin as a likely source. The infiltration of surface-derived fluid into the middle crust requires large travel distances and, as noted by others, has important tectonic implications for crustal fluid flow (McCaig *et al.*, 1990; Morrison 1994; Upton *et al.*, 1995; Cartwright *et al.*, 1999). In order to maintain the original fluid signature minimal fluid-rock interaction is likely to have occurred prior to the hydration of shear zones, due to the significant distance the fluids had to travel in order to reach the middle crust (McCaig *et al.*, 1990). As fluid requires hydraulic head to move downwards through rocks, the infiltration of fluid into the shear zones is likely to have occurred under upper-crustal conditions. The large volumes of surface-derived fluids may have infiltrated the crust during extensional faulting prior to the onset of compression when the brittle-ductile transition was displaced downwards relative to the subsequent shearing within the zones. The tectonic implications of this are discussed in Chapter Five with the geochronological data. The wider shear zones (100 to 300m wide) indicate channelled fluid flow, where significant fluid-rock interaction is restricted to narrow (1 to 5m) domains, whereas the smaller shear zones (1 to 10m) preserve pervasive fluid-rock interaction. In addition, there are sporadic meteoric O-isotope signatures within the shear zones consistent with fluid channelling. Once compression commenced the fluids had penetrated the crust to depths of ~13 km and possibly up to 17 km and became highly focused within the fault/shear zones, as flow became controlled by relative lithological and fluid pressures. As discussed in Sibson (1998), there are several mechanisms for fluid redistribution within active faults including: 1) dilatancy related to the fault loading cycle, for example seismic pumping (Sibson *et al.*, 1975) where fluids are drawn into the rock pre-failure and expelled once

shear stress is reduced, 2) post-seismic redistribution around rupture irregularities such as dilatational jogs and 3) fault-valve action in over-pressured crust were fluid pressures control fluid redistribution following seismic activity. Seismic pumping generates fluid movement through mobile hydrofractures allowing long distance transport of fluids without substantial interaction with wall rocks (Sibson *et al.*, 1975; McCaig, 1990; Sibson, 1990; Cartwright and Buick, 1999). Extreme fault-valve action also produces substantial fluid movement and is likely responsible for many mesothermal Au-quartz lodes hosted within steep reverse faults (Sibson, 1998). Experiments on rock have shown that dilatancy exists at high temperatures and pressures (Edmond and Paterson, 1972; Fischer and Paterson, 1989), and therefore can operate within the ductile regime (Upton, 1998). In addition, over-pressured fluids play a significant role in the faulting (Sibson, 1998). Thus, once the fluids are at depth fault-valving or seismic pumping allow significant fluid to be rapidly redistributed throughout the crust through interconnecting networks of dilatancy zones within the shear zones (Sibson *et al.*, 1975, Sibson, 1998). Fault-valving is suited to compressional or transpressional fault systems due to the misorientation of steep reverse faults to shear failure, thus increases in fluid pressure to supralithostatic pressures occurs prior to faulting (Sibson, 1998). The episodic nature of fault-valving may also explain the large variation in  $\delta^{18}\text{O}$  values of the shear zone rocks where local fluid-rock equilibrium was not attained (McCaig *et al.*, 1990).

#### 4.11 CONCLUSIONS

The penetration of surface-derived fluids into the middle crust is widely documented (Lobato *et al.*, 1983; McCaig, 1988; McCaig *et al.*, 1990; Morrison 1994; Upton *et al.*, 1995; Cartwright and Buick, 1999) and suggests that permeability linking the upper and middle crust frequently occurs at times of crustal reworking. The contribution of surface water reservoirs to the hydration of middle crustal rocks during orogenesis appears to be significant, and may provide the main source of fluids in crustal retrogression where local fluid is unavailable.  $\delta^{18}\text{O}$  and  $\delta\text{D}$  values from greenschist- to amphibolite-facies shear zones in the northern Arunta Inlier indicate that formation waters were significantly channelled through the middle crust, maintaining their isotopic signature. The intraplate setting in central Australia requires that the infiltration of fluid into the crust is achieved without underthrusting or subduction of hydrous slabs to depth. As suggested in Chapter Three, the fluid is likely to have infiltrated during extensional faulting and migrated back up through the shear zones during seismicity associated with intra-plate compression. This requires the ductile shear zones were connected to upper-crustal fault zones during

tectonism. Fluid flow along the network of faults and shear zones within the northern Arunta Inlier stimulated hydration reactions weakening the middle crust and stimulating the development of the crustal-scale pop-up structure that juxtaposed high-grade granulite and amphibolites in the SE Anmatjira and Reynolds Ranges (Fig. 4.7). The extent and characteristics of reworking in the middle crust can be greatly influenced by crustal-scale fluid flow.

## CHAPTER FIVE

### A NEW PERSPECTIVE ON THE TIMING OF SHEARING IN THE NORTHERN ARUNTA INLIER USING Rb-Sr AND $^{40}\text{Ar}/^{39}\text{Ar}$ DATING

#### **Abstract**

Rb-Sr whole rock and mineral age determinations indicate that shearing in the Yalbadjandi Shear Zone of the SE Anmatjira Ranges occurred just prior to ~300 Ma.  $^{40}\text{Ar}/^{39}\text{Ar}$  data indicate that shearing in the granite basement in the SE Reynolds Range occurred at 353 to 358 Ma, while previous  $^{40}\text{Ar}/^{39}\text{Ar}$  and Rb-Sr data from the Reynolds Range (Cartwright *et al.*, 1999) indicate shear zone ages of 333 to 334 Ma. The shear zones in the northern Arunta Inlier record only Alice Springs Orogeny ages, with some protolith granite ages preserved in porphyroclasts, suggesting that they were not active during the Anmatjira Uplift Event. The evolution of the northern Arunta Inlier involved development of E-W extension faults and shear zones during the opening of the Larapinta Seaway (~490 to 460 Ma) followed by thrusting associated with N-S compression of the Alice Springs Orogeny (360 to 300 Ma). Shearing first occurred at ~358 Ma in the southern edge of the SE Reynolds Range and progressed northward, younging by ~50 Ma over 30 km across strike. The shear zones that record 334 Ma ages are ~8 km across strike from those that yield 358 Ma ages. These data suggest that deformation during the Alice Springs Orogeny progressed northward, with different shear zones becoming active at different times, rather than individual shear zones being long lived. The spatial resolution of deformation produced from the geochronological data has led to a new understanding in the tectonic characteristics of the Alice Springs Orogeny.

#### **5.1 INTRODUCTION**

As shear zones represent sites of intense deformation and fluid flow (Beach, 1980; Selverstone *et al.*, 1991; Dipple and Ferry, 1992a; McCaig, 1997; Cartwright and Buick, 1999), and are active during episodes of crustal reworking (Holdsworth *et al.*, 2001), preserving valuable information regarding the tectonic evolution of metamorphic terrains. In high-grade polymetamorphic provinces, evidence of later, lower-grade metamorphic events and crustal recycling may be best preserved in shear zones where new mineral growth is promoted by deformation and fluid flow (Wintsch *et al.*, 1995; Cartwright *et al.*, 1999). Dating shear zones, therefore, aids the interpretation of regional tectonic events. In order to constrain the timing of mineral growth in tectonic events an understanding of the thermal evolution of shearing relative to the closure temperatures of the new growth minerals is required (Dunlap *et al.*, 1991; Dunlap, 1997). In addition, interpreting the ages of mylonites is difficult if they contain inherited phases or internally heterogeneous isotope

exchange has occurred (e.g. West and Lux, 1993; Freeman *et al.*, 1997) requiring careful sample selection and interpretation of the data.

There is some controversy regarding the evolution of the crustal-scale shear zone network in the northern Arunta Inlier. The shear zones cut all other geological structures and contain lower-grade metamorphic assemblages than their host rocks, varying in mineralogy from lower greenschist-facies to amphibolite-facies. The shear zones are proposed to have developed during both the Proterozoic Anmatjira Uplift Event (1400 to 1500 Ma) and the Palaeozoic Alice Springs Orogeny (Black *et al.*, 1983; Dirks and Wilson, 1990; Collins and Shaw, 1995). The different grades of the shear zone assemblages were interpreted as indications of the different tectonic events, with amphibolite-facies shearing representing the Anmatjira Uplift Event and greenschist-facies shearing indicative of the Alice Springs Orogeny (Dirks *et al.*, 1991; Collins and Shaw, 1995). To date, however, only Palaeozoic Alice Springs Orogeny ages have been documented from the shear zones of the Reynolds Range and Mount Boothby (333 to 334 Ma; Cartwright *et al.*, 1999) and recent interpretations of the tectonic evolution of the region omit the Anmatjira Uplift Event (Hand and Buick, 2001). The aims of this chapter are to: 1) constrain the timing of shearing in the northern Arunta Inlier by dating shear zones discussed in Chapters Three and Four using Rb-Sr and  $^{40}\text{Ar}/^{39}\text{Ar}$  techniques; 2) present a revised tectonic model for the evolution of the northern Arunta Inlier, specifically the regional fluid flow; 3) contribute to the overall understanding of the regional Palaeozoic Alice Springs Orogeny.

## 5.2 GEOLOGICAL SETTING

The northern Arunta Inlier, as discussed in Chapter Two, underwent an extensive Proterozoic geological history of repeated sedimentation, granite emplacement, and high-temperature and low-pressure metamorphism. Shear zones that cut the Anmatjira and Reynolds Ranges form an anastomosing network orientated NW-SE and W-E (Fig. 5.1). Dominantly reverse and some dextral movement directions suggest a transpressional tectonic setting (Collins and Teyssier, 1989, Dirks *et al.*, 1991; Collins and Shaw, 1995). The shear zones contain lower-grade metamorphic assemblages than their host rocks, varying from lower greenschist-facies to amphibolite-facies along strike of both the Anmatjira and Reynolds Ranges (Fig. 5.1). Peak shearing conditions are estimated from kyanite- and sillimanite-bearing schists in the SE Reynolds Range as 550 to 600°C and 500 to 550 MPa (Dirks *et al.*, 1991). While other shear zones cutting granites in the SE Reynolds Range record temperatures of 420 to 535°C at 400 to 650 MPa (Cartwright and Buick, 1999) and 335°C at 400 MPa (Chapter Four). The shear zones, as stated above, are

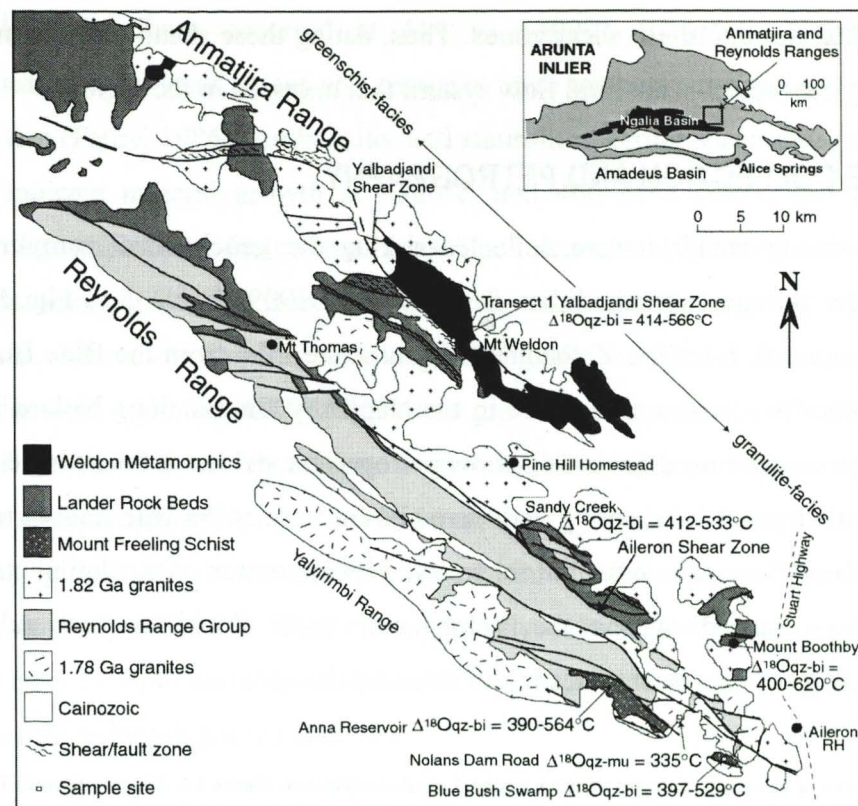


**Figure 5.1.** General geological map of the Anmatjira and Reynolds Ranges, northern Arunta Inlier, showing the location of major shear and fault zones and sample sites for dating samples including the Yalbadjandi Shear Zone (AGR2917-7530) in the SE Anmatjira Range, a 10m wide shear zone in the Napperby Gneiss off Nolans Dam Road (AGR3184-4962) and sheared Mount Freeling Schist at Blue Bush Swamp (AGR3236-4903) in the SE Reynold Range. In addition oxygen isotope thermometry of shear zones rocks (data from Chapter Four and Cartwright and Buick, 1999) for the region are displayed.

proposed to have developed during the Proterozoic Anmatjira Uplift Event (1400 to 1500Ma) and the Palaeozoic Alice Springs Orogeny (300 to 400Ma). The Anmatjira Uplift Event was documented by Black *et al.* (1983) from deformed granites in the Anmatjira Range, and the term was coined by Collins and Shaw (1995) based on these and other 1500 to 1400 Ma ages in the Central Province of the Arunta Inlier. Initially, Alice Springs Orogeny shearing was interpreted as being confined to greenschist-facies mineral growth (Shaw and Black, 1991). However, recently, shear zones in the Strangways Ranges (Bendall *et al.*, 1998; Ballèvre *et al.*, 2000) and re-analysis of the Redbank High Strain Zone (Chapter Seven) in the southern Arunta Inlier indicate that the Alice Springs Orogeny produced at least amphibolite-facies assemblages during peak metamorphic conditions. Work by Cartwright *et al.* (1999) in the Reynolds Range also indicates shear zones that reached temperatures of 535 to 600°C record Alice Springs Orogeny ages.

Oxygen isotope, petrological, and geochemical analyses of sheared rocks in the Anmatjira and Reynolds Ranges, as discussed previously (Chapters Three and Four), indicate that large volumes of fluid derived from a surface reservoir infiltrated the middle-crust, and

were channelled through these shear zones. Thus, dating these shear zones is important to understanding the crustal-scale fluid flow system that operated in the region.

### 5.3 SAMPLE COLLECTION AND PETROGRAPHY

Samples for dating analysis were collected during the geochemical sampling transect program in the northern Arunta Inlier from 1997 to 1999 (Table 5.1, Fig. 5.1). Three samples were chosen from the Yalbadjandi Shear Zone, five from the Blue Bush Swamp Shear Zone, and two from a shear zone in the Napperby Gneiss along Nolans Dam Road (Fig. 5.1). The samples used for dating show petrographic evidence for a single generation of new minerals formed by shearing and were chosen from rocks with known temperature constraints. These factors are essential for tectonic interpretation of the dating analysis. Rb-Sr analysis was carried out on the Yalbadjandi Shear Zone samples and  $^{40}\text{Ar}/^{39}\text{Ar}$  thermochronology on the shear zones in the Reynolds Range.

Table 5.1 Location of shear zone samples used for dating. Locations shown on Figure 5.1. Abbreviations in Table 1.1.

Sample	Location	Australian Grid Reference	Rock Type	Protolith Rock	Mineralogy	Shear Fabric
CR97AR10	YSZ	2922-5330	Mica Schist	Weldon Metamorphic	qz, mu, bt, fs	linear
CR97AR25	YSZ	2917-7530	Protomylonite	Mount Airy Orthogneiss	fs, qz, bi, epi, ap	anastomosing
CR97AR27	YSZ	2917-7530	Mylonite	Mount Airy Orthogneiss	fs, qz, bi, epi, ap	anastomosing
CR99NG29	NGSZ	3184-4962	Bi-Phyllonite	Napperby Gneiss	bi, qz, mu	linear
CR99NG30	NGSZ	3184-4962	Mu-Phyllonite	Napperby Gneiss	mu, chl, qz	linear
CR98BBS40	BBS	3236-4903	Mica Schist	Mount Freeling Schist	qz, bi, mu, fs	anastomosing
CR98BBS79	BBS	3238-4905	Mu-Schist	Mount Freeling Schist	qz, mu, chl, fs	anastomosing
CR98BBS84	BBS	3238-4905	Ky-schist	Mount Freeling Schist	qz, bi, ky, chl, mu, fs	anastomosing
CR98BBS126	BBS	3238-4908	Mica Schist	Mount Freeling Schist	qz, bi, fs, mu	anastomosing
CR98BBS138	BBS	3238-4908	Mica Schist	Mount Freeling Schist	qz, bi, mu, fs	anastomosing

#### 5.3.1 Yalbadjandi Shear Zone

The Yalbadjandi Shear Zone represents the lithological boundary between the pelitic Lander Rock Beds and the Weldon Metamorphics in the SE Anmatjira Range. Structural and compositional similarities suggest that the Weldon Metamorphics are a higher-grade equivalent of the Lander Rock Beds, and that these two units juxtaposed during reverse movement along the Yalbadjandi Shear Zone (Collins and Shaw, 1995). The shear zone is 300m wide, dips steeply to the north and contains an anastomosing NW-SE-trending foliation with strong down-dip lineations. The sheared rocks comprise predominantly heterogeneously-deformed granitic protomylonite and mica schist, equivalents of the granitic Mount Airy Orthogneiss and Weldon Metamorphics pelitic granulite wall rocks. The petrography and oxygen isotope thermometry indicate that shearing within the

Yalbadjandi Shear Zone occurred at 414 to ~500°C (Chapters Three and Four). Recrystallisation of feldspar, micas and apatite at these temperatures should reset the Rb-Sr isotope system (Faure, 1986). Andalusite- and staurolite-bearing shear zones cutting pelitic granulites indicate mineral growth at ~580°C and 400 MPa (Hand and Buick, 2001) consistent with amphibolite-facies conditions. The mica schist (CR97AR10) is fine grained with an anastomosing fabric defined by muscovite and biotite that together represent ~35% of the schist. Muscovite appears to overgrow biotite and is the dominant mica. The quartzofeldspathic mylonite (CR97AR27) and granitic protomylonite (CR97AR25) in the footwall of the Yalbadjandi Shear Zone comprises K-feldspar porphyroclasts surrounded by a matrix of recrystallised quartz and feldspar, newly grown biotite, epidote, and apatite. Biotite and epidote form an anastomosing mylonitic fabric wrapping around feldspar clasts. The mylonite CR97AR27 is more intensely deformed with greater abundance of biotite and epidote. Both samples contain relic K-feldspar that was also dated to provide an indication of the protolith granite age.

### **5.3.2 Blue Bush Swamp Shear Zone**

The Mount Freeling Schist is part of the regional basement sedimentary sequence located in the SE Reynolds Range, and comprises sillimanite-bearing pelitic schists. At Blue Bush Swamp, a 400m wide E-W-oriented shear zone cuts the Mount Freeling Schist. The shear zone dips steeply south with strong down dip lineations, rodded quartz-rich layers, and abundant kyanite-quartz veins. The shear zone at Blue Bush Swamp forms part of the anastomosing network associated with the crustal-scale Aileron Shear Zone that juxtaposes granulites with upper-amphibolite rocks. Petrology and oxygen isotope thermometry indicate metamorphic temperatures were likely to have reached 400 to 500°C (Chapters Three and Four). These temperatures are sufficient to totally reset the  $^{40}\text{Ar}/^{39}\text{Ar}$  system of biotite during shearing (McDougall and Harrison, 1988). Other kyanite-bearing shear zones that cut SE Reynolds Range pelites record slightly higher temperatures of 550 to 600°C (Dirks *et al.*, 1991). The sheared Mount Freeling Schist at Blue Bush Swamp is fine to medium grained, compositionally layered with an anastomosing mylonitic fabric defined by biotite, muscovite, chlorite and kyanite. Muscovite and biotite occur in variable abundances within mafic layers with chlorite. The dated samples are predominantly biotite-rich with the exception of CR98BBS79 that contains muscovite and chlorite as the only phyllosilicates.

### 5.3.3 Napperby Gneiss-hosted shear zones

The Napperby Gneiss is a  $1780 \pm 10$  Ma granitic body of unknown thickness in the SE Reynolds Range (Collins and Williams, 1995). Several 10-100 m wide shear zones cut the Napperby Gneiss in the SE Reynolds Range as part of the Aileron Shear Zone network. The shear zones contain hydrated orthoschists and phyllonites in compositional domains that represent strain partitioning over metre scales. Petrology and oxygen isotope thermometry indicate metamorphic temperatures were likely to be around  $335^\circ\text{C}$  during shearing in the Napperby Gneiss (Chapters Three and Four). These temperatures are sufficient to totally reset the  $^{40}\text{Ar}/^{39}\text{Ar}$  systems of biotite and muscovite and so provide an age estimate of mineral growth (McDougall and Harrison, 1988). A biotite-phyllonite (CR99NG29) and a muscovite-phyllonite (CR99NG30) were collected from a 10m wide shear zone on the road to Nolans Dam (Fig. 5.1). Both phyllonites have linear fabrics parallel to the shear zone wall due to their phyllosilicate-rich composition. The samples represent high-strain domains within the shear zone that have experienced significant fluid flow. The biotite-phyllonite contains 85% biotite with a minor amount of muscovite. The muscovite-phyllonite contains ~70% muscovite with intergrown chlorite.

**Table 5.2. Mineral and whole rock Rb-Sr isotope data for mica-schist (CR97AR10) protomylonite (CR97AR25) and mylonite (CR97AR27) from the Yalbadjandi Shear Zone. Concentrations are in ppm. Internal ( $2\sigma$ ) precision for  $^{87}\text{Sr}/^{86}\text{Sr}$  is  $\pm 0.00002$  to  $0.00004$ ; external precision ( $2s$ ) based on standard runs is  $0.005$  to  $0.05\%$ , depending on sample homogeneity.  $^{87}\text{Rb}/^{86}\text{Sr} \pm 0.5\%$ . Sr isotope ratios relative to SRM987 =  $0.710250$  ( $n=10$ ).**

	Rb (ppm)	Sr (ppm)	$^{87}\text{Rb}/^{86}\text{Sr}$	$\pm 0.5\%$	$^{87}\text{Sr}/^{86}\text{Sr}$	$\pm 0.05\%$
<i>CR97AR10</i>						
whole rock	107.6	66.9	4.69730	0.2349	0.79215	0.0004
muscovite	232.4	41.8	16.30400	0.8152	0.85259	0.0004
biotite ("clean")	983.0	48.0	61.15100	3.0576	1.03999	0.0005
<i>CR97AR25</i>						
whole rock	256.0	98.0	8.28800	0.4144	0.88578	0.0004
apatite	3.3	66.4	0.14610	0.0073	0.84806	0.0004
feldspar	306.0	87.7	10.35900	0.5180	0.96165	0.0005
biotite ("red")	904.0	50.8	53.29700	2.6649	1.07595	0.0005
<i>CR97AR27</i>						
whole rock	248.0	100.3	7.28100	0.3641	0.88331	0.0004
apatite	6.2	76.8	0.23630	0.0118	0.83957	0.0004
feldspar	76.0	126.6	1.76300	0.0882	0.85343	0.0004
biotite	965.0	13.2	237.30000	11.8650	1.90946	0.0010
<i>standards (<math>\pm 2</math> standard deviations of the population)</i>						
BCR-1					0.70500 $\pm 4$	
BHVO-1					0.70346 $\pm 7$	
SRM607	523.5	65.7	24.128 $\pm 51$		1.20061 $\pm 62$	

## 5.4 DATING

### 5.4.1 Rb-Sr results

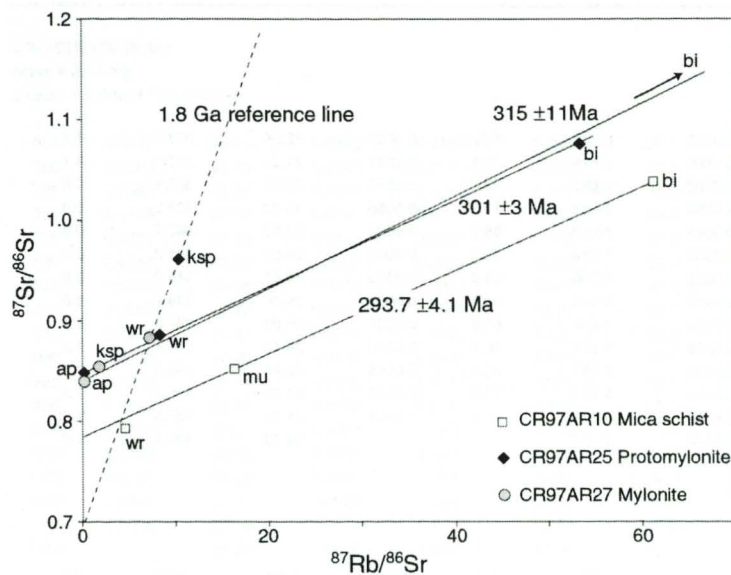


**Figure 5.2.**  $^{87}\text{Sr}/^{86}\text{Sr}$  plotted against  $^{87}\text{Rb}/^{86}\text{Sr}$  for CR97AR10 (mica schist), CR97AR25 (protomylonite) and CR97AR27 (mylonite). Isochrons indicate crystallisation of the three samples at  $293.7 \pm 4.1$  Ma,  $301 \pm 3$  Ma and  $315 \pm 11$  Ma. Sample errors are calculated from external errors of 0.5% for  $^{87}\text{Rb}/^{86}\text{Sr}$  ratios and 0.01% for  $^{87}\text{Sr}/^{86}\text{Sr}$ . Labelled data points depict muscovite, biotite, apatite, K-feldspar, and whole rock for the three different samples. Abbreviations in Table 1.1. Data in Table 5.2.

Results from the Rb-Sr mineral and whole rock analyses for the Yalbadjandi Shear Zone are presented in Table 5.2 and plotted in Figure 5.2. The feldspar of protomylonite samples CR97AR25 lies well above the isochron, indicating it comprises predominantly relic protolith grains. The whole rock samples produce large errors when used to constrain isochrons with biotite, apatite and muscovite for all three

rocks. The large errors are likely due to the presence of inherited feldspar grains within the whole rock sample and are thus whole rocks samples are also not used to constrain the age of shearing. A two-point isochron using biotite and apatite for the protomylonite sample CR97AR25 yields an age of  $301 \pm 3$  Ma. A three-point isochron yields an age of  $315 \pm 11$  Ma for the mylonite CR97AR27. Both samples have very high initial  $^{87}\text{Sr}/^{86}\text{Sr}$  ratios of 0.85. As the Mount Airy Orthogneiss protolith is  $\sim 1.8$  Ga in age, production of radiogenic  $^{87}\text{Sr}$  during the period following formation until recrystallisation at  $\sim 300$  Ma is likely to have caused the high initial  $^{87}\text{Sr}/^{86}\text{Sr}$  ratio. A two-point isochron using muscovite and biotite for the mica schist sample CR97AR10 yields an age of  $293.7 \pm 4.1$  Ma (CR97AR10). All three whole rock data points and CR97AR25 K-feldspar plot close to the 1.8 Ga reference line, with  $\text{Sr}_i$  close to 0.700, close to the mantle value at that time (Faure, 1986). These data are consistent with the 1.8 Ga age of the protolith granite.

### 5.4.2 $^{40}\text{Ar}/^{39}\text{Ar}$ results

In the sheared Mount Freeling Schist at Blue Bush Swamp, age spectra of the biotite (Table 5.3, Fig. 5.3) produced plateau ages of  $345 \pm 2$  Ma,  $353 \pm 2$  Ma and  $358 \pm 2$  Ma. Biotite sample CR98BBS138 from the edge of the shear zone exhibits a reasonably flat age

**Table 5.3**  $^{40}\text{Ar}/^{39}\text{Ar}$  step-heating results for biotite and muscovite from sheared Mount Freeling Schist at Blue Bush Swamp. Sample location and description provided in Table 5.1.

Temp (°C)	Cum $^{39}\text{Ar}$	$^{40}\text{Ar}$	$^{39}\text{Ar}$	$^{37}\text{Ar}$	$^{39}\text{Ar}$	$^{36}\text{Ar}$	$^{39}\text{Ar}$	Vol. $^{39}\text{Ar}$ $\times 10^{-16}$ mol	%Rad. $^{40}\text{Ar}$	Ca/K	$^{40}\text{Ar}/^{39}\text{Ar}$	Age (Ma)	$\pm$ 1s.d. (Ma)
<b>CR88BBS40 Biotite</b>													
Mass = 0.60 mg													
J-value = 0.008472 $\pm$ 0.000025													
650	0.0121	47.42		0.0005		0.0962		0.745	40.0	0.0009	18.96	268.8	6.7
700	0.0515	41.54		0.0014		0.0686		2.429	51.1	0.0027	21.23	298.4	4.1
750	0.1791	31.78		0.0029		0.0288		7.867	73.0	0.0056	23.21	323.9	1.6
775	0.3262	26.81		0.0027		0.0094		9.068	89.5	0.0050	24.00	333.9	0.9
800	0.4885	25.79		0.0017		0.0041		10.00	95.2	0.0032	24.53	340.7	0.8
825	0.6580	25.77		0.0000		0.0030		10.44	96.3	0.0001	24.82	344.3	0.8
850	0.7992	25.95		0.0019		0.0035		8.706	95.9	0.0035	24.87	345.0	0.8
875	0.8709	26.82		0.0002		0.0060		4.419	93.2	0.0003	25.00	346.6	1.5
900	0.8948	30.29		0.0125		0.0176		1.474	82.6	0.0237	25.03	347.0	1.9
950	0.9131	31.72		0.0123		0.0255		1.125	76.1	0.0233	24.13	335.6	2.3
1050	0.9626	27.84		0.0028		0.0129		3.053	86.1	0.0054	23.96	333.5	1.5
1150	0.9979	31.11		0.0027		0.0232		2.173	77.8	0.0050	24.20	336.4	1.2
1300	1.0000	220.5		0.0422		0.6639		0.131	11.0	0.0801	24.28	337.5	76.0
Total		28.59		0.0022		0.0148		61.63			24.18	336.2	1.4
<b>CR88BBS79 Muscovite (chloritised)</b>													
Mass = 0.55 mg													
J-value = 0.008466 $\pm$ 0.000025													
650	0.0520	65.32		0.0910		0.2003		0.203	9.3	0.173	6.08	90.6	14.9
700	0.1279	37.80		0.0612		0.1098		0.296	14.0	0.116	5.30	79.2	9.6
800	0.2824	45.62		0.0013		0.0782		0.603	49.2	0.002	22.46	314.0	5.2
850	0.4459	40.82		0.0006		0.0460		0.637	66.6	0.001	27.20	373.8	3.8
900	0.5577	45.04		0.0189		0.0637		0.436	58.1	0.036	26.18	361.2	4.4
950	0.6333	54.93		0.0436		0.0999		0.295	46.2	0.083	25.35	350.8	7.3
1050	0.7772	47.83		0.0287		0.0761		0.561	52.9	0.055	25.30	350.2	4.4
1150	0.9208	58.37		0.0207		0.1088		0.560	44.8	0.039	26.18	361.2	6.6
1250	0.9591	211.2		0.0698		0.6313		0.149	11.6	0.133	24.59	341.2	67.2
1350	1.0000	317.1		0.0176		0.9918		0.160	7.5	0.033	23.83	331.6	109
Total		65.50		0.0256		0.1444		3.900			22.79	318.3	12.6
<b>CR88BBS84 Biotite</b>													
Mass = 0.60 mg													
J-value = 0.008456 $\pm$ 0.000025													
650	0.0116	64.39		0.0007		0.1607		3.095	26.1	0.0012	16.83	240.1	7.4
700	0.0707	47.16		0.0001		0.0816		15.79	48.8	0.0002	23.01	320.8	2.8
720	0.1619	32.93		0.0001		0.0298		24.34	73.1	0.0002	24.07	334.2	1.3
740	0.2779	27.99		0.0001		0.0104		30.98	88.9	0.0001	24.87	344.4	1.6
760	0.4198	26.58		0.0002		0.0038		37.88	95.6	0.0004	25.42	351.3	1.3
780	0.5584	26.28		0.0001		0.0020		36.99	97.6	0.0001	25.64	354.0	1.0
800	0.6648	26.23		0.0008		0.0020		28.41	97.5	0.0016	25.58	353.3	1.2
830	0.7242	26.21		0.0015		0.0023		15.86	97.3	0.0029	25.50	352.2	1.6
880	0.7698	26.47		0.0002		0.0035		12.16	95.9	0.0003	25.39	350.9	2.1
950	0.8526	26.27		0.0001		0.0020		22.12	97.5	0.0002	25.62	353.8	1.6
1050	0.9728	26.48		0.0001		0.0026		32.08	96.9	0.0001	25.67	354.4	1.2
1150	0.9938	27.76		0.0031		0.0089		5.608	90.3	0.0060	25.08	347.0	3.3
1300	1.0000	26.74		0.0688		0.0148		1.648	83.5	0.1310	22.34	312.1	8.7
Total		28.87		0.0008		0.0127		266.9			25.06	346.8	1.6

i) Errors are one sigma uncertainties and exclude uncertainties in the J-value.

ii) Data are corrected for mass spectrometer backgrounds, discrimination and radioactive decay.

iii) Interference corrections are: ( $^{40}\text{Ar}/^{39}\text{Ar}$ )<sub>cor</sub> = 3.2E-4; ( $^{36}\text{Ar}/^{39}\text{Ar}$ )<sub>cor</sub> = 7.54E-4; ( $^{37}\text{Ar}/^{39}\text{Ar}$ )<sub>cor</sub> = 3.80E-2

iv) J-value is based on an age of 97.9Ma for GIA1550 biotite

v)  $^{40}\text{Ar}/^{39}\text{Ar}$  ratios and ages are corrected for interfering reactions and atmospheric contamination.

vi) Age excludes: errors in J-value determination; error associated with age of std. GIA1550 (~1%); errors associated with decay constants.

Table 5.3. cont.  $^{40}\text{Ar}/^{39}\text{Ar}$  step-heating results for biotite and muscovite from sheared Mount Freeling Schist at Blue Bush Swamp. Sample location and description provided in Table 5.1.

Temp (°C)	Cum $^{39}\text{Ar}$	$^{40}\text{Ar}/^{39}\text{Ar}$	$^{37}\text{Ar}/^{39}\text{Ar}$	$^{36}\text{Ar}/^{39}\text{Ar}$	$^{38}\text{Ar}/^{39}\text{Ar}$	Vol. $\times 10^{-15}$ mol	$^{39}\text{Ar}$ %Rad. $^{40}\text{Ar}$	Ca/K	$^{0}\text{Ar}/^{39}\text{Ar}$	$^{39}\text{Ar}$ Age (Ma)	$\pm 1\text{s.d.}$ (Ma)
<b>CR98BBS126 Biotite</b>											
Mass = 0.47 mg											
J-value = 0.008451 $\pm$ 0.000025											
650	0.0112	55.81	0.0092	0.1159	1.028	38.5	0.0175	21.51	301.3	9.8	
700	0.0393	44.72	0.0018	0.0770	2.567	49.0	0.0034	21.92	306.6	5.2	
725	0.0952	35.26	0.0010	0.0340	5.117	71.4	0.0020	25.17	347.9	2.0	
750	0.1789	29.08	0.0018	0.0117	7.664	87.9	0.0034	25.58	353.1	1.1	
775	0.2791	26.93	0.0007	0.0041	9.178	95.3	0.0013	25.67	354.2	1.0	
800	0.4065	26.44	0.0009	0.0021	11.66	97.4	0.0017	25.77	355.5	1.1	
825	0.5560	26.48	0.0012	0.0016	13.69	98.0	0.0022	25.96	357.8	0.9	
850	0.6902	26.72	0.0005	0.0019	12.28	97.7	0.0009	26.09	359.5	0.9	
875	0.7772	26.92	0.0010	0.0027	7.960	96.8	0.0020	26.07	359.2	1.0	
900	0.8133	27.99	0.0013	0.0064	3.309	93.1	0.0025	26.05	358.9	1.1	
925	0.8334	29.14	0.0006	0.0116	1.838	88.1	0.0012	25.67	354.2	1.7	
950	0.8542	29.43	0.0002	0.0117	1.903	88.1	0.0004	25.93	357.5	1.7	
1000	0.8885	28.2	0.0031	0.0084	3.140	91.0	0.0058	25.67	354.2	1.0	
1050	0.9336	28.03	0.0033	0.0077	4.131	91.7	0.0064	25.72	354.8	1.0	
1100	0.9797	28.32	0.0013	0.0085	4.223	90.9	0.0024	25.76	355.4	1.3	
1200	0.9991	33.7	0.0008	0.0244	1.775	78.4	0.0015	26.44	363.8	1.6	
1300	1.0000	275.9	0.0711	0.8754	0.081	6.2	0.1350	17.17	244.5	152	
Total		28.88	0.0013	0.0107	91.54			25.66	354.1	1.4	
<b>CR98BBS138 Biotite</b>											
Mass = 0.73 mg											
J-value = 0.008448 $\pm$ 0.000025											
650	0.0193	48.25	0.0087	0.1093	1.722	32.9	0.0166	15.89	227.2	7.8	
700	0.0671	36.93	0.0049	0.0573	4.273	54.0	0.0094	19.95	281.0	2.6	
750	0.1877	31.03	0.0029	0.0271	10.76	74.1	0.0056	22.98	320.1	2.0	
800	0.3955	27.19	0.0034	0.0093	18.55	89.7	0.0065	24.38	337.8	0.9	
825	0.5361	26.75	0.0015	0.0050	12.55	94.3	0.0028	25.23	348.5	1.0	
850	0.6559	27.06	0.0026	0.0047	10.70	94.7	0.0050	25.62	353.5	0.9	
875	0.7227	27.91	0.0050	0.0071	5.962	92.3	0.0095	25.76	355.2	1.5	
900	0.7503	30.02	0.0060	0.0167	2.470	83.4	0.0114	25.05	346.3	4.3	
950	0.7867	28.70	0.0050	0.0141	3.247	85.4	0.0095	24.51	339.4	2.0	
1050	0.8952	26.59	0.0080	0.0083	9.686	90.6	0.0152	24.08	334.1	2.0	
1175	0.9966	28.40	0.0034	0.0131	9.054	86.2	0.0064	24.49	339.2	1.0	
1300	1.0000	166.4	0.0698	0.4838	0.306	14.0	0.1330	23.35	324.7	57.1	
Total		29.16	0.0041	0.0166	89.28			24.19	335.5	1.8	

i) Errors are one sigma uncertainties and exclude uncertainties in the J-value.

ii) Data are corrected for mass spectrometer backgrounds, discrimination and radioactive decay.

iii) Interference corrections are: ( $^{36}\text{Ar}/^{37}\text{Ar}$ )<sub>ca</sub> = 3.2E-4; ( $^{38}\text{Ar}/^{37}\text{Ar}$ )<sub>ca</sub> = 7.54E-4; ( $^{40}\text{Ar}/^{39}\text{Ar}$ )<sub>K</sub> = 3.80E-2

iv) J-value is based on an age of 97.9Ma for GIA1550 biotites

v)  $^{40}\text{Ar}/^{39}\text{Ar}$  ratios and ages are corrected for interfering reactions and atmospheric contamination.

vi) Age excludes: errors in J-value determination; error associated with age of std. GIA1550 (~1%); errors associated with decay constants.

spectrum with a weighted mean age of 339  $\pm$  0.41 Ma. Chloritised muscovite produced a plateau age of 356  $\pm$  3 Ma.

In the Napperby Gneiss-hosted shear zone off Nolans Dam Track, the biotite phyllonite CR99NG29 produced a biotite step-heating plateau age of 357  $\pm$  2 Ma (1 $\sigma$ ) (Table 5.4, Fig. 5.4). The muscovite in phyllonite sample CR99NG30 was too substantially intergrown with chlorite to yield a plateau.

## 5.5 INTERPRETATION OF AGE DATA

The data from the Yalbadjandi Shear Zone suggest almost complete isotopic resetting of the mineral Rb-Sr systems at around 293 to 315 Ma. The whole rock samples and one of the feldspar fractions appear to define the Proterozoic Mount Airy Orthogneiss protolith age (~1.8 Ga), which is consistent with the feldspar being preserved as a relic phase within the sheared rocks. Long-term accumulation of radiogenic  $^{87}\text{Sr}$  in the three samples prior to 300 Ma established the high and variable  $\text{Sr}_i$ .

**Table 5.4.**  $^{40}\text{Ar}/^{39}\text{Ar}$  step-heating data for CR98NG29 (biotite-phylionite) and CR98NG30 (muscovite-phylionite) in a Napperby Gneiss-hosted shear zone off Nolans Dam Track (AGR3184-4962) in the SE Reynolds Range. Sample location and description in Table 5.1.

Temp (°C)	Cum $^{39}\text{Ar}$	$^{40}\text{Ar}/^{39}\text{Ar}$	$^{37}\text{Ar}/^{39}\text{Ar}$	$^{36}\text{Ar}/^{39}\text{Ar}$	Vol. $\times 10^{-14}$ mol	%Atmos. $^{40}\text{Ar}$	Ca/K	$^{40}\text{Ar}/^{39}\text{Ar}$	Age (Ma)	$\pm 1\text{s.d.}$ (Ma)
<b>CR98NG29 Biotite</b>										
Mass = 0.60mg										
J-value = 0.009140 $\pm$ 0.000365										
600	0.0054	38.95	0.0240	0.0798	0.164	57.2	0.0456	15.34	236.7	6.5
680	0.0387	25.42	0.0042	0.0131	1.012	14.4	0.0079	21.52	323.9	1.6
710	0.1116	24.43	0.0029	0.0034	2.211	3.7	0.0057	23.39	349.5	0.9
730	0.2072	24.51	0.0020	0.0017	2.899	1.7	0.0037	23.97	357.4	0.9
750	0.2953	24.36	0.0016	0.0013	2.673	1.3	0.0031	23.94	356.9	0.8
770	0.3632	24.39	0.0006	0.0013	2.061	1.1	0.0011	23.97	357.4	0.8
800	0.4349	24.23	0.0006	0.0011	2.176	0.9	0.0010	23.88	356.1	1.2
850	0.5375	24.37	0.0007	0.0010	3.113	0.9	0.0014	24.04	358.4	0.8
900	0.6028	24.14	0.0027	0.0020	1.981	2.0	0.0052	23.50	351.1	1.1
950	0.6617	24.05	0.0062	0.0034	1.787	3.6	0.0119	23.02	344.5	1.0
1000	0.7441	23.99	0.0051	0.0020	2.500	2.1	0.0098	23.36	349.1	1.5
1100	0.9557	24.05	0.0012	0.0014	6.417	1.5	0.0022	23.60	352.5	1.0
1200	0.9958	24.68	0.0001	0.0042	1.218	4.3	0.0002	23.41	349.8	1.3
1300	1.0000	38.66	0.0011	0.0511	1.272	34.7	0.0021	23.53	351.4	6.7
<b>CR98NG30 Muscovite</b>										
Mass = 0.60mg										
J-value = 0.009140 $\pm$ 0.000365										
650	0.0135	23.89	0.0251	0.0327	0.549	33.9	0.0477	14.18	219.9	9.9
750	0.0411	32.43	0.0002	0.0192	1.120	15.2	0.0003	26.71	394.1	7.5
800	0.0796	30.33	0.0031	0.0169	1.568	12.0	0.0059	25.29	375.2	4.9
850	0.1894	18.76	0.3212	0.0231	4.460	33.7	0.6104	11.92	186.6	6.3
900	0.5331	21.49	0.0823	0.0060	13.970	7.6	0.1565	19.68	298.4	2.6
950	0.7704	21.13	0.0470	0.0006	9.647	0.3	0.0893	20.91	315.5	3.5
1000	0.8488	20.64	0.0921	0.0006	3.188	0.5	0.1751	20.44	308.9	3.9
1050	0.8841	18.92	0.1713	0.0019	1.435	2.1	0.3255	18.33	279.4	6.8
1100	0.9276	20.10	0.0951	0.0002	1.765	0.2	0.1807	20.02	303.2	1.5
1150	0.9733	21.23	0.0745	0.0013	1.861	1.7	0.1416	20.83	314.4	9.0
1200	0.9884	15.87	0.7494	0.0237	0.613	21.5	1.4246	8.91	141.3	8.4
1300	1.0000	14.18	1.2578	0.0239	0.471	16.7	2.3921	7.21	115.2	8.9

i) Errors are one sigma uncertainties and exclude uncertainties in the J-value.

ii) Data are corrected for mass spectrometer backgrounds, discrimination and radioactive decay.

iii) Interference corrections are: ( $^{40}\text{Ar}/^{39}\text{Ar}$ )<sub>ca</sub> = 3.2E-4; ( $^{37}\text{Ar}/^{39}\text{Ar}$ )<sub>ca</sub> = 7.54E-4; ( $^{36}\text{Ar}/^{39}\text{Ar}$ )<sub>ca</sub> = 3.80E-2

iv) J-value is based on an age of 97.9Ma for GA1550 biotite

v)  $^{40}\text{Ar}/^{39}\text{Ar}$  ratios and ages are corrected for interfering reactions and atmospheric contamination.

vi) Age excludes: errors in J-value determination; error associated with age of std. GA1550 (~1%); errors associated with decay constants.

Mineral resetting was probably the consequence of deformation-driven recrystallisation and mineral growth during shearing. At 1.8 Ga the Sr was equilibrated at the scale of the

granite pluton and its contact aureole (some hundreds to thousands of metres), but at 300 Ma, the Sr was equilibrated on much smaller scale (a few metres) within the Yalbadjandi shear zone. This is typical of these types of systems (Faure, 1986). The closure temperatures for the Sr system in muscovite is around  $500 \pm 50^\circ\text{C}$  Jäger (1979) while that in biotite is  $320 \pm 40^\circ\text{C}$  for biotite (Harrison *et al.*, 1985). As the temperatures for this shear zone (414 to  $550^\circ\text{C}$ ) are higher than the closure temperature for biotite, which constrains the isochrons, the ages are minima for shearing and likely represent cooling of the shear zone.

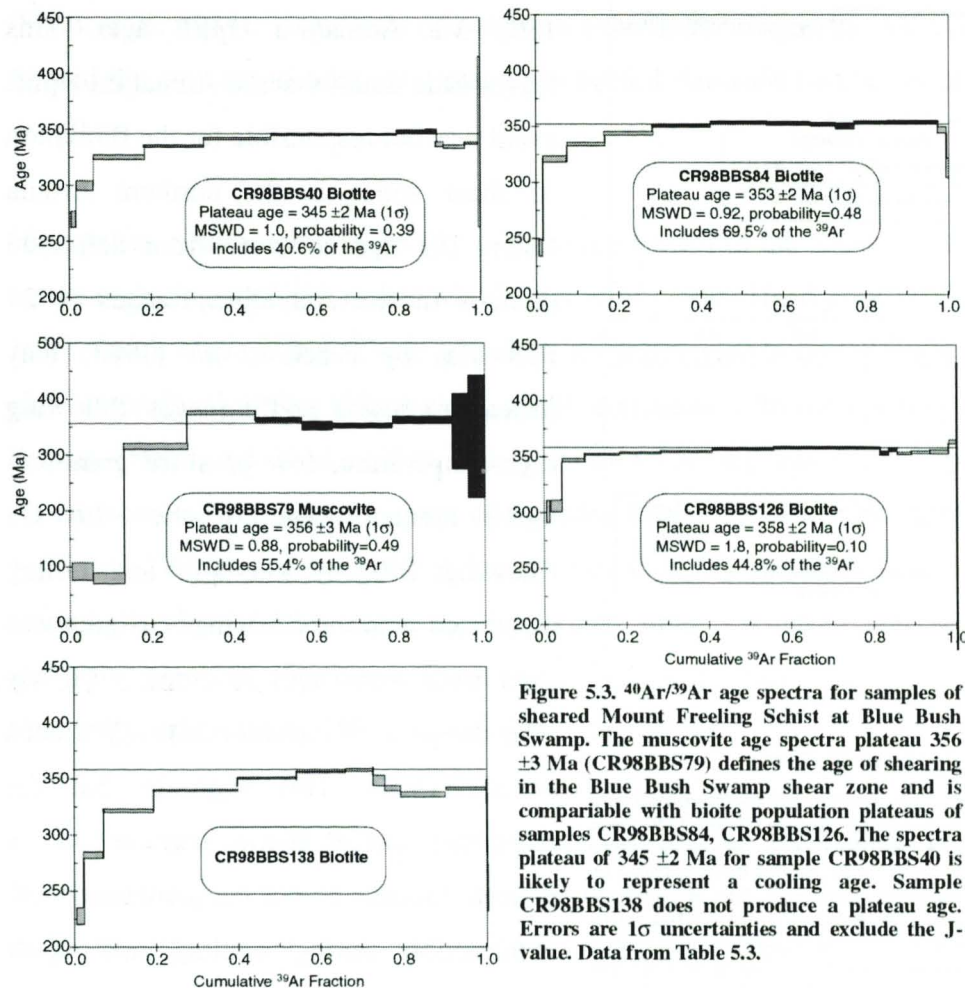


Figure 5.3.  $^{40}\text{Ar}/^{39}\text{Ar}$  age spectra for samples of sheared Mount Freeling Schist at Blue Bush Swamp. The muscovite age spectra plateau  $356 \pm 3$  Ma (CR98BBS79) defines the age of shearing in the Blue Bush Swamp shear zone and is comparable with biotite population plateaus of samples CR98BBS84, CR98BBS126. The spectra plateau of  $345 \pm 2$  Ma for sample CR98BBS40 is likely to represent a cooling age. Sample CR98BBS138 does not produce a plateau age. Errors are  $1\sigma$  uncertainties and exclude the J-value. Data from Table 5.3.

As the shear zones in the Napperby Gneiss record shearing temperatures of  $335^\circ\text{C}$ , similar to the blocking temperature of the Ar system in biotite ( $\sim 300^\circ\text{C}$ , Dodson, 1973), the  $^{40}\text{Ar}/^{39}\text{Ar}$  mineral age for biotite phyllonite sample CR99NG29 ( $357 \pm 0.4$  Ma) should be that of recrystallisation during shearing. The variation in  $^{40}\text{Ar}/^{39}\text{Ar}$  mineral ages in the sheared Mount Freeling Schists at Blue Bush Swamp may be cooling ages, as this shear zone reached temperatures of 400 to  $500^\circ\text{C}$ . However, as the closure temperature for muscovite in the Ar system is  $\sim 400^\circ\text{C}$  (Wijbrans and McDougall, 1986), the muscovite-schist sample CR98BBS79 should yield the age of shearing. The plateau age of sample CR98BBS79 of  $356 \pm 3$  Ma is within error of two biotite samples from the kyanite- and

mica-schists CR98BBS84 ( $353 \pm 2$  Ma) and CR98BBS126 ( $358 \pm 2$  Ma), respectively. These ages are also consistent with that of the Napperby Gneiss-hosted shear zone biotite-phyllosite sample CR99NG29 ( $357 \pm 0.4$  Ma). Therefore, it is concluded that samples CR98BBS79, CR98BBS84, CR98BBS126 and CR99NG29 yield ages close to that of recrystallisation in the shear zones and that shearing occurred at  $\sim 356$  Ma in the shear zone at Blue Bush Swamp and that off Nolans Dam Track in the SE Reynolds Range (Fig. 5.1).

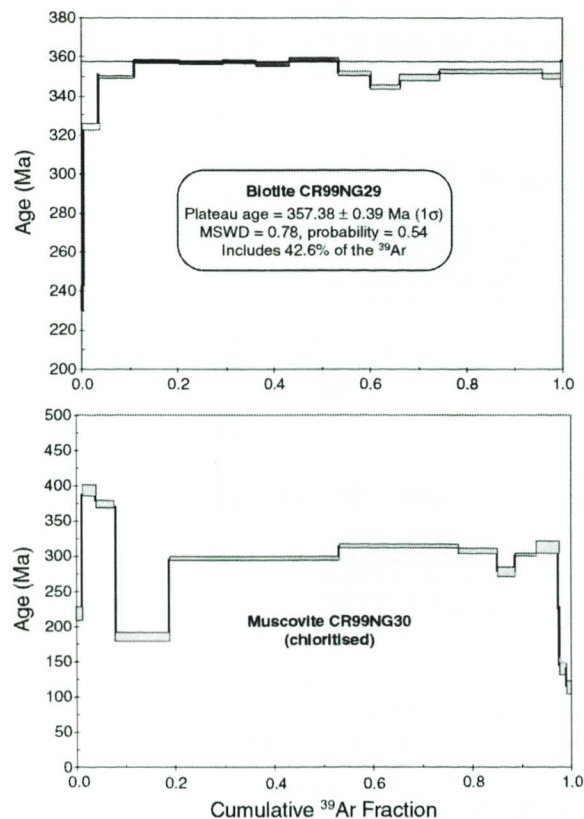


Figure 5.4.  $^{40}\text{Ar}/^{39}\text{Ar}$  age spectra for biotite-phyllosite CR99NG29 and muscovite-phyllosite CR99NG30 from a Napperby Gneiss-hosted shear zone off Nolans Dam Track (Fig. 5.1). The criteria for the plateau is three or more consecutive steps comprising  $>40\%$  of the total  $^{39}\text{Ar}$  with ages within two sigma of the weighted mean age. The biotite samples provide a plateau at  $357 \pm 0.4$  Ma. The error on the plateau is  $1\sigma$ . The muscovite has a humped spectra typical of samples that are chloritized, and do not produce a geologically meaningful plateau age. Data in Table 5.4.

The shear zones do not record any 1400 to 1500 Ma Anmatjira Uplift ages. This leaves little doubt that the Anmatjira Uplift event was not responsible for the formation of shear zones in the northern Arunta Inlier. The age collected from deformed granites in the Anmatjira Ranges ( $1424 \pm 58$  Ma) by Black *et al.* (1983) may instead represent cooling ages following high-temperature, low-pressure granulite-facies metamorphism of the  $\sim 1.6$  Ga Chewings Orogeny. The uplift and cooling associated with the Chewings Orogeny was slow with some ages recorded  $\sim 100$  My after the peak of metamorphism (Williams *et al.*, 1996). This suggests that the Anmatjira Uplift Event may not be a discrete tectonic event, but associated with deformation during cooling and uplift following the Chewings Orogeny.

## 5.6 TECTONIC SYNTHESIS

### 5.6.1 Stratigraphic and geochronological constraints

By the end of the Proterozoic (900 Ma), central Australia was part of the large Australian continental block and became blanketed in a thick sequence of lacustrine and marine sediments forming the Centralian Superbasin (Lindsay, 1999). The opening of the Larapintine Seaway during a period of extension at  $\sim 490$  Ma (Hand *et al.*, 1999) is

recorded in fossil, lithological and palaeomagnetic data within the sediments of the Centralian Superbasin (Webby, 1978). This period of extension represents the onset of tectonic activity that developed into the compressive Alice Springs Orogeny at 400 Ma (Hand and Buick, 2001). Timing of Alice Springs-age deformation that followed is indicated within the basins predominantly by the disruption of post-Cambrian (post Petermann Orogeny at 560 to 520 Ma: Scrimgeour and Close, 1999) sediments (Shaw *et al.*, 1992). There is no evidence for sedimentation in the Amadeus Basin after the late Devonian, suggesting the Alice Springs Orogeny was the last tectonic event in this region (Shaw *et al.*, 1984). The effects of basement exhumation during the Alice Springs Orogeny formed the structural basins now present in central Australia (Walter *et al.*, 1995; Read *et al.*, 1999).

High-grade metamorphic rocks (up to granulite-facies) in the eastern Arunta Inlier record metamorphic ages of 490 to 460 Ma (Miller *et al.*, 1998; Hand *et al.*, 1999; Mawby *et al.*, 1999; Buick *et al.*, 2001). These granulites are interpreted to have formed within an intra-plate extensional setting (Hand *et al.*, 1999) consistent with the opening of the Larapinta Seaway (Hand and Buick, 2001). This extensional setting was rapidly transformed into a contractional setting with the onset of thrusting during the Alice Springs Orogeny, just 60 My later. To date, ages of the Alice Springs Orogeny are restricted to greenschist- to amphibolite-facies shear zones in the Arunta Inlier (Windrim and McCulloch, 1986; Cooper *et al.*, 1988; Black and Shaw, 1991; Collins and Shaw, 1995; Bendall *et al.*, 1998; Cartwright *et al.*, 1999; Ballèvre *et al.*, 2000; this study).

In the northern Arunta Inlier,  $^{40}\text{Ar}/^{39}\text{Ar}$  and Rb-Sr ages from other shear zones in the Reynolds Range at Mount Boothby and Sandy Creek (Fig. 5.1, 5.5) record shearing at 333 to 334 Ma (Cartwright *et al.*, 1999). Taken together with the ages from this study, these data indicate that shearing occurred over a protracted interval in the area. The oldest shear zones occur in the south, with progressively younger shearing recorded northwards (Fig. 5.5). Although biotite records cooling ages equivalent to temperatures of  $320 \pm 40^\circ\text{C}$  (Harrison *et al.*, 1985) at  $\sim 300$  Ma within the Yalbadjandi Shear Zone, the shear zones in the SE Reynolds Range had cooled past  $300^\circ\text{C}$  (Dodson, 1973) at  $\sim 356$  Ma and, therefore, the younger age of the Yalbadjandi Shear Zone can not be explained by cooling across the region. This indicates that although the actual shearing age is not constrained within the Yalbadjandi Shear Zone it is younger than the shear zones to the south. This data indicates a  $\sim 50$  My difference in ages is recorded over 30 km across-strike distance, suggesting a northward progression in the active deformation front of  $0.6 \text{ kmMy}^{-1}$  or  $6 \text{ mmy}^{-1}$ . This

implies that the mechanisms controlling deformation were being rapidly transmitted through the crust from the south to north.

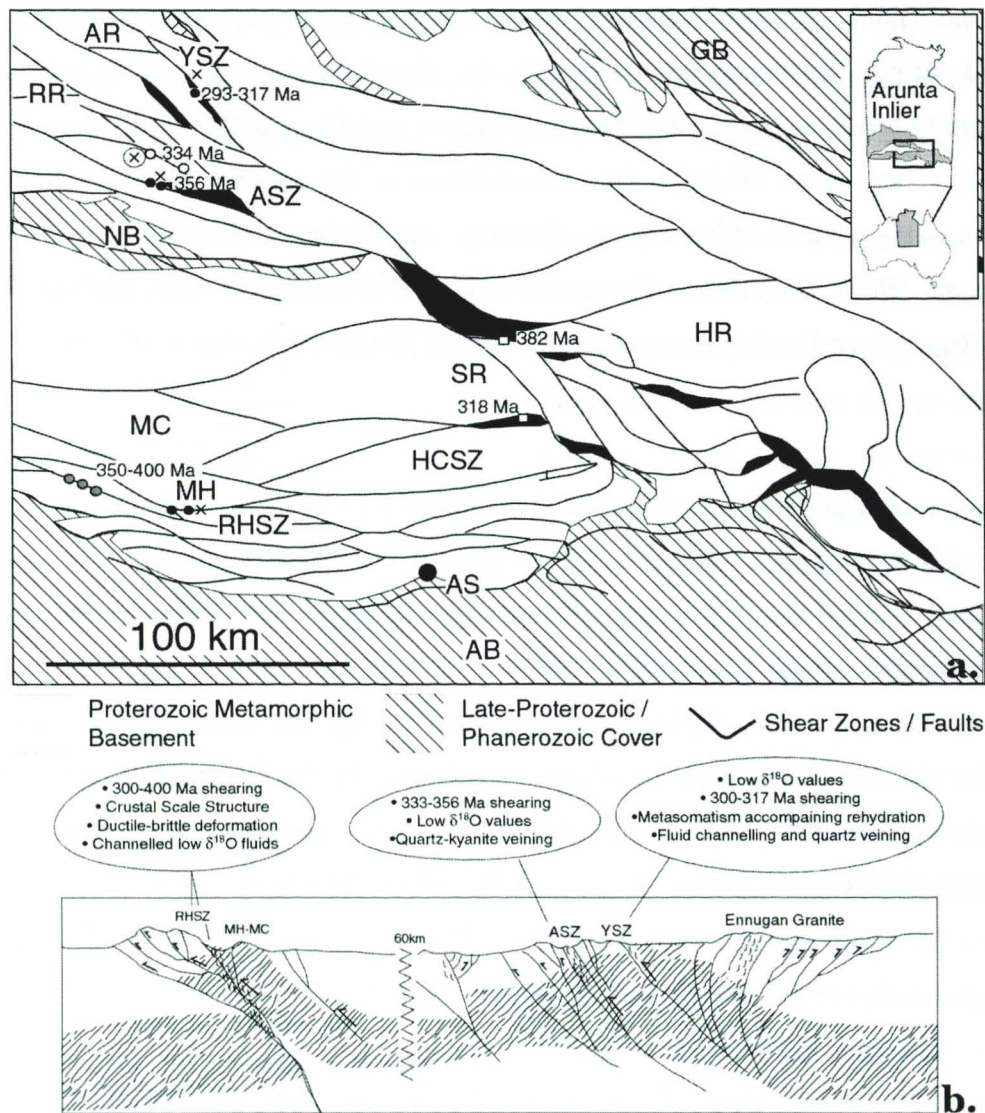


Figure 5.5. a) General tectonic map of the central and eastern Arunta Inlier showing the location of the major faults and shear zones (after Cartwright and Buick, 1999). Shear zones: Aileron Shear Zone, ASZ; Harry Creek Shear Zone, HSCZ; Redbank High Strain Zone, RHSZ; Yalbadjandi Shear Zone, YSZ. Geological regions: Amadeus Basin, AB; Anmatjira Range, AR; Georgina Basin, GB; Harts Range, HR; Mount Chapple, MC; Mount Hay, MH; Ngalia Basin, NB; Reynolds Range, RR; Strangways Range, SR. Alice Springs, AS. Also shown are locations of ages of shear zones from this study (closed circles) Cartwright *et al.* (1999) (open circles), Shaw and Black (1991) (grey circles) and Ballèvre *et al.* (2000) (open square). The crosses denote shear zones that contain  $\delta^{18}\text{O}$  values  $<5\%$  from this study and Cartwright and Buick (1999) (circled crosses). b) Schematic cross-section across the central Arunta Inlier, showing the distribution of fault and shear zones and associated distribution of granulite-facies rocks (diagonal stippled) uplifted during the Alice Springs Orogeny. Also shown are summaries of the data from Chapters 3, 4, 5 and 7 for the Reynolds and Anmatjira Ranges, and Redbank High Strain Zone.

On a larger scale, however, the distribution of ages is not as regular (Fig. 5.5). Sm-Nd ages of garnet in Alice Springs amphibolite-facies shear zones from the SE Arunta Inlier are

318 to 382 Ma during the Alice Springs Orogeny (Bendall *et al.*, 1998; Ballèvre *et al.*, 2000). Rb-Sr data from the Redbank High Strain Zone in the south of the Arunta Inlier indicates thrusting may have occurred at 350 to 400 Ma (Shaw and Black, 1991). These data indicate that deformation progressed from north to south in the SE Arunta Inlier. The lack of data in the region between the Anmatjira-Reynolds Ranges and those in the SE Arunta Inlier leaves doubt over the connection of the deformation trends. However, it is clear that some mechanism, likely a response to the change from extension to contraction during the early Devonian, controlled deformation spatially within the Arunta Inlier. The geochronological data indicates the Alice Springs Orogeny produced local deformation over ~50 My cycles throughout a ~100 My period indicating that deformation during the Alice Springs Orogeny occurred as discrete events throughout the region.

### **5.6.2 Structural constraints**

The shear zones in the northern Arunta Inlier represent the last major tectonic activity in the region (Shaw *et al.*, 1984; Hand and Buick, 2001). The shear zones form a crustal- to lithospheric-scale network (Goleby *et al.*, 1989) with predominantly north-dipping structures (Fig. 5.5). Kinematic indicators imply reverse movement across the shear zones with some sinistral strike slip movement indicative of a transpressional environment (Collins and Teyssier, 1989; Chapter Three). Collins and Teyssier (1989) have interpreted substantial movement involving the juxtaposition of granulites against amphibolite-facies rocks during shearing as a crustal pop-up structure with granulite-facies gneisses in the core. The transpressive setting in the Anmatjira and Reynolds Ranges is consistent with an Arunta-wide inversion of the crust during compression associated with the Alice Springs Orogeny responsible for the exhumation of the middle crustal rocks of the Arunta Inlier.

### **5.6.3 Shear zone development through time**

The spread of ages indicated by the dating suggests that the shear zones within the pop-up structure were active incrementally over an extended period of time (Fig. 5.5). This may have been a response to the combination of internal heterogeneities and thermal conditions within the crust during the Alice Springs Orogeny. The larger crustal-scale shear zones that define the pop-up structure may represent a re-activated deeply penetrating graben structure (Fig. 5.6). In the eastern Arunta, just prior to the Alice Springs Orogeny, extensional tectonism associated with the Larapinta Event (490 to 460 Ma) produced high-grade metamorphism of basinal sediments in the Harts Range region (Mawby *et al.*, 1998; Buick *et al.*, 2001). It is possible that the rifting evident in the Harts Range at this time may have caused some extension in Reynolds and Anmatjira Ranges area (Fig. 5.6). The lack of

metamorphosed basinal sediments in the Reynolds and Anmatjira Ranges region suggests the degree of tectonism and subsequent sedimentation associated with the Larapinta Event in the central Arunta was minimal in comparison to the eastern Arunta. In this scenario, crustal extension, in the Reynolds and Anmatjira Ranges region produced a series of extensional faults forming a graben structure during the Larapinta Event. The graben then became inverted as the stress fields reversed to compression 60 My later during the Alice Springs Orogeny and created the now exposed pop-up structure (Fig. 5.6). The NW-SE gradation in metamorphic temperatures from greenschist- to amphibolite-facies in the shear zones along the Reynolds and Anmatjira Ranges, and the complimentary gradation in the country rocks, may be associated with shallowing of the Graben structure westward, as a response to the centre of tectonism being to the east. The compression uplifting granulite-facies rocks along amphibolite-facies shear zones in the SE and only greenschist-facies rocks to the NW. The only evidence of extensional activity of the shear zones seen in the field was asymmetric folding preserving normal shear sense in steeply north dipping shear zone in Tyson Creek that were cut by small reverse sense shear bands (Chapter Three). The degree of erosion associated with exhumation of the pop-up structure has also removed the sediments that may indicate a period of extension in the region.

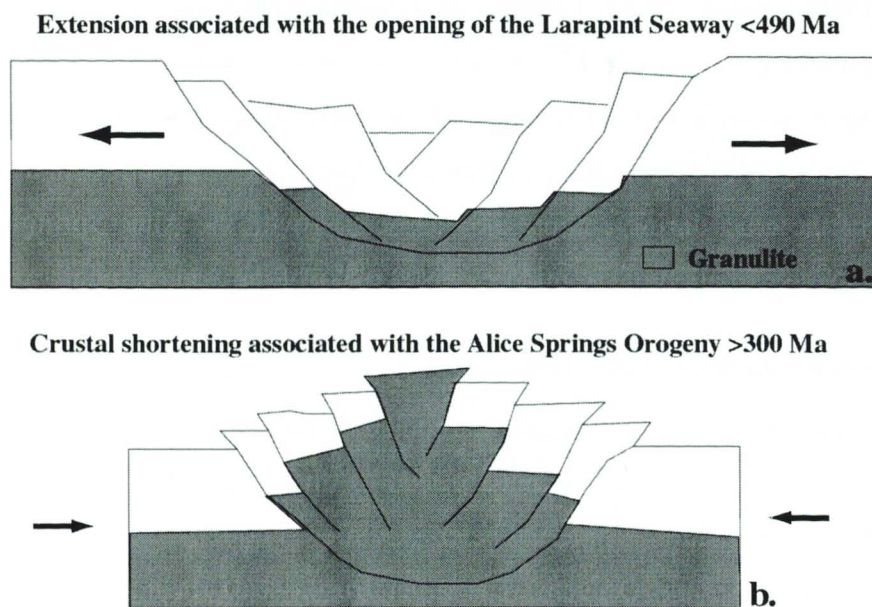


**Figure 5.6.** Schematic representation of the late tectonic evolution of the northern Arunta Inlier, a) Development of a graben structure in response to region extension associated with the opening of the Larapinta Seaway at 490 to 460 Ma, b) crustal shortening during the Alice Springs Orogeny (300 to 360 Ma) causing inversion of the normal faulting to form a crustal pop-up structure, with granulites in the core.

In the northern Arunta Inlier, rises in ambient lithospheric temperatures due to the depth of sedimentation in the overlying basins, and internal heat production within the granitic crust may have produced amphibolite-facies temperatures during the Alice Springs Orogeny (Sandiford and Hand, 1998b; Hand and Sandiford, 1999; Sandiford, 1999; Sandiford *et al.*, 2001). These temperatures would have enabled complete recrystallisation of the shear

zones during large upward movements of granulites in the core of the inverted graben (Fig. 5.6). In addition, the locus of sedimentation may have also controlled the south-north reactivation of the shear zones.

#### **5.6.4 Fluid flow during Alice Springs Age shearing**

Hydration of the granulite-facies metamorphic provinces from 357 to 294 Ma across the northern Arunta Inlier caused major metasomatism with a dramatic lowering of  $\delta^{18}\text{O}$  values during shearing (Chapter Four; Cartwright and Buick, 1999). These data indicate that during shearing, large volumes of fluid were channelled through the shear zones in the northern Arunta Inlier. The  $\delta^{18}\text{O}$  and  $\delta\text{D}$  values within the shear zones indicate that the fluids were surface derived, probably originating from the overlying Centralian Superbasin (Chapter Four). The major reduction in grain size, combined with the mineralogy and in conjunction with mineral fractionation temperature estimates, suggests that shearing occurred at greenschist- to amphibolite-facies conditions (Chapter Three and Four; Cartwright and Buick, 1999). This requires that the large-scale shear zones were connected to fault systems at the surface during ductile shearing. The proposed tectonic evolution linking the extension of the Larapinta Event with the Alice Springs Orogeny would provide an environment where extension fault zones controlled the infiltration of fluids into the crust that were subsequently trapped during compression and seismically pumped back up towards the surface during thrusting.

### **5.7 CONCLUSIONS**

Following regional low-pressure metamorphism of the Chewings Orogeny at 1600 Ma the northern Arunta Inlier crust is likely to have first been disrupted during crustal extension, associated with the opening of the Larapinta Seaway at 490 Ma (Hand *et al.*, 1999). The extension may have development of an elongate (50 km wide and >100 km long) graben structure in the northern Arunta Inlier, parallel to the Larapinta Seaway. The graben became inverted during compression in the early Devonian to form an inversion structure with extensive steeply north- and south-dipping thrusts. Although the fault/shear system was long-lived connection to the surface and infiltration of fluids occurred throughout this period.



## CHAPTER SIX

### CHARACTERISTICS OF FLUID FLOW IN THE REDBANK HIGH STRAIN ZONE, CENTRAL AUSTRALIA

#### **Abstract**

The Redbank High Strain Zone is a crustal-scale faulted boundary where deep-crustal mafic granulites are juxtaposed against amphibolite-facies felsic gneisses. Substantial gains in silica and quartz veining within the mylonites, in addition to an up to sixfold increase in biotite within ultramylonite bands indicate substantial and channelled fluid flow during shearing. Low  $\delta^{18}\text{O}$  values (3.4 to 5.4‰) are recorded extensively from Redbank High Strain Zone mylonites, particularly from the metasomatic quartz-epidote rocks and mafic mylonites, indicating infiltration by low  $^{18}\text{O}$  surface-derived fluids. The protomylonites that host the high-strain mylonites have whole rock  $\delta^{18}\text{O}$  values of 5.1 to 9.6‰ (predominantly <7‰). These values are lower than those recorded from the protolith gneisses (8.0 to 11.0‰) indicating that they have been reset during shearing. Reworked quartz-epidote mylonites contain a muscovite-biotite assemblage and have higher  $\delta^{18}\text{O}$  values that probably reflect continued infiltration by fluids which had equilibrated with crustal rocks. Amphibolite- and greenschist-facies rocks have the same kinematics and similar  $\delta^{18}\text{O}$  values, and are probably recording the same period of shearing and fluid infiltration.

#### **6.1 INTRODUCTION**

Reactivation and the heterogenous nature of deformation within shear zones can lead to complex patterns of fluid-rock interaction. Heterogenous recrystallisation and chemical transfer make deciphering fluid-rock interaction in large structures difficult. Studies have shown that structurally-controlled permeability, as may be present in fractures and shear zones, enable the movement of large quantities of fluid through the crust (McCaig, 1988; Dipple *et al.*, 1990; Buick *et al.*, 1994; Cartwright *et al.*, 1997; McCaig, 1997; Buick *et al.*, 1999, Cartwright and Buick, 1999; Bons 2001). The Redbank High Strain Zone is a major structure in the southern Arunta Inlier that connects the upper and lower crust, providing a potential pathway for the movement of fluid through the entire crust. This study combines field and petrological observations, in conjunction with O and H isotope data, to investigate fluid flow during shearing along the Redbank High Strain Zone. The petrographic features and isotopic changes within the Redbank High Strain Zone investigated in this study form the basis for the geochronological investigation in Chapter Seven. Due to the diversity in composition of the host rocks, geochemical analysis across

the Redbank High Strain Zone is unlikely to distinguish specific chemical changes that occurred during shearing to any finer scale than petrographic analyses, and thus is not included within this study.

## 6.2 GEOLOGICAL SETTING

The Redbank High Strain Zone (Fig. 6.1) is one of the largest fault structures in the Arunta Inlier, comprising abundant, sub-parallel, north-dipping, mylonite-zones within a protomylonite matrix (Shaw and Black, 1991; Collins and Shaw, 1995). It forms a crustal-scale thrust zone that offsets the Moho by  $\sim 15$  km (Lambeck and Penney, 1984; Lambeck, 1991; Korsch *et al.*, 1998), producing major discontinuities in gravity, teleseismic travel-times and seismic structure (Goleby *et al.*, 1990; Lambeck, 1991; Korsch *et al.*, 1998). The exposed mylonites of the Redbank High Strain Zone form a WNW-ESE-trending belt, 400 km long and up to 20 km wide, across the SW Arunta Inlier (Fig. 6.1) and dips at  $\sim 40^\circ$  N. Reverse sense movement was substantial as deep-crustal granulites (700 to 800°C and 7 to 9 kbar) are exposed in the hangingwall juxtaposed against mid-crustal amphibolite-facies gneisses in the footwall to the south.

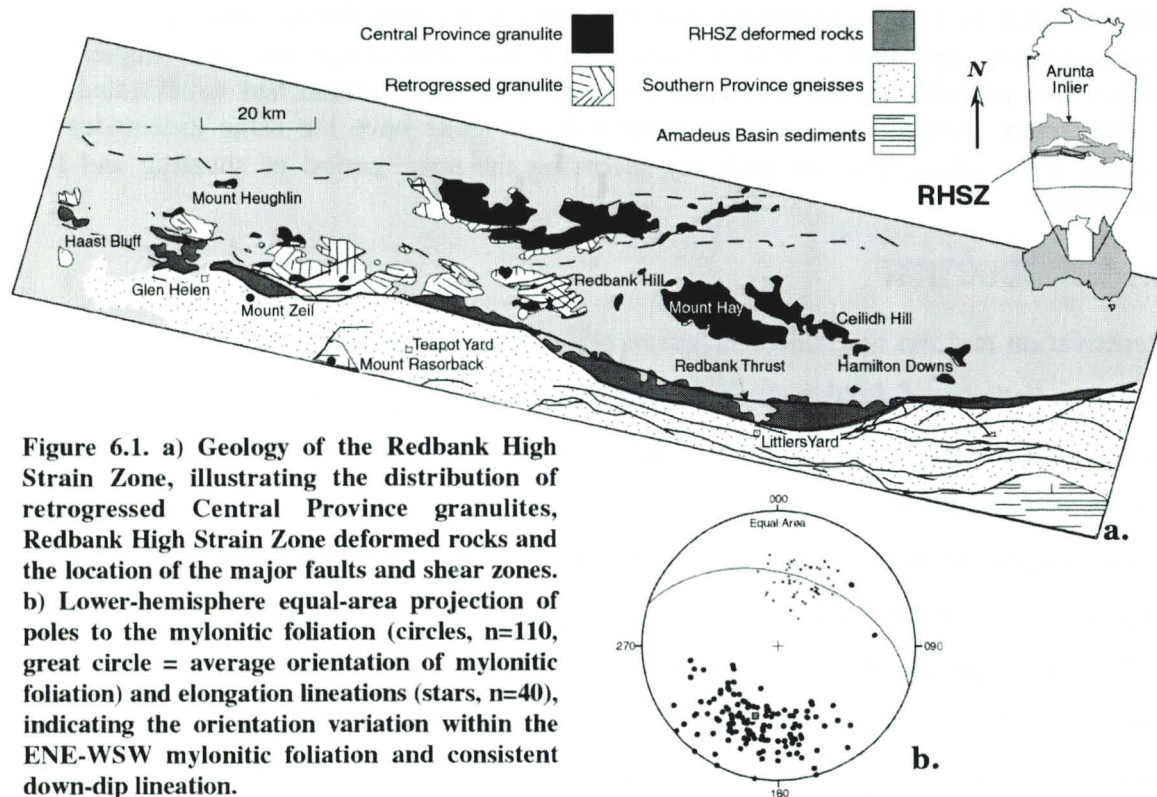


**Figure 6.1.** a) Geology of the Redbank High Strain Zone, illustrating the distribution of retrogressed Central Province granulites, Redbank High Strain Zone deformed rocks and the location of the major faults and shear zones. b) Lower-hemisphere equal-area projection of poles to the mylonitic foliation (circles,  $n=110$ , great circle = average orientation of mylonitic foliation) and elongation lineations (stars,  $n=40$ ), indicating the orientation variation within the ENE-WSW mylonitic foliation and consistent down-dip lineation.

Interpretation of teleseismic travel-time anomalies and deep seismic reflection data of the present structure of the central Australian crust indicate that substantial movement across the Redbank High Strain Zone occurred during the Alice Springs Orogeny (Lambeck,

1991; Shaw *et al.*, 1995). The tectonic evolution of the Redbank High Strain Zone is outlined in Table 6.1.

**Table 6.1. Tectonothermal History of the Central and Southern Provinces, Arunta Inlier. Information from Collins and Teyssier, 1989; Shaw and Black, 1991; Shaw *et al.*, 1992; Zhao and McCulloch, 1993; Black and Shaw, 1994; Collins *et al.*, 1995; Collins and Shaw, 1995; Balevre *et al.*,**

Age (Ma)	Central Province	Southern Province Redbank Zone	Southern Province Wigley Zone	Southern Province Chewings Zone
c. 1880	Yuendumu Tectonic Event	Deposition of Meddierns Yard Metamorphic Complex (MYMC) protolith rocks		
1780 -1730	<b>Strangways Event</b> Igneous crystallisation ages granulite-facies metamorphism 850°C and 6-9kbar			
1670 - 1680		<b>Arglike Tectonic event</b> regional amphibolite-facies metamorphic event associated with granitoid magmatism emplacing the Elery Granitic Complex migmatisation of the MYMC		
1610 - 1600	<b>Chewings Orogeny</b> granulite-facies metamorphism 800°C and 7-8kbar	<b>Chewings Orogeny</b> upper amphibolite-facies metam. N-directed overthrusting granitoid magmatism N-directed retrogressive shear zones?	<b>Chewings Orogeny</b> amphibolite-facies metamorphism N-directed overthrusting migmatisation of the MYMC & the EGC N-directed retrogressive shear zones	<b>Chewings Orogeny</b> greenschist-facies metamorphism N-directed overthrusting N-directed retrogressive shear zones
1500-1400	<b>Anmatjira Uplift Phase</b> south-directed shearing 650°C and 6-7kbar	<b>Anmatjira Uplift Phase?</b> S-directed thrusting at amphibolite-facies conditions		
1200-1150	<b>Teapot Magmatic Event</b> pegmatite emplacement	<b>Teapot Magmatic Event</b> intrusion of the Teapot Granite and associated pegmatites	<b>Teapot Magmatic Event</b> intrusion of the Teapot Granite extensive pegmatite emplacement	<b>Teapot Magmatic Event</b> development of zircon overgrowths in Ormiston Pound
1080-900	<b>Stuart Pass Dyke Swarm</b> intrusion of a dolerite dykes	<b>Stuart Pass Dyke Swarm</b> intrusion of a dolerite dykes	<b>Stuart Pass Dyke Swarm</b> intrusion of a dolerite dykes	<b>Stuart Pass Dyke Swarm</b> intrusion of a dolerite dykes
400-300	<b>Alice Springs Orogeny</b> south-directed shearing greenschist-facies	<b>Alice Springs Orogeny</b> S-directed amphibolite to greenschist-facies? shearing	<b>Alice Springs Orogeny</b> S-directed brittle-ductile shearing	<b>Alice Springs Orogeny</b> S-directed brittle-ductile shearing

Some mylonite zones are cut by pegmatites of the Teapot Tectonothermal Event (~1120 Ma), while others deform mafic dykes of the Stuart Pass Dyke Swarm (~900 Ma) (Chapter Two; Marjoribanks and Black, 1974; Shaw and Black, 1991), suggesting that the Redbank High Strain Zone is a long-lived structure with multiple phases of movement. However, due to consistent foliations and kinematics within the mylonites, it is difficult to discern the timing of the major phases of movement from field relationships. In addition, apparent changes in mylonite foliation orientations, rather than providing overprinting criteria, may instead reflect strain intensity (Fliervoet *et al.*, 1997). Metamorphic conditions based on mineral assemblages that are discussed in Shaw and Black (1991) have been used to infer the shearing history. Amphibolite-facies mineral assemblages of garnet, amphibole, K-feldspar, plagioclase, quartz and biotite within coarser-grained mylonites were interpreted to have formed during the Proterozoic Anmatjira Uplift Event (1400 to 1500Ma). In contrast, greenschist-facies assemblages of muscovite, biotite, clinozoisite, K-feldspar, quartz and plagioclase and locally chlorite were interpreted to have formed by shearing during the Devonian Alice Springs Orogeny (300 to 400Ma). It has been suggested that

shearing during the Alice Springs Orogeny did not produce temperatures greater than 350°C (Shaw *et al.*, 1992). However, as shown in this thesis (Chapters Three and Five) and by others (eg. Cartwright and Buick, 1999; Ballèvre *et al.*, 2000), this distinction does not seem to generally hold for other shear zones of the Arunta Inlier. In addition, TEM and SEM data for the mylonites of the Redbank High Strain Zone indicate that both amphibolite- and greenschist-facies mylonites were dominated by grain-boundary sliding deformation (Obee and White, 1985; Fliervoet *et al.*, 1997), suggesting they may have been part of the same deformation event. This textural, mineralogical and isotopic study of several mylonite zones within the Redbank High Strain Zone aims to provide some further insights into its shearing history and the extent of the Alice Springs Orogeny.

### **6.2.1 Host rocks**

The rocks in the footwall of the eastern Redbank High Strain Zone are derived from the Southern Province and comprise predominantly strongly-foliated, variably-megacrystic migmatite gneisses and augen gneisses (Fig. 6.2a) of granitic origin. Garnet-bearing pelitic gneisses and quartzites are also present in lower volumes. Folded and sheared magmatic contacts and melt segregations are common in the gneisses (Fig. 6.2b). Regional metamorphism at 1600 Ma during the Chewings Orogeny produced upper amphibolite-facies assemblages in the north of the Southern Province (Collins and Shaw, 1995).

The rocks in the hangingwall of the eastern Redbank High Strain Zone comprise predominantly layered mafic granulites of the Mount Hay Granulite and Bunghara Metamorphics (Chapter Two). The Mount Hay Granulite comprises contains numerous bands of intermediate (leucogabbro-anorthosite) and felsic (tonalitic-granodioritic) gneisses with minor intercalated paragneiss layers (Glikson, 1987; Warren and Shaw, 1995). Further to the west, the Mount Chapple Metamorphics, are predominantly felsic gneisses, with intermediate and felsic migmatites. The Bunghara Metamorphics comprises gneisses of mafic to intermediate meta-igneous composition with minor meta-sediments containing granulite-facies assemblages and minor melt segregations (Warren and Shaw, 1995). Rocks in the Mount Hay and Mount Chapple region underwent granulite-facies (700 to 850°C and 6 to 8kbar) metamorphism during the Chewings Orogeny and represent an exhumed lower-crustal section of the Arunta Inlier (Collins, 2000). The uplift of Central Province rocks is in the order of 20 km, as indicated by the change in peak pressure estimates across the Redbank High Strain Zone (Shaw and Black, 1991), deep seismic reflect profiles (Goleby *et al.*, 1989), and teleseismic travel times (Lambeck *et al.*, 1988).

### 6.2.2 Mylonite Zones

Protomylonites comprise a significant portion (~66%) of the rock within the Redbank High Strain Zone, and contain multiple, narrow high-strain zones of mylonite and ultramylonite that have undergone extensive grainsize reduction (Fliervoet *et al.*, 1997). The mylonite zones are typically 15 to 300m wide and sub-parallel to the Redbank High Strain Zone, dipping 40-60°N (Fig. 6.2c). Pegmatites and mafic dykes that cut the mylonitic fabric have been subsequently sheared (Fig. 6.2d), as documented from elsewhere in the region (Marjoribanks and Black, 1974). The rocks in the mylonite zones have an WNW-ENE-trending anastomosing mylonitic foliation that dips 38-72°N (Fig. 6.1), and consistent down-dip stretching lineations defined predominantly by elongated grains and felsic aggregates (Fig. 6.2e). Asymmetric folds, rotated porphyroclasts, shear bands and SC-fabrics indicate a dominantly reverse sense of shear across the mylonite zones (Fig. 6.2f). Minor slickensides along shear plane surfaces also indicate dip-slip movement, while some narrow ultramylonite zones indicate a component of sinistral strike-slip movement. There is typically a gradual transition from weakly-foliated protomylonite gneiss to strongly foliated augen-rich mylonite, and a clear transition in strain intensity can be recognised in outcrop (Figs. 6.3a,b). Porphyroclast size decreases within the higher strain mylonites from >5cm to <2cm. Core-mantle structures occur where feldspar clasts are recrystallised along their margins and form mantles of fine feldspar, commonly becoming tails entrained in the shear fabric and indicating sense of shear. Ultramylonite forms narrow continuous and discontinuous bands (1mm to 5m wide) within both protomylonite and mylonite. They are commonly dark, containing predominantly very fine-grained (<10µm) biotite and thin (<1mm) quartz layers. Tight folds (Fig. 6.3c) within the quartz layers likely developed as a local distortion in the flow field during shearing (Passchier and Trouw, 1996). Porphyroclasts within the ultramylonites are typically rounded and reworked, floating within a very fine-grained matrix (Fig. 6.3c). Pseudotachylyte is also described from several areas within and to the south of the Redbank High Strain Zone (Obee and White, 1985; Fliervoet *et al.*, 1997). The dark green, commonly parallel, pseudotachylyte veins have a very fine-grained matrix, rounded porphyroclasts and small injection-like veins oblique to the main veins. The pseudotachylytes cut the mylonitic foliation and are themselves sheared (Fig. 6.3d). The sharp vein walls have recrystallised, and the pseudotachylyte material is devitrified and hydrated.

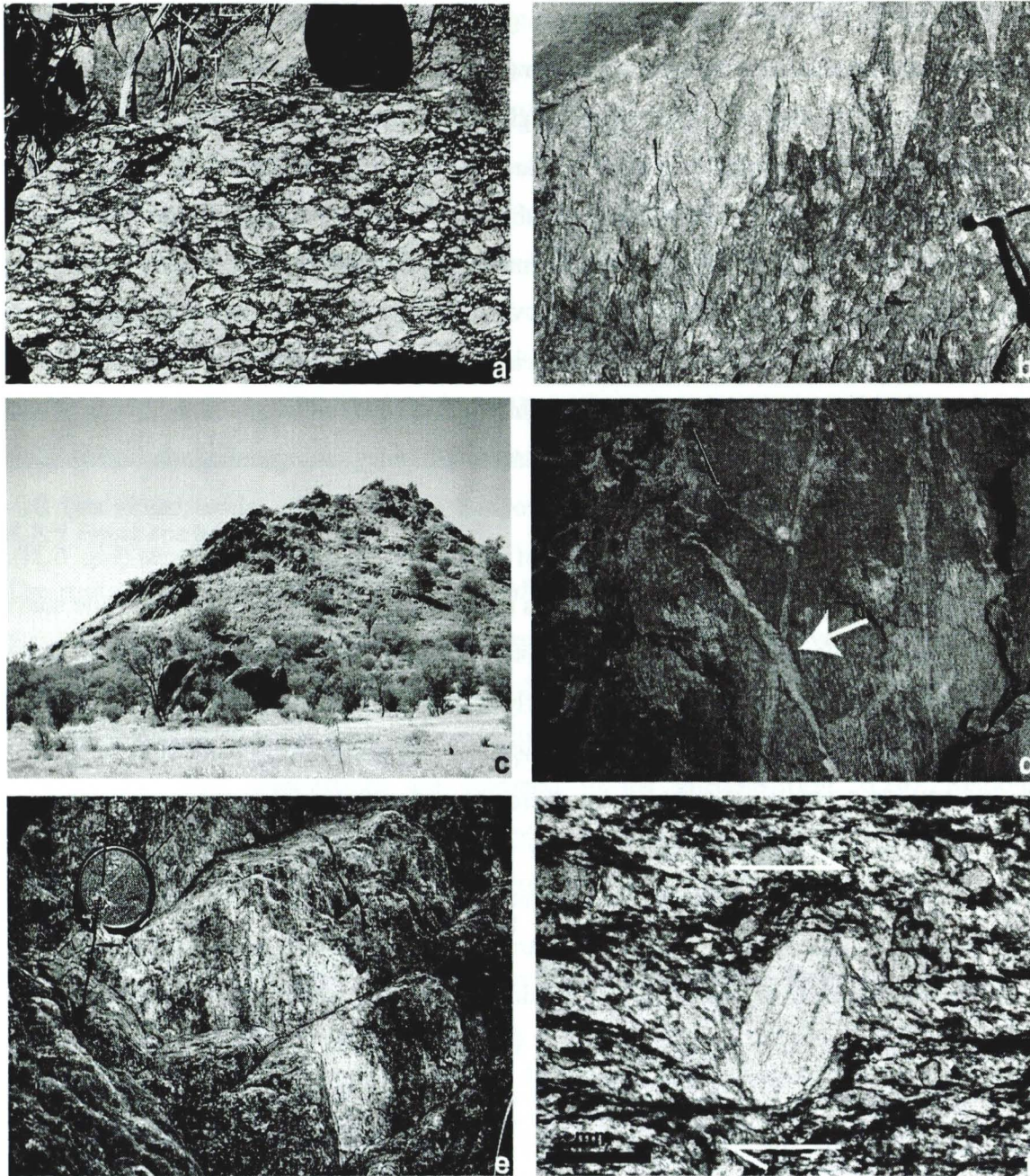


Figure 6.2. a) Augen Gneiss, Mount Forster. b) Sheared contact between augen gneiss and felsic gneiss, Hamilton Downs. c) North-dipping shear zone at Illyabba Dam. d) Deformed pegmatite truncating a pegmatite/vein (arrow) within low strain mylonite at Hamilton Downs, pencil is aligned with mylonitic foliation, showing both earlier pegmatites are deformed within the mylonite. e) Well-developed down-dip lineations at Mount Forster. f) Rotated porphyroclasts of feldspar showing reverse sense of shear, within a mylonite zone at Brumby Bore.

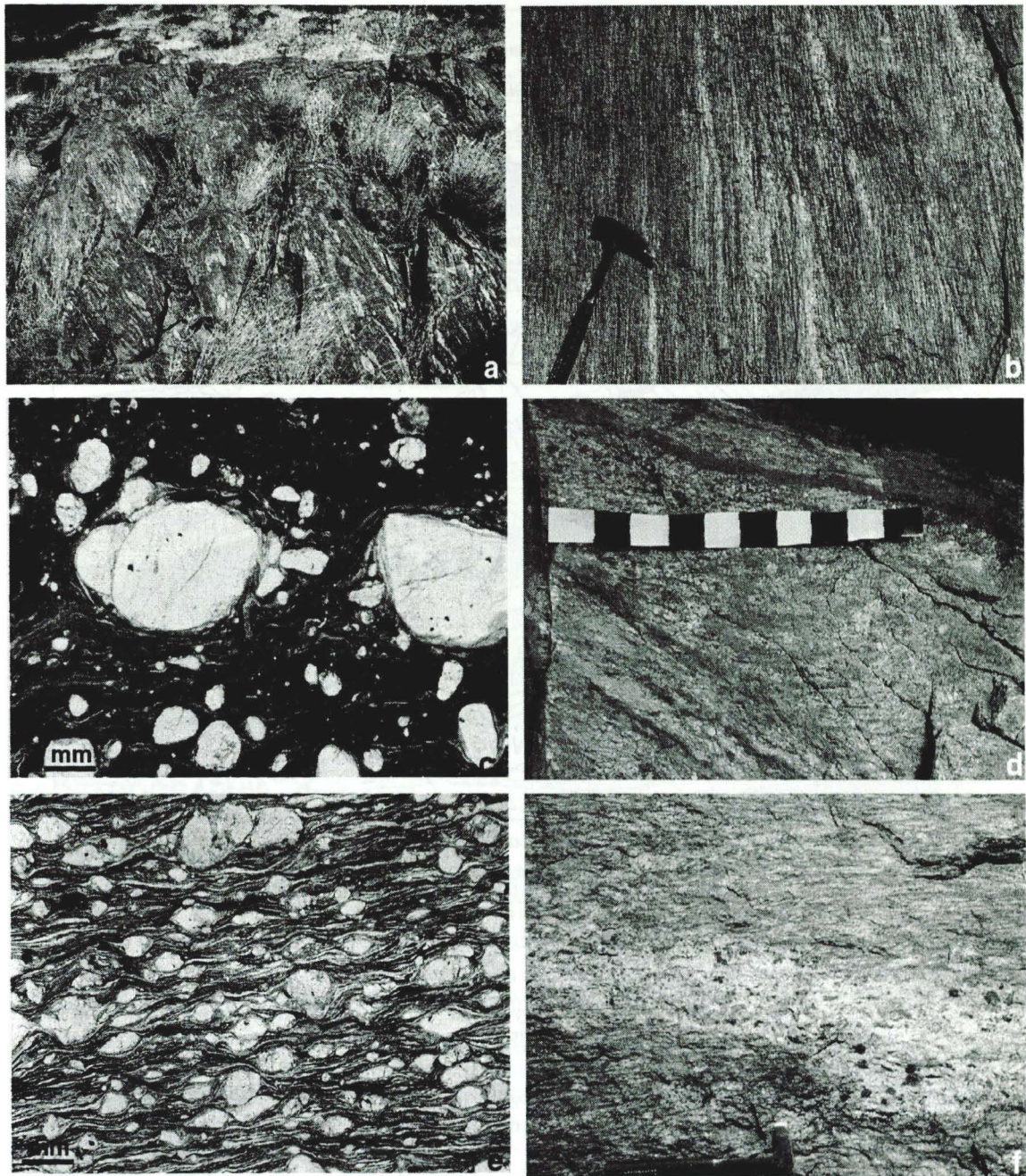
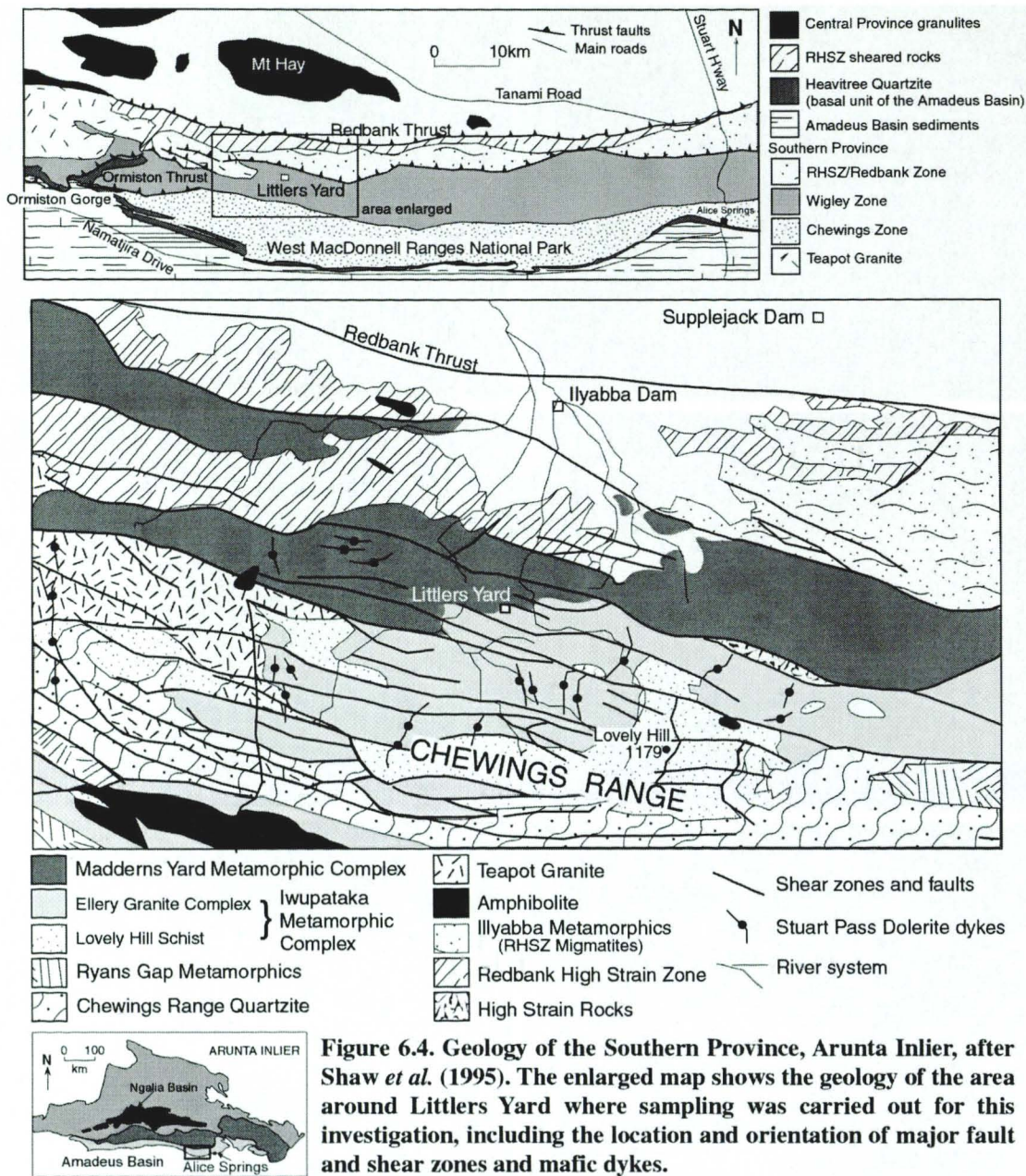


Figure 6.3. a) Low strain, folded and deformed migmatite gneiss, Hamilton Downs. b) High strain mylonite, Hamilton Downs. c) Feldspar porphyroclasts floating in a very fine-grained matrix of biotite and quartz with folded quartz layers representing local distortion in the strain field during shearing, PPL. d) Altered and deformed pseudotachylyte veins cutting the earlier mylonite foliation, Mount Forster, scale has centimetre stripes. e) Layered mylonite typical of the Redbank High Strain Zone, with abundant feldspar porphyroclasts. The layers comprise quartz, quartz-feldspar and biotite, PPL. f) Coarse-grained pegmatite cutting protomylonite at Hamilton Downs, that was subsequently sheared and recrystallised at the edges.



**Figure 6.4. Geology of the Southern Province, Arunta Inlier, after Shaw *et al.* (1995). The enlarged map shows the geology of the area around Littlers Yard where sampling was carried out for this investigation, including the location and orientation of major fault and shear zones and mafic dykes.**

Shear zones are also abundant to the south of the Redbank High Strain Zone in the Southern Province. Several of the shear zones in the Littlers Yard area (Fig. 6.4) offset dolerite dykes of the Stuart Pass Dyke Swarm, to the west and east, inferring movement predominantly during the Alice Springs Orogeny (Warren and Shaw, 1995). The shear zones cut both the Madderns Yard Metamorphic Complex and Iwupataka Metamorphic Complex, forming lenses of interleaved gneisses. The shear zones are 5m to 100m wide, oriented NE-SW to E-W with steep ( $65\text{-}85^\circ$ ) north or south dips (Fig. 6.4), and have well-developed down-dip lineations. They show extensively developed SC fabrics and asymmetric folds indicating reverse senses of shear.

## 6.3 SAMPLE COLLECTION

Sampling transects were conducted perpendicular to the mylonitic foliation across discrete mylonite zones in order to establish a fluid flow regime throughout the Redbank High Strain Zone and to the south within the Southern Province (Figs. 6.4, 6.5). Samples along strike of the mylonite zones were also collected to identify any lateral variations. Samples of less-strained protomylonites and, where possible, gneisses and granulites were collected in order to identify changes within the shear zones.

The shear zones are described using the following names throughout the text, from west to east: Brumby Bore Shear Zone (KP9294), Hamilton Downs Shear Zone (LP0492) Ilyabba Dam Shear Zone (LP1091) and Supplejack Dam Shear Zone (LP1491), (Table 6.2). Other areas are referred to as Littlers Yard (LP0686), Mount Forster (LP7493), west Brumby Bore (KP8995) and eastern Redbank High Strain Zone (LP0093-0591) (Tables 6.2, 6.3). Details of the analytical procedures for oxygen and hydrogen isotope extraction and calibration are presented in Chapter One.

## 6.4 PETROGRAPHY

### 6.4.1 Quartzofeldspathic mylonite zones

#### 6.4.1.1 Brumby Bore Shear Zone

The shear zone at Brumby Bore is ~400m wide, oriented E-W, and dips steeply (~50°) to the north. The footwall rocks exposed to the south comprise migmatitic granitic gneiss. The hangingwall rocks to the north are completely covered by colluvium, but are probably mafic granulites of the Central Province, as the trace of the Redbank Thrust is inferred immediately north of the exposure (Fig. 6.1). Protomylonite is the dominant rock type at Brumby Bore, hosting multiple narrow mylonite and ultramylonite zones (2 to 15m wide).

The rocks have an anastomosing mylonitic foliation (078-128°/38-62°N) and down-dip stretching lineations plunging north 34-50°. Asymmetric folding,  $\delta$ - and  $\alpha$ -type clasts and SC fabrics indicate reverse sense of shear (Fig. 6.2f).

The low-strain protomylonites are medium to fine grained (50-500 $\mu$ m), layered with an anastomosing mylonitic fabric, and contain quartzofeldspathic and amphibole-bearing granitic assemblages (Table 6.4). Fine-grained quartz, feldspar, and biotite bands wrap corroded and elongated feldspar and hornblende porphyroclasts. K-feldspar, plagioclase

and quartz porphyroclasts form augen-shaped aggregates that are elongated within the foliation. Recrystallisation and perthitic intergrowths are common with the feldspar porphyroclasts with some undulose extinction of quartz. Biotite shear bands are common and truncate the quartz and feldspar bands. In discrete high strain zones (5 to 15 m wide), the mylonites have anastomosing layers of (50 to 150 $\mu$ m) quartz, very fine-grained biotite (<10 $\mu$ m) and quartz, feldspar, and biotite (Fig. 6.3e). Biotite shear bands are common and

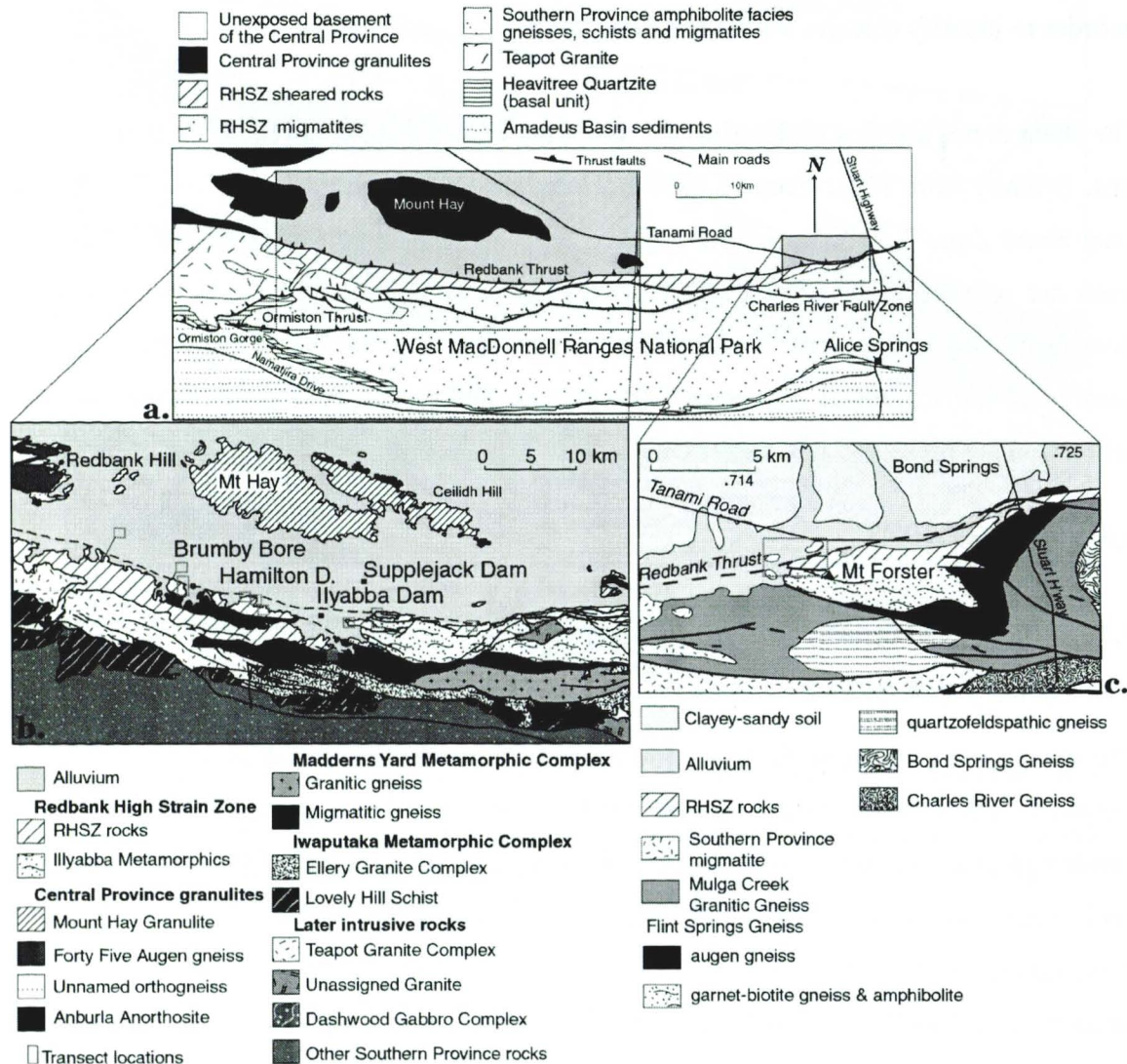


**Figure 6.5.** a) General geology of the southern Arunta Inlier, including the Redbank High Strain Zone, showing the location maps b) and c). b) Geological units of the Central and Southern Province (after Shaw *et al.*, 1995) with deformed Redbank High Strain Zone rocks and locations of the sampling transects in order from west to east: west of Brumby Bore, Brumby Bore, Hamilton Downs (3 areas), Ilyabba Dam and Supplejack Dam and eastern Redbank. c) Geology of the Southern Province (after Shaw *et al.*, 1983) at Bond Springs showing the location of the sampling area north of Mount Foster.

**Table 6.2 Location, description and  $\delta^{18}\text{O}$  and  $\delta\text{D}$  whole rock values (‰) of samples. Metamorphic grade estimated on mineral assemblages and deformation microstructures.**

Sample	Location	Grid Reference	Rock Type	Estimated Metamorphic Grade	$\delta^{18}\text{O}_{\text{wr}}$	$\delta\text{D}_{\text{wr}}$
<b>Brumby Bore Shear Zone</b>						
CR98BB546	Brumby Bore	KP9294	protomylonite	amphibolite-facies	6.7	
CR98BB233	Brumby Bore	KP9294	protomylonite	amphibolite-facies	6.9	
CR98BB235	Brumby Bore	KP9294	protomylonite	amphibolite-facies	6.7	
CR98BB236	Brumby Bore	KP9294	ultramylonite	amphibolite-facies	7.1	
CR98BB237	Brumby Bore	KP9294	pelitic schist	amphibolite-greenschist	7.2	
CR98BB239	Brumby Bore	KP9294	pelitic schist	amphibolite-greenschist	8.4	
CR98BB242	Brumby Bore	KP9294	protomylonite	amphibolite-facies	9.6	
CR98BB245	Brumby Bore	KP9294	mylonite	greenschist-facies	6.2	
CR98BB246	Brumby Bore	KP9294	protomylonite	amphibolite-facies	5.8	
CR98BB249	Brumby Bore	KP9294	protomylonite	amphibolite-facies	5.1	
CR98BB251	Brumby Bore	KP9294	ultramylonite	greenschist-facies	7.0	
CR98BB254	Brumby Bore	KP9294	ultramylonite	greenschist-facies	5.1	
CR98BB255	Brumby Bore	KP9294	ultramylonite	greenschist-facies	6.5	
CR98BB256	Brumby Bore	KP9294	mylonite	greenschist-facies	6.9	
CR98BB257	Brumby Bore	KP9294	protomylonite	amphibolite-facies	6.7	
CR98BB261	Brumby Bore	KP9294	mylonite	amphibolite-greenschist	8.1	
CR98BB265	Brumby Bore	KP9294	mylonite	amphibolite-facies	7.1	
CR98BB267	Brumby Bore	KP9294	mylonite	amphibolite-facies	7.2	
CR98BB269	Brumby Bore	KP9294	mylonite	amphibolite-facies	6.9	
CR98BB274	Brumby Bore	KP9294	mylonite	amphibolite-facies	7.3	
CR98BB278	Brumby Bore	KP9294	protomylonite	amphibolite-facies	7.1	
CR98BB287	Brumby Bore	KP9294	protomylonite	amphibolite-facies	5.1	
CR98BB288	Brumby Bore	KP9294	mylonite	amphibolite-greenschist	6.5	
CR98BB294	Brumby Bore	KP9294	mylonite	amphibolite-facies	6.5	
CR98BB307	Brumby Bore	KP9294	ultramylonite	greenschist-facies	7.0	
CR98BB319	Brumby Bore	KP9294	mylonite	amphibolite-facies	5.8	
CR98BB328	Brumby Bore	KP9294	qz-epi mylonite	amphibolite-facies	7.2	
CR98BB337	Brumby Bore	KP9294	mylonite	amphibolite-greenschist	7.6	
CR98BB342	Brumby Bore	KP9294	mylonite	amphibolite-greenschist	8.0	
CR98BB344	Brumby Bore	KP9294	protomylonite	amphibolite-facies	6.8	
CR98BB345	Brumby Bore	KP9294	qz-epi mylonite	amphibolite-greenschist	4.8	-68.83
CR98BB346	Brumby Bore	KP9294	qz-epi mylonite	amphibolite-greenschist	5.0	
CR98BB347	Brumby Bore	KP9295	qz-epi mylonite	amphibolite-greenschist	3.7	
CR99BB5	Brumby Bore	KP9295	ultramylonite	amphibolite-greenschist	6.6	
<b>West Brumby Bore</b>						
CR98BB514	W Brumby Bore	KP8995	qz-epi mylonite	amphibolite-facies		-74.8
CR98BB515	W Brumby Bore	KP8995	qz-epi mylonite	amphibolite-facies	3.4	
CR98BB516	W Brumby Bore	KP8995	qz-epi mylonite	amphibolite-facies	3.7	-75.8
CR98BB517	W Brumby Bore	KP8995	qz-epi mylonite	greenschist-facies	5.4	
CR98BB518	W Brumby Bore	KP8995	muscovite phyllonite	greenschist-facies	5.4	
CR98BB519	W Brumby Bore	KP8995	epidote vein	greenschist-facies	4.7	
CR98BB520	W Brumby Bore	KP8995	migmatite gneiss	amphibolite-facies	8.1	
CR98BB521	W Brumby Bore	KP8995	qz-epi mylonite	amphibolite facies	6.3	
CR99WBB	W Brumby Bore	KP8995	qz-epi mylonite	amphibolite facies		-66.1
<b>Hamilton Downs Shear Zone and associated sample</b>						
CR99HD41	East RHSZ	LP0591	mylonite	amphibolite-greenschist	6.8	
CR98RTZ522	Hamilton Downs	LP0492	mylonite	amphibolite-greenschist	8.9	
CR98RTZ523	Hamilton Downs	LP0492	mylonite	greenschist-facies	8.2	
CR97RTZ59	Hamilton Downs	LP0492	protomylonite	amphibolite-facies	8.5	
CR97RTZ58	Hamilton Downs	LP0492	ultramylonite	amphibolite-greenschist	7.0	
CR98RTZ524	Hamilton Downs	LP0492	mylonite	greenschist-facies	8.1	
CR98RTZ525	Hamilton Downs	LP0492	qz-epi mylonite	greenschist-facies	7.6	
CR98RTZ526	Hamilton Downs	LP0492	mylonite	greenschist-facies	8.0	
CR97RTZ60	Hamilton Downs	LP0492	mylonite	amphibolite-greenschist	7.6	
CR97RTZ61	Hamilton Downs	LP0492	ultramylonite	greenschist-facies	6.0	
CR97RTZ62	Hamilton Downs	LP0492	protomylonite	amphibolite-facies	5.4	

**Table 6.2 cont. Location, description and  $\delta^{18}\text{O}$  and  $\delta\text{D}$  whole rock values (%) of samples. Metamorphic grade estimated on mineral assemblages and deformation microstructures.**

Sample	Location	Grid Reference	Rock Type	Estimated Metamorphic Grade	$\delta^{18}\text{O}_{\text{wr}}$	$\delta\text{D}_{\text{wr}}$
<b>Ilyabba Dam Shear Zone and associated samples</b>						
CR98HD532	E Ilyabba Dam	LP1091	protomylonite	greenschist-facies	7.1	
CR98HD534	E Ilyabba Dam	LP1091	ultramylonite	greenschist-facies	6.6	
CR98HD538	E Ilyabba Dam	LP1091	mylonite	greenschist-facies	7.0	
CR98HD539	E Ilyabba Dam	LP1091	mylonite	greenschist-facies	7.4	
CR98HD540	E Ilyabba Dam	LP1091	quartzite	greenschist-facies	11.4	
CR98HD541	E Ilyabba Dam	LP1091	mylonite	greenschist-facies	8.4	
CR98HD544	E Ilyabba Dam	LP3391	quartzite	greenschist-facies	11.0	
CR98HD545	E Ilyabba Dam	LP3391	mylonite	greenschist-facies	7.0	
CR98HD527	E Ponding Dams	LP1691	mylonite	amphibolite-facies	8.1	
CR98HD528	E Ponding Dams	LP1691	ultramylonite	amphibolite-facies	7.3	
CR98HD529	E Ponding Dams	LP1691	protomylonite	amphibolite-facies	7.0	
<b>Supplejack Dam Shear Zone</b>						
CR98SJ395	S Supplejack Darr	LP1491	protomylonite	amphibolite-facies	6.6	
CR98SJ398	S Supplejack Darr	LP1491	mylonite	amphibolite-facies	7.5	
CR98SJ400	S Supplejack Darr	LP1491	mylonite	greenschist-facies	8.5	
CR98SJ401	S Supplejack Darr	LP1491	protomylonite	greenschist-facies	8.2	
CR98SJ403	S Supplejack Darr	LP1491	mylonite	greenschist-facies	8.8	
CR98SJ404	S Supplejack Darr	LP1491	mylonite	amphibolite-facies	4.9	-79.1
CR98SJ407	S Supplejack Darr	LP1491	protomylonite	amphibolite-facies	5.4	-111.4
CR98SJ411	S Supplejack Darr	LP1491	mylonite	amphibolite-facies	5.0	-93.3
CR98SJ413	S Supplejack Darr	LP1491	mylonite	amphibolite-facies	6.3	
CR98SJ414	S Supplejack Darr	LP1491	mylonite	amphibolite-facies	7.9	
CR98SJ415	S Supplejack Darr	LP1491	mylonite	amphibolite-facies	7.2	
CR98SJ417	S Supplejack Darr	LP1491	protomylonite	amphibolite-facies	6.9	
<b>Bond Springs Shear Zone and associated samples</b>						
CR99TR1	Bond Springs	LP7494	mylonite	low-grade	6.7	
CR99TR2	Bond Springs	LP7494	mylonite gneiss	low-grade	5.3	
CR99TR3	Bond Springs	LP7494	cataclasite	low-grade	5.0	
CR99TR4	Bond Springs	LP7494	pelitic gneiss	granulite	8.3	
CR99TR37	Bond Springs	LP7493	cataclasite	low-grade		
CR99TR38	Bond Springs	LP7493	phyllonite	low-grade	6.8	
CR99TR39	Bond Springs	LP7493	mylonite	greenschist-facies	8.7	
CR99TR40	Bond Springs	LP7493	protomylonite	greenschist-facies	7.4	
CR98TR473	Bond Springs	LP7393	foliated cataclasite	low-grade	6.8	
CR98TR474	Bond Springs	LP7393	mylonite	greenschist-facies	7.4	
CR98TR475a	Bond Springs	LP7393	mylonite	greenschist-facies	6.9	
CR98TR475b	Bond Springs	LP7393	mylonite	greenschist-facies	6.7	
CR98TR476	Bond Springs	LP7393	mylonite	greenschist-facies	8.3	
CR98TR477	Bond Springs	LP7393	protomylonite	greenschist-facies	8.7	
CR98TR478	Bond Springs	LP7393	mylonite	greenschist-facies	6.6	
CR98TR479	Bond Springs	LP7393	protomylonite	greenschist-facies	7.6	
CR98TR418	Bond Springs	LP7393	protomylonite	greenschist-facies	6.9	
<b>Mafic mylonites, Bond Springs</b>						
CR98TR420	Bond Springs	LP7495	mafic mylonite	greenschist-facies	5.3	
CR98TR425	Bond Springs	LP7495	mafic mylonite	greenschist-facies	4.4	
CR98TR428	Bond Springs	LP7495	mafic mylonite	greenschist-facies	4.9	
CR98TR435	Bond Springs	LP7495	mafic mylonite	greenschist-facies	5.3	
CR98TR441	Bond Springs	LP7495	mafic mylonite	greenschist-facies	7.3	
CR98TR444	Bond Springs	LP7495	mafic mylonite	greenschist-facies	6.9	
CR98TR445	Bond Springs	LP7495	mafic mylonite	greenschist-facies	7.4	
CR98TR456	Bond Springs	LP7495	mafic mylonite	greenschist-facies	9.5	
CR98TR462	Bond Springs	LP7495	mafic mylonite	greenschist-facies	7.6	
CR98MF220	Bond Springs	LP7294	mafic mylonite	greenschist-facies	5.4	
CR98BS547	Bond Springs	LP7294	mafic mylonite	greenschist-facies	7.4	
CR98BS550	Bond Springs	LP7392	pyroxene-granulite	granulite-facies	8.0	
CR98BS551	Bond Springs	LP7392	augen gneiss	amphibolite-granulite	11.0	
CR98BS552	Bond Springs	LP7392	augen gneiss	amphibolite-granulite	8.9	

Table 6.3.  $\delta^{18}\text{O}$  and  $\delta\text{H}^2$  values of migmatite gneisses and associated rocks at Littlers Yard, Southern Arunta Inlier. \* denotes the samples analysed at Monash University, the rest were analysed at Cape Town University, South Africa.

Sample	Location	Grid Reference	Rock Type	Transect (m)	$\delta^{18}\text{O}$ (‰)	$\delta\text{D}$ (‰)
<i>Shear Zone 1</i>						
CR98SP814	Littlers Yard Track	LP0686	protomylonite	2	6.4	-43.17
CR98SP815	Littlers Yard Track	LP0686	protomylonite	4	6.6	-62.73
CR98SP816	Littlers Yard Track	LP0686	migmatite	8	6.5	
CR98SP817	Littlers Yard Track	LP0686	quartz vein	8	6.4	
CR98SP818	Littlers Yard Track	LP0686	mylonite	10	5.9	
CR98SP819	Littlers Yard Track	LP0686	ultramylonite	14	6.2	-106.70
CR98SP821	Littlers Yard Track	LP0686	ultramylonite	27	7.1	
CR98SP822	Littlers Yard Track	LP0686	migmatite gneiss	37	5.2	-120.94
CR98SP823	Littlers Yard Track	LP0686	pegmatite	38	6.0	-49.41
CR98SP824	Littlers Yard Track	LP0686	migmatite gneiss	53	1.6	-117.61
CR98SP825	Littlers Yard Track	LP0686	quartz-rich layer	54	3.1	
CR98SP826	Littlers Yard Track	LP0686	migmatite gneiss	59	4.9	-49.14
<i>Shear Zone 2</i>						
CR98LY827	Littlers Yard	LP0786	orthogneiss	0	4.4*	
CR98LY828	Littlers Yard	LP0786	orthogneiss	20	2.3	
CR98LY829	Littlers Yard	LP0786	ultramylonite	28	6.4	
CR98LY830	Littlers Yard	LP0786	ultramylonite	31	8.0	
CR98LY834	Littlers Yard	LP0786	quartz vein	43	10.6*	
CR98LY835	Littlers Yard	LP0786	mylonite	47	10.3*	
CR98LY836	Littlers Yard	LP0786	mylonite	51	6.3*	
CR98LY837	Littlers Yard	LP0786	ultramafic	61	4.3*	
<i>Shear Zone 3</i>						
CR98LY841	S Littlers Yard	LP0785	mylonite	14	7.3*	
CR98LY842	S Littlers Yard	LP0785	migmatite gneiss	22	6.4*	
CR98LY843	S Littlers Yard	LP0785	mylonite	42	6.6*	
CR98LY844	S Littlers Yard	LP0785	amphibolite	42	6.1*	

generally are very fine grained ( $<10\mu\text{m}$ ). Epidote becomes abundant within the more hydrous mylonites (Table 6.4), forming small clasts wrapped within the biotite foliation. The ultramylonites comprise a fine to very fine grained matrix of biotite with minor quartz and feldspar and variable abundances of porphyroclasts of quartz and/or feldspar (Fig. 6.3c). The porphyroclasts are well rounded and in the coarser grained ultramylonite contain well-formed tail systems. Epidote occurs in minor abundances as equant grains, and as small clasts wrapped in biotite.

#### 6.4.1.2 Hamilton Downs Shear Zone

The Hamilton Downs shear zone is 35m wide, flanked by amphibolite-bearing augen-rich protomylonite gneiss to the south and quartzofeldspathic protomylonite gneiss to the north. The shear zone trends  $116^\circ/60^\circ\text{N}$ , and forms an eroded gully between two small hills 5km north of a 871m (unnamed) peak (LP0188; Fig. 6.5).



Table 6.5. Petrographic summary of samples. Crudester: v<-10mm, p-10-100mm, m-100-200mm, co->200mm. Minerals in % Mineral abbreviations in Table 1.1.

Sample	Rock Type	Foliation Intensity	Matrix Granulite	Porphyroblast size (mm)	PlC (%)	fsp	qz	bl	epi	ms	grt	amp	il	opq	sil	sp	accessory phases
<b>West Brunby Bore</b>																	
CR98B614	qr-epi mylonite	strong	l	0.5-2.0	10	30	45	0	25	0	0	0	0	0	0	0	il, B
CR98B515	qr-epi mylonite	strong linear	m-c		0	0	18	2	78	0	0	0	2	0	0	0	
CR98B516	qr-epi mylonite	strong linear	m-c		<1	8	20	1	88	0	0	0	3	0	0	0	
CR98B517	qr-epi mylonite	moderate	m		0	1	50	5	26	17	0	0	0	0	0	0	il
CR98B518	muscovite phylonite	strong	f-m		<1	0	39	5	20	36	0	0	0	0	0	0	il
CR98B519	epidote vein	moderate	f		0	0	20	0	78	0	0	0	2	0	0	0	
CR98B519	hoof of vein	moderate	f		0	90	10	1	0	0	0	0	0	0	0	0	il
CR98B520	hydrothermal greases	moderate	m-l	0.5-100.0	85	40	35	20	20	0	0	0	0	0	0	0	il
CR98B521	qr-epi mylonite	moderate	m	3.0	18	30	50	10	5	5	0	0	0	0	0	0	
<b>Hamilton Downs Shear Zone and associated samples</b>																	
CR98H241	mylonite	strong	f-vf	2.0	25	28	22	35	15	0	0	2	0	0	0	0	il, B
CR98H232	mylonite	strong	m	0.5-3.0	15	30	49	15	6	1	<1	0	0	0	0	0	il
CR98H233	mylonite	strong	m	0.5-3.0	15	40	40	10	<1	10	0	0	0	0	0	0	il
CR97H229	protonylonite	moderate	m-l	0.5-1.0	70	40	35	22	0	0	2	0	0	1	0	0	
CR97H228	ultramylonite	strong linear	f	0.4	40	45	45	0	15	0	0	0	0	0	0	0	
CR98H2324	mylonite	strong	m-l	5.0	10	43	42	7	8	0	0	0	0	0	0	0	
CR98H2325	qr-epi mylonite	strong	m	0.5-1.0	15	58	50	2	10	0	0	0	0	0	0	0	
CR98H2326	mylonite	strong	m	0.3-1.0	12	40	50	10	<1	0	0	0	0	0	0	0	
CR97H220	mylonite	moderate	m	1.0-5.0	30	35	32	20	10	0	0	3	0	0	0	0	
CR97H221	ultramylonite	strong linear	f-vf	2.0-3.0	2	7	47	28	18	0	0	0	0	0	0	0	
CR97H222	protonylonite	moderate	m	1.0-3.0	80	32	37	15	1	0	0	15	0	0	0	0	act
<b>Hybble Dam Shear Zone and associated samples</b>																	
CR98H252	protonylonite	moderate	m-l	0.5-5	55	50	25	13	0	0	0	10	0	2	0	0	il, ep, sp
CR98H254	ultramylonite	strong	vf	1.0-1.25	10	10	10	70	10	0	0	0	0	0	0	0	il
CR98H258	mylonite	strong	f	0.3-1.5	45	39	39	16	0	0	0	4	0	2	0	0	zf, ep
CR98H259	mylonite	strong	f-vf	0.3	15	40	64	5	0	0	0	0	0	1	0	0	ep
CR98H260	quartzite	v. strong linear	f	N/A	0	0	80	0	14	1	0	0	0	5	0	0	
CR98H261	mylonite	strong	f	0.7	35	35	55	7	0	0	0	0	0	3	0	0	zf
CR98H264	quartzite	v. strong linear	f-vf	N/A	0	0	65	0	28	2	0	0	0	5	0	0	
CR98H265	mylonite	strong	f	0.5-1.0	45	40	45	10	2	0	0	0	0	3	0	0	ep, B
CR98H267	ultramylonite	strong linear	m	0.5	2	20	80	7	13	0	0	0	0	0	0	0	
CR98H268	ultramylonite	v. strong linear	f	1.0	5	5	43	40	5	0	5	0	2	0	0	0	
CR98H269	protonylonite	weak	m (vf sb)	0.8	70	39	25	18	0	0	0	18	0	0	0	0	il, B

Table 6.6. Petrographic summary of samples. Grainsize: v&lt;-10mm, f=10-100mm, m=100-200mm, c&gt;200mm. Minerals in %. Mineral abbreviations in Table 1.1.

Sample	Rock Type	Foliation Intensity	Matrix Grainsize	Porphyroblast size (mm)	P/C (%)	fsp	qz	bl	epi	mu	gnt	amp	tl	opq	stl	ap	accessory phases
<b>Supplejack Dam Shear Zone</b>																	
CR98SJ395	protomylonite	weak-mod	m-f	1.0-4.0	65	40	45	15	0	0	<1	0	0	0	0	0	ap, tl
CR98SJ396	mylonite	strong	f	1.0	20	34	40	20	1	0	0	0	0	5	0	0	ap, tl, zr
CR98SJ400	mylonite	strong	f (vf mica)	1.0-7.0	30	30	30	28	10	2	0	0	0	0	0	0	ap, tl, zr
CR98SJ401	protomylonite	moderate	f-m	1.0	55	45	37	15	3	0	0	0	0	0	0	0	ap, tl
CR98SJ403	mylonite	strong	m-f	1.0	40	38	45	5	2	10	<1	0	0	0	0	0	tl
CR98SJ404	mylonite	strong	f	1.0-3.0	20	40	50	10	<1	0	0	0	0	0	0	0	tl
CR98SJ407	protomylonite	weak-mod	m (f mica)	0.8	60	43	40	15	0	0	1	1	0	1	0	0	ap, tl, zr
CR98SJ411	mylonite	moderate	m (f mica)	0.3-5.0	45	45	43	10	0	0	0	1	1	1	0	0	
CR98SJ413	mylonite	strong	f	0.3-1.5	40	45	43	10	0	0	0	1	1	1	0	0	
CR98SJ414	mylonite	strong linear	f-vf	0.5	35	30	50	20	<1	<1	0	0	0	0	0	0	tl
CR98SJ415	mylonite	moderate	f	0.5-5.0	20	40	43	17	0	0	<1	0	0	0	0	0	tl
CR98SJ417	protomylonite	moderate	m (f mica)	0.5-0.8	60	42	40	10	6	0	0	0	1	2	0	0	
<b>Bond Springs Shear Zone and associated samples</b>																	
CR98TR1	mylonite	strong	m-vf	1.0	20	35	30	0	15	18	0	0	0	2	0	0	
CR98TR2	mylonite gneiss	weak	c-m		15	50	15	0	35	0	0	0	0	0	0	0	
CR98TR3	cataclastite		c-m	2.0-7.0	80	48	1	0	48	0	0	0	3	0	0	0	
CR98TR4	migmatite gneiss	strong	c-f		30	20	15	0	0	15	0	0	0	0	20	0	
CR98TR37	cataclastite	strong	f	0.3-0.7	30	28	37	0	20	15	0	0	0	0	0	0	
CR98TR473	foliated cataclastite	moderate	m-vf	0.5-5.0	40	25	10	15	10	0	0	0	0	0	0	0	
CR98TR474	mylonite	strong	f	0.8	20	25	30	1	15	29	0	0	0	0	0	0	
CR98TR475a	mylonite	strong	f-m	0.3-0.7	30	37	48	0	7	8	0	0	0	0	0	0	
CR98TR475b	mylonite	strong	f	0.3-0.7	20	35	35	12	16	0	0	0	1	0	0	1	
CR98TR476	mylonite	strong	f-vf	0.5	25	35	30	0	15	20	0	0	0	0	0	0	
CR98TR477	protomylonite	strong	f-m	0.3-0.5	70	45	40	0	15	0	0	0	0	0	0	0	
CR98TR478	mylonite	strong	vf	0.5	5-20	25	35	0	15	25	0	0	0	0	0	0	
CR98TR479	protomylonite	weak	c-m		75	40	30	15	13	0	0	0	2	0	0	0	
CR98TR418	protomylonite	moderate	c-f	up to 100	60-70	45	30	15	8	0	0	0	2	0	0	0	
<b>Mafic mylonites, Bond Springs</b>																	
CR98TR425	mafic mylonite	strong	m-f	0.5	20	25	35	10	0	0	14	15	0	1	0	0	
CR98TR436	mafic mylonite	strong	m (fine bl)	0.5-1.0	25	20	40	10	0	0	15	15	0	0	0	0	
CR98TR441	mafic mylonite	strong	c-m	0.5-1.0	25	25	35	7	0	0	16	18	0	0	0	0	
CR98TR444	mafic mylonite	strong	m (fine bl)	0.3-0.8	25	30	35	14	0	0	20	1	0	0	0	0	
CR98TR462	mafic mylonite	strong	f-m	0.3-0.5	15	25	35	10	0	0	15	15	0	0	0	0	
CR98MF220	mafic mylonite	strong	m	0.5-2.0	40	32	33	14	0	0	5	14	0	2	0	0	
CR98BS547	mafic mylonite	strong	m-vf	0.3-1.0	35	30	35	20	0	0	2	10	0	3	0	0	
CR98BS550	pyroxene-granulite	weak	c	N/A		40	5	10	0	0	0	0	0	0	0	0	45% cpx
CR98BS551	augen gneiss	weak	c	N/A		30	50	15	0	0	5	0	0	0	0	0	
CR98BS552	augen gneiss	weak	c	N/A		43	35	15	0	5	2	0	0	0	0	0	

The protomylonite north of the high-strain zone is composed of migmatite gneiss with a relict ~15m wide leucocratic segregation at the edge of the high strain zone. The leucocratic protomylonite comprises quartz, K-feldspar, plagioclase, biotite and garnet. The amphibolite-bearing augen-rich protomylonite gneiss to the south comprises quartz, K-feldspar, plagioclase, biotite and hornblende (Table 6.4). The higher-strain mylonites comprise layers of quartz, quartzofeldspathic and phyllosilicate-rich composition. Muscovite-bearing quartzofeldspathic mylonites also occur to the north of the main shear zone, separated by a band of protomylonite. Two bands of ultramylonite are present at each edge of the main shear zone. They are 1 to 2m wide and are biotite and epidote rich.

The felsic, layered mylonites to the north of the main shear zone contain quartz, K-feldspar, plagioclase, variable biotite, muscovite, epidote, and relic garnet, and have accessory titanite and ilmenite (Table 6.4). They comprise strongly-foliated, millimetre-sized feldspar-rich layers, biotite-muscovite-quartz-rich layers, and aligned recrystallised, undulose, quartz ribbons. Feldspar porphyroclasts are also aligned in the fabric. Some small anhedral garnet grains (~200µm) occur and these are partially replaced by biotite and epidote. Some K-feldspar porphyroclasts have a dirty appearance with biotite and some associated muscovite replacement. Commonly, the feldspar porphyroclast edges are recrystallised with large lobate embayments and inclusions developed during grain boundary migration. Some symplectite structures are also present. New growth minerals within these mylonites include 100 to 200µm muscovite, epidote-clinozoisite and titanite. Muscovite pseudomorphs biotite grains, titanite commonly rims ilmenite grains, and biotite and epidote rim garnet clasts.

The quartzofeldspathic mylonites appear to have accommodated more strain. Feldspar porphyroclasts are flattened and stretched. They have fine grainsize (20 to 100µm) and are partitioned into phyllosilicate-rich and quartz-rich layers within a strong laminar foliation. The feldspar porphyroclasts have recrystallised grain boundaries parallel to the foliation and pressure shadows have developed. Silicic mylonites within the main shear zone are predominantly quartz rich with minor biotite and abundant epidote. They are equigrained with thin layers of epidote, a strong laminar foliation and fine to medium-grainsize (100 to 200µm). The ultramylonites have a strong planar fabric with few or no porphyroclasts remaining. They are fine grained (~20µm) and comprise biotite, quartz, feldspar, epidote and titanite (Table 6.4). The matrix comprises layered, sub-grained quartz lenses and very

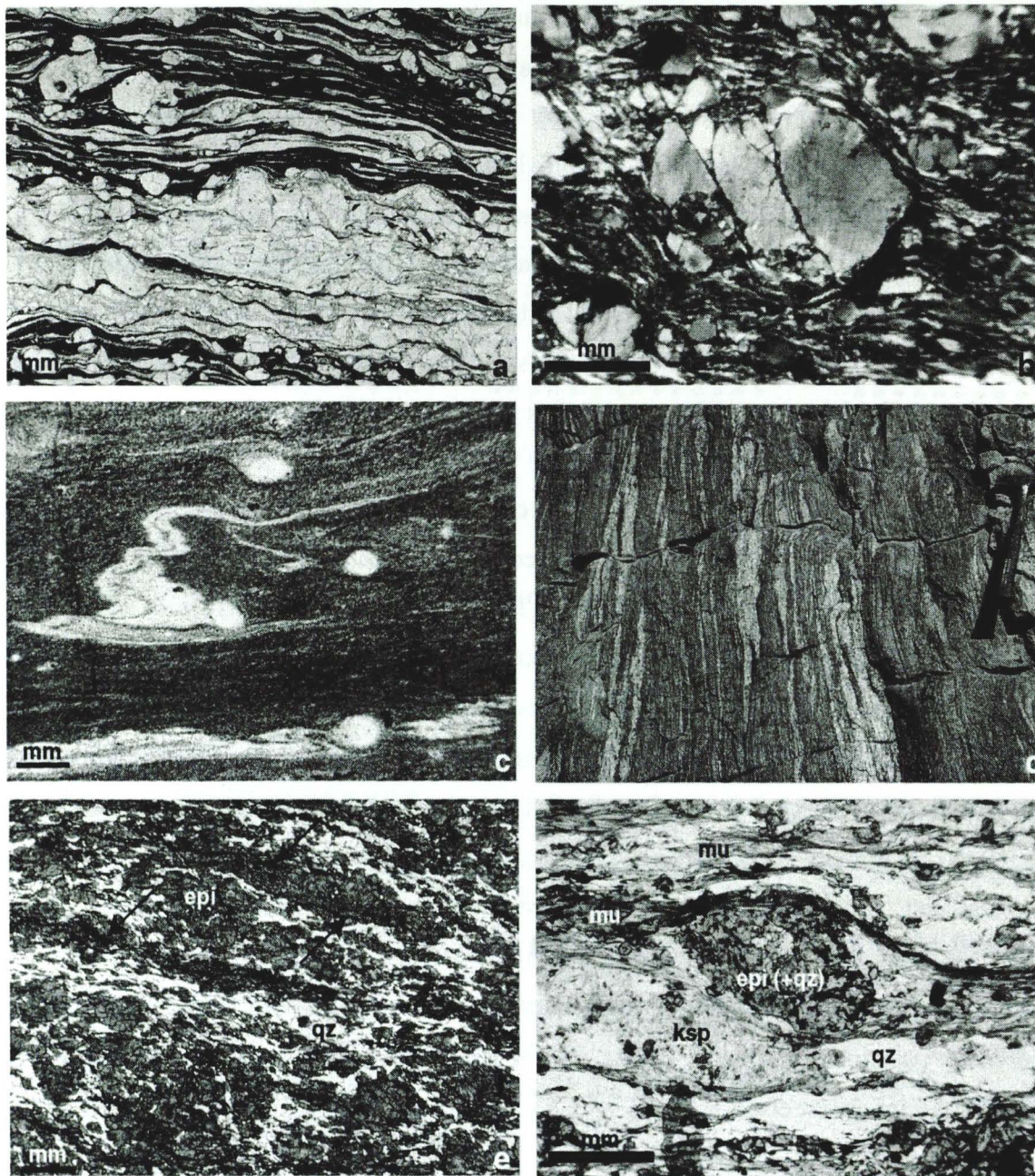


Figure 6.6. a) Layered mylonite showing abundant angular feldspar fragments wrapped in biotite and quartz layers, indicating both brittle and ductile deformation, PPL. b) Fractured feldspar porphyroclast in a quartzofeldspathic mylonite at Illyabba Dam, XPL. c) Folded quartz vein in an ultramylonite, PPL. d) Melt segregations entrained within a high strain mylonite at Supplejack Dam. e) Epidote-rich quartz-epidote mylonite, Brumby Bore, PPL. f) Epidote and quartz augen wrapped in muscovite and recrystallised quartz, indicating reworking of the quartz-epidote mylonites.

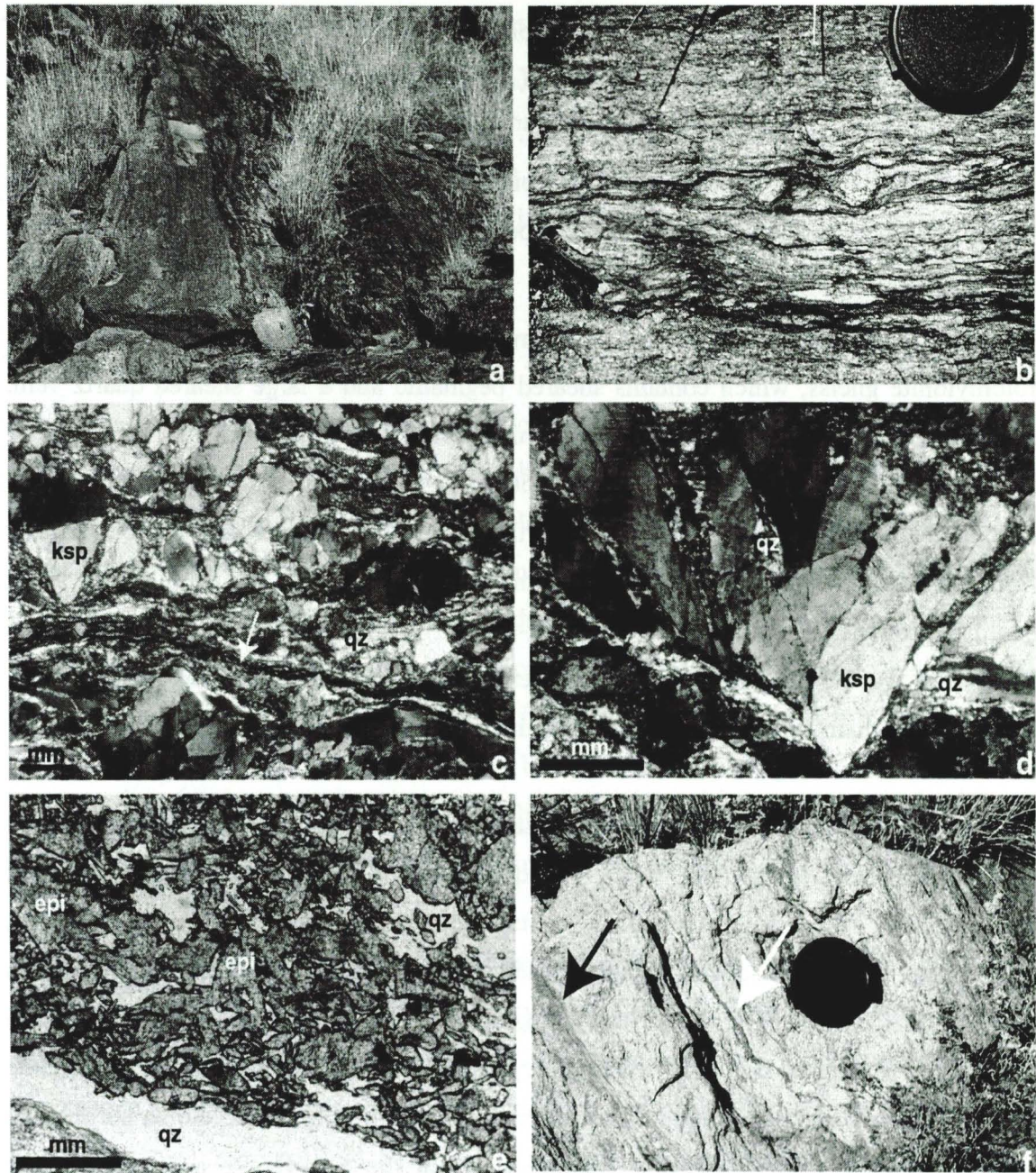


Figure 6.7. a) Migmatite gneiss at Mount Forster. b) Rotated fragments within a biotite-rich shear band, Mount Forster. c) Fractured feldspar clasts within an annealed quartz and feldspar matrix with abundant dissolution seams (arrow) of opaque material. d) Close up of a fractured feldspar within the foliated cataclasite at Mount Forster, with recrystallised quartz filling fractures. e) Recrystallised epidote vein. f) Small shear band (black arrow) and epidote vein (white arrow) cutting quartz-epidote mylonite at Mount Forster.

fine-grained ( $\leq 10\mu\text{m}$ ) green-brown biotite forming a SC fabric with a sinistral sense of shear. Flattened K-feldspar porphyroclasts have recrystallised edges, pressure shadows and tails that also indicate sinistral sense of shear. Titanite occurs associated with the epidote. Straight, corroded grain boundaries of clinozoisite with biotite rims parallel to the foliation suggest that pressure solution-mass transfer operated during shearing.

#### *6.4.1.3 Ilyabba Dam Shear Zone*

The shear zone near Ilyabba Dam is 55m wide and cuts a leucocratic migmatitic protomylonite gneiss, which contains sheared pegmatite and a large sheared quartz vein. The shear zone trends  $120^\circ/50^\circ\text{N}$  with mylonitic foliation ranging from  $75\text{-}126^\circ/48\text{-}68^\circ\text{N}$  and down-dip stretching lineation plunging  $50$  to  $68^\circ$  towards  $\sim 016^\circ$ . The protomylonite fabric intensifies to mylonite fabric in the northern part of the shear zone, with one narrow ( $\sim 1\text{m}$ ) ultramylonite zone occurring within the protomylonite. To the south of the shear zone, the protomylonite comprises quartz, K-feldspar, plagioclase, biotite, and hornblende (Table 6.4). To the north hornblende is absent and the protomylonite has a more felsic composition. Ilmenite and titanite are the dominant accessory phases.

The mylonites are strongly layered, with quartz ribbons, biotite bands and fine-grained quartz and feldspar layers (Fig. 6.6a). The quartz and feldspar layers contain abundant porphyroclasts. The sheared assemblage contains quartz, K-feldspar, plagioclase, biotite, epidote, and locally muscovite or hornblende (Table 6.4). Hornblende only occurs as porphyroclasts, with K-feldspar and plagioclase. The hornblende clasts contain microscales, fractures and only minor recrystallisation. The recrystallised hornblende occurs in higher strain layers and in association with ilmenite and biotite. Some hornblende clasts are present as small angular fragments within the fine biotite and quartz shear matrix, indicating brittle deformation. Extensive perthitic exsolution, undulose extinction and deformation twins are all present within the feldspar porphyroclasts, in addition to abundant microfaulting and fracturing (Fig. 6.6b). Microfaulting of the feldspars is more abundant in the higher strain mylonites that contain less biotite. Epidote occurs as rounded small ( $200\mu\text{m}$ ) clasts within the very fine ( $10$  to  $50\mu\text{m}$ ) matrix. Quartz ribbons are abundant and define the strong foliation within the shear zone, reducing in size as strain increases. The quartz ribbons have undulose extinction and contain minor subgraining with serrated grain boundaries. Very fine-grained biotite ( $\sim 10\mu\text{m}$ ) also occurs in bands within the high-strain mylonites. Layers of very fine-grained biotite contain seams of opaque material, likely representing dissolution seams. Some feldspar porphyroclasts have their edges truncated and fibrous biotite occurs within feldspar pressure shadows. Pressure

solution seams are abundant within the ultramylonites. The ultramylonite comprises biotite (70%) with epidote and quartz and contains well-rounded clasts of quartz and feldspar and small elongate clasts of epidote in a very fine-grained biotite matrix. Micro-folding within fine quartz layers (Fig. 6.6c) and pressure shadows of rounded porphyroclasts indicate sinistral sense of shear parallel to the foliation plane, consistent with reverse dip-slip movement across the shear zone.

#### 6.4.1.4 Supplejack Dam Shear Zone

The shear zone south of Supplejack Dam is 70m wide, trends  $140^{\circ}/50^{\circ}\text{N}$  and cuts granitic migmatite gneiss with a sub-parallel foliation. Pegmatites and large leucosomes produce compositional variation within the granitic host that ranges from felsic (two feldspar and quartz with garnet) to granodioritic (hornblende-bearing) compositions (Table 6.5). The shear zone rocks have an anastomosing mylonitic foliation of  $132\text{-}164^{\circ}/30\text{-}55^{\circ}\text{N}$  and a down-dip stretching lineation defined by feldspar as well as feldspar and quartz aggregates. Deformed melt segregations within the shear zone rocks define a fabric parallel to the shear zone walls (Fig. 6.6d). The mylonitic foliation varies from weak to strong in several narrow bands throughout the shear zone, likely reflecting changes in strain. Grainsize reduction mirrors the changes in fabric. Ultramylonite occurs within the more intensely sheared rocks, as narrow, biotite-rich, very fine-grained bands.

The protomylonite and mylonite comprise feldspar, quartz and biotite with minor amphibole and garnet (Table 6.5). Accessory phases include ilmenite, titanite and apatite, with zircon present in the sheared garnet-bearing leucosomes. K-feldspar, plagioclase, hornblende and garnet occur as 2 to 10mm diameter porphyroclasts within a matrix of fine ( $\sim 10$  to  $50\mu\text{m}$ ) recrystallised feldspar, quartz and aligned biotite. The anastomosing mylonitic foliation is predominantly defined by abundant bands of sub-grained quartz ( $\sim 50\mu\text{m}$ ). The bands have serrated to straight sub-grain boundaries, and undulose extinction depending on strain intensity. The quartz-feldspar layers do not have a strong grain-shape fabric or preferred orientation. The grains are angular and are finer-grained than the pure-quartz layers, similar in style to the mylonites described by Fleirvoet *et al.* (1997). K-feldspar porphyroclasts contain abundant exsolution lamellae. In addition, some symplectite textures occur at clast boundaries along the foliation plane. Core-mantle textures produced by recrystallisation at the boundaries of porphyroclasts are common, as are pressure shadows with fibrous biotite, feldspar and quartz. Garnet forms fine euhedral grains in the matrix. Biotite is present in all the mylonites, but is more abundant in the high strain mylonites. Epidote occurs within some higher strain mylonites, as small ( $\sim 20\mu\text{m}$ )

equant grains in association with biotite. In the felsic leucocratic mylonites muscovite occurs in variable abundance (Table 6.4).

#### **6.4.2 Quartz-epidote mylonites**

Finely layered, silicified and epidotised mylonite occurs at the northern extent of the exposed mylonites at Brumby Bore, on a small hill west of Brumby Bore, at Ilyabba Dam and at Mount Forster (Fig. 6.5). It is light green to yellow and contains large pink K-feldspar augen. The green colouration is due to abundant epidote, varying from 11 to 35% (Table 6.5). The mylonitic fabric is anastomosing to laminar, depending on the augen content, and ranges from 140-130°/60-54°N. Variation in strain throughout the silicified mylonites are implied by changes in grain size and augen abundance. The compositional layering and relict K-feldspar porphyroclasts present in the quartz-epidote mylonites indicates that they are altered equivalents of the quartzofeldspathic mylonites.

The mylonites are typically medium grained (100 to 500µm) and layered with variable quartz and epidote contents (Table 6.5). Compositional layering, alignment of biotite flakes, and feldspar augen define the foliation. K-feldspar porphyroclasts are flattened and recrystallised with feldspar-rich pressure shadows and abundant flame perthites. K-feldspar aggregates also occur aligned in lenses and contain recrystallised irregular shaped grains with abundant cross-hatched twinning. Where strain is higher, the feldspar porphyroclasts are completely flattened, forming elongate lenses. Quartz occurs as 50 to 100µm equigranular sub-grains with straight grain boundaries. Epidote occurs as equant 20 to 50µm grains (Fig. 6.6e). Ilmenite (20 to 50µm) forms an important accessory mineral, commonly occurring in very thin layers parallel to the foliation and defining dissolution seams (Fig. 6.6e). The mylonites have distinctively different composition from the granitic mylonite (Fig. 6.10). Epidote-rich layers contain up to 90% epidote (Fig. 6.6e). Discrete shear bands of muscovite and muscovite and biotite truncate the quartz-epidote foliation. The micas form euhedral needles and are medium-grained (~80µm). In some cases, epidote-quartz aggregates form augen wrapped by the fine muscovite-biotite shear bands (Fig. 6.6f). In addition, some larger epidote clasts occur and are wrapped by the fine epidote, indicating heterogenous reworking of the mylonites.

##### *6.4.2.1 Cataclasis and shearing at Mount Forster*

Mount Forster (Fig. 6.5) comprises granitic and quartzofeldspathic gneisses with abundant augens (Fig. 6.2a), felsic leucosomes, and foliated migmatites (Fig. 6.7a). Shear bands that cut the gneisses commonly contain rotated, angular fragments of gneiss (Fig. 6.7b). The phyllonites contain abundant fine-grained (20µm) biotite, subgrained quartz and relict

feldspar grains. Foliated cataclasites are also present and contain abundant dissolution seams (Fig. 6.7c) and annealed quartz. Large feldspars are extensively fractured and have quartz filling the fractures (Fig. 6.7d). Phyllonite exposed in creeks and along the base of the hill at Mount Forster contains cataclastic layers, and fragmented feldspars and epidote suggesting it developed from hydration of the cataclasite. To the south of Mount Forster, a large pod/lens of quartz-epidote mylonite-gneiss is exposed as a steeply sided hill. The mylonite forms a large block that is rimmed by a cataclastic zone. The cataclastic zone is 1 to 5m wide and cemented with epidote. Many epidote veins occur throughout the surrounding country rock which has substantially fractured (Fig. 6.7e). The cataclasite is foliated, with lenses of quartz-epidote mylonite gneiss wrapped in recrystallised quartz and epidote. Annealed quartz in the foliated cataclasites contains abundant fluid inclusion trails.

#### **6.4.3 Mafic mylonites at Mount Forster**

To the North of the Redbank Thrust, the mylonites are derived from rocks of the Central Province. The low hills to the north of Mt Forster comprise 120 m height of exposed mafic-intermediate mylonite, with no exposed boundaries. The mylonitic foliation is north dipping ( $60-86^{\circ}/40-50^{\circ}\text{N}$ ), with a clear SC fabric indicating sinistral sense of shear parallel to the lineation, consistent with reverse movement along the foliation.

The mylonites are dark and finely laminated, with well-formed down-dip stretching lineation and highly-attenuated felsic layers. Garnet–amphibole aggregates give the mylonite a peppered appearance in outcrop (Fig. 6.8a). The mylonites comprise fine-grained (20 to 50 $\mu\text{m}$ ) layers containing plagioclase, amphibole, garnet, K-feldspar, quartz, and biotite (Table 6.6). Throughout the exposure, grain size and foliation intensity vary, with some more garnetiferous felsic layers representing pre-shearing partial melting. Composition is consistent throughout the exposure with the only variation being where garnet and hornblende reduce and biotite increase in abundance in the finer-grained, higher-strain layers (Table 6.6). Extensive undulose quartz ribbons that wrap around aligned composite augens comprising garnet, plagioclase and hornblende (Figs. 6.8b, e) define the mylonitic foliation. In addition, minor very fine-grained biotite (<10 $\mu\text{m}$ ) and

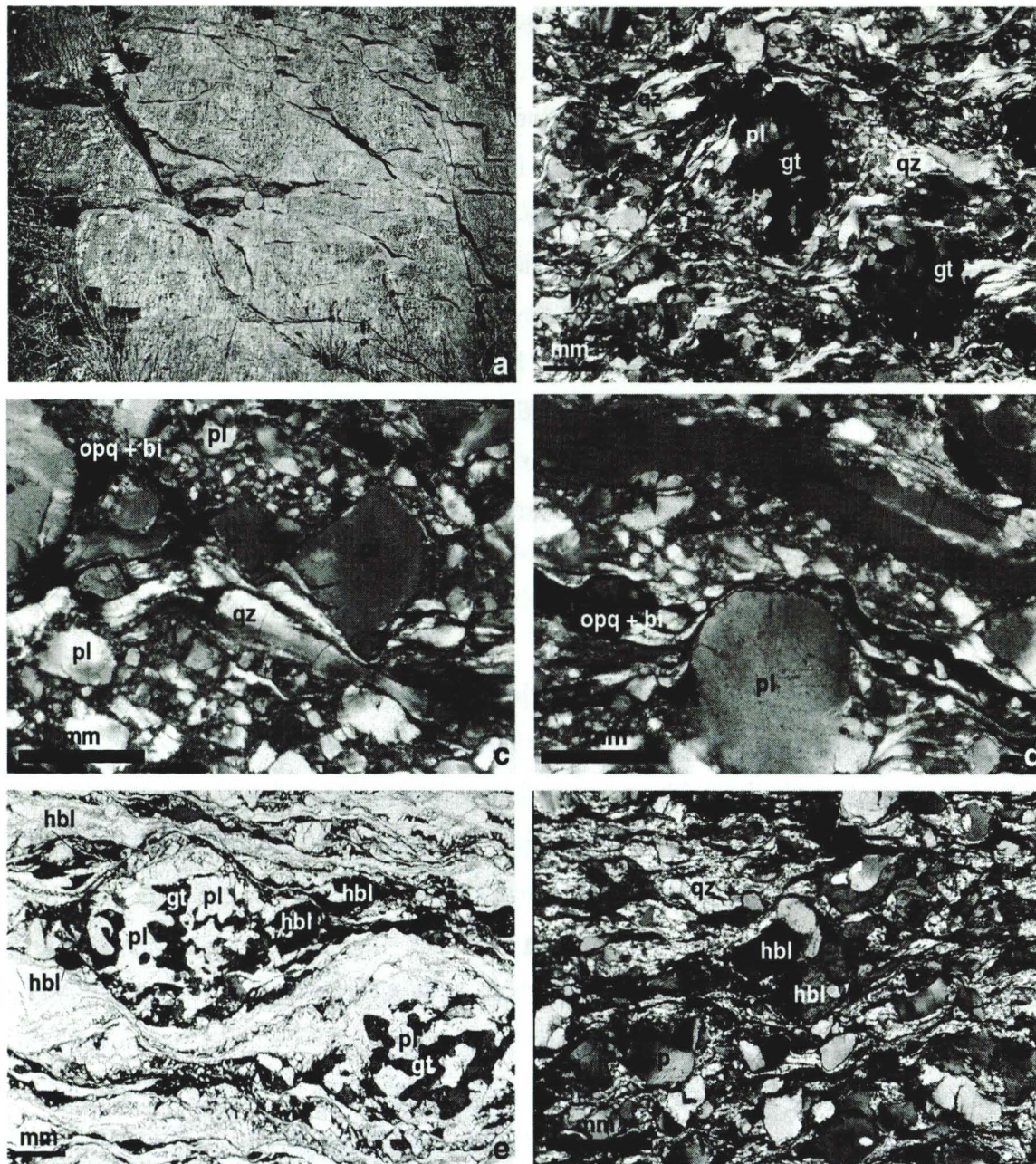


Figure 6.8. a) Peppered mafic mylonites north of Mount Forster, with a well developed down-dip lineation. b) Embayed garnet and plagioclase porphyroclasts surrounded by a matrix of fine quartz and feldspar with abundant quartz ribbons, XPL. c) Fractured plagioclase clast with slip along the fracture plane surrounded by quartz ribbons and cataclastic matrix of angular feldspar fragments and fine recrystallized quartz with some opaque material and biotite, XPL. d) Plagioclase porphyroclasts surrounded by annealed cataclasite of feldspar and quartz with a seam of opaque material and biotite, XPL. e) High-grade decompression texture of garnet altering to plagioclase and locally hornblende, PPL. f) Angular hornblende clasts entrained in recrystallized quartz and feldspar matrix, and surrounded by fine recrystallized amphibole and biotite, XPL.

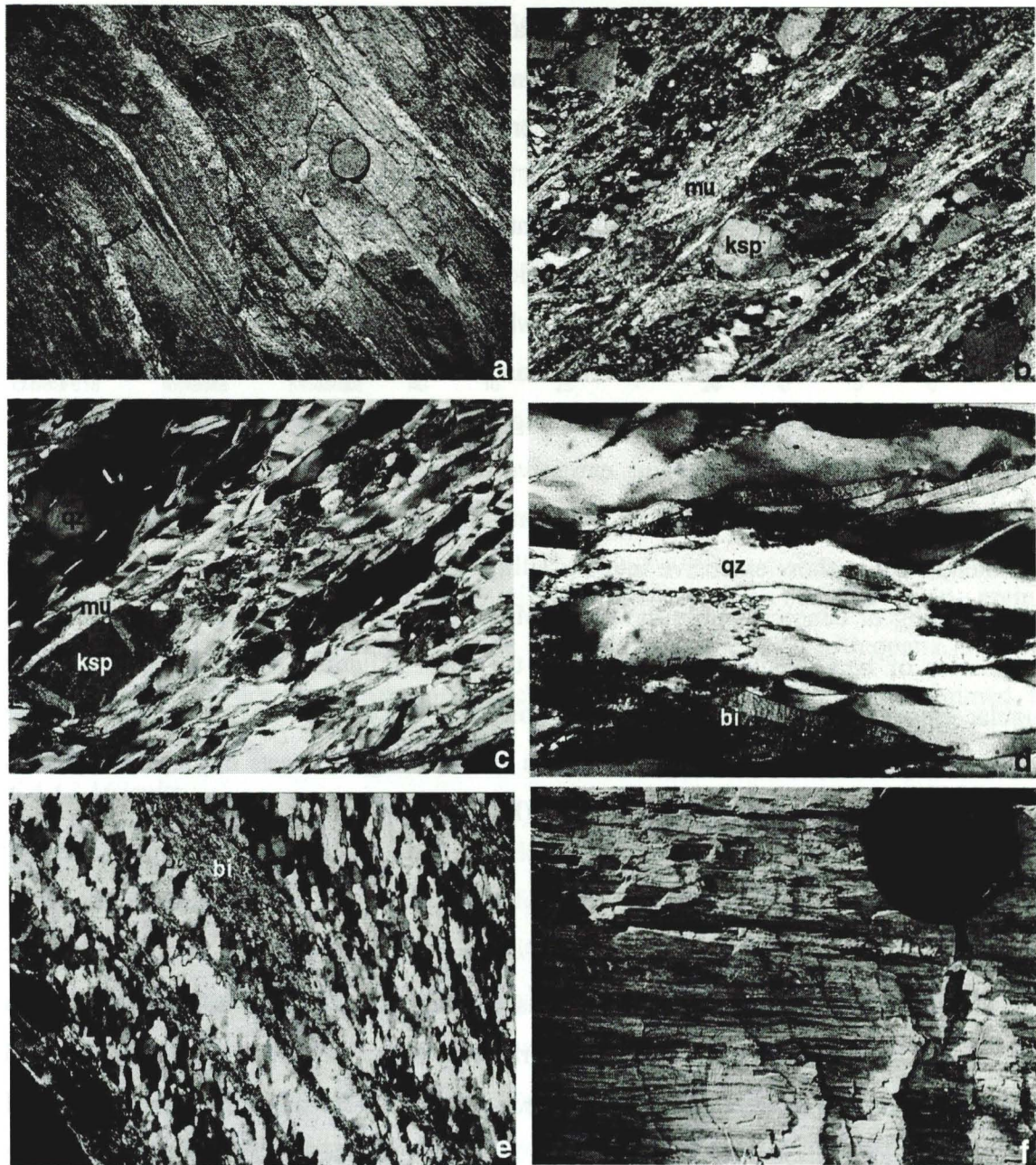


Figure 6.9. Mylonites from the Littlers Yard area, Southern Province. a) Banded mylonite. b) K-feldspar wrapped by fibrous muscovite, with abundant angular feldspar clasts and recrystallised quartz, XPL. c) K-feldspar porphyroclast with mica fringes, XPL. d) Quartz showing serrated grain boundaries and undulose extinction with deformed biotite grains, XPL. e) Quartz-rich layer with strong preferred orientation and biotite s-bands, showing sinistral shear sense, XPL. f) Finely-laminated ultramylonite.

ilmenite form fine anastomosing bands parallel to the quartz ribbons. Small (0.5mm) angular clasts of feldspar, amphibole and garnet are commonly entrained within the very-fine biotite bands. Biotite is also present in pressure shadows, along the grain boundaries and filling fractures in garnet and hornblende clasts. The quartz ribbons have fine serrated boundaries and some sub-graining is apparent. In the finer grained mylonites, the quartz ribbons reduce in size but maintain undulose extinction and shape, suggesting low temperatures and high strain. The feldspars, which form angular, variable sized clasts have extensive undulose extinction, exsolution and deformation lamellae. Some antithetic micro-faults occur in large feldspar clasts (Fig. 6.8c). The finer-grained mylonites contain brittle textures that have undergone extensive recrystallisation (Fig. 6.8d). The coarser-grained mylonites show extensive rotation and recrystallisation of feldspars. The hornblende clasts show extensive intercrystalline deformation as undulose extinction and some kinking or bending within the grain. Minor recrystallisation occurs along the grain boundaries of hornblende clasts parallel to the shear foliation, and alignment of small angular grains defines an anastomosing mylonitic foliation (Fig. 6.8f). In addition to the larger embayed prophyroclasts, garnet occurs as small angular clasts in pressure shadows of larger clasts and within brittle shear bands (Fig. 6.8d).

#### **6.4.4 Littlers Yard shear zones**

##### *6.4.4.1 Ellery Granitic Complex migmatite gneiss*

The Ellery Granite Complex occurs as intensely-folded granitic migmatite in the Littlers Yard area. The gneiss is medium- to coarse-grained (200µm to 1mm) equigranular, layered and folded. The average composition comprises quartz, K-feldspar, plagioclase, biotite and muscovite (Table 6.7). The folded, predominantly layer-parallel leucosomes are more quartz-rich with coarse-grained (0.5 to 2mm) and equigranular, with a granitic composition. The mylonite zones within the Ellery Granite Complex contain a progression of intensities of strain from protomylonite through mylonite and ultramylonite. The sheared rocks are commonly banded (Fig. 6.9a), with compositional changes coupled with intensity of deformation.

##### *6.4.4.2 Protomylonite*

The quartzofeldspathic protomylonites are medium- to coarse-grained ( $\leq 1$ mm) and layered. The protomylonites comprise quartz, K-feldspar, plagioclase, biotite, and muscovite (Table 6.7). Small micaceous shear bands commonly form layer-parallel discrete ultramylonite bands within the protomylonites. Quartz forms ribbons that are commonly rimmed by fine-grained recrystallised quartz with undulose extinction.

**Table 6.7. Modal mineral abundances (%) for unsheared and sheared Ellery Granitic Complex rocks at Littlers Yard. Abbreviations in Table 1.1.**

Sample	Rock Type	Foliation Intensity	qz	ksp	pl	fsp	bi	mu	epi	ti	chl
CR98SP616	Migmatite Gneiss	weak	40	40	13	-	5	2	0	0	0
CR98SP622	Migmatite Gneiss	weak	40	40	10	-	10	0	0	0	0
CR98SP624	Migmatite Gneiss	weak	40	32	15	-	13	0	0	0	0
CR98SP626	Migmatite Gneiss	weak	50	35	5	-	10	0	0	0	0
CR98SP614	protomylonite	weak	70	5	5	-	10	10	0	0	0
CR98SP615	protomylonite	weak	60	4	1	-	15	20	0	0	<1
CR98SP617	quartz layer/vein	strong	90	-	-	5	0	5	0	0	0
CR98SP618	mylonite	moderate	40	10	25	-	24	0	0	0	0
CR98SP619	ultramylonite	strong	70	-	-	10	0	15	5	<1	0
CR98SP621	ultramylonite	strong	60	-	-	9	0	15	13	3	0
CR98SP625	quartz mylonite	strong linear	80	-	-	5	0	10	5	0	0
CR98SP630	mylonite	strong	50	-	-	25	4	5	15	1	0

Deformation lamellae and fluid inclusion trails are common within the larger quartz grains. The edges of the elongated quartz grains are serrated. Mica is aligned with quartz, defining a preferred orientation. Feldspar porphyroclasts are large (<2mm) and are rimmed by muscovite and biotite.

#### 6.4.4.3 Mylonite

Continued grain size reduction and reworking of feldspar and quartz porphyroclasts produced medium-grained, layered quartzofeldspathic mylonite. The mineral assemblage comprises quartz, feldspar, biotite, muscovite, epidote, and chlorite (Table 6.7). Aligned biotite and muscovite form a strong mylonitic foliation, wrapping around feldspar porphyroclasts. Biotite typically occurs in two forms, as large elongate grains with internal deformation and abundant kinking and as fine masses of recrystallised biotite that both rim the larger grains or K-feldspar porphyroclasts. Overprinting textures indicate muscovite or chlorite infrequently formed at the expense of biotite. Muscovite also occurs as large kinked grains in association with the kinked biotite. Biotite and muscovite commonly form aligned grains along embayed edges of feldspars indicating fluid-assisted mass transfer occurred during deformation (Fig. 6.9b). The more intensely strained mylonites contain flattened feldspar porphyroclasts, with pressure shadows and tails of recrystallised feldspar, quartz and muscovite that indicate sinistral shear sense (Fig. 6.9c). Brittle fractures locally offset the feldspar grains, with abundant microfractures and cracks. Plagioclase porphyroclasts are also commonly rimmed by biotite and epidote and have well-developed pressure shadows. Quartz occurs as irregular, elongate undulose ribbons that are typically surrounded by biotite, with minor sub-grain development along the edges of some ribbons (Fig. 6.9d).

Quartz-rich layers within the mylonite contain ~90% quartz, with some relic feldspar porphyroclasts and fine-grained muscovite. The quartz is extensively dynamically recrystallised, forming a crystallographic preferred orientation (Fig. 6.9e). Muscovite forms thin elongate anastomosing shear bands. Feldspar grains are aligned within the mylonitic fabric and have variable development of pressure shadows. They are smaller in size (~2mm) than within the quartzofeldspathic mylonite. The SC fabric in the quartz layers indicates sinistral shear sense, representing reverse movement across the shear zone (Fig. 6.9e). Rounded, reworked feldspar porphyroclasts occur in a biotite, epidote and quartz matrix forming a strong foliation. Quartz ribbons are typically sub-grained and flattened. Feldspar porphyroclasts contain fractures that are filled with biotite and quartz. The high-strain fabric is defined by fine-grained (20-100 $\mu$ m) bands of muscovite, epidote titanite and recrystallised feldspar  $\pm$  biotite. Quartz forms layers of dynamically-recrystallised rotated sub-grains, with some larger grains remaining as undulose augens.

#### *6.4.4.4 Ultramylonite*

Fine- to very fine-grained (10 to 100 $\mu$ m) ultramylonite occurs in narrow bands within mylonite zones (Fig. 6.9f). The ultramylonite comprises quartz, feldspar, muscovite, epidote, titanite, biotite, chlorite (Table 6.7). Major grain size reduction appears to have occurred by dynamic recrystallisation, especially sub-grain rotation recrystallisation of the quartz. Dynamically recrystallised albite, K-feldspar, quartz and sericite occur in pressure shadows and as tails associated with feldspar porphyroclasts. Finely recrystallised white mica associated with minor epidote form an anastomosing shear fabric. Large muscovite grains also occur, with muscovite comprising the dominant mica and are associated with abundant epidote and titanite. Biotite is rare, having been replaced by muscovite, epidote and, occasionally, chlorite. A major increase in epidote and muscovite abundance occurs with a decrease in feldspar porphyroclast grain size. Fine-grained shear bands that comprise sericite, quartz and epidote ( $\pm$  albite) anastomose around feldspar porphyroclasts. Titanite is also variably abundant, occurring in layers parallel with the shear foliation, as well as in association with epidote.

#### **6.4.5 Shearing characteristics**

The mylonites of the Redbank High Strain Zone show extensive variation in strain across individual shear zones. The variation in strain is typically associated with a variation in composition. The high strain rocks comprise both biotite- and/or epidote-rich ultramylonites and quartz-rich mylonites, while the low strain protomylonites contain assemblages resembling their granitic, granodioritic or pelitic protoliths.

The shear zones commonly develop at lithological boundaries within the granitic protomylonites, indicating that deformation was in part controlled by pre-existing discontinuities in the wall rocks. Predominantly, the wide shear zones with visibly progressive increases in strain represent the higher-temperature mylonite zones. These zones have predominantly been reworked at lower grades, producing hydrous greenschist-facies mineral assemblages and abundant brittle deformation.

Due to the fine grain size with consistent lack of preferred orientation or shape fabric, the finer-grained quartz-feldspar matrix material of the mylonites are likely to have deformed by grain boundary sliding (Passchier and Trouw, 1996), suggesting very high strains during shearing producing superplasticity. Similar evidence of grain-boundary sliding has been discussed from elsewhere in the Redbank High Strain Zone by Fleirvoet *et al.* (1997). The abundance of core-mantle structures and grain-boundary sliding suggests shearing occurred above  $\sim 400^{\circ}\text{C}$ , with banded ribbon textures common in medium- to high-grade quartzofeldspathic rocks (Passchier and Trouw, 1996). The conditions of metamorphism within the quartzofeldspathic mylonites is not well constrained through mineral assemblages, but the deformation characteristics discussed above indicate that the mylonites formed under at least upper greenschist-facies conditions. Temperatures of mineral growth are further discussed in Chapter Seven. There is abundant evidence of lower grade reworking of the mylonites throughout the Redbank High Strain Zone, with the growth of epidote and muscovite within ultramylonites and as shear bands through the lower strain rocks. These hydrated assemblages probably indicate focused flow during deformation due to strain partitioning that continued as metamorphism subsided.

Fractured feldspars indicate that brittle processes were also significant during shearing in the eastern Redbank High Strain Zone, and suggest that at least some shear zones deformed at conditions close to those of the brittle-ductile transition (Imber *et al.*, 1997). Fluid inclusion trails in quartz within the protomylonite are indicative of healed fluid filled fractures. The occurrence of ultramylonite bands within protomylonites indicates variations in strain that may have resulted from brittle fracturing at sites of high strain as pressure and temperature decreased during shearing. In addition, cataclasis and epidote veining (Fig. 6.7) substantially reworked both quartz-epidote and quartzofeldspathic mylonites. The cataclasis also occurred at sites of very high strain within the shear zones. The subsequent recrystallisation of quartz and phyllosilicate growth within the cataclasites and the development of phyllonites indicate hydration following brittle deformation occurred at

temperatures greater than 300°C (Passchier and Trouw, 1996). This suggests reworking within the shear zones occurred under conditions representing the brittle-ductile transition.

The quartzofeldspathic mylonites vary in composition (Tables 6.4, 6.5, 6.6). Increases in strain are coupled with consistent loss of feldspar and growth of biotite, muscovite and epidote (Fig. 6.10). The high strain zones within the protomylonites typically contain quartz-rich mylonites, biotite-rich ultramylonites and less commonly quartz- and epidote-rich mylonites. The coupling of increasing strain with quartz loss and biotite gain in the mylonites zones, as also recognised in the northern Arunta Inlier (Chapter Three), is likely to reflect the preferential dissolution of quartz under high normal stress (Bos and Spiers, 2001).

The biotite and less common muscovite shear bands throughout the protomylonites likely represent fluid flow pathways and indicate variable fluid infiltration at grain scale in the lower strain rocks. The mylonites contain pressure solution seams and truncated porphyroclasts, indicating more pervasive fluid-driven mass transfer occurred during shearing in the higher strain rocks. The fine-grained, biotite-rich ultramylonite bands contain abundant dissolution seams and would have channelled the bulk of the fluid flow during shearing.

#### 6.4.5.1 Quartz-epidote mylonites

The medium grainsize, strain-free quartz aggregates with polygonal subgrain boundaries and large, equant epidote grains suggest the quartz-epidote mylonites crystallised at moderately high temperatures. The abundant K-feldspar

porphyroclasts with similar morphology and deformation textures indicate that they were produced from the quartzofeldspathic mylonites. The quartz-epidote mylonites contain

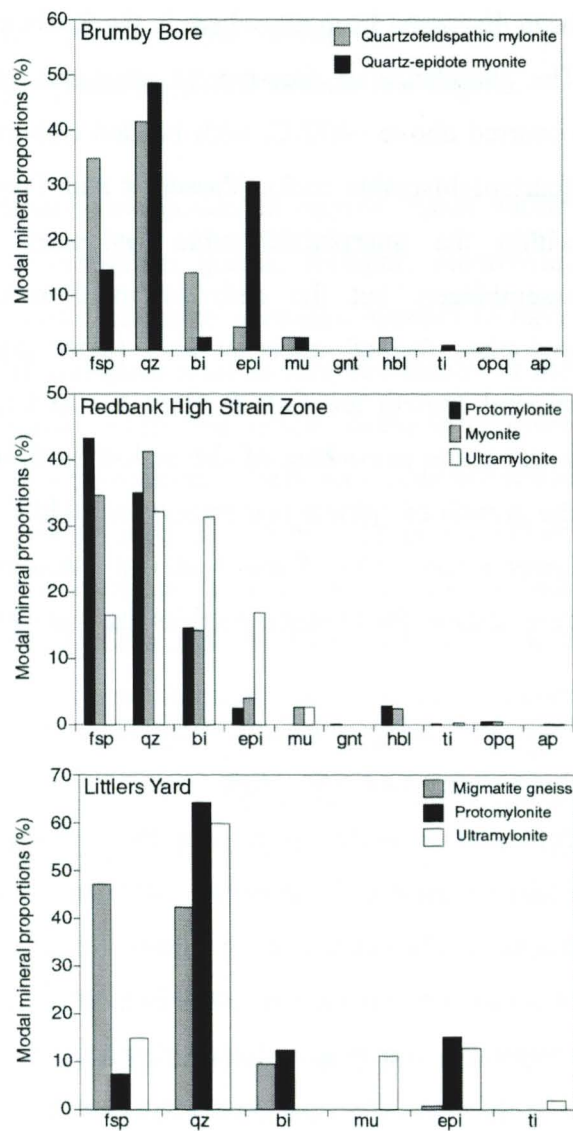


**Figure 6.10.** Comparison of average modal mineral proportions of rocks from the Redbank High Strain Zone and Southern Province.

substantially more epidote, more quartz and less feldspar and biotite than the quartzofeldspathic mylonites (Fig. 6.10). The abundant epidote implies substantial gains in CaO and FeO and the increase of quartz suggests a gain in SiO<sub>2</sub> within these mylonites. Therefore, the presence of quartz-epidote mylonites along the eastern Redbank High Strain Zone indicates extensive and focused metasomatism of the footwall gneisses during high-temperature shearing. The reworked textures within the mylonites, comprising muscovite and biotite growth with recrystallisation of the epidote and quartz are consistent with the retrogression and reworking within the higher-temperature quartzofeldspathic mylonites.

#### *6.4.5.2 Mafic mylonites*

The mafic composition of the mylonites at Mount Forster suggests they are likely sheared Central Province rocks in the hangingwall of the Redbank High Strain Zone. Garnet-plagioclase-hornblende porphyroclasts within the mafic mylonites indicate decompression textures that may have formed during the initial movement along the Redbank Thrust. Further composition analyses of these minerals are needed to constrain the conditions of their formation. However, brittle deformation and rotation of the plagioclase, hornblende and garnet grains within the mylonites, and abundant undulose quartz ribbons, suggests low temperatures of mylonitization. This is consistent with the brittle-ductile deformation in the quartzofeldspathic mylonites to the south. The preservation of garnet and the low proportion of biotite growth within the mylonites suggest that little fluid-rock interaction occurred during deformation.

#### *6.4.5.3 Littlers Yard shear zones*

The mylonite zones hosted by Ellery Granite Complex migmatite gneisses at Littlers Yard show significant grainsize reduction and a progressive increase in shearing intensity that produced protomylonite to ultramylonite rocks. The major mineralogical changes between the protolith migmatite gneiss and the sheared rocks include the dramatic decrease in feldspar abundance (both K-feldspar and plagioclase) and the increase in quartz, muscovite, epidote, and titanite contents (Fig. 6.10). The protomylonite show a decrease in feldspar (primarily K-feldspar) that is coupled with an increase in muscovite and quartz, whereas the mylonite and ultramylonite gained significant epidote and titanite at the expense of biotite. The large mineralogical changes that occurred across the shear zone and the formation of veins indicate that substantial fluid infiltration occurred during shearing.

The sheared rocks at Littlers Yard contain abundant pressure shadows and fibrous rims. Within the mylonite at Littlers Yard the growth of mica along feldspar grain boundaries parallel to the shear fabric are also indicative of pressure solution mechanisms. This suggests low temperature and high-strain conditions (Passchier and Trouw, 1996) and indicates that shearing involved pressure solution, requiring fluid flow through the shear zone.

The banded ultramylonite-mylonite rocks contain quartz layers of recrystallised sub-grains that indicate dynamic recrystallisation. Abundant fractured feldspar indicates shearing occurred at conditions near the brittle-ductile transition. Fluid infiltration along fractures stimulating hydration reactions, coupled with increases in strain, may have led to the formation of the ultramylonite bands.

The altered mineral assemblage of quartz, muscovite, epidote-clinzoisite, titanite and locally chlorite suggest greenschist-facies conditions during shearing (Yardley, 1989). There is a direct relationship between titanite abundance and shearing intensity, reflecting dissolution of the more mobile minerals such as quartz. The recrystallisation of biotite and muscovite within the mylonites and ultramylonites suggests the infiltration of water-rich fluids. The mineral assemblage, grain size and brittle-ductile deformation structures indicate that shearing occurred near the brittle-ductile transition under greenschist-facies conditions.

Overall, there is plenty of evidence of mass transport in shear zones of the southern Arunta Inlier. The fluid flow appears to be governed by strain variations and caused heterogeneous fluid rock interaction.

## **6.5 STABLE ISOTOPE GEOCHEMISTRY**

Oxygen and hydrogen isotope ratios of the shear zone samples along the Redbank High Strain Zone are presented in Table 6.2. The range of whole rock  $\delta^{18}\text{O}$  values within the Redbank High Strain Zone is 3.4 to 11.4‰ (Fig. 6.11). The migmatite, augen gneisses and quartzite samples range from 8.0 to 11.4‰. These rocks preserve the highest  $\delta^{18}\text{O}$  values within the Redbank High Strain Zone and, as they are predominantly unaffected by shearing, are assumed to reflect the pre-shearing protolith  $\delta^{18}\text{O}$  values. The quartzofeldspathic gneisses have  $\delta^{18}\text{O}$  values of 8.1‰ to 11.0‰, consistent with granitic

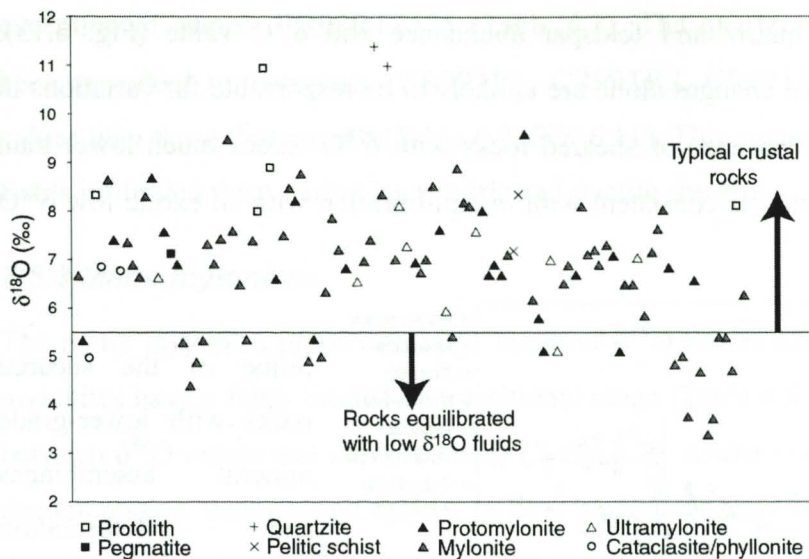


**Figure 6.11.**  $\delta^{18}\text{O}$  whole rock values (‰) for rocks of the Redbank High Strain Zone showing the typical variation in values between 9 and 6‰. Several samples show a lowering of  $\delta^{18}\text{O}$  values that indicate partial re-equilibration with a low  $\delta^{18}\text{O}$  fluid.

rocks (Sheppard, 1986) and sedimentary gneisses that have experienced contact metamorphism and fluid flow associated with the intrusion of granitic rocks. Contact metamorphism was widespread during the Teapot Tectonothermal Event and may have caused this shift in

$\delta^{18}\text{O}$  values. A greater number of analyses of unshered samples from the wall rocks of the Redbank High Strain Zone are required to verify this interpretation.

### 6.5.1 Quartzofeldspathic mylonite zones

The quartzofeldspathic mylonite zones have a range of  $\delta^{18}\text{O}$  values from 4.9 to 9.6‰. Although some mylonites have similar  $\delta^{18}\text{O}$  values to their granitic protoliths, the sheared rocks generally have lower values than their wall rocks (Fig. 6.12). As the protolith lithologies have consistently higher  $\delta^{18}\text{O}$  values, the isotope resetting of the mylonites probably resulted from fluid infiltration during shearing. There is little correlation between the intensity of shearing and  $\delta^{18}\text{O}$  values (Fig. 6.12), suggesting that the sheared rocks in general interacted with sufficient fluid to reset their oxygen isotope values, but that volumes of fluid in all shear zones were locally variable.

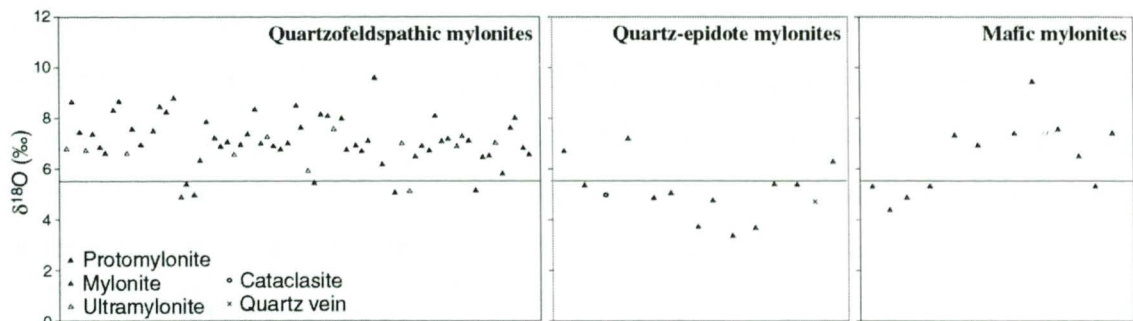


**Figure 6.12.**  $\delta^{18}\text{O}$  value plots for quartzofeldspathic, quartz-epidote and mafic mylonites of the Redbank High Strain Zone. The line at 5.4‰ denotes the lowest primary crustal rock signatures (Sheppard, 1986).

$\delta^{18}\text{O}$  values increase with increasing  $\text{SiO}_2$  content, due to the observed tendency of  $^{18}\text{O}$  to concentrate in quartz (Faure, 1986). However, in the quartzofeldspathic mylonites there is

little correlation between quartz and feldspar abundance and  $\delta^{18}\text{O}$  value (Fig. 6.13), indicating that compositional changes alone are unlikely to be responsible for variations in  $\delta^{18}\text{O}$  values. Rather, the occurrence of sheared rocks with  $\delta^{18}\text{O}$  values much lower than expected for their composition is consistent with re-equilibration with an exotic low  $\delta^{18}\text{O}$  fluid during shearing.

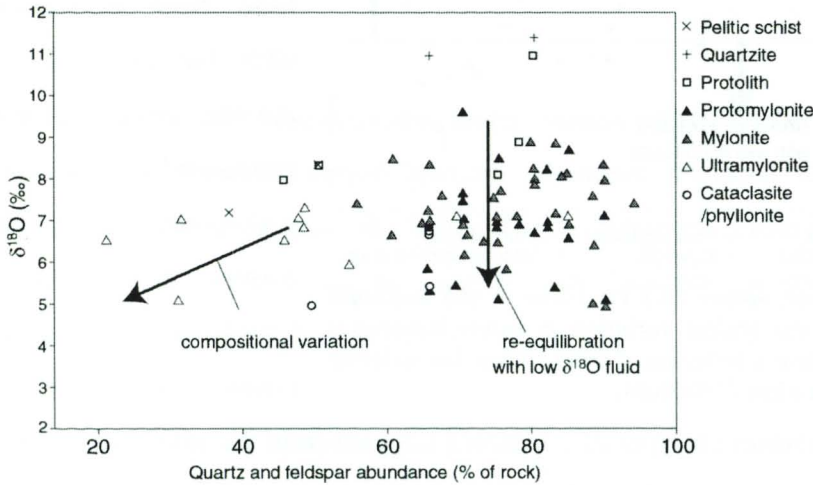


**Figure 6.13.**  $\delta^{18}\text{O}$  value plotted against quartz and feldspar abundance for rocks from the Redbank High Strain Zone, showing some compositional variation, but substantial lowering of  $\delta^{18}\text{O}$  in rocks with proportional quartz and feldspar, probably due to re-equilibration with a low  $^{18}\text{O}$  fluid.

Some of the sheared rocks with lower-grade mineral assemblages and deformation microstructures have higher  $\delta^{18}\text{O}$  value compared to the higher-grade mylonites. This suggests that the volume of fluids decreased as shearing proceeded with

the available local fluids having equilibrated with the local rocks.

Two narrow quartzite layers, CR98HD540 in the Ilyabba Dam shear zone transect and CR98HD544, 20 km to the east, are similar in composition and appearance. The two quartzites preserve  $\delta^{18}\text{O}$  values of 11.4‰ and 11.0‰ respectively. These two values are anomalously high within the Redbank High Strain Zone and probably reflect their sedimentary protolith signature.

### 6.5.2 Quartz-epidote mylonites

The quartz-epidote mylonites have low  $\delta^{18}\text{O}$  values, ranging from 3.4 to 7.6‰. The mylonites with greater epidote abundance have consistently lower  $\delta^{18}\text{O}$  values (Fig. 6.14), suggesting a systematic variation due to compositional changes. Quartz-epidote mylonites cut by mica shear

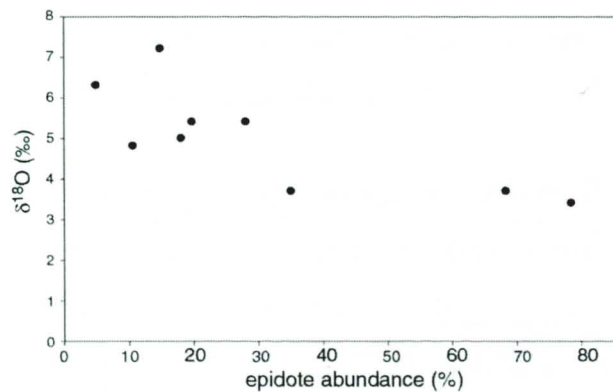


**Figure 6.14.**  $\delta^{18}\text{O}$  plotted against epidote abundance (%) within the quartz-epidote mylonites, showing a general decrease in  $\delta^{18}\text{O}$  value with increasing epidote content.

bands and epidote veins (CR98BB517, CR98BB518, CR98BB519, CR98BB521, and CR98BB328) have higher  $\delta^{18}\text{O}$  values than the other quartz-epidote mylonites with the

exception of sample CR98RTZ525 (Table 6.2). The quartz-epidote mylonites that have been reworked by cataclasis (CR99TR1, CR99TR2, CR99TR3) also have higher  $\delta^{18}\text{O}$  values than those that are not (Table 6.2, Fig. 6.11). This suggests that locally-equilibrated fluids infiltrated them during later brittle and ductile shearing.

### 6.5.3 Mafic mylonites

The mafic mylonites preserve a large range of  $\delta^{18}\text{O}$  values from 4.4 to 7.6‰. The mafic mylonites have a fairly limited compositional range (Table 6.5) and there is no correlation between  $\delta^{18}\text{O}$  values and shear intensity (Table 6.2). As the mylonites preserve high-grade decompression textures and appear to have undergone very minor fluid-rock interaction during shearing, the  $\delta^{18}\text{O}$  values may reflect inherited heterogeneous fluid-rock interaction signatures from the protolith granulite. Unexpectedly low  $\delta^{18}\text{O}$  values are recorded from high-grade mafic gneisses elsewhere in the Arunta Inlier (Miller *et al.*, 1997). In the Reynolds Range and Mallee Bore region the low  $\delta^{18}\text{O}$  values of granulites are attributed to the preservation of early hydrothermal alteration by meteoric fluids as the result of little fluid-rock interaction during high-grade metamorphism. This is consistent with the low  $\delta^{18}\text{O}$  values from the mafic mylonites. Examples of fluid infiltration into igneous provinces where circulation cells of heated meteoric fluids are active during plutonism and igneous activity include the Scottish Hebrides and the San Juan Mountains, where  $^{18}\text{O}$  depletion of up to 13‰ occurs within Tertiary volcanics (Taylor, 1974).

### 6.5.4 Hydrogen isotopes

Epidote from quartz-epidote mylonites has  $\delta\text{D}$  values of -66.1 to -75.8‰. Biotite from weakly to strongly sheared mylonites CR98SJ407 and CR98SJ411, and biotite, muscovite and epidote mixture from CR98SJ403 has  $\delta\text{D}$  values of -111.4‰ -93.3‰ and -79.1‰, respectively (Table 6.2). Shearing is estimated to have occurred at amphibolite-facies conditions for all of these samples except CR98SJ403. Using the biotite-water fractionation factors from Suzuoki and Epstein (1976) for temperatures of 500°C  $\delta\text{D}_{\text{fluid}}$  values are estimated as -73‰ and -54‰ for samples CR98SJ407, CR98SJ411. Epidote to water fractionation factors from Chacko *et al.* (1999) indicates  $\delta\text{D}_{\text{fluid}}$  values of -19.8 to -29.5‰. Combined biotite, muscovite and epidote to water fractionation factors at 350°C from Suzuoki and Epstein (1976) and Chacko *et al.* (1996, 1999) provide a  $\delta\text{D}_{\text{fluid}}$  value for CR98SJ403 of -35.4‰. These data are within the overlapping fields of formation and metamorphic waters. Equivalent  $\delta^{18}\text{O}_{\text{fluid}}$  values calculated for these samples and plotted on Figure 6.15 show that the rocks preserve fluid values that are at the edge of the

metamorphic fluid field and may indicate original meteoric fluids that became partially re-equilibrated with the metamorphic rocks they infiltrated. Similar fluid compositions occur in the shear zones of the Anmatjira and Reynolds Ranges (Chapter Four).

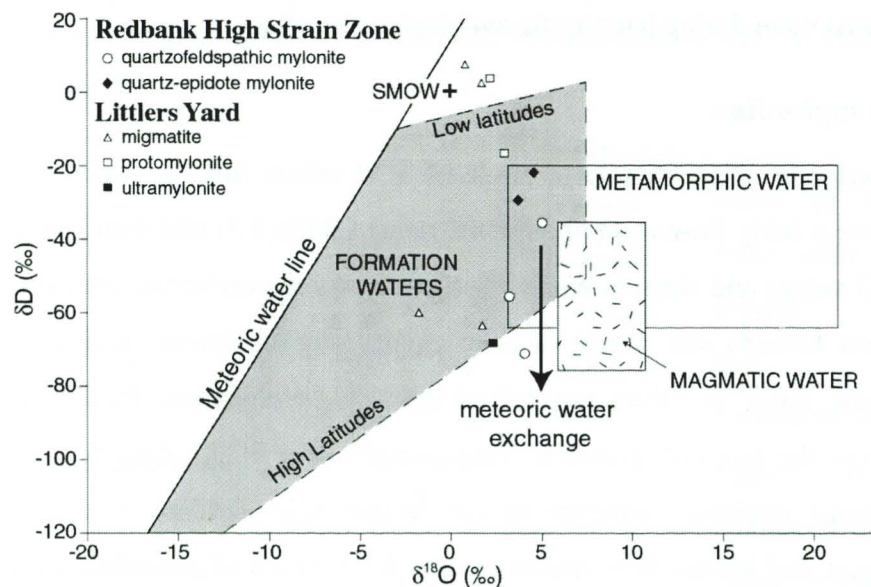


Figure 6.15.  $\delta D_{\text{fluid}}$  and  $\delta^{18}O_{\text{fluid}}$  values for the shear zone rocks of the Redbank High Strain Zone and Littlers Yard, and migmatite gneiss from Littlers Yard. Formation water, metamorphic water and magmatic water fields after Rollinson, (1993) from data of Taylor, (1974) and Sheppard, (1986). The rocks predominantly occur within the formation waters field with an overlap with metamorphic waters, suggesting some mixing, or local fluid equilibration during fluid-rock interaction. The migmatites indicate two distinct hydrogen signatures, both indicative of surface-derived fluids. The lowering of the hydrogen values in the Redbank High Strain Zone samples may indicate exchange with meteoric fluids, similar to data presented by Satir and Taubald (2001) from the Merendes Massif, Turkey.

### 6.5.5 Littlers Yard shear zones

The migmatite gneiss and orthogneiss wall rocks at Littlers Yard preserve  $\delta^{18}O$  values of 0.6 to 6.4‰ (Table 6.3), significantly lower than expected granitic  $\delta^{18}O$  values of 8 to 10.5‰ (Sheppard, 1986). The low  $\delta^{18}O$  migmatites at Littlers Yard, as with the mafic mylonites, may be explained by early hydrothermal alteration by meteoric fluids and subsequent low fluid-rock interaction during upper amphibolite-facies metamorphism. However, a detailed investigation of the high-grade gneisses is required to substantiate this interpretation.

The shear zone rocks at Littlers Yard have  $\delta^{18}O$  values of 4.4 to 10.0‰ (Table 6.3, Fig. 6.16). These  $\delta^{18}O$  values are consistently higher than those of the host gneisses, implying isotopic resetting probably occurred as a result of fluid infiltration during shearing. A quartz vein records a  $\delta^{18}O$  value of 10.6‰ and is thus likely to have formed from the same

fluid. In this case the fluid flow increased  $\delta^{18}\text{O}$  values within the shear zones suggesting that the fluids were derived from, or had equilibrated with, crustal rocks.

Quartz and biotite  $\delta^{18}\text{O}$  values of a protomylonite (CR98SP615) at Littlers Yard (Table 6.8) record oxygen isotopic resetting at  $\sim 580^\circ\text{C}$ , possibly representing metamorphic temperatures of their gneissic protolith. Quartz and muscovite  $\delta^{18}\text{O}$  values of an ultramylonite (CR98SP619) and a sheared pegmatite (CR98SP623) at Littlers Yard show retrogressive muscovite growth within the shear zones occurred during shearing at  $305$  to  $330^\circ\text{C}$ , consistent with the brittle-ductile deformation observed.

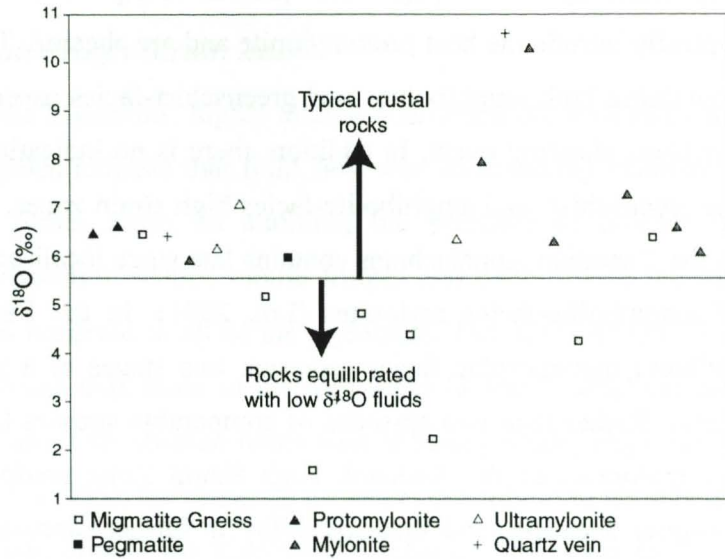


**Figure 6.16.**  $\delta^{18}\text{O}$  whole rock values (‰) for rocks from the Southern Province showing lower  $\delta^{18}\text{O}$  values of the protolith migmatite gneiss and higher  $\delta^{18}\text{O}$  of the sheared rocks.

**Table 6.8.** Quartz, biotite and muscovite  $\delta^{18}\text{O}$  values from sheared rocks at Littlers Yard, Southern Province. Calculated crystallisation temperatures based on qz-bi and qz-mu fractionation factors of Chacko *et al.*, 1996.

Sample	Rock Type	$\delta^{18}\text{O}_{\text{qtz}}$	$\delta^{18}\text{O}_{\text{omu}}$	$\delta^{18}\text{O}_{\text{obi}}$	$\Delta\text{qz-min}$	T °C
CR98SP615	protomylonite	8.7		4.2	4.5	578
CR98SP619	ultramylonite	8.4	4.5		3.9	330
CR98SP623	pegmatite	7.5	3.3		4.2	305

The  $\delta\text{D}$  values from the Littlers Yard shear zones preserve two distinct compositions. Muscovite from the sheared pegmatite CR98SP623, biotite from the migmatite gneiss CR98SP626, and muscovite-biotite mixtures from the protomylonites CR98SP614 and CR98SP615 in shear zone 1 (Table 6.3) have  $\delta\text{D}$  values of  $-43.2$  to  $-62.7\text{‰}$ . Biotite from the migmatite gneiss samples CR98SP622 and CR98SP624 and muscovite and epidote from ultramylonite CR98SP619 have combined  $\delta\text{D}$  values of  $-120.9\text{‰}$ ,  $-117.6\text{‰}$  and  $-106.7\text{‰}$ , respectively. There is no apparent correlation between the oxygen and hydrogen isotope compositions of these rocks. As lower volumes of water-rich fluids are required to reset hydrogen isotopes (Bickle and MacKenzie, 1987) the  $\delta\text{D}$  values may indicate fluid infiltration from multiple sources during shearing.

The  $\delta\text{D}$  values from the Littlers Yard shear zones preserve two distinct compositions. Muscovite from the sheared pegmatite CR98SP623, biotite from the migmatite gneiss CR98SP626, and

## 6.6 DISCUSSION

The mafic dykes and pegmatites present along the eastern Redbank High Strain Zone typically intrude the host protomylonite and are sheared. This suggests that the shear zones containing both amphibolite- and greenschist-facies assemblages were reactivated during the latest shearing event. In addition, there is no indication of different kinematics within the greenschist- and amphibolite-facies high strain zones. A similar large-scale shear zone in the Canadian Appalachians contains late stage localised greenschist-facies retrogression of amphibolite-facies mylonites (Lin, 2001). In the Eastern Highlands shear zone the different metamorphic facies represent two stages of a single deformation episode (Lin, 1995). Rather than two episodes of comparable stresses (Shaw and Black, 1991), perhaps the mylonites of the Redbank High Strain Zone predominantly contain Alice Springs Orogeny shearing, and this possibility is further discussed using  $^{40}\text{Ar}/^{39}\text{Ar}$  *in situ* laser probe dating in Chapter Seven.

The westernmost shear zones from this study contain predominantly amphibolite-facies mylonites and grade decreases to the east. This suggests that the Redbank High Strain Zone shallows to the east, consistent with the presence of cataclasite at Mount Forster and in the Charles River Fault Zone (Obee and White, 1985). As shear zones tend to widen with depth this interpretation is consistent with the Redbank High Strain Zone widening toward the west.

As discussed by Shaw and Black (1991), the early shear zones in the Redbank High Strain Zone are amphibolite-facies grade and are cut by pegmatites of 1150 Ma age. However, their distinction from the younger shear zones, active during the Alice Springs Orogeny, is not clear. There are proportionately more amphibolite-facies or upper greenschist-facies shear zones and protomylonites making up the Redbank High Strain Zone than the relatively narrow, extensively hydrated high-strain mylonite zones. However, the low- to high-strain mylonites in the eastern Redbank High Strain Zone represent predominantly reactivated older structures, with extensive shearing of pegmatites and mafic dykes. The stable isotope data indicates that pervasive lowering of  $\delta^{18}\text{O}$  values occurred during shearing throughout the Redbank High Strain Zone and suggest that they all equilibrated with a surface-derived fluid. The reworked textures, prolific throughout the mylonites, may be the result of continued deformation during one period of shearing, rather than reactivation during different events. Without substantial geochronological data the relative

extent of shearing during the Anmatjira Uplift Event and the Alice Springs Orogeny remains unclear.

### **6.6.1 Fluid flow in the Redbank High Strain Zone**

The presence of low strain granitic mylonites, highly altered quartz-epidote mylonites and highly strained biotite-rich mylonites indicate that fluid flow was substantially channelled throughout the Redbank High Strain Zone. In addition, the presence of biotite and muscovite shear bands, pressure solution seams, biotite fringes and overgrowths indicate that fluid-mass transfer processes occurred in all of the mylonites. The lower  $\delta^{18}\text{O}$  (3.4 to 9.6‰) values of the shear zone rocks than those of the wall rocks (8.0 to 11.0‰) indicate that the oxygen isotope ratios of all of the sheared rocks were at least partially reset during shearing. As pointed out by Giletti (1985), the presence of water, in addition to stimulating deformation in quartz and feldspar, speeds the kinetics of exchange of oxygen isotopes. Diffusion occurs between minerals in a hydrous system at two to three orders of magnitude higher than in anhydrous systems (Jenkin *et al.*, 1994). Therefore, oxygen isotope diffusion at grain boundaries is increased by the presence of an aqueous fluid (Jenkin *et al.*, 1994). Thus, the lower  $\delta^{18}\text{O}$  values within the sheared rocks of the Redbank High Strain Zone suggest that a low  $^{18}\text{O}$  fluid infiltrated during shearing. The variation in  $\delta^{18}\text{O}$  values suggests that variable oxygen isotope equilibration of the infiltrating fluid occurred due to interaction with the rocks in and around the shear zones during sustained fluid-rock interaction. The higher  $\delta^{18}\text{O}$  values in the reworked mylonites are consistent with fluid volumes diminishing over time resulting in a loss of distinctive  $\delta^{18}\text{O}$  values. The presence of lowered  $\delta^{18}\text{O}$  values within the higher-grade shear zones indicates low  $\delta^{18}\text{O}$  fluids infiltrated the shear zone during shearing. The possible increase of  $\delta^{18}\text{O}$  values within the lower grade mylonites may be explained by partial re-equilibration with the host rocks during continued fluid recycling and deformation.

As discussed in Chapter Four, O and H isotope geochemistry of the shear zones of the Northern Arunta Inlier also indicate surface-derived fluid infiltration during shearing. There is a lack of other potential fluid reservoirs for the brittle-ductile and ductile shear zones in central Australia as the rocks hosting them are predominantly high-grade gneisses and occur within a continental interior. It may be that surface reservoirs are important in the hydration of shear zones within continental interiors and where there are limited other fluid sources, such as the dehydrating middle crust, down-going slabs in subduction zones or synorogenic igneous rocks. The significance of surface-derived fluids hydrating the

middle crust and the process of fluid flow throughout the shear zones is discussed further in Chapter Eight.

## **6.7 CONCLUSIONS**

Some of the shear zones in the Arunta Inlier, including the Redbank High Strain Zone are crustal-scale and steeply dipping, with offsets that indicate reworking during the Alice Springs Orogeny entailed extensive vertical movement. There are similarities of heterogenous strain and fluid-rock interaction within all of the shear zones throughout the Arunta Inlier associated with the Alice Springs Orogeny, suggesting that this event caused significant metasomatism as a result of substantial fluid flow. Particularly within the Redbank High Strain Zone, deformation at very high strain is predicted during the Alice Springs Orogeny. A model of fluid flow throughout the Arunta Inlier during the Alice Springs Orogeny is present in Chapter Eight.

## CHAPTER SEVEN

### EXCESS ARGON IN REACTIVATED MYLONITES OF THE REDBANK HIGH STRAIN ZONE: IMPLICATIONS FOR FLUID FLOW DURING SHEARING

#### **Abstract**

The Redbank High Strain Zone is a crustal-scale thrust in central Australia. It is 9 to 20 km wide and 400 km long and is characterised by multiple sub-parallel high-strain mylonite zones. Previous Rb-Sr, K-Ar and  $^{40}\text{Ar}/^{39}\text{Ar}$  data have not resolved the relative importance of movement during the Proterozoic Anmatjira Uplift Event and the Devonian Alice Springs Orogeny. Step-heating  $^{40}\text{Ar}/^{39}\text{Ar}$  analyses of multiple biotite grains, and *in situ* laser probe  $^{40}\text{Ar}/^{39}\text{Ar}$  analyses of biotite and amphibole grains yield a variety of apparent ages. Hornblende apparent ages of 561 to 1508 Ma indicate partial argon loss during the Alice Springs Orogeny and suggest that this event occurred at temperatures above 500°C (higher than previously thought). Biotite apparent ages of 487 to 1570 Ma are interpreted as being due to heterogenous uptake of excess argon during fluid flow in the Alice Springs Orogeny. The heterogeneity of apparent ages reflects heterogenous strain partitioning, recrystallisation and fluid flow at the millimetre scale within the mylonites. Older  $^{40}\text{Ar}/^{39}\text{Ar}$  ages from the biotite porphyroclasts, biotite matrix grains and K-feldspar porphyroclasts reported by Shaw *et al.* (1992) are likewise interpreted to be the result of excess argon contamination. These data illustrate the difficulty in obtaining geologically meaningful ages within mylonite zones.

#### **7.1 INTRODUCTION**

Shear zones represent sites of intense deformation and fluid-rock interaction, and are common in most mid-crustal metamorphic terrains (Holdsworth *et al.*, 1997, and references therein). Interpreting the regional tectonic evolution of metamorphic provinces requires an understanding of the kinematics, deformation mechanisms, metamorphic reactions, and the timing of deformation within shear zones. Tectonic evaluation of metamorphic terrains can thus be substantially aided by direct dating of shear zones. The use of  $^{40}\text{Ar}/^{39}\text{Ar}$  dating for mid-crustal shearing events is possible because micas are commonly formed during shearing. However, interpretation of argon isotope ratios of sheared mineral populations can be difficult due to the heterogenous nature of mylonites (Dunlap *et al.*, 1991; West and Lux, 1993; Dunlap, 1997). The interpretation of  $^{40}\text{Ar}/^{39}\text{Ar}$  data depends on the timing of mineral growth within the thermal evolution of the shear zone in relation to the relevant blocking temperature of the mineral for argon diffusion

(Dunlap, 1997). Step-heating analysis on mineral populations from sheared rocks may yield ambiguous results (Wets and Lux, 1993). For example, greenschist-facies deformation and metamorphism in mid-crustal shear zones commonly produces mylonites that contain both new and relict minerals, and will thus produce geologically-meaningless mixed ages (West and Lux, 1993). Heterogeneous deformation and chemical re-equilibration on a grain-scale within partially-recrystallised rocks can also cause disturbances within  $^{40}\text{Ar}/^{39}\text{Ar}$  isotopic systems with inter- and intra-grain isotope exchange (Wright *et al.*, 1991; Wartho, 1995; Villa *et al.*, 2000; Reddy *et al.*, 2001).

Excess argon incorporated in K-bearing minerals also produces older geologically-meaningless apparent ages. Excess argon is typically introduced by metamorphic fluids, and is therefore a problem when dating open-system, fluid-dominated shear zones (Arnaud and Kelley, 1995). “Saddle” shaped age spectra are typical of excess argon (Foster *et al.*, 1990; Ruffet *et al.*, 1995), and have been documented from mica in high-pressure metamorphic terrains (Arnaud and Kelley, 1995; Ruffet *et al.*, 1995, 1997; Reddy *et al.*, 1996; Scaillet, 1996; de Jong *et al.*, 2001). For example, in the European Alps  $^{40}\text{Ar}/^{39}\text{Ar}$  data initially suggested two thermal events, a high-pressure event at ~110 Ma and a younger greenschist-facies overprint at ~30 to 45 Ma (Arnaud and Kelley, 1995; Scaillet, 1996). Later Rb-Sr, U-Pb and Sm-Nd data indicated that high-pressure metamorphism occurred just prior to the greenschist-facies overprint at around 45 Ma (Arnaud and Kelley, 1995; Ruffet *et al.*, 1997 and references therein), implying a significantly different tectonic evolution of the Alps. The incorporation of excess argon into white micas during fluid-rock interaction is likely to have produced  $^{40}\text{Ar}/^{39}\text{Ar}$  apparent ages that were too old (Arnaud and Kelley, 1995; Scaillet, 1996; Ruffet *et al.*, 1997).

The Alps example indicates the complexity of argon isotope systematics within individual mineral grains and the resulting difficulties of traditional step-heating analyses that assume homogeneous mineral populations. Individual step-heating analysis of grains can provide better resolution on the thermal evolution of mineral assemblages (Ruffet *et al.*, 1995; Phillips *et al.*, 1998; Villa *et al.*, 2000; de Jong *et al.*, 2001). Chemical mapping of individual amphibole grains may also resolve compositional heterogeneity within grains (Wartho, 1995; Villa *et al.*, 2000) that might indicate multiple phases of growth or partial recrystallisation. Laser probe analysis of *in situ* grains reduces the resolution difficulties by allowing the direct analysis of different mineral generations in addition to intra-grain analysis. Therefore, analysis by *in situ* laser probe can separate minerals into different textural settings to establish multiple generation mineral growth and constrain partial

exchange along grain boundaries or within grain heterogeneities, allowing for a finer-scale resolution to be achieved within individual grains and poly-metamorphic mylonites (Phillips, 1991; Hodges and Bowring, 1995; Ruffet *et al.*, 1995; Reddy *et al.*, 2001). As biotite is a common mineral in mylonites and thus is often used in geochronological studies, laser probe analysis also has the advantage of reducing the problems of homogenisation during *in vacuo* heating, as often occurs with the step-heating technique (Phillips, 1991; Hodges and Bowring, 1995).

In central Australia, the Redbank High Strain Zone is an important structural feature, representing a long-lived crustal-scale thrust zone (Fig. 7.1). Previous research has ascribed two different metamorphic assemblages to two different shearing events within the Redbank High Strain Zone (Table 7.1; Shaw and Black, 1991; Black and Shaw, 1992, Shaw *et al.*, 1992). The older, known as Type 1 mylonites, were dated using Rb-Sr and  $^{40}\text{Ar}/^{39}\text{Ar}$  techniques at 1560 to 1370 Ma and assigned to the Anmatjira Uplift Event (Shaw and Black, 1991; Black and Shaw, 1992; Shaw *et al.*, 1992). The younger, Type 2 mylonites, deform pegmatites, migmatites and mafic dykes of 1200 to 1150 Ma and 1000 to 900 Ma age respectively (Table 7.1; Black *et al.*, 1980; Shaw and Black, 1991; Zhao and McCulloch, 1993). Type 2 mylonites have been dated by Rb-Sr whole rock isochrons at  $415 \pm 50$  Ma and biotite isochrons at  $348 \pm 3$  Ma, and are part of the Alice Springs Orogeny (Shaw and Black, 1991).

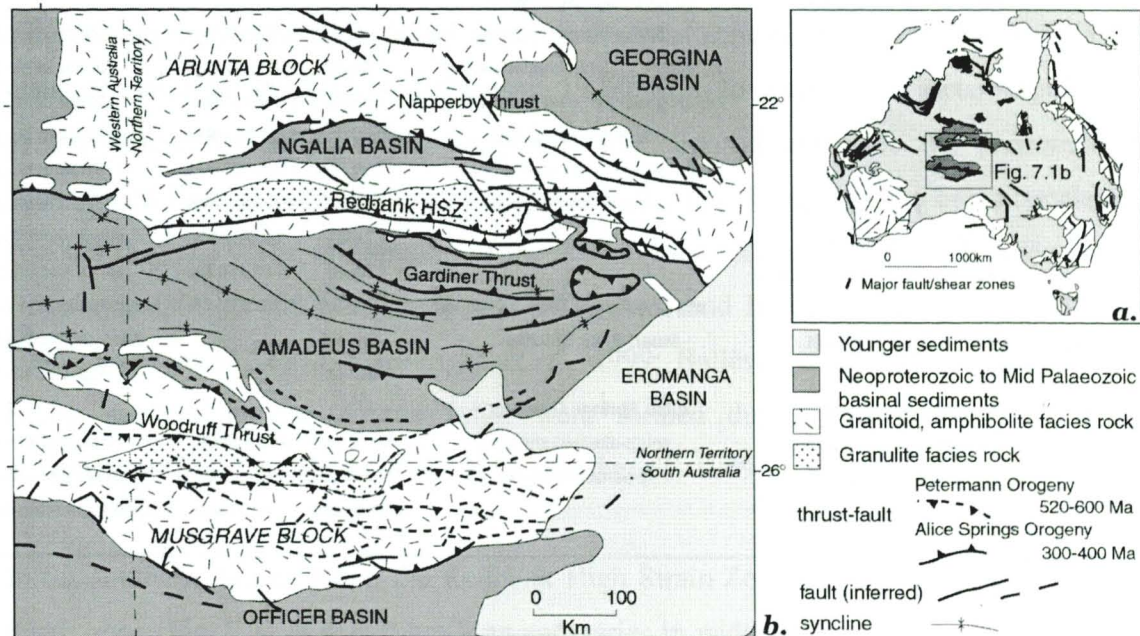


Figure 7.1. a) Australian Orogenic Provinces, after Shaw *et al.* (1991) showing location of Figure 1b. b) Geology of central Australia including location of major thrust and fault zones corresponding to the Petermann (dashed lines) and Alice Springs (full lines) Orogenies, after Sandiford and Hand (1998b).

**Table 7.1. Tectonothermal History of the southern Arunta Inlier including associated geochronological data with references.**

Age (Ma)	Central Province	Southern Province	Method	Date	Reference
c. 1880	Yuendumu Tectonic Event		U-Pb		Young et al. (1995)
1780 -1730	<b>Strangways Event</b>				
	Megacrystic diorite		U-Pb	1788±5 Ma	Black and Shaw (1992)
	Redbank Hill microgranite		U-Pb	1760±11 Ma	Black and Shaw (1992)
	Central Prov. metadolerite		U-Pb	1763±2 Ma	Black and Shaw (1992)
	Redbank Hill megacrystic gneiss		U-Pb	1754±9 Ma	Black and Shaw (1992)
	Mount Hay Granulite		Rb-Sr	1768±20 Ma	Black et al. (1983)
	Mount Hay Granulite		SHRIMP	~1770 ma	Collins (2000)
1670 - 1660		<b>Argilke Tectonic event</b> <b>(Warren and Shaw, 1995)</b>			
		Glen Helen banded gneiss	U-Pb	1663±13 Ma	Black and Shaw (1992)
		felsic gneisses	U-Pb	1678±6 Ma	Black and Shaw (1992)
		genissic xenolith zr core in OPG	U-Pb	1678 ±14 Ma	Collins et al. (1995)
1610 - 1600		<b>Chewings Orogeny</b> <b>(Collins and Shaw, 1995)</b>			
	Mount Chapple Granulite		U-Pb	~1660 Ma	Collins (2000)
		Ormiston Pound Granite	U-Pb	1603±10 Ma	Collins et al. (1995)
		meta-rims of zr in OPG xenolith		1575 ±20 Ma	Collins et al. (1995)
		Rungtjirba Gneiss	U-Pb	1615 ±11 Ma	Zhao and Bennett (1995)
		Burts Bluff Gneiss	U-Pb	1603 ± 7 Ma	Zhao and Bennett (1995)
		Chewings Zone Potrock gneiss	Rb-Sr	1620 ±70 Ma	Marjoribanks and Black (1974)
1500-1400	<b>Anmatjira Uplift Phase</b>	<b>Anmatjira Uplift Phase?</b>			
	south-directed shearing				
	650°C and 6-7kbar		Rb-Sr	1560-1370 Ma	Shaw and Black (1991)
	hornblende retrogressed granulite		<sup>40</sup> Ar/ <sup>39</sup> Ar	1421 ±7	Shaw et al. (1992)
1200-1150	<b>Teapot magmatic event</b>	<b>Teapot magmatic event</b>			
		OPG meta-rim on zircon	U-Pb	1183 ±52Ma	Collins et al. (1995)
		pegmatite in OP (recrystallisation?)	Rb-Sr	1097-1029Ma	Collins et al. (1995)
		biotite gneiss OP (recrystallisation)	Rb-Sr	1120-1078Ma	Collins et al. (1995)
		hnb in amphibolites	<sup>40</sup> Ar/ <sup>39</sup> Ar	1210-1139Ma	Shaw et al. (1992)
		mu in (leucocratic) granite gneiss	<sup>40</sup> Ar/ <sup>39</sup> Ar	1125-1085Ma	Shaw et al. (1992)
		biotite in granite gneiss	K-Ar	1125 ± 10Ma	Shaw et al. (1992)
	Mount Zeil pegmatite		U-Pb	1137±9 Ma	Black and Shaw (1992)
	pegmatite west of Mount Zeil		Rb-Sr	1140 ±56 Ma	Shaw and Black (1991)
		mig-gneiss near Teapot Granite	Rb-Sr	1076 ± 50 Ma	Marjoribanks and Black (1974)
1080-900	<b>Dolerite Dyke Intrusion</b>	<b>Stuart Pass Dolerite</b>	Sm-Nd		Zhao and McCulloch (1993)
			Rb-Sr		Black et al. (1980)
400-300	<b>Alice Springs Orogeny</b>	<b>Alice Springs Orogeny</b>			
	south-directed shearing	south-directed shearing	Rb-Sr (wr)	415 ± 50Ma	Shaw and Black (1991)
	greenschist-facies	greenschist-facies	Rb-Sr (bi)	348 ± 3 Ma	Shaw and Black (1991)
			Rb-Sr (bi)	~400 Ma	Marjoribanks and Black (1974)

Because <sup>40</sup>Ar/<sup>39</sup>Ar and K-Ar data for biotite and K-feldspar preserved older apparent ages Shaw *et al.* (1992) suggested that the Alice Springs Orogeny did not produce temperatures greater than 350°C within the Redbank High Strain Zone. However, the work by Shaw and Black (1991) indicated upper-greenschist- to amphibolite-facies shearing (350 to 500°C at

>200 MPa) as the Rb-Sr system was reset during the Alice Springs Orogeny. If the mylonites of the Redbank High Strain Zone contain Alice Springs Orogeny Rb-Sr ages, then, as the closure of biotite and K-feldspar is lower in the  $^{40}\text{Ar}/^{39}\text{Ar}$  system than the Rb-Sr system, these minerals should be reset and record Alice Springs ages as well. Elsewhere in the Arunta Inlier, Alice Springs age shear zones contain amphibolite-facies assemblages, suggesting that, at least locally, temperatures were elevated during that event (Dunlap and Teyssier, 1995; Cartwright *et al.*, 1999; Ballèvre *et al.*, 2000; Chapter Five). In addition, lithospheric rheology modelling by Sandiford and Hand (1998b) suggests re-activation along the Redbank High Strain Zone may have been a response to thermal weakening of the lithosphere created by the thickness of the overlying sedimentary basin (Sandiford and Hand, 1998b; Hand and Sandiford, 1999; Sandiford *et al.*, 2001). This implies that the temperature of the crust during re-activation of the Redbank High Strain Zone was elevated. This investigation addresses the contrasting interpretations of the thermal history of the Redbank High Strain Zone using laser *in situ*  $^{40}\text{Ar}/^{39}\text{Ar}$  analyses of individual grains within the mylonites. This allows ages of the K-bearing minerals to be determined in different textural settings within the complex mylonites and provides some constraints on the thermal character of shearing by incorporating both amphibole and biotite analysis.

## 7.2 TECTONIC FRAMEWORK

Central Australia has been in an intra-continental setting since at least the late Proterozoic, when a massive supercrustal basin developed across central and southern Australia as a result of the break up of Rodinia (Lindsay, 1999). Mid- to deep-crustal metamorphic rocks of the Arunta Inlier (~200,000 km<sup>2</sup>) are now exposed alongside the predominantly undeformed Proterozoic sedimentary basins, due to uplift along regional crustal-scale fault systems (Fig. 7.1). The exhumation of the Arunta Inlier occurred during the Alice Springs Orogeny at 300 to 400 Ma (Lambeck, 1991; Shaw and Black, 1991; Collins and Shaw, 1995; Shaw *et al.*, 1995; Cartwright *et al.*, 1999; Ballèvre *et al.*, 2000). The structural basins surrounding the Arunta Inlier were formed during this period of basement exhumation (Fig. 7.1; Walter *et al.*, 1995; Read *et al.*, 1999).

In the southern Arunta Inlier, the Redbank High Strain Zone forms a major north-dipping thrust zone (Fig. 7.1). It is 400 km long and varies in width from a few hundred metres up to 20 km (Fig. 7.2). Deep seismic reflection profiles and teleseismic travel time data indicate that vertical uplift across the Redbank High Strain Zone was approximately 15 km (Goleby *et al.*, 1990; Lambeck, 1991; Korsch *et al.*, 1998) juxtaposing deep-crustal granulite rocks to the north against mid-crustal amphibolite-facies gneisses to the south.

The presence of shear zones that are cut by, and others that offset, 1200 to 1150 Ma granitic pegmatites and 1000 to 900 Ma dolerite dykes implies that the Redbank High Strain Zone is a long-lived structure (Shaw and Black, 1991; Shaw *et al.*, 1992; Collins and Shaw, 1995). However, changes in foliation and metamorphic grade are less convincing as indicators of reactivation during different tectonic events due to the similarity in kinematic indicators, foliation and lineation orientations, and deformation microstructures within both greenschist- and amphibolite-facies shear zones (Chapter Six). Petrography and isotope data presented in Chapter Six suggests that both the greenschist- and amphibolite-facies shearing assemblages may have formed during a single shearing event. In addition, the rotation of fabrics through increases in strain intensity may explain apparent crosscutting fabrics within the shear zones (Fleirvoet and White, 1995). Although the conditions of shearing during the Alice Springs Orogeny are ambiguous, structural interpretation of teleseismic travel-time anomalies and deep seismic reflection data suggest that extensive movement across the Redbank High Strain Zone occurred during the Alice Springs Orogeny (Lambeck, 1991; Shaw *et al.*, 1995). Thus, the relative importance and extent of Alice Springs verse Anmatjira Uplift age movement remains unresolved.

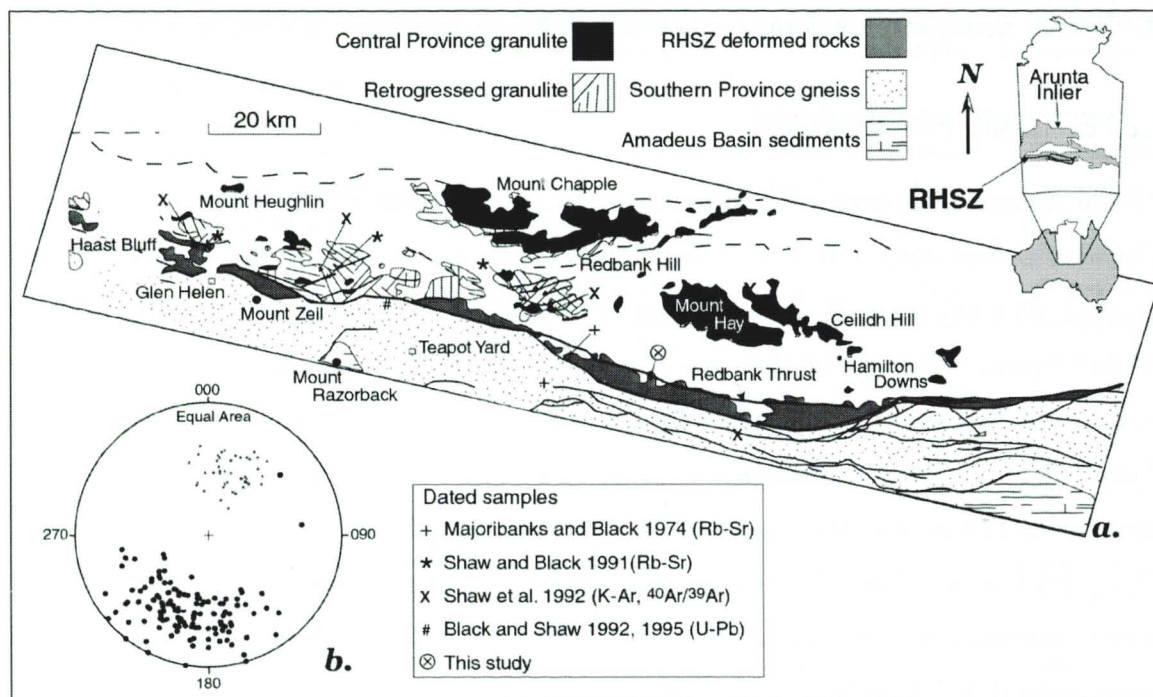


Figure 7.2. a) Geology of the southern Arunta Inlier, central Australia, after Shaw *et al.* (1992), with locations of dating samples as shown. b) Lower hemisphere equal area projection of poles to the planes of the mylonitic foliation within the Redbank High Strain Zone (full circles, n=139) and elongation lineations (stars, n=48), indicating an anastomosing NE-dipping WNW-ESE-oriented foliation with down-dip lineation.

### 7.3 GEOLOGY OF THE REDBANK HIGH STRAIN ZONE

The Redbank High Strain Zone comprises multiple sub-parallel shear zones that form the boundary between the Southern and Central Provinces in the Arunta Inlier (Fig. 7.2). The Southern Province comprises strongly-foliated variably-megacrystic amphibolite-facies augen gneisses and migmatites (Fig. 7.3a), while the Central Province, immediately adjacent to the Redbank High Strain Zone, comprises layered mafic granulites. The shear zones are consistently north dipping (40-60°) with down-dip stretching lineations (Figs. 7.2, 7.3b) defined predominantly by elongated grains and felsic aggregates. Asymmetric folds, rotated  $\delta$ -, and  $\alpha$ -type porphyroclasts and shear bands indicate reverse sense of shear (Fig. 7.3c). Some narrow ultramylonite zones within protomylonite-gneiss also indicate a component of sinistral strike-slip movement.

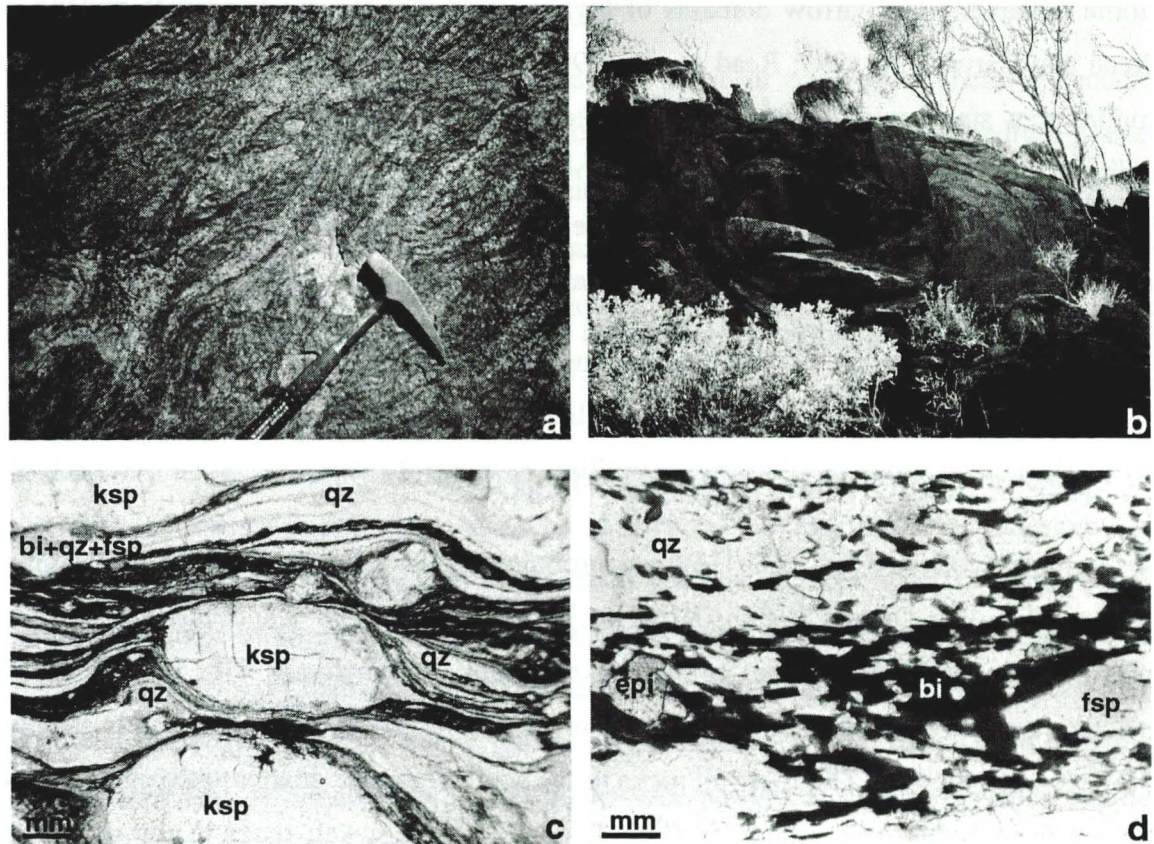


Figure 7.3. a) polydeformed migmatite gneiss in the footwall of the shear zone at Brumby Bore. b) North-dipping protomylonite at Brumby Bore with well developed down-dip lineation. c) K-feldspar porphyroclast wrapped in finely recrystallised quartz, feldspar and biotite showing sinistral sense of shear. d) Sample CR98BB342 from Brumby Bore, used for step-heating analysis, showing, a single generation of biotite growth in the fine-grained mylonite.

The shear zones within the Redbank High Strain Zone contain variable abundances of protomylonite, mylonite and ultramylonite rocks. The protomylonites have a coarse-grained (>100 $\mu$ m) matrix with variable sized augen (1mm to 2cm). They represent low-strain deformation and make up a significant portion of the Redbank High Strain Zone.

Mylonites are commonly medium-grained (50 to 100 $\mu\text{m}$ ) with planar foliation and represent higher-strain domains within the shear zones. Where they cut augen gneisses, they are variably augen-rich. Ultramylonite typically forms 1mm to 5m bands commonly within mylonite zones. These bands are predominantly dark and very fine-grained (<10 $\mu\text{m}$ ). Augen are typically rounded and reworked, and are suspended within the very fine-grained matrix. The characteristic mineral assemblages of protomylonites are K-feldspar, plagioclase, quartz, amphibole, biotite and garnet. The typical ultramylonite assemblage includes K-feldspar, quartz, plagioclase muscovite, biotite, clinozoisite and may or may not contain chlorite. Mylonite contains variations of both assemblages.

The presence of narrow linear zones of high-strain ultramylonite containing up to 80% biotite (Chapter Six), narrow domains of highly-metasomatised quartz-epidote mylonites (Read and Cartwright, 1999; Read *et al.*, 1999), and abundant late stage epidote veining, implies that strain partitioning and channelled fluid flow occurred during shearing. In addition, discrete mica and epidote shear bands, pressure solution seams, and fibrous fringes around porphyroclasts throughout the lower strain protomylonites and mylonites indicate fluid-assisted deformation and crystallisation (Passchier and Trouw, 1996). This shearing was accompanied by the infiltration of variable volumes of fluid throughout the Redbank High Strain Zone.

#### **7.4 SAMPLE SELECTION AND DESCRIPTION**

The samples collected for  $^{40}\text{Ar}/^{39}\text{Ar}$  geochronological investigations are from Brumby Bore on Hamilton Downs Station (KP9294, Table 7.2, Fig. 7.2). The exposed mylonites form a 480m wide shear zone, containing abundant protomylonite with thin bands of mylonite and ultramylonite. The shear zone is oriented approximately E-W and is steeply (38-62°) north dipping. The footwall rocks to the south comprise quartzofeldspathic gneiss derived from Proterozoic granitoids (Fig. 7.3a). The hangingwall rocks to the north are completely covered by colluvium, but are probably mafic granulites of the Central Province. Within the shear zone, the mylonites are dominantly quartzofeldspathic with local porphyroclasts of garnet. Asymmetric folding with top-to-the-south direction exposes granodioritic mylonites with abundant amphibole and minor pelitic schist intercalated with the quartzofeldspathic mylonites. Laser probe analysis of *in situ* and individual grains of biotite and hornblende were undertaken from six mylonite samples from Brumby Bore and step-heating of one biotite separate from mylonite sample CR98BB342. Analytical procedures are outlined in Chapter One. The samples chosen for analysis represent both

**Table 7.2. Location and description of samples from Brumby Bore. Rock classification, after Sibson (1977); protomylonites contain 0-50% matrix, mylonites contain 50-90% matrix. Metamorphic grade estimated from mineral assemblage and deformation microstructures.**

Sample	Location	Universal Grid Reference	Rock Type	Estimated Metamorphic Grade	Transect (m)
CR98BB235	Brumby Bore	KP9294	protomylonite	amphibolite-facies	13
CR98BB245	Brumby Bore	KP9294	mylonite	greenschist-facies	45
CR98BB246	Brumby Bore	KP9294	protomylonite	amphibolite-facies	50
CR98BB269	Brumby Bore	KP9294	mylonite	greenschist-facies	120
CR98BB342	Brumby Bore	KP9294	mylonite	amphibolite-greenschist	447
CR98BB546	Brumby Bore	KP9294	protomylonite	amphibolite-facies	0

quartzofeldspathic (quartz, K-feldspar, plagioclase, biotite  $\pm$  epidote) and amphibole-rich (amphibole, K-feldspar, plagioclase, quartz, biotite) compositions.

#### **7.4.1 CR98BB235 granitic protomylonite**

Sample CR98BB235 is from the southern edge of the shear zone where shearing becomes distinctive in the foliated granitic migmatitic wall rock. This sample is a medium-grained (55 to 75 $\mu$ m) granitic protomylonite containing quartz, K-feldspar, plagioclase and biotite, some epidote and ilmenite (Table 7.3). It has a whole rock  $\delta^{18}\text{O}$  value of 6.7‰ (Chapter Six). Anastomosing bands of fine-grained (20 to 25 $\mu$ m) quartz and biotite occur throughout the rock and define the protomylonitic fabric. K-feldspar and plagioclase porphyroclasts occur within a matrix of medium-grained quartz, and finer-grained quartz-feldspar-biotite layers. Quartz forms recrystallised equigranular domains elongated into the direction of shearing and finer sub-grained ribbons aligned with the anastomosing foliation. Both plagioclase and K-feldspar predominantly occur as augens of relict grains. Recrystallisation at their edges has produced core and mantle texture of fine-grained feldspar. Where recrystallisation is more advanced, fine-grained feldspar is interspersed with larger polycrystalline quartz. Relic K-feldspar porphyroclasts show perthitic intergrowths and deformation twinning. Plagioclase porphyroclasts are typically smaller, commonly with multiple twinning. Biotite occurs as both euhedral grains associated with feldspar porphyroclasts and as fine-grained matrix clusters, either aligned into microshear bands or inter-grown with quartz and quartz-feldspar matrix. Kinking of the larger biotite grains is common where they are in proximity to a shear band, and these grains are often rimmed with recrystallised fine-grained biotite, ilmenite and quartz. Minor amounts of new-growth epidote rim the larger biotite grains, while ilmenite is associated with the fine-grained biotite masses.

**Table 7.3. Petrographic summary of samples from Brumby Bore. Grainsize: vf=<10mm, f=10-50mm, m=50-100mm. Minerals in %. Abbreviations in Table 1.1.**

Sample	Rock Type	Foliation Intensity	Matrix Grainsize	fsp	qz	bl	epi	gnt	hbl	ap	accessory phases
CR98BB546	protomylonite	weak	m-f	45	35	15	0	0	5	0	zr, il, ap, ti
CR98BB235	protomylonite	moderate	f-m	50	35	15	0	0	0	0	ti, epi, ap, il
CR98BB245	mylonite	strong	f-vf	35	35	25	5	0	0	0	il, ap, epi, zr
CR98BB246	protomylonite	moderate	m-vf	40	25	10	0	0	25	0	ti, blue am, epi
CR98BB269	mylonite	strong	m	35	29	20	0	0	15	1	opq, ti, zr
CR98BB342	mylonite	strong	f-vf	20	55	15	10	<1	0	0	

#### **7.4.2. CR98BB245 mica-rich quartzofeldspathic mylonite**

Sample CR98BB245 is from 45m north of the southern edge of the shear zone where the shearing fabric is stronger, grainsize is reduced, and there is an increase in mica abundance. The sample is a mica-rich layered mylonite with large augen-shaped porphyroclasts and aggregates of feldspar in a fine-grained matrix of biotite, epidote, quartz and ilmenite, with a whole rock  $\delta^{18}\text{O}$  value of 6.2‰ (Chapter Six). The rock comprises quartz, K-feldspar, biotite, and epidote (Table 7.3) with titanite, ilmenite and zircon as accessory phases. It is compositionally banded, and contains crosscutting microshears. The mylonitic foliation is defined by quartz, biotite-quartz, and biotite bands that anastomose around aligned feldspar porphyroclasts. Fibrous biotite occurs in some pressure shadows. Quartz occurs as sub-grained domains of variable grainsize where the larger grains commonly have undulose extinction, with some serrated grain boundaries in areas of lower strain. K-feldspar porphyroclasts contain abundant deformation twinning and flame perthites, with rare microfaulting also present. The porphyroclasts range in size up to 5mm and are very well rounded with fine-grained recrystallised rims. Very fine-grained (~10 $\mu\text{m}$ ) masses of biotite occur in bands throughout the rock in association with fine-grained quartz, feldspar and ilmenite. The ilmenite occurs preferentially in stringers and clusters within some of the shear bands. Epidote forms equant grains throughout the rock and is entrained within the fine shear bands of quartz and biotite.

#### **7.4.3. CR98BB246 granitic protomylonite**

Sample CR98BB246 was collected 50m from the southern edge of the shear zone, just to the north of a narrow ultramylonite zone. It is a protomylonite, comprising the assemblage; hornblende, biotite, plagioclase, K-feldspar and quartz (Table 7.3). It has a whole rock  $\delta^{18}\text{O}$  value of 5.8‰ (Chapter Six). It is medium- to coarse-grained (100-300 $\mu\text{m}$ ) with a

gneissic–protomylonite texture. The sample contains hornblende, feldspar and biotite porphyroclasts within a fine-grained matrix of biotite, quartz and feldspar. Large biotite clasts are kinked and bent with some slip along cleavage planes and abundant recrystallisation at grain boundaries. Recrystallised biotite forms stringy shear bands, as well as large masses frequently containing relict kinked clasts. K-feldspar porphyroclasts have extensive perthitic intergrowths and deformation twinning, rimmed with fine-grained quartz and feldspar. Amphibole porphyroclasts are extensively microfractured, with some minor grain boundary recrystallisation. Biotite and minor ilmenite are also present along internal cleavage planes. Dynamically recrystallised quartz occurs in polycrystalline bands with serrated sub-grain boundaries that have been rotated into alignment with the shear direction. Undulose extinction is common within the larger quartz grains. The fine-grained biotite shear bands are not strongly aligned but lie parallel to the gneissic fabric.

#### **7.4.4. CR98BB269 granodioritic mylonite**

Sample CR98BB269 is a layered mylonite that contains K-feldspar, plagioclase, hornblende, quartz and biotite (Table 7.3), with a whole rock  $\delta^{18}\text{O}$  value of 6.8‰ (Chapter Six). The sample was collected 120m from the southern edge of the shear zone in an area of intense shearing. It is rich in 6mm diameter, rounded porphyroclasts of feldspar and hornblende wrapped in a matrix of fine-grained quartz, feldspar and biotite. The mylonites are layered with a strong anastomosing fabric comprising quartz layers; quartz, feldspar and biotite layers and biotite shear bands. The K-feldspar porphyroclasts are mantled by fine-grained recrystallised feldspar that is also entrained along microshears throughout the rock. The quartz layers comprise aligned aggregates of recrystallised medium-grained (50 to 75 $\mu\text{m}$ ) quartz with polygonal grain boundaries. The quartz and feldspar polycrystalline aggregates are fine-grained and create a very distinct bimodal grain-size distribution with the porphyroclasts. Some minor myrmekite texture occurs along the feldspar edges. Biotite occurs dominantly as recrystallised aggregates, often entrained with quartz and feldspar into anastomosing microshears. The relict larger biotite clasts are still present, though their size is much reduced. Hornblende occurs as large porphyroclasts with abundant microfractures and mantles of fine-grained recrystallised amphibole, biotite and ilmenite. Pressure shadows of the hornblende clasts frequently have fibrous biotite fringes.

#### **7.4.5. CR98BB546 granodioritic protomylonite-gneiss**

This sample is from the southern edge of the shear zone. It forms a medium-grained protomylonite-gneiss, with evidence of subsequent deformation and shearing, forming small micro-shears and deformation textures. The rock contains K-feldspar, plagioclase,

quartz, biotite and hornblende, with minor apatite, ilmenite and zircon (Table 7.3). It has a whole rock  $\delta^{18}\text{O}$  value of 6.7‰ (Chapter Six). Large K-feldspars are rimmed with myrmekite textures and fine-grained recrystallised aggregates. Some feldspar porphyroclasts are fractured, with biotite and recrystallised feldspar infill. All the quartz is present in recrystallised sub-grained aggregates, with relative straight grain-boundaries. Biotite is present as large deformed grains with some kinking, all mantled by very fine-grained recrystallised aggregates. Biotite inclusions in the large K-feldspars are not deformed, some also contain apatite. Hornblende is a minor component, and occurs as relic fractured grains mantled by fine recrystallised biotite. Small microshears occur throughout the rock.

#### **7.4.6. CR98BB342 quartzofeldspathic mylonite**

Sample CR98BB342 was collected 446.5 m from the southern edge of the shear zone. It is a layered quartzofeldspathic mylonite with small augens (1mm) and abundant quartz layers and a strong planar foliation. It contains K-feldspar, quartz, biotite, epidote garnet, minor zircon and titanite, and has a whole rock  $\delta^{18}\text{O}$  value of 8.0‰ (Table 7.3, Chapter Six). Porphyroclasts are dominantly feldspar with some rounded epidote and anhedral garnet. Biotite forms an anastomosing foliation with equigranular, acicular grains indicating a single generation growth (Fig. 7.3d). A sample of biotite was obtained from this mylonite for  $^{40}\text{Ar}/^{39}\text{Ar}$  step-heating analysis, as a comparison to the *in situ* laser analyses.

#### **7.4.7. Discussion**

Deformation microstructures within the mylonites, including core and mantle textures and rotation recrystallisation domains in quartz, are consistent with variable strain at moderate temperatures (>400°C for core-mantle textures; Passchier and Trouw, 1996). Heterogenous strain partitioning occurs on a millimetre scale throughout all the samples. For example, in protomylonite CR98BB546, porphyroclasts were recrystallised in shear bands while their immediate neighbours are undeformed. Fibrous biotite growth within pressure shadows and ilmenite accumulation along dissolution seams within biotite shear bands indicates that fluid-assisted mass transfer operated during shearing. Samples with a range of deformation microstructures and strain intensities were chosen in order to account for the heterogenous nature of deformation within the mylonites (Table 7.2). All the samples contain biotite, and all except CR98BB235 and CR98BB245 contain amphibole. In order to identify any differences in the age of the porphyroclasts and fine-grained matrix biotite, samples containing both were chosen for analysis.

These samples describe a range of shearing characteristics throughout the Brumby Bore Shear Zone from low-strain protomylonites (CR98BB546) to the extensively-sheared mylonites (CR98BB245). All samples experienced fluid infiltration during shearing, although to different degrees. Pressure solution and mass transfer indicate pervasive fluid infiltration in CR98BB269 and CR98BB245, while other samples contain biotite shear bands (CR98BB546, CR98BB246 and CR98BB235) suggesting highly focused fluid infiltration. The mylonites all preserve  $\delta^{18}\text{O}$  values within 2‰. Given that there is a range in compositions, this suggests that they reached equilibrium with a common fluid during shearing. The whole rock  $\delta^{18}\text{O}$  value is lower than expected for a granitic rock (8 to 10‰; Sheppard, 1986) and suggests that the fluid was exotic. As discussed in Chapter Six, the fluid was probably derived from a surface reservoir and infiltrated the Redbank High Strain Zone through strain- and reaction-controlled conduits during the last shearing event.

## 7.5 RESULTS

### 7.5.1 Step-heating analyses

Table 7.4.  $^{40}\text{Ar}/^{39}\text{Ar}$  step-heated analytical data for biotite from the mylonite CR98BB342 at Brumby Bore, Redbank Hig

Temp (°C)	Cum $^{39}\text{Ar}$	Vol. $^{39}\text{Ar}$ $\times 10^{-15}\text{mol}$	$^{40}\text{Ar}/^{39}\text{Ar}$	$^{37}\text{Ar}/^{39}\text{Ar}$	$^{36}\text{Ar}/^{39}\text{Ar}$	Ca/ K	$^{40}\text{Ar}^*$ (%)	$^{40}\text{Ar}^*/^{39}\text{Ar}$	Age (Ma)	$\pm 1$ s.d. (Ma)
<i>Mass = 0.55 mg</i>										
<i>J-value = 0.01020 <math>\pm</math> 0.000025</i>										
650	0.0210	0.26749	666.390	0.0268	209.700	0.0509	92.988	46.671	702.5	49.8
700	0.0514	0.38753	235.900	0.0016	0.60597	0.0031	75.907	56.774	824.2	22.0
750	0.0755	0.30782	165.060	0.0004	0.34751	0.0008	62.213	62.309	887.6	16.3
775	0.1522	0.97795	80.938	0.0001	0.04390	0.0002	16.027	67.905	949.5	3.3
800	0.2383	1.09720	71.679	0.0002	0.00517	0.0002	2.131	70.091	973.1	1.8
825	0.3686	1.66070	72.181	0.0001	0.00287	0.0001	1.173	71.274	985.7	2.1
850	0.5657	2.51270	72.542	0.0020	0.00214	0.0034	0.872	71.849	991.9	2.5
860	0.7146	1.89940	72.366	0.0001	0.00234	0.0001	0.957	71.613	989.1	2.7
870	0.8243	1.39430	72.379	0.0013	0.00278	0.0026	1.137	71.495	988.1	1.8
885	0.8943	0.08969	72.176	0.0047	0.00385	0.0088	1.575	70.978	982.6	2.2
910	0.9325	0.04865	71.699	0.0030	0.00490	0.0058	2.018	70.191	974.2	3.4
950	0.9516	0.02432	73.171	0.0007	0.01165	0.0014	4.702	69.670	968.6	3.8
1000	0.9682	0.02120	72.659	0.0094	0.01534	0.0178	6.236	68.068	951.3	5.7
1100	0.9929	0.03153	69.198	0.0118	0.01474	0.0225	6.291	64.785	915.2	3.0
1200	0.9980	0.00639	61.911	0.0627	0.01244	0.1191	4.730	58.185	840.6	7.7
1350	1.0000	0.00261	91.017	0.5902	0.27333	1.1218	88.674	10.253	179.4	45.3

1. Isotopic ratios are corrected for mass spectrometer backgrounds, mass discrimination and radioactive decay.

2. J-values are based on an age of 98.8 Ma for the GA1550 biotite monitor.

3. Errors are 1s uncertainties and exclude the error in the J-value.

4. Correction factors:  $(^{36}\text{Ar}/^{37}\text{Ar})\text{Ca} = 3.5\text{E-}4$ ;  $(^{39}\text{Ar}/^{37}\text{Ar})\text{Ca} = 7.86\text{E-}4$ ;  $(^{40}\text{Ar}/^{39}\text{Ar})\text{K} = 0.040$ ;  $140\text{K} = 5.543\text{E-}10$ .

A fine-grained biotite separate from the quartzofeldspathic mylonite sample CR98BB342 was step heated in 16 increments (Table 7.4, Fig. 7.4). The samples produced a slightly hump-shaped age spectrum with an intermediate temperature plateau age of  $988 \pm 1$  Ma (Fig. 7.4) and a total-gas integrated age of  $974 \pm 0.8$  Ma. Grains from this sample were too small for *in situ* probe analysis and the relationship between the step-heating pattern and internal Ar gradients could not be established for this sample.

### 7.5.2 Laser *in situ* analyses

Laser probe analyses were made on the rims and cores of larger hornblende and biotite grains ( $\sim 500$  to  $1000 \mu\text{m}$ ) and clusters of recrystallised fine-grained matrix biotite ( $< 10 \mu\text{m}$ ). In addition, analyses of visibly deformed porphyroclasts (kinked biotite in CR98BB246 and microsheared hornblende in CR98BB269) as well as the recrystallised edges and strain shadows of the porphyroclasts were undertaken. The laser beam analyses produced pits ( $\sim 100$  to  $200 \mu\text{m}$  wide) within the mineral grains denoted by the circle/oval on the backscatter SEM images of the pre-analysed grains (Fig. 7.5).

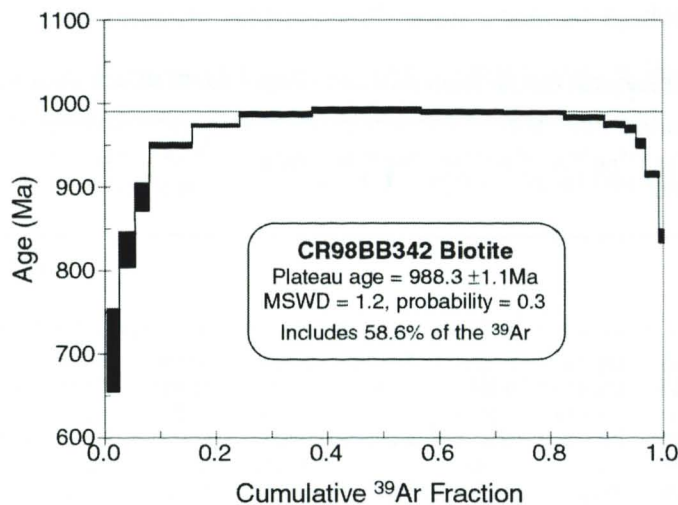


**Figure 7.4.** Age spectra for mylonite sample CR98BB342 from Brumby Bore, Redbank High Strain Zone.

#### 7.5.2.1 Hornblende porphyroclasts

Core and rim laser probe analyses were undertaken on hornblende porphyroclasts from samples CR98BB246 (Disc 2 and 5) CR98BB269 (Disc 1) and CR98BB546 (Disc 3) (Fig. 7.5, 7.6). Core analyses of two large porphyroclasts from sample CR98BB246 yield apparent ages of  $1244 \pm 6$  Ma and  $1048 \pm 6$  Ma, respectively. Rim analyses yield significantly younger apparent ages of  $700 \pm 3$  Ma,  $602 \pm 2$  Ma and  $561 \pm 3$  Ma (Fig. 7.6, Table 7.5). Similar results were recorded for sample CR98BB546, with a core apparent age

of  $1056 \pm 9$  Ma and rim apparent ages of  $832 \pm 6$  Ma and  $865 \pm 5$  Ma. In contrast, core and rim analysis of a porphyroclast from sample CT98BB269 yielded similar apparent ages of  $1472 \pm 11$  Ma and  $1508 \pm 12$  Ma respectively, while a sheared grain from the same sample gave an apparent age of  $1224 \pm 5$  Ma. Calculated Ca/K ratios are generally higher for the core analyses than the rim analyses. These variations could be due to the laser beam impinging on adjacent or underlying grains of different mineralogy. However, there is no systematic variation in Ca/K ratios with apparent age, suggesting that the change in Ca/K values may result from compositional zonation of the hornblende itself. The change in composition could also result from partial recrystallisation of the hornblende, although there is no evidence of this from the backscatter SEM imaging or light microscopy.

#### *7.5.2.2 Biotite porphyroclasts*

Core and rim laser probe analyses were undertaken on biotite porphyroclasts from samples CR98BB235 (Disc 2), CR98BB245, (Disc 7), CR98BB246 (Discs 2 and 5) and CR98BB269 (Discs 1 and 7) (Figs. 7.5, 7.6). Core and rim analysis of a porphyroclast from sample CT98BB235 yielded apparent ages of  $789 \pm 3$  Ma and  $716 \pm 3$  Ma, respectively (Fig. 7.6, Table 7.5). Similar results were recorded for one biotite porphyroclast in sample CR98BB269 with core apparent ages of  $760 \pm 3$  Ma and  $707 \pm 3$  Ma. A second porphyroclast in sample CR98BB269 yields slightly older core apparent ages of  $878 \pm 6$  Ma,  $972 \pm 7$  Ma,  $767 \pm 2$  Ma and a rim age of  $915 \pm 5$  Ma (Fig. 7.6, Table 7.5) with the rim apparent age older than two of the core analyses. Core and rim results were also recorded for sample CR98BB546 yielding apparent ages of  $915 \pm 4$  Ma and  $897 \pm 3$  Ma, respectively.

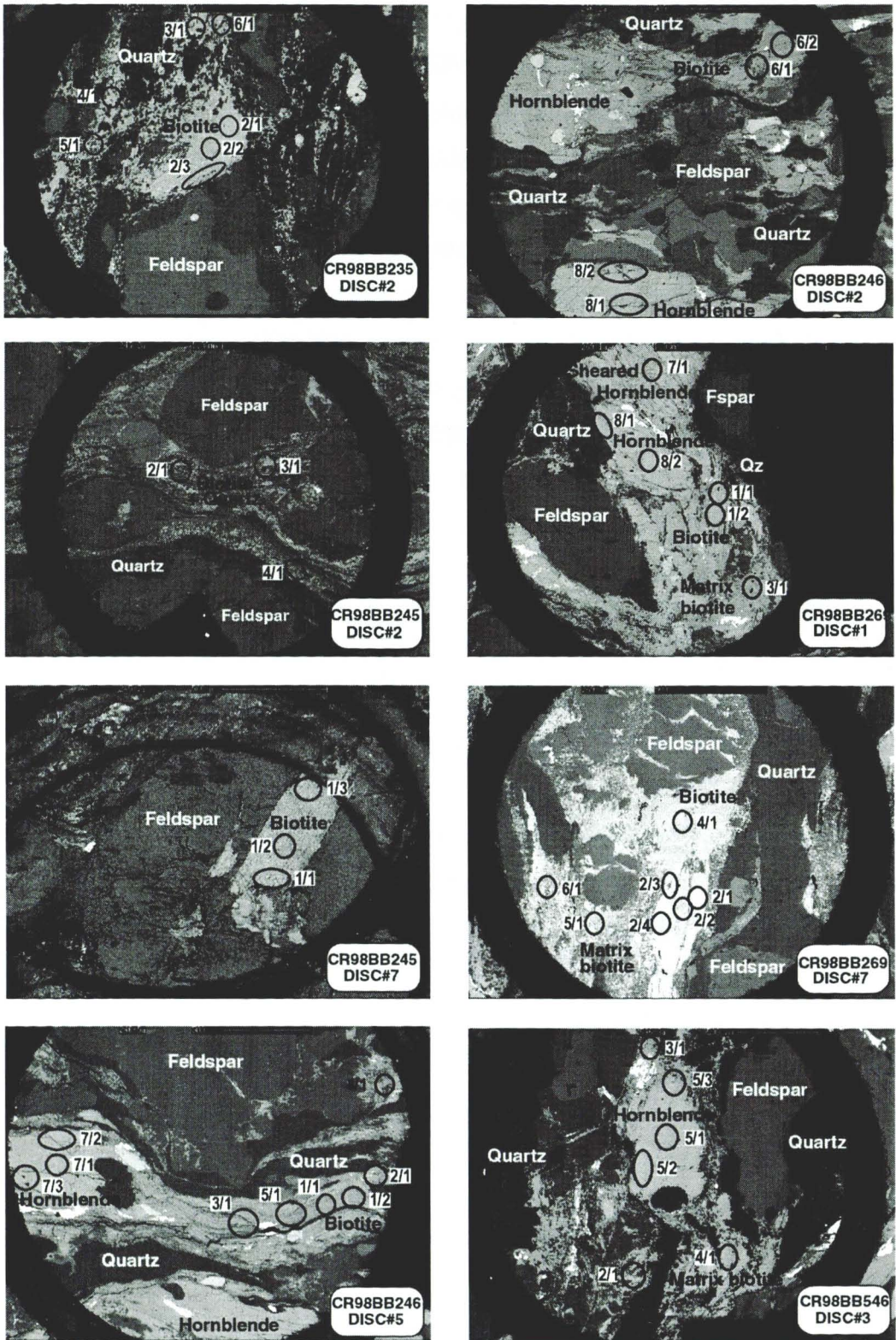


Figure 7.5. Laser *in situ*  $^{40}\text{Ar}/^{39}\text{Ar}$  analysis samples with location and reference number for single analyses on backscatter SEM images of the dating samples. Minerals are labelled. For mylonite location and description see Table 7.2 and 7.3. The ovals/circles refer to actual size of laser probe analysis.

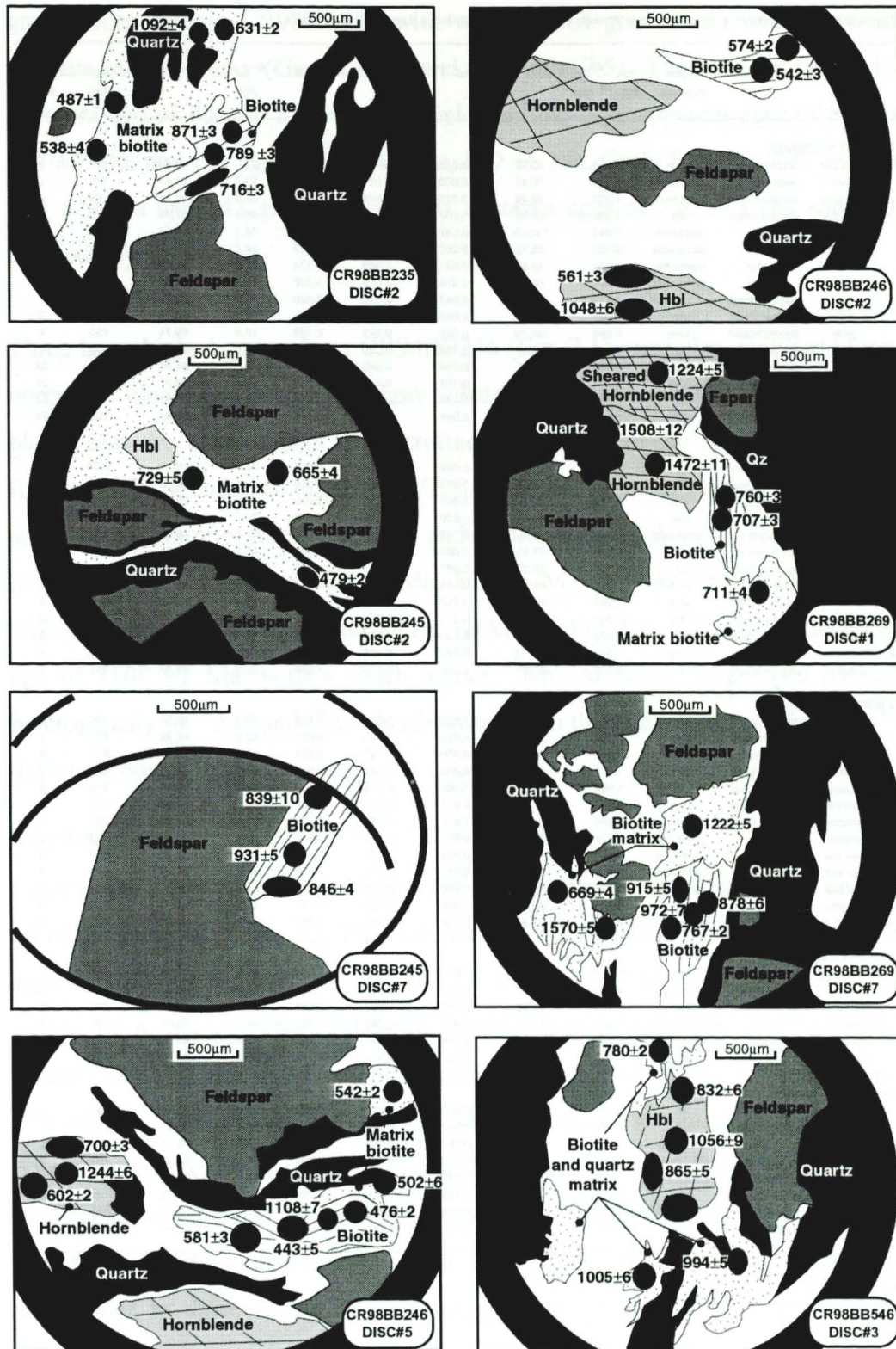


Figure 7.6. Laser  $^{40}\text{Ar}/^{39}\text{Ar}$  apparent ages *in situ* within the mylonite chips (after Figure 7.5.). Data is listed in Table 7.4.

Table 7.5.  $^{40}\text{Ar}/^{39}\text{Ar}$  laser probe analytical data for samples from Brumby Bore, Redbank High Strain Zone, central Australia.

Grain No.	Mineral	Sample Type	Texture	Spot Position	Vol. $\times 10^{-18}$	$^{39}\text{Ar}$ mol	$^{40}\text{Ar}/^{39}\text{Ar}$	$^{37}\text{Ar}/^{39}\text{Ar}$	$^{36}\text{Ar}/^{39}\text{Ar}$	$^{38}\text{Ar}/^{39}\text{Ar}$	Ca/K	$^{40}\text{Ar}$ (%)	$^{40}\text{Ar}/^{39}\text{Ar}$	$^{36}\text{Ar}$	Age (Ma)	$\pm 1\text{s.d.}$ (Ma)
<b>CR98BB235 (J = 0.008367 <math>\pm</math> 0.000025)</b>																
111	biotite	grain	porphyroblast	core	1.826	90.76	0.015	0.081	0.028	73.6	66.83	807	4			
211	biotite	grain	porphyroblast	rim/core	3.009	78.41	0.003	0.017	0.006	93.7	73.47	871	3			
212	biotite	T/section	porphyroblast	core	4.235	78.44	0.018	0.045	0.034	82.8	64.97	789	3			
213	biotite	T/section	porphyroblast	rim	1.880	60.30	0.006	0.009	0.011	95.7	57.73	718	3			
311	biotite	T/section	matrix	composite	0.945	133.03	0.042	0.117	0.080	74.1	98.54	1092	4			
411	biotite	T/section	matrix	composite	28.681	38.72	0.080	0.007	0.113	94.7	36.69	487	1			
511	biotite	T/section	matrix	composite	1.964	42.83	0.091	0.006	0.174	96.0	41.13	538	4			
611	biotite	T/section	matrix	composite	4.397	53.11	0.004	0.012	0.008	93.3	49.55	631	2			
711	biotite	grain	porphyroblast	core	1.479	134.35	0.047	0.228	0.090	49.7	86.79	807	7			
711	biotite	grain	porphyroblast	rim	1.067	72.09	0.065	0.030	0.124	87.8	63.28	772	3			
712	biotite	grain	porphyroblast	core	0.866	126.79	0.082	0.193	0.155	55.0	69.74	835	6			
712	biotite	grain	porphyroblast	rim	0.518	84.45	0.158	0.052	0.301	81.8	69.07	829	6			
811	biotite	grain	porphyroblast	core	0.337	337.3	0.208	0.942	0.395	17.4	58.80	727	29			
811	biotite	grain	porphyroblast	core	0.727	310.51	0.163	0.846	0.310	19.4	60.37	743	21			
811	biotite	grain	porphyroblast	rim	0.381	174.91	0.197	0.387	0.374	34.7	60.64	746	13			
811	biotite	grain	porphyroblast	rim	0.122	180.03	0.058	0.399	0.111	34.4	62.03	760	23			
<b>CR98BB246 (J = 0.008348 <math>\pm</math> 0.000025)</b>																
111	biotite	T/section	kinked grain	core	0.491	135.21	0.028	0.117	0.053	74.4	100.63	1108	7			
112	biotite	T/section	porphyroblast	rim	1.096	48.66	0.010	0.043	0.019	73.6	35.79	476	2			
211	biotite	T/section	kinked grain	rim	1.572	63.20	0.050	0.085	0.096	60.2	38.08	502	6			
311	biotite	T/section	kinked grain	rim	3.941	57.77	0.028	0.043	0.052	78.1	45.13	581	3			
411	biotite	T/section	matrix	composite	3.550	49.08	0.124	0.025	0.238	84.8	41.61	542	2			
511	biotite	T/section	porphyroblast	rim	6.044	76.35	0.003	0.146	0.005	43.3	33.07	443	5			
611	bio + hbl	T/section	porphyroblast	rim	8.798	56.03	0.067	0.039	0.127	79.4	44.47	574	2			
612	biotite	T/section	porphyroblast	core	2.933	44.44	0.043	0.010	0.082	93.5	41.55	542	3			
711	hornblende	T/section	porphyroblast	core	1.897	164.46	1.253	0.159	2.382	71.6	117.80	1244	6			
712	hornblende	T/section	porphyroblast	rim	1.999	68.13	0.222	0.040	0.421	82.5	56.21	700	3			
713	hornblende	T/section	porphyroblast	rim	3.574	56.92	0.846	0.034	1.609	82.8	47.04	802	2			
811	hornblende	T/section	porphyroblast	core	1.342	124.43	0.792	0.105	1.505	75.1	93.47	1048	6			
812	hornblende	T/section	porphyroblast	rim	2.979	47.67	0.559	0.015	1.063	90.8	43.29	561	3			
<b>CR98BB269 (J = 0.008348 <math>\pm</math> 0.000025)</b>																
111	biotite	T/section	porphyroblast	core	4.650	72.96	0.032	0.036	0.060	85.3	62.20	760	3			
112	biotite	T/section	porphyroblast	core	2.701	58.44	0.019	0.005	0.037	97.5	56.95	707	3			
211	biotite	T/section	porphyroblast	core	1.606	76.52	0.030	0.007	0.057	97.2	74.38	878	6			
212	biotite	T/section	porphyroblast	core	1.612	91.50	0.008	0.023	0.014	92.6	84.76	972	7			
213	biotite	T/section	porphyroblast	rim	1.962	82.66	0.006	0.014	0.012	94.8	78.37	915	5			
214	biotite	T/section	porphyroblast	core	3.205	66.49	0.031	0.012	0.058	94.5	62.84	767	2			
311	biotite	T/section	matrix	composite	0.948	70.37	0.012	0.044	0.023	81.4	57.30	711	4			
411	biotite	T/section	matrix	composite	1.814	124.91	0.097	0.034	0.184	92.0	114.93	1222	5			
511	biotite	T/section	matrix	composite	0.967	195.81	0.061	0.106	0.116	84.1	164.61	1570	5			
611	biotite	T/section	matrix	composite	0.773	67.12	0.016	0.047	0.030	79.3	53.25	669	4			
711	hornblende	T/section	porphyroblast	sheared	2.078	131.36	0.456	0.055	0.867	87.7	115.19	1224	5			
811	hornblende	T/section	porphyroblast	rim	0.618	190.82	1.986	0.122	3.779	81.2	155.11	1508	12			
812	hornblende	T/section	porphyroblast	core	0.378	158.46	2.238	0.031	4.260	94.3	149.63	1472	11			
<b>CR98BB245 (J = 0.008348 <math>\pm</math> 0.000025)</b>																
111	biotite	T/section	porphyroblast	rim	11.050	108.19	0.022	0.126	0.041	65.6	70.98	946	4			
112	biotite	T/section	porphyroblast	core	4.691	95.50	0.003	0.052	0.005	94.0	80.20	931	5			
113	biotite	T/section	porphyroblast	rim	5.189	98.98	0.032	0.097	0.061	71.0	70.24	839	10			
211	biotite	T/section	matrix	composite	1.454	62.82	0.091	0.013	0.173	94.0	59.06	729	5			
311	biotite	T/section	matrix	composite	1.970	56.90	0.052	0.014	0.098	92.9	52.88	665	4			
411	biotite	T/section	matrix	composite	1.933	39.81	0.007	0.013	0.012	90.6	36.06	479	2			
<b>CR98BB546 (J = 0.008348 <math>\pm</math> 0.000025)</b>																
111	biotite	T/section	porphyroblast	rim	2.788	81.46	0.005	0.017	0.009	93.8	76.44	897	3			
112	biotite	T/section	porphyroblast	core	1.764	82.42	0.007	0.013	0.014	95.2	78.42	915	4			
211	biotite	T/section	matrix	composite	1.281	118.84	0.057	0.103	0.108	74.5	88.49	1005	6			
311	biotite	T/section	matrix	composite	1.477	67.72	0.455	0.012	0.864	94.8	64.20	780	2			
411	biotite	T/section	matrix	composite	2.519	98.34	0.140	0.038	0.296	88.7	87.24	994	5			
511	hornblende	T/section	porphyroblast	core	0.118	122.48	2.165	0.096	4.120	76.9	94.36	1056	9			
512	hornblende	T/section	porphyroblast	rim	0.497	84.52	2.074	0.040	3.947	86.3	73.02	865	5			
513	hornblende	T/section	porphyroblast	rim	1.600	72.53	0.611	0.011	1.162	95.8	69.48	832	6			

1. Isotopic ratios are corrected for mass spectrometer backgrounds, mass discrimination and radioactive decay.
2. J-values are based on an age of 98.8 Ma for the GA1550 biotite monitor.
3. Errors are 1s uncertainties and exclude the error in the J-value.
4. Correction factors: ( $^{36}\text{Ar}/^{37}\text{Ar}$ )<sub>ca</sub> = 3.5E-4; ( $^{36}\text{Ar}/^{37}\text{Ar}$ )<sub>ca</sub> = 7.86E-4; ( $^{40}\text{Ar}/^{39}\text{Ar}$ )<sub>ca</sub> = 0.040;  $^{40}\text{K}$  = 5.543E-10.

Similar results were recorded for sample CR98BB245 with a core apparent age of  $931 \pm 5$  Ma and younger rim apparent ages of  $846 \pm 4$  Ma and  $839 \pm 10$  Ma (Fig. 7.6, Table 7.5).

Due to the substantial deformation break-up of the biotite grains and their orientation perpendicular to the C-axis in thin section there was some difficulty in discerning cores and rims during the analysis. Therefore, to further assess core/rim variations, three biotite

grains from sample CR98BB235 with well-defined grain boundaries were analysed as separate single grains (Grains 1, 7 and 8; Table 7.5). The core of Grain 1 yields an apparent age of  $807 \pm 4$  Ma. Grain 7 yields similar core apparent ages of  $807 \pm 4$  Ma and  $835 \pm 6$  Ma, and rim ages of  $772 \pm 3$  Ma,  $829 \pm 6$  Ma. Grain 8 yields core apparent ages of  $727 \pm 29$  Ma and  $743 \pm 21$  Ma and rims apparent ages of  $746 \pm 13$  Ma and  $760 \pm 23$  Ma, respectively.

Three large kinked grains from CR98BB246 (Fig. 7.5) were also analysed along a surface normal to cleavage. The grains show substantial deformation by slip along the cleavage planes and the development of microfractures at  $45^\circ$  to the cleavage that subsequently formed grain boundaries. Analyses 1/2, 3/1 and 5/1 from this sample represent deformed areas of the biotite where rotation and cleavage-parallel slip occurred (Fig. 7.5) and preserve apparent ages of  $476 \pm 2$  Ma,  $502 \pm 6$  Ma and  $443 \pm 5$  Ma. Analysis 1/1 occurs within the least deformed section of the kinked biotite (Fig. 7.5) and produced an apparent age of  $1108 \pm 7$  Ma, with a much higher  $^{40}\text{Ar}/^{39}\text{Ar}$  ratio. These data indicate internal heterogeneity of  $^{40}\text{Ar}^*$  and  $^{39}\text{Ar}$  distribution within the grain, with variably less  $^{40}\text{Ar}^*$  at the deformed edges.

#### 7.5.2.3 Biotite matrix

Laser probe analyses of accumulations of fine-grained biotite matrix were undertaken from all of the samples (Table 7.5, Fig. 7.5). Sample CR98BB235 yields biotite matrix apparent ages of  $1092 \pm 4$  Ma,  $631 \pm 2$  Ma,  $538 \pm 4$  Ma and  $487 \pm 1$  Ma with all the analysis sites within 1mm of each other, indicating a major spatial variability of  $^{40}\text{Ar}$  within the fine-grained biotite. Three areas of biotite matrix in Sample CR98BB245 yield apparent ages of  $479 \pm 2$  Ma,  $665 \pm 4$  Ma and  $729 \pm 5$  Ma and record substantially lower  $^{39}\text{Ar}$  than the porphyroclasts within the sample (Table 7.5). Sample CR98BB245 yields an apparent age of the biotite matrix of  $542 \pm 2$  Ma. Sample CR98BB546 yields slightly higher apparent ages for the biotite matrix of  $780 \pm 2$  Ma,  $994 \pm 5$  Ma and  $1005 \pm 6$  Ma. These apparent ages are similar to those of the biotite porphyroclast within the sample and record similar volumes of  $^{39}\text{Ar}$ . Sample CR98BB269 yields the highest apparent ages for biotite matrix of  $669 \pm 4$  Ma,  $711 \pm 4$  Ma,  $1222 \pm 5$  Ma and  $1570 \pm 12$  Ma.

## 7.6 INTERPRETATION OF DATA

### 7.6.1 *Hornblende porphyroclasts*

The variation in apparent ages recorded from core and rim laser probe analyses of the hornblende porphyroclasts is symptomatic of partial argon loss in response to a thermal overprint (eg. Wartho, 1995; Villa *et al.*, 2000). The data would indicate formation/resetting of the hornblende prior to 1.5 Ga, ie. the oldest apparent age, perhaps during the Chewings Orogeny, followed by partial argon loss after ~600 Ma (the youngest hornblende apparent age), presumably during the Alice Springs shearing. This scenario would require elevated temperatures above ~500°C, the closure temperature for argon diffusion in hornblende (McDougall and Harrison, 1988) after 600Ma. Alternatively, the younger apparent ages reflect impingement on younger adjacent or underlying grains, such as matrix biotite. Although, Ca/K ratios decrease towards hornblende grain margins, as expected of analyses with combined hornblende and biotite, there is no systematic correlation between Ca/K ratios and apparent ages, suggesting that this is not a major cause of the younger rim ages. Another alternative is partial recrystallisation of the hornblende rims. However, there is little evidence of recrystallisation from backscatter SEM imaging and light microscopy. Therefore, it is concluded that the variation in hornblende ages is most likely due to thermal overprinting during the Alice Springs Orogeny.

### 7.6.2 *Biotite porphyroclasts*

The lack of systematic variation in core-rim apparent ages preserved in the individual biotite grains suggests that they were completely reset during shearing. This is consistent with temperatures of >500°C predicted by the hornblende partial resetting. Consistent low Ca/K ratios for the biotite porphyroclast analyses indicate that the variation in apparent ages of biotite porphyroclasts is not associated with impingement of hornblende grains into the laser beam. As discussed below, the old apparent ages may be the result of variable incorporation of excess argon during recrystallisation. The apparent ages of biotite porphyroclasts indicate resetting occurred after 476 Ma, presumably during Alice Springs shearing.

### 7.6.3 *Biotite matrix*

The matrix biotite also yields old and variable apparent ages. This may be due to the release of argon from quartz and interstitial gas containing excess argon. However, visual estimates of the proportion of quartz in each analysis do not correlate with apparent age. Also, a separation of fine biotite from CR98BB342 gives older apparent ages. This

suggests that there are variations in the apparent ages of the matrix biotite. As the biotite matrix apparent ages are not within error, yet the grains were from within ~1mm of each other, this implies chemical disequilibrium and a heterogeneous distribution of excess argon within the mylonites.

## 7.7 EXCESS ARGON CONTAMINATION

The data from this investigation, combined with that of other workers, indicates that the mylonites of the Redbank High Strain Zone were contaminated with excess argon during the Alice Springs Orogeny. This interpretation is based on: i) Rb-Sr whole rock and biotite isochrons give Alice Springs ages of 350 to 400 Ma, indicating isotopic resetting under lower amphibolite- to upper greenschist-facies conditions at that time. However, K-feldspar K-Ar and biotite  $^{40}\text{Ar}/^{39}\text{Ar}$  ages along the Redbank High Strain Zone give older apparent ages (This study; Shaw *et al.*, 1992); ii) Some K-feldspar spectra of Shaw *et al.* (1992) exhibit unusual “hump” shapes that are characteristic of excess argon (Foster *et al.*, 1990) as noted by Shaw *et al.*, (1992); iii) Hornblende argon systematics are partially reset, implying relatively high temperatures (>500°C) during the Alice Springs Orogeny in keeping with Rb-Sr data, yet biotite ages are older than Alice Springs. The published diffusion data for hornblende and biotite (Dodson, 1973; Villa *et al.*, 1996) indicate that biotite should be completely reset to Alice Springs ages if hornblende is partially reset (notwithstanding alternative explanations); iv) Some apparent ages from the matrix biotite, formed during shearing, are older than hornblende and biotite porphyroclast ages.

The data show that even apparently fully-recrystallised mineral populations can give old geologically-meaningless, apparent ages. The large variation in apparent ages, with high variable  $^{40}\text{Ar}/^{39}\text{Ar}$  ratios of the matrix biotite, indicate that excess argon distribution throughout the mylonites at Brumby Bore is heterogeneous at a millimetre-scale. The disequilibrium of  $^{40}\text{Ar}/^{39}\text{Ar}$  isotope ratios across grains can be attributed to the introduction of excess argon via an external fluid source, where the uptake and distribution of excess argon is controlled by fluid-rock interaction and heterogeneous deformation-controlled diffusion (Villa *et al.*, 2000).

Though there is clear distinction between amphibolite and greenschist-facies mineral growth, the deformation zones are gradational and have similar kinematics, likely representing two stages of mineral growth within a single episode of shearing. The uptake of argon into hornblendes indicates that the Alice Springs Orogeny reached temperatures of >500°C. The hornblende data may be interpreted as formation/resetting of the

porphyroclasts prior to 1.5 Ga, perhaps related to the Chewing Orogeny, followed by partial argon loss during the Alice Springs shearing. The data do not constrain whether mineral crystallisation or resetting occurred during the Anmatjira Uplift Event. The lack of consistency of the ages within the hornblende cores may be explained by slow cooling following the 1.6 Ga high-grade Chewings Orogeny, or partial resetting during the 1200 to 1050 Ma Teapot Tectonomagmatic Event. Due to the contamination of excess argon there are no specific age constraints on the Alice Springs Orogeny obtained from these data.

## 7.8 IMPLICATIONS FOR FLUID FLOW DURING SHEARING

Excess argon incorporation into minerals may occur during subsequent thermal events, and through fluid-rock interaction during recrystallisation (de Jong *et al.*, 2001). Chemical analyses of intracratonic thermal fluids in central-western India show enrichment in crustal  $^{40}\text{Ar}$  of deep, old, circulating meteoric fluids (Minissale *et al.*, 2000), thus suggesting that given sufficient supply of K-bearing rocks, circulating fluids may transfer argon during fluid-rock interaction in intracontinental settings.

The Redbank High Strain Zone is likely to have been infiltrated by argon-bearing fluids during the Alice Springs Orogeny. The presence of fluid-assisted deformation mechanisms and metasomatic layering within the mylonites indicates that fluid-assisted mass transfer operated at variable scales during shearing (Chapter Six). Features of deformation and fluid-rock interaction throughout the Redbank High Strain Zone mylonites suggest that strain was partitioned into ultramylonite bands and that deformation was heterogenous at a millimetre-scale within all the lower strain mylonites. Excess argon brought into the mylonites during fluid-rock interaction likely became heterogeneously distributed throughout the mylonites, producing scattered and geologically-meaningless  $^{40}\text{Ar}/^{39}\text{Ar}$  apparent ages. As previously noted, this type of contamination by excess argon is also characteristic of the high-pressure terrains in the Alps. High-pressure phengites within eclogitized rocks of the western Alps contain excess argon that was trapped in the early stages of high-pressure metamorphism following continent-continent collision. In the case of the Alps, fluid-rock interaction during subduction-related high-pressure metamorphism led to excess argon contamination.

## 7.9 CONCLUSIONS

Extensive investigations of the Alpine orogenesis have been important in contributing to the understanding of continental collision (Arnaud and Kelley, 1995). Identification of the

evolution of continental tectonics requires, in addition to mechanical processes, the timing of thermal events. Therefore the controversy over the timing of high-pressure metamorphism within the western Alps provides important insights into the limitations of isotopic systems as geochronometers. In the case of the Alps excess argon was incorporated into the rocks from an argon-rich fluid during high-pressure metamorphism (Villa *et al.*, 1996). The excess argon was retained within white micas throughout the eclogite to greenschist-facies metamorphic evolution (Scaillet, 1996). However, only minimal uptake of excess argon within the retrograde biotite phase produced the apparent younging of metamorphism, indicating mixing and re-equilibration of the minerals never reached completion following the initial fluid-rock interaction (Villa *et al.*, 1996). The extent of excess argon incorporation within metamorphic minerals in different tectonic settings can only be assessed by continued analysis. The data presented in this study suggest that, in addition to the retention of excess argon within high-pressure rocks, open systems such as shear zones can experience extensive excess argon contamination through fluid rock interaction. This implies that the contamination of excess argon during fluid-rock interaction is a significant problem for the application of the  $^{40}\text{Ar}/^{39}\text{Ar}$  dating technique. This study illustrates that the use of high-resolution methods, such as *in situ* laser probe analyses, are important in order to understand  $^{40}\text{Ar}/^{39}\text{Ar}$  apparent ages and decipher the tectonic evolution within fluid-affected terrains.



## CHAPTER EIGHT

### THE ROLE OF SHEAR ZONES IN CRUSTAL FLUID FLOW

#### **Abstract**

Shear zones in the Arunta Inlier hosted substantial crustal-scale fluid flow during the intracontinental Alice Springs Orogeny. This study suggests that surface reservoirs may provide the fluid required for hydrating the middle crust during periods of tectonic rejuvenation. This requires permeability connectivity across the brittle-ductile transition during tectonism. Examples of fluid-assisted mass transfer, vein formation, cataclasis and dynamic recrystallisation within the shear zones suggests that they formed near the brittle-ductile transition, and may indicate changes in predominant deformation mechanisms as the shear zones evolved. Therefore, fluid flow through the crust during periods of continental reworking may influence the location of the brittle-ductile transition.  $^{40}\text{Ar}/^{39}\text{Ar}$  *in situ* laser probe analysis of Redbank High Strain Zone mylonites shows that excess argon contamination occurred during the Alice Springs Orogeny, and provides geologically meaningless ages. This study illustrates the sensitivity of mylonites to isotope exchange during recrystallisation associated with fluid-rock interaction.

#### **8.1 INTRODUCTION**

It has been well established that fluids play an important role in shearing and reworking of the middle crust during orogenesis (Beach, 1976; Dipple et al., 1990; Koons and Craw, 1991; Dipple and Ferry, 1992; Knipe and McCaig, 1994; Winsch et al., 1995). Fluids affect the chemistry of rocks in the middle crust through fluid-rock interaction and stimulate changes in rheology. As orogenic activity occurs more readily where continental plates converge, fluid flow studies have often involved the input of a down-going hydrous slab (Bebout and Barton, 1993), or the underthrusting of sedimentary piles (McCaig, 1988). However, within central Australia, Devonian-Carboniferous compression during the intraplate Alice Springs Orogeny caused widespread hydration of middle crustal rocks, requiring large-scale fluid flow. Chapters three to seven of this thesis discussed in detail the characteristics and timing of fluid flow in shear zones of the Arunta Inlier. This chapter provides a discussion of these data in a general context of fluid flow during continental reworking.

## 8.2 CHARACTERISTICS OF SHEARING DURING THE ALICE SPRINGS OROGENY

The Arunta Inlier is cut by abundant NW-SE- and E-W-oriented faults and shear zones with predominantly reverse displacements. Teleseismic travel time and deep-seismic reflection profiles indicate that the Aileron Shear Zone in the northern Arunta Inlier and the Redbank High Strain Zone in the south are crustal-scale thrusts that have sustained significant vertical movement (Lambeck and Penney, 1984; Goleby et al., 1990; Lambeck, 1991; Korsch et al., 1998; Fig 8.1). Deep-crustal mafic granulites were juxtaposed against middle-crustal granitic gneisses across the Redbank High Strain Zone, indicating 15 to 20 km of uplift during intraplate compression (Shaw and Black, 1991). These deep-crustal features and the abundance of shear zones across the Arunta Inlier suggest that, in common with ancient continental crust worldwide, the central Australian crust has been significantly reworked during exhumation.

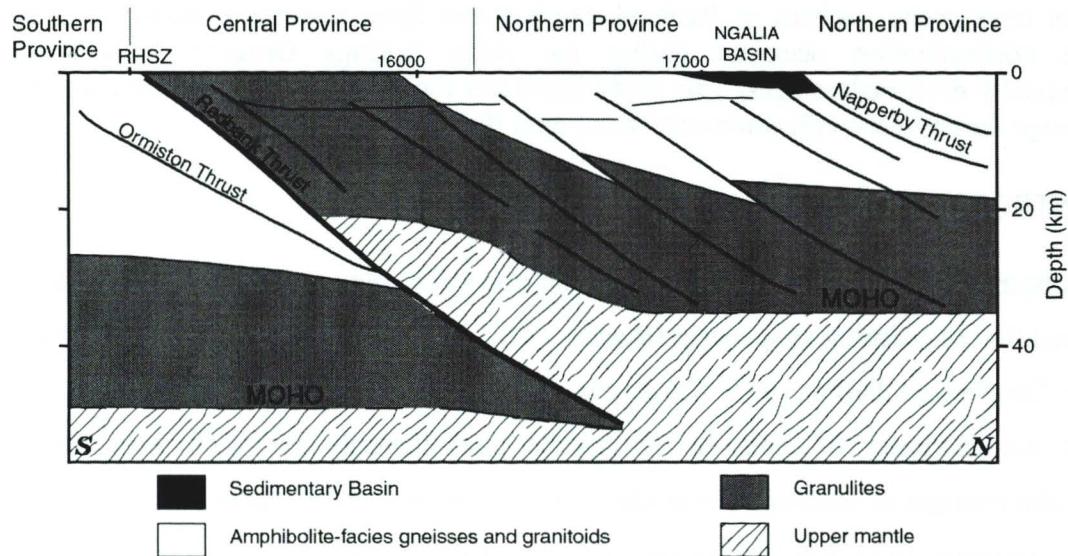


**Figure 8.1.** Combination of seismic and lithological interpretation across the southern Arunta Inlier, representing the thick-skinned nature of deep crustal structures such as the Redbank High Strain Zone (from models presented by: Goleby *et al.*, 1990; Lambeck, 1991; Shaw *et al.*, 1991; Korsch *et al.*, 1998).

### 8.2.1 Geochronology

The timing of shearing within the Arunta Inlier has been constrained by two sets of radiogenic isotopic ages (Shaw and Black, 1991; Shaw *et al.*, 1992; Cartwright *et al.*, 1999; Bendall *et al.*, 1998; Ballèvre *et al.*, 2000). Chapter Five and Seven discuss the geochronology of the shear zones in part of the Arunta Inlier, and suggest that they were predominantly, or only, active in the Alice Springs Orogeny at 300 to 400 Ma. Rb-Sr and  $^{40}\text{Ar}/^{39}\text{Ar}$  dating of shear zones in the northern Arunta Inlier, presented in Chapter Five and

Cartwright *et al.* (1999), yield ages of 300 to 356 Ma and indicate a northward progression in active deformation of  $6\text{mm}\cdot\text{y}^{-1}$  in the region. A possible southward migration of deformation from  $\sim 315$  to  $\sim 400$  Ma in the south of the Arunta Inlier may also have occurred given the age data of Shaw and Black (1991), Bendall *et al.* (1998) and Ballèvre *et al.* (2000) (Fig 8.2). This geochronological data indicates that the Alice Springs Orogeny produced local deformation during discrete events throughout a  $\sim 100$  My period.

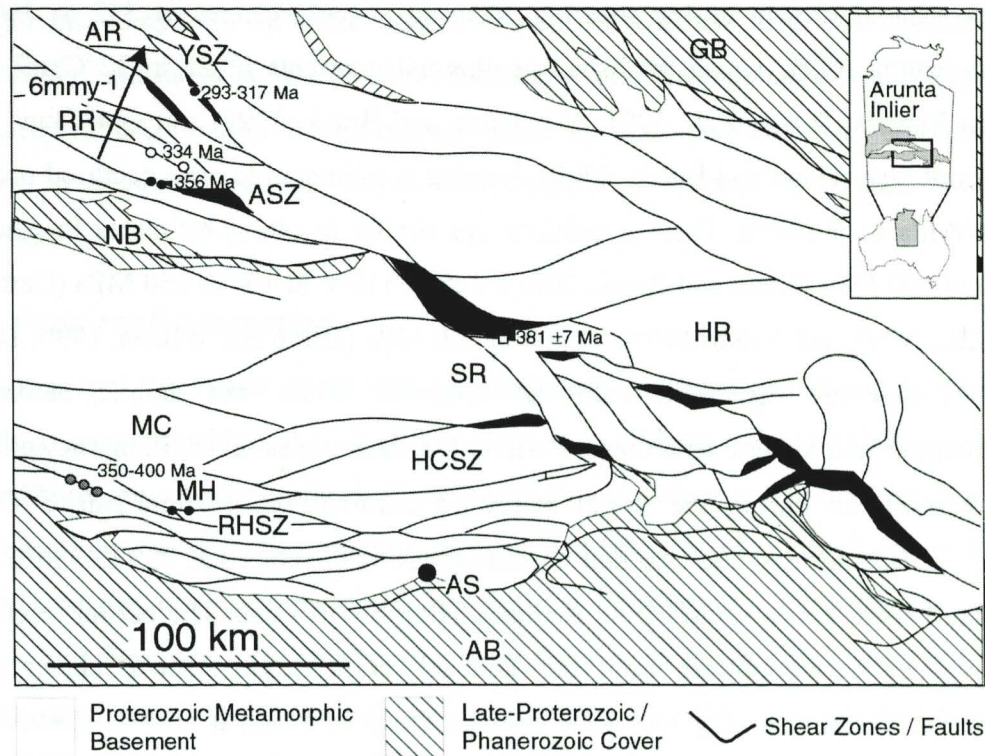


**Figure 8.2.** General tectonic map of the central and eastern Arunta Inlier showing the location of the major faults and shear zones (after Cartwright and Buick, 1999). Shear zones: Aileron Shear Zone, ASZ; Harry Creek Shear Zone, HCSZ; Redbank High Strain Zone, RHSZ; Yalbadjandi Shear Zone, YSZ. Geological regions: Amadeus Basin, AB; Anmatjira Range, AR; Georgina Basin, GB; Harts Range, HR; Mount Chapple, MC; Mount Hay, MH; Ngalia Basin, NB; Reynolds Range, RR; Strangways Range, SR. Alice Springs, AS. Also shown are locations of ages of shear zones from this study (closed circles) Cartwright *et al.* (1999) (open circles), Shaw and Black (1991) (grey circles) and Ballèvre *et al.* (2000) (open square), and the direction and speed of the Alice Springs age deformation front in the northern Arunta Inlier

Thus, the Alice Springs Orogeny was a long-lived and extensive period of crustal reworking within the Arunta Inlier. This is contrary to orogenic belts at collisional margins, such as the European Alps and the Southern Alps in New Zealand, where deformation and uplift are rapid, and is likely a response to the intraplate setting. In addition, tectonism during the Alice Springs Orogeny is recorded from deformed and reworked sediments within the overlying basins (Shaw, 1991). During the Devonian to Carboniferous extensive tectonism is recorded throughout the Australian continent and

may have been driven by rifting and associated microplate rotation at the northern margin (Braun and Shaw, 2001 and references therein).

### **8.2.3 Conditions of shearing**

The shear zones investigated in this study contain hydrous assemblages, abundant quartz veining, and fluid-driven deformation microstructures, suggesting that fluid flow played an important role during crustal reworking. Mineral-pair  $\delta^{18}\text{O}$  data presented in Chapter Four indicates mineral growth during shearing occurred at temperatures of 312 to 566°C in northern Arunta Inlier. Using published geothermal gradients of 25 to 32°Ckm<sup>-1</sup> in the Reynolds Ranges (Dirks et al., 1991; Cartwright and Buick, 1999) and ~44°Ckm<sup>-1</sup> in the Anmatjira Range (Hand and Buick, 2001) shearing is estimated to have occurred pressures of at 340MPa to 500MPa. These conditions are similar to others estimates for shearing: 580°C and 400 MPa (Hand and Buick, 2001); 425 to 535°C at 400 to 650 MPa (Cartwright and Buick, 1999); and 550 to 600°C at 500 to 600 MPa (Dirks and Wilson, 1990; Dirks et al., 1991) and are consistent with the observed brittle and ductile deformation microstructures and mineral assemblages within the shear zones. In addition, they allow for brittle deformation during the initial stages of deformation. Mineral-pair  $\delta^{18}\text{O}$  data, presented in Chapter Six, indicate that muscovite growth occurred at 305 to 330°C in the Littler Yard shear zones south of the Redbank High Strain Zone. The partial resetting of argon isotopes in amphiboles from the Redbank High Strain Zone (Chapter Seven) suggests that shearing during the Alice Springs Orogeny reached 500°C. However, the observed brittle and ductile reworking of mylonites and the growth of muscovite and epidote assemblages suggests that temperatures dropped to lower greenschist-facies conditions prior to the end of movement across the Redbank High Strain Zone. All of the shear zones investigated preserve evidence of retrogression as metamorphism waned during the Alice Springs Orogeny. The presence of brittle deformation in the Redbank High Strain Zone and Yalbadjandi Shear Zone, and the extensive vein networks throughout the Napperby Gneiss and Blue Bush Swamp shear zones, are consistent with deformation at the brittle-ductile transition. However, the resulting temperatures of 550°C within the Yalbadjandi Shear Zone and the ductile overprint of the Napperby Gneiss-hosted shear zones in the northern Arunta Inlier indicate that the brittle-ductile transition was displaced upwards during shearing. Extensional faulting within the Arunta Inlier prior to the Alice Springs Orogeny may have resulted in the downward displacement of the brittle-ductile transition initially during shear zone development, followed by weakening of shear zones, though prograde metamorphism and fluid-assisted deformation. Imber et al. (1997) and Holdsworth et al. (2001) describe fluid-assisted weakening of shear zones leading to

changes in the dominant deformation mechanisms from brittle to ductile from the Great Glen Fault Zone and the Outer Hebrides Fault Zone in Scotland, suggesting that fluid can control deformation, and displace the brittle-ductile transition. In the Redbank High Strain Zone, brittle deformation overprints ductile shearing as temperatures reached at least 500°C initially and decreased as shearing continued. Oxygen isotope data suggests that fluid infiltration also diminished during shearing, with locally-available fluid recycling through narrow high-strain zones. The different shearing characteristics within the Arunta highlight the complexity of shear zone evolution in response to crustal conditions and permeability, and likely are the result of location within the regional tectonic regime. The movement of deformation fronts through time, as discussed above is consistent with changes in regional tectonic forces and associated thermal conditions within the lithosphere.

### **8.2.2. Fluid-rock interaction**

Hydrous assemblages with up to 90% phyllosilicates, massive quartz and kyanite veins, and metasomatism within the shear zones of the northern Arunta Inlier discussed in Chapter Three represent significant fluid flow during shearing. In addition, muscovite- and epidote-rich mylonites cutting granitic gneisses at Littlers Yard in the Southern Province also indicate that there was hydration associated with shearing. Quartz-epidote mylonites suggest fluid flow was substantial during early shearing in the Redbank High Strain Zone. The results of geochemical analysis across the shear zones in the northern Arunta Inlier indicate that substantial fluid-rock interaction can cause extensive alteration even to assumed immobile elements such as Ti, Zr, and the REE's. This type of alteration has also been documented in shear zones by O'Hara (1988) and Selverstone et al. (1991). In addition, the geochemical trends vary significantly within individual shear zones in the northern Arunta Inlier, corresponding to compositional domains. Transient fluid flow may be responsible for the formation of adjacent silica-poor phyllonite domains and abundant quartz veins within these shear zones. As suggested in Chapter Three, this may occur through the dissolution of silica under conditions of high normal stress and the expulsion of the silica-saturated fluid along seismically-activated hydrofractures with local quartz precipitation within the steeply-dipping shear zones. This interpretation suggests that changes in the composition of shear zone rocks may be controlled by local fluid pressure changes, rather than uniform temperature changes along the flow path. This has important implications for the use of temperature-dependant and chemical-based alteration calculations in determining volumes and directions of fluid flow such as time integrated fluid flux calculations (Dipple and Ferry, 1992a). Specifically, the calculations assume

uniform flow along the flow path but if there is lateral redistribution of elements reintegration of those changes is required to make use of the calculations. The progressive alteration of the shear zones rocks is likely to have occurred over time as cycles of seismic activity pumped large volumes of fluid through the shear zones. Alteration calculations based on immobile elements forming an isocon (Grant, 1989) also may not provide the resolution to describe shear zones with complex fluid flow evolutions, as changes in element mobility may occur throughout the life time of the shear zones.

### **8.3 CENTRAL AUSTRALIAN CONTINENTAL REWORKING: A FAILED RIFT?**

Tectonism during the Alice Springs Orogeny (300 to 400 Ma) caused the inversion of the Centralian Superbasin and lead to the exhumation of middle- to deep-crustal rocks within central Australia. Metamorphism and deformation during the Alice Springs Orogeny produced greenschist- to amphibolite-facies shear zone assemblages throughout the Arunta Inlier while sedimentation and deformation occurred within the overlying basins.

The dominant orientation of structures within the Arunta Inlier is NW-SE and E-W and was caused by repeated N-S compression and extension since the Proterozoic. As central Australia formed a continental interior during the Alice Springs Orogeny failure along existing structures may explain the orientation of shear zones and faults. As discussed by Sandiford (1999) a deformation-induced imbalance in the thermal regime within the lithosphere as a response to rifting and sedimentation may play a key role in the mechanics of basin inversion that occurs 50 to 100My after rifting. In addition, high-heat production from granites within the crust, can explain the significantly-weakened crust of central Australia during the Phanerozoic (Sandiford and Hand, 1998b). Modelling by Roberts and Houseman (2001) also indicated weakening of the intracontinental crust by mantle delamination can contribute to periods of orogenic activity at great distances to tectonic forces at the continental edge.

The steeply-dipping orientation and reverse movement along the Alice Spring Orogeny age shear zones in the northern Arunta Inlier form an inversion structure (Collins and Teyssier, 1989). Prior to the onset of the Alice Springs Orogeny, the opening of the Larapinta Seaway at ~490 Ma may have created an extensional rift-type setting, in which deep extensional faults and graben structures developed throughout the region (Fig. 8.3). Surface topography models from Braun and Shaw (2001) are consistent with this, indicating that a lineament across the Australian continent that denotes the Larapinta Seaway had negative (~1km) topography at 450 Ma and became positive at 385 Ma,

becoming perhaps 5 km high by 300 Ma. Abundant sedimentation within the deepened basins during the rifting and lithospheric heating within the thinning lithosphere may have stimulated thermal weakening of the crust. As a response, compressional forces reactivated the extensional faults leading to the formation of substantial topography (Fig. 8.3), while shear zones beneath were recrystallised under amphibolite-facies conditions. Thrusting along these structures producing a regional inversion structure that led to the exhumation of the Arunta Inlier.

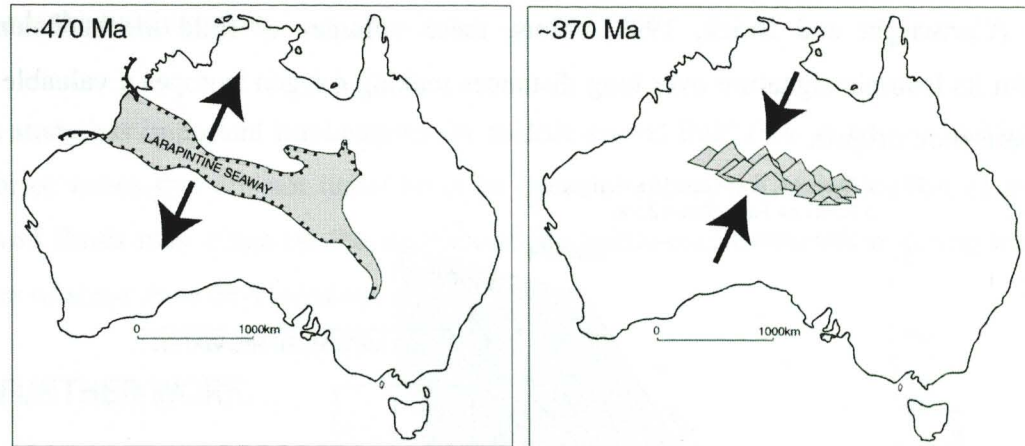


**Figure 8.3.** Schematic representation of rifting associated with the Larapinta Seaway at ~470 Ma (after Webby 1978) and the formation of large mountains in central Australia during the Alice Springs Orogeny (~370 Ma). Topography location approximately from Braun and Shaw (2001).

Substantiating a Palaeozoic failed rift-setting in central Australia is beyond the scope of this study, but, it is clear that substantial tectonic rejuvenation occurred during the Ordovician to Carboniferous periods involving extension followed by compression.

#### 8.4 SHEAR ZONE HYDRATION: IMPLICATIONS FOR MIDDLE-CRUSTAL FLUID RECYCLING

Oxygen and hydrogen isotope data presented in Chapters Four and Six indicate that the shear zones in the northern Arunta Inlier and the Redbank High Strain Zone hosted low  $\delta^{18}\text{O}$  surface-derived fluids, likely to be formation waters from the overlying sedimentary basins (Fig 8.4). The variable low  $\delta^{18}\text{O}$  signatures throughout the shear zones suggest that, at least locally, fluid volumes were sufficient to preserve their source isotopic signature over long distances. The petrography of the shear zones, presented in Chapters Three and Six, indicates they occurred at or near the brittle-ductile transition. This being the case, the distance fluid must have flowed from its surface reservoir to the onset of the ductile crust is

likely to be a minimum of 10km. PT estimates of the shear zones indicate depths of ~13km for the northern Arunta Inlier shear zones that host surface-derived fluids. Given:

$$q = K_e * z$$

where  $q$  is the time-integrated fluid flux (in  $m^3 m^{-2}$ ),  $K_e$  is the water-rock partition coefficient ( $\sim 1.8 m^3 m^{-1}$ ) and  $z$  (m) is the distance along the flow path (Cartwright and Buick, 1999), the time-integrated fluid fluxes within the shear zones of the Arunta Inlier must have been at least  $2.3 \times 10^4 m^3 m^{-2}$ . This is similar in magnitude to the calculated time-integrated fluid fluxes from shear zones in the SE Reynolds Range of  $5.9 \times 10^4$  to  $4.2 \times 10^5 m^3 m^{-2}$  (Cartwright and Buick, 1999). Thus, these volumes of fluid are sufficient to maintain its isotopic signature over long distances making oxygen isotopes a valuable tool to discern fluid origins.

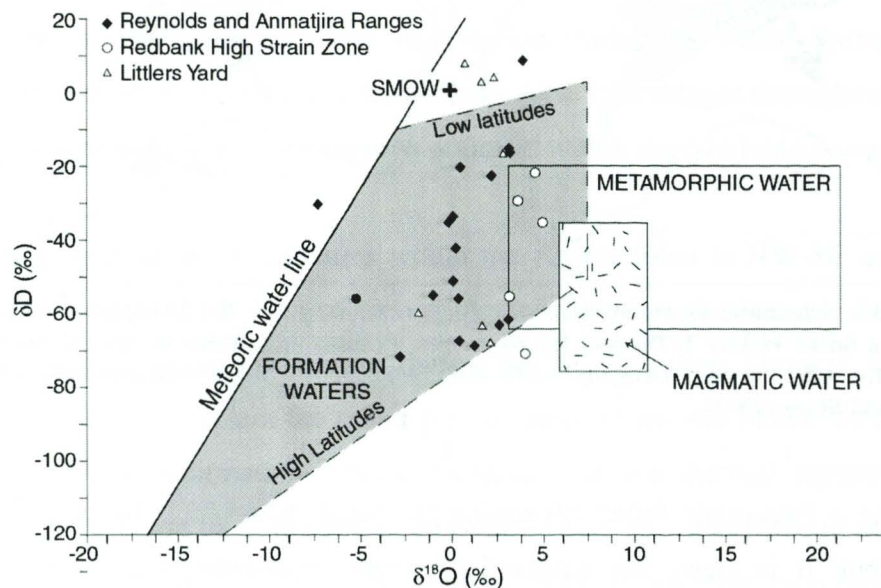


**Figure 8.4.**  $\delta D_{fluid}$  and  $\delta^{18}O_{fluid}$  values for the shear zone rocks of the SE Anmatjira and Reynolds Ranges, Redbank High Strain Zone and Littlers Yard, southern Arunat Inlier. Formation water, metamorphic water and magmatic water fields after Rollinson, 1993 from data of Taylor, 1974 and Sheppard, 1986. The data indicate fluids originated as formation waters.

The large sedimentary basin covering central Australia from 900 Ma (Lindsay, 1999) provides a substantial fluid reservoir. In addition, the opening of the Larapinta Seaway would have produced further hydrous sediments. Seismic activity and deep faulting at the onset of extension associated with the opening of the Larapinta Seaway may have driven substantial fluid circulation throughout the brittle upper crust. Thus, extensive fluid flow down through the crust may have predominantly occurred during extension and brittle deformation, becoming entrapped with a ductile crust at the onset of compression before being pumped back out during ductile shearing. As discussed by Holdsworth *et al.* (2001 and references therein), the flow of fluids within shear zones drives ductility enhancing

chemical reactions and diffusive mass transfer leading to the softening of the wall rocks and the upward displacement of the brittle-ductile transition. This process of shallowing the brittle-ductile transition by pumping volumes of fluids into fault zones may have some relevance to the shear zones of central Australia, where large quantities of fluid have infiltrated shear zones within a thick continental block. Once fluid penetrated the fracture networks within the middle crust reaction weakening and strain partitioning become emphasised trapping fluids within the fault zones as permeability rapidly decreased. Fault-valving networks may then have driven the ascent of fluids through the shear zones back towards the brittle regime.

This study has important implications for middle crustal fluid flow in continental interiors or thrust zones that are not underthrust by hydrous material. The infiltration of surface-derived fluids may hinge on the location of the brittle-ductile transition during the early stages of shear zone development.

## **8.5 FURTHER WORK**

The extent and significance of the newly defined Larapinta Event in the tectonic evolution of central Australia remains unclear and is currently the focus of investigations by other researchers in the area. Further high-resolution geochronological work is necessary to constrain the timing of the Alice Springs Orogeny within the Redbank High Strain Zone where  $^{40}\text{Ar}/^{39}\text{Ar}$  fails to determine geologically meaningful ages due to excess argon contamination. In addition, the extent of excess argon contamination within other shear zones in the Arunta Inlier remains unknown.



- Allen, A. R., and Black, L. P., 1979, The Harry Creek Deformed Zone, a retrograde schist zone of the Arunta Block, central Australia: *Journal of the Geological Society of Australia*, v. 26, p. 17-28.
- Arnaud, N. O., and Kelley, S. P., 1995, Evidence for excess argon during high pressure metamorphism in the Dora Maira Massif (western Alps, Italy), using an ultra-violet laser ablation microprobe  $^{40}\text{Ar}/^{39}\text{Ar}$  technique: *Contributions to Mineralogy and Petrology*, v. 121, p. 1-11.
- Arnold, J., Sandiford, M., and Wetherley, S., 1995, Metamorphic events in the eastern Arunta Inlier, Part 1. Metamorphic petrology: *Precambrian Research*, v. 71, p. 183-205.
- Ballèvre, M., Möller, A., and Hensen, B. J., 2000, Exhumation of the lower crust during crustal shortening: an Alice Springs (380 Ma) age for a prograde amphibolite facies shear zone in the Strangways Metamorphic Complex (central Australia): *Journal of Metamorphic Geology*, v. 18, p. 737-747.
- Barker, A. J., Bennett, D. G., Boyce, A. J., and Fallick, A. E., 2000, Retrogression by deep infiltration of meteoric fluids into thrust zones during late-orogenic rapid unroofing: *Journal of Metamorphic Geology*, v. 18, p. 307-318.
- Beach, A., 1980, Retrogressive metamorphic processes in shear zones with special reference to the Lewisian complex: *Journal of Structural Geology*, v. 2, p. 257-263.
- Bebout, G. E., and Barton, M. D., 1993, Metasomatism during subduction: products and possible paths in the Catalina Schist, California: *Chemical Geology*, v. 108, p. 61-92.
- Becker, H., Jochum, K. P., and Carlson, R. W., 2000, Trace element fractionation during dehydration of eclogites from high-pressure terranes and the implications for element fluxes in subduction zones: *Chemical Geology*, v. 163, p. 65-99.
- Bendall, B., Hand, M., and Foden, J., 1998, Sm-Nd evidence for mid-Palaeozoic regional amphibolite-facies metamorphism in the Strangways Range, central Australia: *Geological Society of Australia Abstracts*, v. 49, p. 27.
- Best, M. G., 1982, *Igneous and Metamorphic Petrology*: W. H. Freeman and Company, New York.
- Bickle, M. J., and MacKenzie, D. M., 1987, The transport of heat and matter by fluids during metamorphism: *Contributions to Mineralogy and Petrology*, v. 95, p. 384-392.
- Black, L. P., 1984, U-Pb zircon ages and a revised chronology for the Tennant Creek Inlier, Northern Territory: *Australian Journal of Earth Sciences*, v. 31, p. 123-131.

- Black, L. P., and Shaw, R. D., 1992, U-Pb zircon chronology of prograde Proterozoic events in the Central and Southern Provinces of the Arunta Blocks, central Australia: *Australian Journal of Earth Sciences*, v. 39, p. 153-171.
- Black, L. P., Shaw, R. D., and Offe, L. A., 1980, The age of the Stuart Dyke Swarm and its bearing on the onset of Late Precambrian sedimentation in central Australia: *Journal of the Geological Society of Australia*, v. 27, p. 151-155.
- Black, L. P., Shaw, R. D., and Stewart, A. J., 1983, Rb-Sr geochronology of Proterozoic events in the Arunta Inlier, central Australia: *BMR Journal of Australian Geology & Geophysics*, v. 8, p. 129-137.
- Bons, P. D., 2001, The formation of large quartz veins by rapid ascent of fluids in mobile hydrofractures: *Tectonophysics*, v. 336, p. 1-17.
- Bos, B., and Spiers, C. J., 2001, Experimental investigation into the microstructural and mechanical evolution of phyllosilicate-bearing fault rock under conditions favouring pressure solution: *Journal of Structural Geology*, v. 23, p. 1187-1202.
- Boullier, A. M., Charoy, B., and Pollard, P. J., 1994, Fluctuation in porosity and fluid pressure during hydrothermal events: textural evidence in the Emuford District, Australia: *Journal of Structural Geology*, v. 16, p. 1417-1429.
- Bowman, J. R., and Willett, S. D., 1991, Spatial patterns of oxygen isotope exchange during one-dimensional fluid infiltration: *Geophysical Research Letters*, v. 18, p. 971-974.
- Bowman, J. R., Willett, S. D., and Cook, S. J., 1994, Oxygen isotopic transport and exchange during fluid flow: one-dimensional models and applications: *American Journal of Science*, v. 294, p. 1-55.
- Braun, J. and Shaw, R., 2001, A thin-plate model of Palaeozoic deformation of the Australian lithosphere: implications for understanding the dynamics of intracratonic deformation: *Geological Society Special Publication*, v. 184, p. 165-194.
- Buick, I. S., Cartwright, I., Hand, M., and Powell, R., 1994, Evidence for pre-regional metamorphic fluid infiltration of the Lower Calcsilicate Unit, Reynolds Range Group (central Australia): *Journal of Metamorphic Geology*, v. 12, p. 789-810.
- Buick, I. S., Cartwright, I., and Harley, S. L., 1998, The retrograde P-T-t path for low-pressure granulites from the Reynolds Range, central Australia: petrological constraints and implications for low-P/high-T metamorphism: *Journal of Metamorphic Geology*, v. 16, p. 511-529.
- Buick, I. S., Hand, M., Vry, J. K., Cartwright, I., and Read, C. M., 1999a, Polymetamorphism and reactivation of the Reynolds Range area, northern Arunta Inlier, central Australia: petrological, geochronological, geochemical and structural

- constraints: Specialist Group in Geochemistry, Mineralogy and Petrology Field Guide No. 2 Geological Society of Australia.
- Buick, I. S., Frei, R., and Cartwright, I., 1999b, The timing of high-temperature retrogression in the Reynolds Range, central Australia: constraints for single mineral Pb-Pb dating: *Contributions to Mineralogy and Petrology*, v. 135, p. 244-254.
- Buick, I. S., Miller, J. A., Williams, I. S., and Cartwright, I., 2001, Ordovician high-grade metamorphism of a newly recognised late Neoproterozoic terrane in the northern Harts Range, central Australia: *Journal of Metamorphic Geology*, v. 19, p. 373-394.
- Cartwright, I., and Valley, J. W., 1992, Oxygen isotope geochemistry of the Scourian complex, NW Scotland: *Journal of the Geological Society London*, v. 149, p. 115-126.
- Cartwright, I., and Oliver, N. H. S., 1994, Fluid flow during contact metamorphism, Mary Kathleen, Australia: *Journal of Petrology*, v. 35, p. 1493-1519.
- Cartwright, I., and Buick, I. S., 1999, The flow of surface-derived fluids through Alice Springs age middle-crustal ductile shear zones, Reynolds Range, central Australia: *Journal of Metamorphic Geology*, v. 17, p. 397-414.
- Cartwright, I., Valley, J. W., and Hazelwood, A. M., 1993, Extent and causes of resetting of oxybarometers and oxygen isotopes in granulite-facies orthogneisses: Diana and Stark complexes, NW Adirondack Mountains, New York: *Contributions to Mineralogy and Petrology*, v. 113, p. 208-225.
- Cartwright, I., Vry, J. K., and Sandiford, M., 1995, Changes in stable isotope ratios of metapelites and marbles during metamorphism, Mount Lofty Ranges, South Australia: implications for crustal scale fluid flow: *Contributions to Mineralogy and Petrology*, v. 120, p. 292-310.
- Cartwright, I., Buick, I. S., and Vry, J. K., 1996, Polyphase metamorphic fluid flow in the lower calc-silicate Unit, Reynolds Range, central Australia: *Precambrian Research*, v. 77, p. 211-229.
- Cartwright, I., Buick, I. S., and Mass, R., 1997, Fluid flow in Marbles at Jervois, central Australia: oxygen isotope disequilibrium and zoning produced by decoupling of mineralogical and isotopic resetting: *Contributions to Mineralogy and Petrology*, v. 128, p. 335-351.
- Cartwright, I., Buick, I. S., Foster, D. A., and Lambert, D. D., 1999, Alice Springs age shear zones from the southeastern Reynolds Range, central Australia: *Australian Journal of Earth Sciences*, v. 46, p. 355-363.

- Cartwright, I., Buick, I. S., and Vry, J. K., 2001, Fluid-rock interaction in the Reynolds Range, central Australia: superimposed, episodic, and channelled fluid flow systems: Geological Society Special Publication, v. 184, p. 357-380.
- Chacko, T., Xiangsheng, H., Mayeda, T.K., Clayton, R.N., and Goldsmith, J.R., 1996, Oxygen isotope fractionations in muscovite, phlogopite and rutile: *Geochimica et Cosmochimica Acta*, v. 60, p. 2595-2608.
- Chacko, T., Riciputi L. R., Cole D. R., and Horita J., 1999, A new technique for determining equilibrium hydrogen isotope fractionation factors using the ion microprobe: Application to the epidote-water system: *Geochimica et Cosmochimica Acta*, v. 63, p. 1-10.
- Chamberlain, C. P., Ferry, J. M., and Rumble, D, III, 1990, The effect of net-transfer reactions on the isotopic composition of minerals: *Contributions to Mineralogy and Petrology*, v. 105, p. 322-336.
- Chamberlain, C. P., Zeitler, P. K., Barnett, D. E., Winslow, D., Poulson, S. R., Leathy, T., and Hammer, J. E., 1995, Active hydrothermal systems during the recent uplift of Nanga Parbat, Pakistan Himalaya: *Journal of Geophysical Research*, v. 100, p. 439-495.
- Clarke, G. L., and Powell, R., 1991, Proterozoic granulite facies metamorphism in the southeastern Reynolds Range, central Australia: geological context, P-T path and overprinting relationships: *Journal of Metamorphic Geology*, v. 9, p. 267-281.
- Clarke, G. L., Collins, W. J., and Vernon, R. H., 1990, Successive overprinting granulite-facies metamorphic events in the Anmatjira Range, central Australia: *Journal of Metamorphic Geology*, v. 8, p. 65-88.
- Clayton, R., and Mayeda, T. K., 1963, The use of bromine pentafluoride in the extraction of oxygen from oxides and silicates for isotopic analysis: *Geochimica et Cosmochimica Acta*, v. 27, p. 43-52.
- Close, D., Scrimgeour, I., Hand, M., Flottmann, T., and Edgegoose, C., 1999, Strain partitioning in the intracratonic Petermann Orogeny, central Australia: *Geological Society of Australia Abstracts*, v.49 p. 32.
- Cole, D. R., and Ripley, E.M., 1998, Oxygen isotope fractionation between chlorite and water from 170 to 350°C: A preliminary assessment based on partial exchange and fluid/rock experiments: *Geochimica et Cosmochimica Acta*, v. 63, p. 449-457.
- Collins, W. J., 2000, Granite magma segregation and transfer during compressional deformation in the deep crust? Proterozoic Arunta Inlier, central Australia, FA4 *Geological Society of Australia*, p. 104.

- Collins, W. J., and Teyssier, C., 1989, Crustal scale ductile fault systems in the Arunta Inlier, central Australia: *Tectonophysics*, v. 158, p. 49-66.
- Collins, W. J., and Vernon, R. H., 1991, Orogeny associated with anticlockwise P-T-t paths: Evidence from low-P, high-T metamorphic terranes in the Arunta Inlier, central Australia: *Geology*, v. 19, p. 835-838.
- Collins, W. J., and Shaw, R. D., 1995, Geochronological constraints on orogenic events in the Arunta Inlier: a review: *Precambrian Research*, v. 71, p. 315-346.
- Collins, W. J., and Williams, I. S., 1995, SHRIMP ionprobe dating of short-lived Proterozoic tectonic cycles in the northern Arunta Inlier, central Australia: *Precambrian Research*, v. 71, p. 69-89.
- Collins, W. J., and Sawyer, E. W., 1996, Pervasive granitoid magma transfer through the lower-middle crust during non-coaxial compressional deformation: *Journal of Metamorphic Geology*, v. 14, p. 565-579.
- Collins, W. S., Vernon, R. H., and Clarke, G. L., 1991, Discrete Proterozoic structural terranes associated with low-P, high-T metamorphism, Anmatjira Range, Arunta Inlier, central Australia: tectonic implications: *Journal of Structural Geology*, v. 13, p. 1157-1171.
- Collins, W. J., Williams, I. S., Shaw, S. E., and McLaughlin, N. A., 1995, The age of the Ormiston pound Granite: implications for Mesoproterozoic evolution of the Arunta Inlier, central Australia: *Precambrian Research*, v. 71, p. 91-105.
- Cooper, J. A., Mortimer, G. E., and James, P. R., 1988, Rate of Arunta Inlier evolution at the eastern margin of the Entia Dome, central Australia: *Precambrian Research*, v. 40/41, p. 217-231.
- de Jong, K. F., G. Ruffet, G., Amouric, M., and Wijbrans, J. R., 2001, Excess argon incorporation in phengite of the Mulhacén Complex: submicroscopic illitization and fluid ingress during late Miocene extension in the Betic Zone, south-eastern Spain: *Chemical Geology*, v. 178, p. 159-195.
- Deer, W. A., Howie, R. A., and Zussman, J., 1992, An introduction to the rock-forming minerals: Longman Group Limited, Harlow, p. 696.
- Dipple, G. M., and Ferry, J. M., 1992a, Metasomatism and fluid flow in ductile fault zones: *Contributions to Mineralogy and Petrology*, v. 112, p. 149-164.
- Dipple, G. M., and Ferry, J. M., 1992b, Fluid flow and stable isotopic alteration in rocks at elevated temperatures with applications to metamorphism: *Geochimica et Cosmochimica Acta*, v. 56, p. 3539-3550.

- Dipple, G. M., Wintsch, R. P., and Andrews, M. S., 1990, Identification of the scales of differential element mobility in a ductile fault zone: *Journal of Metamorphic Geology*, v. 8, p. 645-661.
- Dirks, P. H., and Wilson, C. J. L., 1990, The geological evolution of the Reynolds Range, central Australia: evidence for three distinct structural-metamorphic cycles: *Journal of Structural Geology*, v. 12, p. 651-665.
- Dirks, P. H., Hand, M., and Powell, R., 1991, The P-T deformation path for a mid-Proterozoic, low-pressure terrane: the Reynolds Range, central Australia: *Journal of Metamorphic Geology*, v. 9, p. 641-661.
- Dodson, M. H., 1973, Closure temperature in cooling geochronological and petrological systems: *Contributions to Mineralogy and Petrology*, v. 40, p. 259-274.
- Dunlap, W. J., 1997, Neocrystallization or cooling?  $^{40}\text{Ar}/^{39}\text{Ar}$  ages of white micas from low-grade mylonites: *Chemical Geology* v. 143, p. 181-203.
- Dunlap, W. J., and Teyssier, C., 1995, Paleozoic deformation and isotopic disturbances in the southeastern Arunta Block, central Australia: *Precambrian Research*, v. 71, p. 229-250.
- Dunlap, W. J., Teyssier, C., MacDougall, I., and Baldwin, S., 1991, Ages of deformation from K/Ar and  $^{40}\text{Ar}/^{39}\text{Ar}$  dating of white micas: *Geology* v.19, p. 1213-1216.
- Edmond, J. M., and Paterson, M. S., 1972, Volume changes during the deformation of rocks at high pressures: *International Journal of Rock Mechanics and Mineral Science* v. 9, p. 161-182.
- Elberg, M. A., Bons, P. D., Dougherty-Page, J., Janka, C. E., Neumann, N., and Schafer, B., 2001, Age and metasomatic alteration of the Mt Neil Granite at Nooldoonooldoona Waterhole, Mt Painter Inlier, Southern Australia: *Australian Journal of Earth Sciences*, v. 48, p. 721-730.
- Embleton, B. J. J., 1984, Continental Palaeomagnetism, in Veevers, J. J., ed., *Phanerozoic Earth History of Australia: Oxford Monographs on Geology and Geophysics*, Oxford Science Publications, Oxford, p. 11-16.
- Etheridge, M. A., Wall, V. J., and Vernon, R. H., 1983, The role of the fluid phase during regional metamorphism and deformation: *Journal of Metamorphic Geology*, v. 1, p. 205-226.
- Faure, G., 1986, *Principles of isotope geology*: John Wiley and Sons, Singapore, p. 589.
- Ferry, J. M., 1994, A historical view of metamorphic fluid flow: *Journal of Geophysical Research*, v. 99, p. 15487-15498.

- Fliervoet, T. F., and White, S. H., 1995, Quartz deformation in a very fine-grained quartzofeldspathic mylonite: a lack of evidence for dominant grain boundary sliding deformation: *Journal of Structural Geology*, v. 17, p. 1095-1109.
- Fliervoet, T. F., White, S. H., and Drury, M. R., 1997, Evidence for dominant grain-boundary sliding in greenschist- and amphibolite-grade polymetamorphic ultramylonites from the Redbank Deformed Zone, central Australia: *Journal of Structural Geology*, v. 19, p. 1495-1520.
- Fisher, G. J., and Paterson, M. S., 1989, Dilatancy during rock deformation at high temperatures and pressures: *Journal of Geophysical Research*, v. 94, p. 17607-17617.
- Flöttmann, T., and Hand, M., 1999, Folded basement-cored tectonic wedges along the northern edge of the Amadeus Basin, Central Australia: evaluation of orogenic shortening: *Journal of Structural Geology*, v. 21, p. 399-412.
- Flöttmann, T., Hand, M., Close, D., Edgoose, C., and Scrimgeour, I., 1999, Thrust tectonic styles at the margins of the Amadeus Basin, central Australia: *Geological Society of Australia, Abstracts*, v. 54, p. 30.
- Foden, J., Mawby, J., Kelley, S., Turner, S., and Bruce, D., 1995, Metamorphic events in the eastern Arunta Inlier, Part 2. Nd-Sr-Ar isotopic constraints: *Precambrian Research*, v. 71, p. 207-227.
- Forman, D. J., and Shaw, R. D., 1973, Deformation of the crust and mantle in central Australia: *Bureau of Mineral Resources, Australia, Bulletin*, v. 144.
- Foster, D. A., Harrison, T. M., Miller, C. F., and Howard, K. A., 1990, The  $^{40}\text{Ar}/^{39}\text{Ar}$  thermochronology of the eastern Mojave Desert, California, and adjacent western Arizona with implications for the evolution of metamorphic core complexes: *Journal of Geophysical Research, B, Solid Earth and Planets*, v. 95, p. 20,005-20,024.
- Freeman, S. R., Inger, S., Butler, R. W. H., and Cliff, R. A., 1997, Dating deformation using Rb-Sr in white mica: greenschist-facies deformation ages from the Entrelor shear zone, Italian Alps: *Tectonics*, v. 16, p. 57-76.
- Fyfe, W. S., Kronberg, B. I., and Stumm, W., 1979, Global chemical cycles and their alteration by man; book review: *Chemical Geology*, v. 24, p. 176-178.
- Gascombe, B., 1992, High-grade reworking of central Australian granulites. Part 1: Structural evolution: *Tectonophysics*, v. 204, p. 361-399.
- Giles, D., and Betts, P. G., (in review). Beyond Rodinia: The Early to Middle Proterozoic amalgamation of Australia and North America: *Geology*.

- Giletti, B. J., 1985, The nature of oxygen transport within minerals in the presence of hydrothermal water and the role of diffusion: *Chemical Geology*, v. 53, p. 197-206.
- Glazner, A. F., and Bartley, J. M., 1991, Volume loss, fluid flow and state of strain in extensional mylonites from the central Mojave Desert, California: *Journal of Structural Geology*, v. 13, p. 587-594.
- Glikson, A. Y., 1987, Regional structure and evolution of the Redbank-Mount Zeil thrust zone: a major lineament in the Arunta Inlier, central Australia: *Journal of Australian Geology and Geophysics*, v. 10, p. 89-107.
- Goleby, B. R., Shaw, R. D., Wright, C., Kennett, B. L. N., and Lambeck, K., 1989, Geophysical evidence for "thick-skinned" crustal deformation in central Australia: *Nature*, v. 337, p. 325-330.
- Goleby, B. R., Kennett, B. L. N., Wright, C., Shaw, R. D., and Lambeck, K., 1990, Seismic reflection profiling in the Proterozoic Arunta Block, central Australia: processing for testing models of tectonic evolution: *Tectonophysics*, v. 173, p. 257-268.
- Golyshev, S. I., Padalko, N. L., and Pechenkin, S. A., 1981, Fractionation of stable oxygen and carbon isotopes in carbonate systems: *Geochemistry International*, v. 18, p. 85-99.
- Graham, C. M., Atkinson, J., and Harmon, R. S., 1984, Hydrogen isotope fractionation in the system chlorite-water: NERC 6th Progress Report of Research 1981-1984, v. NERC Publication Series D, p. 139.
- Grant, J. A., 1986, The Isocon diagram – A simple solution to Gresens' equation for metasomatic alteration: *Economic Geology*, v. 81, p. 1976-1982.
- Gray, D. R., and Foster, D. A., 1998, Character and kinematics of faults within the turbidite-dominated Lachlan Orogen; implications for tectonic evolution of eastern Australia: *Journal of Structural Geology*, v. 20, p. 1691-1720.
- Greenfield, J. E., Clarke, G. L., Bland, M., and Clark, D. J., 1996, In-situ migmatite and hybrid diatexite at Mount Stafford: *Journal of Metamorphic Geology*, v. 14, p. 413-426.
- Gueguen, Y., David, C., and Gavrilenko, P., 1991, Percolation networks and fluid transport in the crust: *Geophysical Research Letters*, v. 18, p. 931-934.
- Hand, M., and Dirks, P. H., 1992, The influence of deformation on the formation of axial-planar leucosomes and the segregation of small melt bodies within the migmatitic Napperby Gneiss, central Australia: *Journal of Structural Geology*, v. 14, p. 591-604.
- Hand, M., and Sandiford, M., 1999, Intraplate deformation in central Australia, the link between subsidence and fault reactivation: *Tectonophysics*, v. 305, p. 121-140.

- Hand, M., and Buick, I. S., 2001, Polymetamorphism and reworking of the Reynolds and Anmatjira Ranges, central Australia: Geological Society Special Publication, v. 184, p. 237-260.
- Hand, M., Mawby, J., Kinny, P., and Foden, J., 1999, SHRIMP evidence for multiple high-T Palaeozoic events in the Arunta Inlier, central Australia: Journal of the Geological Society London, v. 156, p. 715-730.
- Harrison, T. M., Duncan, I., and McDougall, I., 1985, Diffusion of  $^{40}\text{Ar}$  in biotite: Temperature, pressure and compositional effects: *Geochimica et Cosmochimica Acta*, v. 49, p. 2461-2468.
- Henderson, I. H. C., and McCaig, A. M., 1996, Fluid pressures and salinity variations in shear zone-related veins, central Pyrenees, France: Implications for the fault-valve model: *Tectonophysics*, v. 262, p. 321-348.
- Hobbs, B. E., Archibald, N. J., Etheridge, M. A., and Wall, V. J., 1984, Tectonic history of the Broken Hill Block, Australia, in Kroener, A. and Greiling, R., ed., *Precambrian Tectonics Illustrated*, Stuttgart, E. Schweizerbart'sche Verlagsbuchhandl, p. 353-368.
- Hodges, K. V., and Bowring, S. A., 1995,  $^{40}\text{Ar}/^{39}\text{Ar}$  thermochronology of isotopically zoned micas: Insights from the southwestern USA Proterozoic orogen: *Geochimica et Cosmochimica Acta*, v. 59, p. 3205-3220.
- Hoefs, J., 1997, *Stable Isotope Geochemistry: Minerals and Rocks 9*, Springer and Verlag, Berlin.
- Holdsworth, R. E., Butler, C. A., and Roberts, A. M., 1997, The recognition of reactivation during continental deformation: *Journal of the Geological Society, London*, v. 154, p. 73-78.
- Holdsworth, R. E., Stewart, M., and Imber, J., 2001, The structure and rheological evolution of reactivated continental fault zones: a review and case study: *Geological Society Special Publication*, v. 184, p. 115-138.
- Holland, T., and Powell, R., 1998, An internally-consistent thermodynamic dataset for phases of petrological interest: *Journal of Metamorphic Geology*, v. 16, p. 309-343.
- Imber, J., Holdsworth, R. E., Butler, C. A., and Lloyd, G. E., 1997, Fault-zone weakening processes along the reactivated Outer Hebrides Fault Zone, Scotland: *Journal of the Geological Society, London*, v. 154, p. 105-109.
- Iyer, S. S., Woodford, P. J., and Wilson, A. F., 1976, Rb-Sr isotopic studies of a polymetamorphic granulite terrain, Strangways Range, central Australia: *Lithos*, v. 9, p. 211-224.

- Jäger, E., 1979, The Rb-Sr method, in Jäger, E., Hunziker, J. C., eds. *Lectures in Isotope Geology*, Springer, Berlin, p. 12-26
- Jambon, A., and Zimmerman, J. L., 1990, Water in oceanic basalts: evidence for dehydration of recycled crust: *Earth and Planetary Science Letters*, v. 101, p. 323-331.
- Jenkin, G. R. T., Craw, D., and Fallick, A. E., 1994, Stable isotope and fluid inclusion evidence for meteoric fluid penetration into an active mountain belt; Alpine Schist, New Zealand: *Journal of Metamorphic Geology*, v. 12, p. 429-444.
- Kerrick, R., and Hyndman, D., 1986, Thermal and fluid regimes in the Bitterroot Lobe Sapphire Block detachment zone, Montana; evidence from  $^{18}\text{O}/^{16}\text{O}$  and geological relationships: *Geological Society of America Bulletin*, v. 97, p. 147-155.
- Klootwijk, C. T., 1980, Early Palaeozoic palaeomagnetism in Australia; I, Cambrian results from the Flinders Ranges, South Australia; II, Late Early Cambrian results from Kangaroo Island, South Australia; III, Middle to early-Late Cambrian results from the Amadeus Basin, Northern Territory: *Tectonophysics*, v. 64, p. 249-332.
- Knipe, R. J., 1989, Deformation mechanisms - recognition from natural tectonics: *Journal of Structural Geology*, v. 11, p. 127-146.
- Koons, P. O., and Craw, D., 1991, Evolution of fluid driving forces and composition within collisional orogens: *Geophysical research letters*, v. 18, p. 935-938.
- Korsch, R. J., Goleby, B. R., Leven, J. H., and Drummond, B. J., 1998, Crustal architecture of central Australia based on deep seismic reflection profiling: *Tectonophysics*, v. 288, p. 57-69.
- Lambeck, K., 1991, Teleseismic travel-time anomalies and deep crustal structure of the northern and southern margins of the Amadeus Basin: *BMR Bulletin*, v. 236, p. 409-427.
- Lambeck, K., and Penney, C., 1984, Teleseismic travel time anomalies and crustal structure in central Australia: *Physics of the Earth and Planetary Interiors*, v. 34, p. 46-56.
- Lambeck, K., Bergess, G., and Shaw, R. D., 1988, Teleseismic travel-time anomalies and deep crustal structure in central Australia: *Geophysical Journal of the Royal Astronomical Society*, v. 94, p. 212-224.
- Lin, S., 1995, Structural evolution and tectonic significance of the Eastern Highlands shear zone in Cape Breton Island, the Canadian Appalachians: *Canadian Journal of Earth Sciences*, v. 32, p. 545-554.

- Lin, S., 2001,  $^{40}\text{Ar}/^{39}\text{Ar}$  age pattern associated with differential uplift along the Eastern Highlands shear zone, Cape Breton Island, Canadian Appalachians: *Journal of Structural Geology*, v. 23, p. 1031-1042.
- Lindsay, J. F., 1999, Heavitree Quartzite, a Neoproterozoic (ca 800-760 Ma), high energy, tidally influenced, ramp association, Amadeus Basin, central Australia: *Australian Journal of Earth Sciences*, v. 46, p. 127-139.
- Lobato, L. M., Forman, J. M. A., Fazikawa, K., Fyfe, W. S., and Kerrich, R., 1983, Uranium in overthrust Archaean basement, Bahia, Brazil: *Canadian Mineralogist*, v. 21, p. 647-654.
- Manatschal, G., Marquer, D., and Fruh-Green, G. L., 2000, Channellized fluid flow and mass transfer along a rift-related detachment fault (Eastern Alps, southeast Switzerland): *Geological Society of America Bulletin*, v. 112, p. 21-33.
- Marjoribanks, R. W., and Black, L. P., 1974, Geology and geochronology of the Arunta Complex north of Ormiston Gorge, central Australia: *Journal of the Geological Society of Australia*, v. 21, p. 291-299.
- Marquer, D., and Burkhard, M., 1992, Fluid circulation progressive deformation and mass transfer processes in the upper crust: the example of basement-cover relationships in the External Crystalline Massifs, Switzerland: *Journal of Structural Geology*, v. 14, p. 1047-1057.
- Mawby, J., Hand, M., and Foden, J., 1999, Sm-Nd evidence for high-grade Ordovician metamorphism in the Arunta Block, central Australia: *Journal of Metamorphic Geology*, v. 17, p. 653-668.
- Mawby, J., Hand, M., Foden, J. and Kinny, P., 1998, Ordovician granulites in the southeastern Arunta Inlier: a new twist in the Palaeozoic history of central Australia: *Geological Society of Australia, Abstracts*, v. 49, p. 296.
- Mawer, C. K., 1986, What is a mylonite?: *Geosciences Canada*, v. 13, p. 33-34.
- McCaig, A. M., 1984, Fluid-rock interaction in some shear zones from the Pyrenees: *Journal of Metamorphic Geology*, v. 2, p. 129-141.
- McCaig, A. M., 1988, Deep Fluid circulation in fault zones: *Geology*, v. 16, p. 867-870.
- McCaig, A. M., 1997, The geochemistry of volatile fluid flow in shear zones, in Holness, M. B., ed., *Deformation-enhanced Fluid Transport in the Earth's Crust and Mantle*, London, Chapman & Hall, p. 228-266.
- McCaig, A. M., Wickham, S. M., and Taylor, H. P. Jr., 1990, Deep fluid circulation in alpine shear zones, Pyrenees, France: field and oxygen isotope studies: *Contributions to Mineralogy and Petrology*, v. 106, p. 41-60.

- McCaig, A. M., Wayne, D. M., Marshall, J. D., Banks, D., and Henderson, I., 1995, Isotopic and fluid inclusion studies of fluid movement along the Gavarnie Thrust, central Pyrenees: reaction fronts in carbonate mylonites: *American Journal of Science*, v. 295, p. 309-343.
- McDougall, I., and Harrison, T. M., 1988, *Geochronology and thermochronology by the  $^{40}\text{Ar}/^{39}\text{Ar}$  method: Monographs on Geology and Geophysics, No. 9: New York, Oxford University Press Inc.*, p. 212.
- McDougall, I., and Harrison, T. M., 1999, *Geochronology and thermochronology by the  $^{40}\text{Ar}/^{39}\text{Ar}$  method: Oxford University Press, New York.*
- Miller, J. A., and Cartwright, I., 1997, Early meteoric fluid flow in high-grade, low  $\delta^{18}\text{O}$  gneisses from the Mallee Bore area, northern Harts Range, central Australia: *Journal of the Geological Society, London*, v. 54, p. 839-848.
- Miller, J. A., Cartwright, I., and Buick, I. S., 1997, Granulite facies metamorphism in the Mallee Bore area, northern Harts Range: implication for thermal evolution of the eastern Arunta Inlier, central Australia: *Journal of Metamorphic Geology*, v. 15, p. 613-629.
- Miller, J. A., Buick, I. S., Williams, I., and Cartwright, I., 1998, Re-evaluating the metamorphic and tectonic history of the eastern Arunta Block, central Australia: *Geological Society of Australia Abstracts*, v. 49, p. 316.
- Miller, S. A., and Nur, A., 2000, Permeability as a toggle switch in fluid-controlled crustal processes: *Earth and Planetary Science Letters*, v. 183, p. 133-146.
- Minissale, A., Vaselli, O., Chandrasekharam, D., Magro, G., Tassi, F., and Casiglia, A., 2000, Origin and evolution of "intracratonic" thermal fluids from central-western peninsular India: *Earth and Planetary Science Letters*, v. 181, p. 377-394.
- Mitchell, M. M., Kohn, B. P., and Foster, D.A., 1998, Post-orogenic cooling history of eastern South Australia from apatite FT thermochronology, in Van Den Haute, P. and de Corte, F., ed., *Advances in Fission-Track Geochronology*, Dordrecht, Kluwer.
- Möller, A., Armstrong, R. A., Ballèvre, M., Hensen, B. J., and Mezger, K., 1999, Crustal growth, metamorphism and deformation in the Strangways Metamorphic complex; a summary of recent U-Pb and Sm-Nd geochronology: *Geological Society of Australia Abstracts*, v. 54, p. 69-70.
- Morrison, J., 1994, Downward circulation of meteoric water into the lower plate of the Wipple Mountains metamorphic core complex, California: *Journal of Metamorphic Geology*, v. 12, p. 827-840.

- Norman, A. R., and Clarke, G. L., 1990, A barometric response to late compression in the Strangways Metamorphic Complex, Arunta Block, central Australia: *Journal of Structural Geology*, v. 12, p. 667-684.
- O'Hara, K., 1988, Fluid Flow and volume loss during mylonitization: an origin for phyllonite in an overthrust setting, North Carolina, U. S. A.: *Tectonophysics*, v. 156, p. 21-36.
- Obee, H. K., and White, S. H., 1985, Faults and associated fault rocks of the southern Arunta block, Alice Springs, central Australia: *Journal of Structural Geology*, v. 7, p. 701-712.
- Oliver, N. S., and Bons, P. D., 2001, Mechanisms of fluid flow and fluid-rock interaction in fossil metamorphic hydrothermal systems inferred from vein-wallrock patterns, geometry and microstructure: *Geofluids*, v. 1, p. 137-162.
- Passchier, C. W., and Trouw, R. A. J., 1996, *Micro-tectonics*: Springer-Verlag, Berlin.
- Phillips, D., 1991, Argon isotope and halogen chemistry of phlogopite from South African kimberlites: a combination step-heating, laser probe, electron microprobe and TEM study: *Chemical Geology*, v. 87, p. 71-98.
- Phillips, D., Machin, K. J., Kiviets, G. B., and Fourie, L. F., 1998, A petrological and  $^{40}\text{Ar}/^{39}\text{Ar}$  geochronological study of the Voorspoed kimberlite, South Africa: implications for the origin of Group II kimberlite magmatism: *South African Journal of Geology*, v. 101, p. 299-306.
- Pin, C., Briot D., Bassin C., and Poitrasson, F., 1994, Concomitant separation of strontium and samarium-neodymium for isotopic analysis in silicate samples, based on specific extraction chromatography: *Analytica Chimica Acta*, v. 298, p. 209-217.
- Ramsay, J. G., 1980, Shear zone geometry: a review: *Journal of Structural Geology*, v. 2, p. 83-99.
- Read, C. M., and Cartwright, I. S., 1999, The role of fluids in a major crustal thrust zone, Redbank High Strain Zone, central Australia, *Geological Society of Australia Abstracts*, v. 54, p. 88-89.
- Read, C. M., and Cartwright, I. S., 2000, Meteoric fluid infiltration in the middle crust during shearing: examples from the Arunta Inlier, central Australia: *Journal of Geochemical Exploration* v. 69-70, p. 333-337.
- Read, C. M., Flottman, T., Hand, M., Shaw, R., Cartwright, I., and Miller, J.A., 1999, Reactivation and reworking in the West MacDonnell Ranges region, southern Arunta Inlier, central Australia: *Specialist Group in Geochemistry, Mineralogy and Petrology Field Guide No. 3 Geological Society of Australia*.

- Reddy, S. M., Kelley, S. P., and Wheeler, J., 1996, A  $^{40}\text{Ar}/^{39}\text{Ar}$  laserprobe study of rocks from the Sesia Zone: excess argon, argon loss and implications for metamorphic and deformation histories: *Journal of Metamorphic Geology*, v. 14, p. 493-508.
- Reddy, S. M., Potts, G. J., and Kelley, S. P., 2001,  $^{40}\text{Ar}/^{39}\text{Ar}$  ages in deformed potassium feldspar: evidence of microstructural control on Ar isotope systematics: *Contributions to Mineralogy and Petrology*, v. 141, p. 186-200.
- Rollinson, H. R., 1993, *Using Geochemical Data: evaluation, presentation, interpretation: Longman geochemistry series: Longman Group Limited, Singapore*, p. 352.
- Roberts, E. A. and Houseman, G. A., 2001, Geodynamics of central Australia during intraplate Alice Springs Orogeny, thin viscous sheet models: *Geological Society Special Publication*, v. 184, p. 139-164.
- Rubatto, D., Williams, I. S., and Buick, I. S., 2001, Zircon and monazite response to prograde metamorphism in the Reynolds Range, central Australia: *Contributions to Mineralogy and Petrology*, v. 140, p. 458-468.
- Ruffet, G., Féraud, G., Malèvre, M., and Kiénast, J. R., 1995, Plateau ages and excess argon in phengites: an  $^{40}\text{Ar}/^{39}\text{Ar}$  laser probe study of Alpine micas (Sesia Zone, Western Alps, northern Italy): *Chemical Geology*, v. 121, p. 327-343.
- Ruffet, G., Gruau, G., Ballèvre, M., Féraud, G., and Philippot, P., 1997, Rb-Sr and  $^{40}\text{Ar}/^{39}\text{Ar}$  laser probe dating of high-pressure phengites from the Sesia zone (Western Alps): underscoring of excess argon and new age constraints on the high-pressure metamorphism: *Chemical Geology*, v. 141, p. 1-18.
- Rumble III, D., 1994, Water circulation in metamorphism: *Journal of Geophysical Research*, v. 99, p. 15499-15502.
- Sandiford, M., 1999, Mechanics of basin inversion: *Tectonophysics*, v. 305, p. 109-120.
- Sandiford, M., and Hand, M., 1998a, Australian Proterozoic high-temperature, low-pressure metamorphism in the conductive limit, in Treloar P. J. O'Brian, P. J., ed., *What Drives Metamorphism and Metamorphic Reactions?*, Geological Society of London, Special Publication, v. 138 p. 109-120.
- Sandiford, M., and Hand, M., 1998b, Controls on the locus of intraplate deformation in central Australia: *Earth and Planetary Science Letters*, v. 162, p. 97-110.
- Sandiford, M., Hand, M., and McLaren, S., 2001, Tectonic feedback, intraplate orogeny and the geochemical structure of the crust: a central Australian perspective: *Geological Society Special Publication*, v. 184, p. 195-218.
- Satir, M., and Taubald, H., 2001, Hydrogen and oxygen isotope evidence for fluid-rock interactions in the Menderes Massif, western Turkey: *International Journal of Earth Sciences*.

- Scaillet, S., 1996, Excess  $^{40}\text{Ar}$  transport and mechanism in high-pressure phengites: A case study from an eclogitized metabasite of the Dora-Maira nappe, western Alps: *Geochimica et Cosmochimica Acta*, v. 60, p. 1075-1090.
- Schmid, S. M., and Handy, M. R., 1991, Towards a genetic classification of fault rocks: geological usage and tectonophysical implications, in Müller, D. W., McKenzie, J. and Weissert, H., eds., *Controversies in modern geology*, New York, New York Academic Press, p. 339-361.
- Scrimgeour, I., and Sandiford, M., 1993, Early Proterozoic metamorphism at The Granites gold mine, Northern Territory; implications for the timing of fluid production in high-temperature, low-pressure terranes: *Economic Geology, Bulletin of the Society of Economic Geologists*, v. 88, p. 1099-1113.
- Scrimgeour, I., and Close, D., 1999, Regional high-pressure metamorphism during intracratonic deformation: the Petermann Orogeny, central Australia: *Journal of Metamorphic Geology*, v. 17, p. 557-572.
- Selverstone, J., Morteani, G., and Staude, J. M., 1991, Fluid channelling during ductile shearing: transformation of granodiorite into aluminous schist in the Tauern Window, eastern Alps: *Journal of Metamorphic Geology*, v. 9, p. 419-431.
- Shaw, R. D., 1991, The tectonic development of the Amadeus Basin, central Australia: *BMR Bulletin*, v. 236, p. 429-461.
- Shaw, R. D., and Black, L. P., 1991, The history and tectonic implications of the Redbank Thrust Zone, central Australia, based on structural, metamorphic and Rb-Sr isotopic evidence: *Australian Journal of Earth Sciences*, v. 38, p. 307-332.
- Shaw, R. D., Langworthy, A. P., Stewart, A. J., Offe, L. A., Jones, B. G., O'Donnell, I. C., and Knight, C. P., 1983, Alice Springs Sheet: Australian Geological Survey Organisation.
- Shaw, R. D., Stewart, A. J., and Black, L. P., 1984, The Arunta Inlier: a complex ensialic mobile belt in central Australia. Part 2: tectonic history: *Australian Journal of Earth Sciences*, v. 31, p. 457-484.
- Shaw, R. D., Korsch, R. J., Wright, C., and Goleby, B. R., 1991, Seismic interpretation and thrust tectonics of the Amadeus Basin, central Australia, along the BMR regional seismic line: *BMR Bulletin*, v. 236, p. 385-408.
- Shaw, R. D., Zeitler, P. K., McDougall, I., and Tingate, P. R., 1992, The Palaeozoic history of an unusual intracratonic thrust belt in central Australia based on  $^{40}\text{Ar}/^{39}\text{Ar}$ , K-Ar and fission track dating: *Journal of the Geological Society, London*, v. 149, p. 937-954.

- Shaw, R. D., Warren, R. G., and Pillinger, D. M., 1995, Hermannsburg Sheet: Australian Geological Survey Organisation.
- Sheppard, S. M. F., 1986, Characterisation of isotopic variations in natural waters, in Valley, J. W., Taylor, H. P. and O'Neil, J. R., ed., *Stable Isotopes in High Temperature Geological Processes*, Mineralogical Society of America, *Reviews in Mineralogy*, p. 165-184.
- Sibson, R. H., 1977, Fault rocks and fault mechanisms: *Journal of the Geological Society London*, v. 133, p. 191-213.
- Sibson, R. H., 1990, Conditions of fault-valve behaviour, in Knipe, R. J. and Rutter, E. H., ed., *Deformation mechanisms, rheology and tectonics*, Geological Society Special Publication, p. 15-28.
- Sibson, R. H., 1996, Structural permeability of fluid-driven fault-fracture meshes: *Journal of Structural Geology*, v. 18, p. 1031-1042.
- Sibson, R. H., 1998, Crustal stress, faulting and fluid flow, *Geological Society Special Publication*, v. 78, p. 69-84.
- Sibson, R. H., Moore, J. McM., and Rankin, A. H., 1975, Seismic pumping - a hydrothermal fluid transport mechanism: *Journal of the Geological Society of London*, v. 131, p. 653-659.
- Silver, P. G., 1996, Seismic anisotropy beneath the continents: probing the depths of geology: *Annual Review Earth and Planetary Science*, v. 24, p. 385-432.
- Simpson, C., and Wintsch, R. P., 1989, Evidence for deformation-induced K-feldspar replacement by myrmekite: *Journal of Metamorphic Geology*, v. 7, p. 261-275.
- Snoke, A. W., and Tullis, J., 1998, An overview of fault rocks, in Snoke, A. W., Tullis, J. and Todd, V. R., ed., *Fault-related rocks a petrographic atlas*, Princetown, Princetown University Press, p. 3-18.
- Spikings, R. A., Foster, D. A., and Kohn, B. P., 1997, Phanerozoic denudation history of the Mount Isa Inlier, Northern Australia: a record of the response of a Proterozoic mobile belt to intraplate tectonics: *International Geology Review*, v. 39, p. 107-124.
- Spikings, R. A., Foster, D. A., Kohn, B. P., and Lister, G. S., 2001, Post-orogenic (<1500 Ma) thermal history of the Proterozoic Eastern Fold Belt, Mount Isa Inlier, Australia: *Precambrian Research*, v. 109, p. 103-144.
- Steiger, R. H., and Jager, E., 1977, Subcommittee on geochronology; convention on the use of decay constants in geo- and cosmochronology: *Earth and Planetary Science Letters*, v. 36, p. 359-362.

- Stern, L. A., Chamberlain, C. P., Barnett, D. E., and Ferry, J. M., 1992, Stable isotopic evidence for regional-scale fluid migration in a Barrovian metamorphic terrain, Vermont, USA: *Contributions to Mineralogy and Petrology*, v. 112, p. 475-489.
- Stewart, A. J., 1981, 1:100 000 Geological Map Commentary, Reynolds Range Region, Canberra, Bureau of mineral resources, geology and geophysics, p. 1 -12.
- Stewart, A. J., Shaw, R. D., and Black, L. P., 1984, The Arunta Inlier: a complex ensialic mobile belt in central Australia. Part 1: stratigraphy, correlations and origin: *Australian Journal of Earth Sciences*, v. 31, p. 445-455.
- Stewart, M., Holdsworth, R. E., and Strachan, R. A., 2000, Deformation processes and weakening within the frictional-viscous transition zone of major faults: insights from the Great Glen Fault Zone, Scotland: *Journal of Structural Geology*, v. 22, p. 543-560.
- Streit, J. E., and Cox, S. F., 1998, Fluid infiltration and volume change during mid-crustal mylonitization of Proterozoic granite, King Island, Tasmania: *Journal of Metamorphic Geology*, v. 16, p. 197-212.
- Suzuoki, T., and Epstein, S., 1976, Hydrogen isotope fractionation between OH-bearing minerals and water: *Geochimica et Cosmochimica Acta*, v. 40, p. 1229-1240.
- Taylor, H. P., 1974, The application of oxygen and hydrogen isotope studies to problems of hydrothermal alteration and ore deposition. *Economic Geology*, v. 69, p. 843-883.
- Taylor, H. P., and Sheppard, S. M. F., 1986, Igneous rocks: I. Processes of isotopic fractionation and isotopic systematics, in Valley, J. W., Taylor, H. P., and O'Neil, J. R., ed., *Stable Isotopes in High-Temperature Geological Processes*, Mineralogical Society of America, *Reviews in Mineralogy*, p. 227-272.
- Tetley, N., MacDougall, I., and Heydegger, H. R., 1980, Thermal neutron interferences in the  $^{40}\text{Ar}/^{39}\text{Ar}$  dating technique: *Journal of Geophysical Research*, v. 85, p. 7201-7205.
- Teyssier, C., 1985, A crustal thrust system in an intracratonic environment: *Journal of Structural Geology*, v. 7, p. 689-700.
- Teyssier, C., Amri, C., and Hobbs, B. E., 1988, South Arunta block: the internal zones of a Proterozoic overthrust in central Australia: *Precambrian Research*, v. 40/41, p. 157-173.
- Tobisch, O. T., and Paterson, S. R., 1988, Analysis and interpretation of composite foliations in areas of progressive deformation: *Journal of Structural Geology*, v. 10, p. 745-754.

- Tobisch, O. T., Barton, M. D., Vernon, R. H., and Peterson, S. R., 1991, Fluid-enhanced deformation: transformation of granitoids to banded mylonites, western Sierra Nevada, California and southeastern Australia: *Journal of Structural Geology*, v. 13, p. 1137-1156.
- Upton, P., 1998, Modelling localization of deformation and fluid flow in a compressional orogen: Implications for the Southern Alps of New Zealand: *American Journal of Science*, v. 298, p. 296-323.
- Upton, P., Koons, P. O., and Chamberlain, C. P., 1995, Penetration of deformation-driven meteoric water into ductile rocks: isotopic and model observations from the Southern Alps, New Zealand: *New Zealand Journal of Geology and Geophysics*, v. 38, p. 535-543.
- van Staal, C. R., Rogers, N., and Taylor, B. E., 2001, Formation of low-temperature mylonites and phyllonites by alkali-metasomatic weakening of felsic volcanic rocks during progressive, subduction-related deformation: *Journal of Structural Geology*, v. 23, p. 903-921.
- Veevers, J. J., 1984, *Phanerozoic Earth History of Australia*: Oxford, Clarendon Press, p. 418.
- Vernon, R. H., Clarke, G. L., and Collins, W. J., 1990, Local, mid-crustal granulite facies metamorphism and melting: an example in the Mount Stafford area, central Australia, in Ashworth, J. R., Brown, M., ed., *High temperature metamorphism and crustal Anatexis*, London, Unwin & Hyman, p. 272-315.
- Villa, I. M., Grobèty, B., Kelley, S.P., Trigila, R., and Wieler, R., 1996, Assessing Ar transport paths and mechanisms in the McClure Mountains hornblende: *Contributions to Mineralogy and Petrology*, v. 126, p. 67-80.
- Villa, I. M., Hermann, J., Müntener, O., and Trommsdorff, V., 2000,  $^{40}\text{Ar}/^{39}\text{Ar}$  dating of multiply zoned amphibole generations (Malenco, Italian Alps): *Contributions to Mineralogy and Petrology*, v. 140, p. 363-381.
- Vry, J. K., and Cartwright, I., 1994, Origins of low- $^{18}\text{O}$  metamorphic rocks in the Early Proterozoic Lander Rock Beds, Reynolds Range, Arunta Block, central Australia: *Geological Society of America Abstracts with Programs*, v. 26, p. 407.
- Vry, J. K., and Cartwright, I., 1998, Stable isotope evidence for early fluid infiltration in a multiply metamorphosed terrane: the Reynolds Range, Arunta Block, central Australia: *Journal of Metamorphic Geology*, v. 16, p. 749-766.
- Vry, J., Compston, W., and Cartwright, I., 1996, SHRIMP II dating of zircon and monazites: reassessing the timing of high-grade metamorphism and fluid flow in

- the Reynolds Range, northern Arunta Block, Australia: *Journal of Metamorphic Geology*, v. 14, p. 335-350.
- Waight, T. E., Weaver, S. D., Ireland, T. R., Maas, R., Muir, R. J., and Shelley, D., 1997, Field characteristics, petrography, and geochronology of the Hohonu Batholith and the adjacent Granite Hill Complex, North Westland, New Zealand: *New Zealand Journal of Geology and Geophysics*, v. 40, p. 1-17.
- Walter, M. R., and Veevers, J. J., 1997, Australian Neoproterozoic palaeogeography, tectonics, and supercontinental connections: *AGSO Journal of Australian Geology and Geophysics*, v. 17 p. 73-92.
- Walter, M. R., Veevers, J. J., Calver, C. R., and Grey, K., 1995, Neoproterozoic stratigraphy of the Centralian Superbasin, Australia: *Precambrian Research*, v. 73, p. 173-195.
- Warren, R. G., 1983, Metamorphic and tectonic evolution of granulites, Arunta Block, central Australia: *Nature*, v. 305, p. 300-303.
- Warren, R. G., and Shaw, R. D., 1985, Volcanogenic Cu-Pb-Zn bodies in granulites of the central Arunta Block: *Journal of Metamorphic Geology*, v. 3, p. 81-99.
- Warren, R. G., and Shaw, R. D., 1995, Hermannsburg SF53-13; 1:250 000 geological Map Series explanatory notes: Northern Territory Geological Survey, p. 81.
- Wartho, J., 1995, Apparent argon diffusive loss  $^{40}\text{Ar}/^{39}\text{Ar}$  age spectra in amphiboles: *Earth and Planetary Science Letters*, v. 134, p. 393-407.
- Webby, B. D., 1978, History of the Orodvician continental platform shelf margin of Australia: *Journal of the Geological Society of Australia*, v. 25, p. 41-63.
- West, D. P., and Lux, D. R., 1993, Dating mylonitic deformation by the  $^{40}\text{Ar}/^{39}\text{Ar}$  method: An example from the Norumbega Fault Zone, Maine: *Earth and Planetary Science Letters*, v. 120, p. 221-237.
- White, S. H., and Knipe, R. J., 1978, Transformation- and reaction-enhanced ductility in rocks: *Journal of the Geology Society, London*, v. 135, p. 513-516.
- White, S. H., Burrows, S. E., Carreras, J., Shaw, N. D., and Humphreys, F. J., 1980, On mylonites in ductile shear zones: *Journal of Structural Geology*, v. 2, p. 175-187.
- Wijbrans, J. R., and McDougall, I., 1986,  $^{40}\text{Ar}/^{39}\text{Ar}$  dating of white micas from an alpine high-pressure metamorphic belt on Naxos (Greece): the resetting of the argon isotopic system: *Contributions to Mineralogy and Petrology*, v. 93, p. 187-194.
- Williams, I. S., Buick, I., and Cartwright, I. S., 1996, An extended episode of early Mesoproterozoic metamorphic fluid flow in the Reynolds Range, central Australia: *Journal of Metamorphic Geology*, v. 14, p. 29-47.

- Windrim, D. P., and McCulloch, M. T., 1986, Nd-Sr isotopic systematics of central Australian granulites: chronology of crustal development and constraints on the evolution of lower continental crust: *Contributions to Mineralogy and Petrology*, v. 94, p. 289-303.
- Wintsch, R. P., Christofferson, R., and Kronenberg, A. K., 1995, Fluid-rock reaction weakening of fault zones: *Journal of Geophysical Research B*, v. 100, p. 13021-13032.
- Wise, D. U., Dunn, D. E., Engelder, J. T., Geiser, P. A., Hatcher, R. D., Kish, S. A., Odom, A. L., and Schamel, S., 1984, Fault-related rocks: suggestions for terminology: *Geology*, v. 12, p. 391-394.
- Wright, C., Goleby, B. R., Collins, C. D. N., Korsch, R. J., Barton, T., Greenhalgh, S. A., and Sugiharto, S., 1990, Deep seismic profiling in central Australia: *Tectonophysics*, v. 173, p. 247-256.
- Wright, N., Layer, P. W., and York, D., 1991, New insights into thermal history from single grain  $^{40}\text{Ar}/^{39}\text{Ar}$  analysis of biotite: *Earth and Planetary Science Letters*, v. 140, p. 70-79.
- Wyborn, L. A. I., Page, R. W., and McCulloch, M. T., 1988, Petrology, geochronology and isotope geochemistry of the post-1820 Ma granites of the Mount Isa Inlier; mechanisms for the generation of Proterozoic anorogenic granites in Wyborn, L. A. I., Etheridge, M. A. ed., *The early to middle Proterozoic of Australia: Precambrian Research*, v. 40-41, p. 509-541.
- Wyborn, L.A.I., Hazell, M., Page, R. W., Idnurm, M., and Sun, S. S., 1998, A newly discovered major Proterozoic granite-alteration system in the Mount Webb region, central Australia and implications for Cu-Au mineralisation: *AGSO Research Newsletter*, v. 28, p. 1-5.
- Yardley, B. W. D., 1989, *An introduction to metamorphic petrology*: Longman Scientific & Technical, New York, p. 248.
- Young, D. N., Fanning, C. M., Shaw, R. D., Edgoose, C. J., Blake, D. H., Page, R. W., and Camacho, A., 1995, U-Pb zircon dating of tectonomagmatic events in the northern Arunta Inlier, central Australia: *Precambrian Research*, v. 71, p. 45-68.
- Zhao, J. -X., and McCulloch, M. T., 1993, Sm-Nd mineral isochron ages of Late Proterozoic mafic dyke swarms in central Australia; evidence for two distinctive events of mafic magmatism and crustal extension: *Chemical Geology*, v. 109, p. 341-354.

- 
- Zhao, J. -X., and Bennett, V. C., 1995, SHRIMP U-Pb zircon geochronology of granites in the Arunta Inlier, central Australia: Implications for Proterozoic crustal evolution: *Precambrian Research*, v. 71, p. 17-43.
- Zhao, J. -X., and McCulloch, M. T., 1995, Geochemical and Nd isotopic systematics of granites from the Arunta Inlier, central Australia: implications for Proterozoic crustal evolution: *Precambrian Research*, v. 71, p. 265-299.
- Zhao, J. -X., McCulloch, M. T., and Bennett, V. C., 1992, Sm-Nd and U-Pb zircon isotopic constraints on the provenance of sediments from the Amadeus Basin, central Australia: Evidence for REE fractionation: *Geochimica et Cosmochimica Acta*, v. 56, p. 921-940.
- Zheng, Y. F., 1991, Calculation of oxygen isotope fractionation in metal oxides: *Geochimica et Cosmochimica Acta*, v. 55, p. 2299-2307.
- Zheng, Y. F., 1993a, Calculation of oxygen isotope fractionation in anhydrous silicate minerals: *Geochimica et Cosmochimica Acta*, v. 57, p. 1079-1091.
- Zheng, Y. F., 1993b, Calculation of oxygen isotope fractionation in hydroxyl-bearing silicates: *Earth and Planetary Science Letters*, v. 120, p. 247-263.